Cx32 Gap Junctions in Human Urothelial Barrier Generation and Restitution

Jennifer Susan Hinley

Doctor of Philosophy

University of York

Biology

July 2015

Abstract

The ability of the urothelium to act as a urinary barrier is afforded by two key features: 1) It has the tightest barrier function of any epithelium, generated by tight junctions which assemble upon differentiation; 2) In response to damage, the quiescent urothelium can rapidly switch to a regenerative phenotype to enable regeneration and restitution of barrier function.

Central to repair is the ability for the urothelium to sense damage; a process hypothesised to involve cell-cell communication. Direct cell-cell communication occurs through gap junctions, channels comprising connexin (Cx) proteins which allow for the passage of signalling molecules. Cxs have been linked to wound healing, as well as to maintenance of polarity and homeostasis in other epithelia, by both communication-dependent and -independent mechanisms. A systematic characterisation of Cx expression has not been performed in urothelium and the significance of specific Cxs to urothelial physiology is not understood.

This study aimed to investigate whether specific Cx proteins contribute to the regulation of barrier maintenance and restitution in human urothelium. Analysis of Cx transcripts identified Cx32, which was expressed *in situ* and highly induced upon *in vitro* differentiation of normal human urothelial (NHU) cells using two independent methods. In differentiated NHU cells, Cx32 proteins assembled into functional gap junction channels at cell borders, co-localising with the barrier-defining tight junction proteins occludin and ZO-2. shRNA studies demonstrated that normal tight junction development and barrier function were dependent on the presence of intercellular Cx32, but not gap junction communication.

In wound-healing experiments, intercellular communication through Cx32 channels inhibited urothelial cell migration and proliferation, in a process which involved suppression of activated SMAD3. Together the evidence presented here supports an unanticipated central role for Cx32 in orchestrating the homeostasis between barrier function and repair in human urothelium.

Table of Contents

List of Figures

List of Tables

Acknowledgements

I would like to thank the following people for their contributions in helping me achieve this research;

I am fully indebted to my supervisor, Professor Jenny Southgate; foremost for giving me the opportunity to achieve, but also for her patience, encouragement, enthusiastic conversations and infuriating attention to detail!

I would like to thank York Against Cancer, for their generous funding and continued support throughout my project.

I am extremely grateful to the clinicians for the supply of surgical specimens used in this study.

I would like to say thank you to Dr Paul Genever and Professor Henry Leese for their ideas and stimulating conversations in my training meetings. Also to Meg Stark for her help with the TEM work and Celina Whalley and Dr. Naveed Aziz from the Technology Facility for their help with all things genomic.

To all of my friends and fantastic colleagues in the Jack Birch Unit, with special thanks to Dr Lisa Kirkwood and Dr Nik Georgopoulos for guiding me with expert molecular biology knowledge.

To my dad, for his encouragement when I was writing and to my gorgeous baby daughter Izzy, whose arrival gave me a much needed early deadline.

My final thank you is to Simon Baker for his endless support as a colleague, friend and husband. For his motivational, but frank words when I felt sluggish and for maintaining his sense of humour when I'd lost mine.

Authors Declaration

The candidate confirms that all work submitted is her own and that appropriate credit has been given where reference has been made to the work of others.

The candidate confirms that this work has not been submitted for academic qualification at this or any other institution.

J. Hinley

July 2015

1. Introduction

1.1 The Urothelium

1.1.1 The Urinary System

The urinary system in man comprises the kidneys, ureters, bladder and urethra. The kidneys function to filter waste products and surplus water from the blood stream, thereby producing urine which drains into the bladder via the ureters, before expulsion via the urethra. The primary function of the urinary bladder is to contain urine at low pressure whilst accommodating large fluctuations in volume, to spare renal damage due to reflux. The kidneys and ureters are derived from intermediate mesoderm, whilst the bladder and urethra develop from the endodermally-derived urogenital sinus, prior to the 10th week of gestation (McHugo et al. 2001).

Despite their different histogenesis, all portions of the urinary tract from the renal pelvis to the proximal urethra are lined by a common epithelium known as urothelium, which acts as a barrier to urine.

1.1.2 Morphology and key features of the urothelium

The thickness of human urothelium can vary from 2-7 cells depending on the degree of bladder distension. A distinct three-layered morphology is apparent with distinct levels of specialisation (or differentiation). The urothelium is separated from the suburothelial lamina propria by a basement membrane. Adjoining the basement membrane are a single layer of small cuboidal basal cells, which sit beneath 1-5 layers of larger polygonal intermediate cells. On the most superficial surface (luminal surface) are a single layer of large, flattened superficial cells (Fig 1.1), the apical surface of which are lumen-facing and therefore interface directly with urine. The urothelium is described as a transitional epithelium since it

contains features in common with both columnar and stratified squamous epithelia.

The superficial cells (often descriptively called umbrella cells) are commonly binucleate. Their apical surface is covered with a layer of rigid hexagonal plaques of asymmetric unit membrane (AUM), composed of proteins restricted to the urothelium known as uroplakins. Uroplakin proteins in mammals are highly conserved and are considered to be the culminating feature of urothelial cell differentiation (Wu et al. 1994). Another key feature of urothelium is that it is mitotically-quiescent with a turnover rate of approximately 200 days (Walker 1960). However, in response to insult or injury the urothrelium has an exceptionally high capacity for regeneration (Hicks 1975).

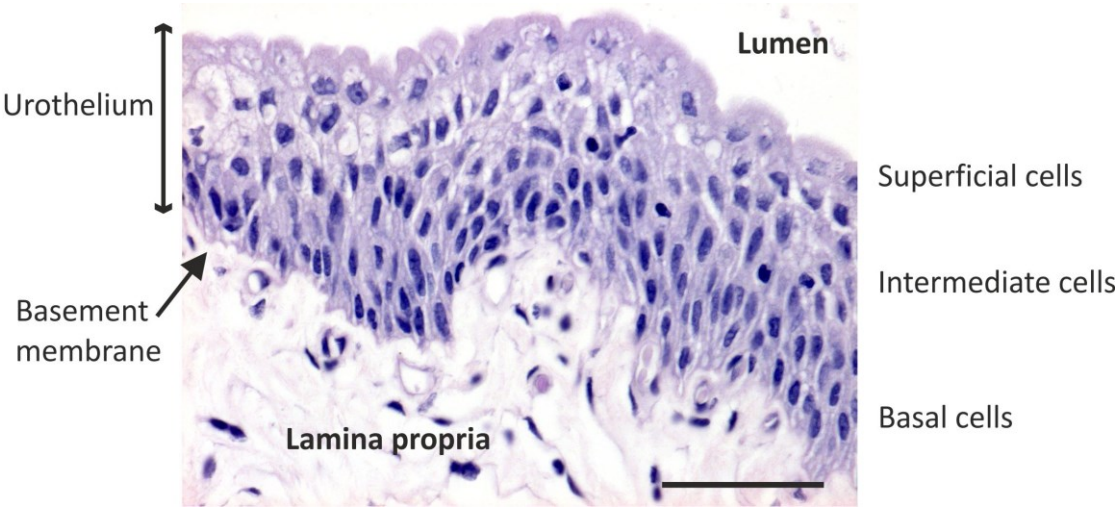

Figure 1.1 Haematoxylin and Eosin stain of normal human ureteric urothelium.

Scale bar = 50µM

1.1.3 Physiological function of the urothelium

The major function of the urothelium is to act as a barrier to urine and it is thought to be the tightest, most impermeable epithelium in the human body. The highest recorded transepithelial electrical resistance (TER) was found to be in the urinary bladder (Lewis et al. 1982, Negrete et al. 1996) and this is thought to be the result of a complex network of interlocking tight junctions.

To maintain barrier function, the urothelium has a remarkable ability to repair damage and urothelial cells are able to rapidly migrate in a coordinated manner to repair damage (Rebel et al. 1994, Shabir et al. 2008). The urothelium is able to flatten and stretch to accommodate large changes in surface area, a feature supported by uroplakin-containing fusiform vesicles in the superficial cells, which insert AUM into the luminal surface to stabilise the apical membrane, reviewed in (Khandelwal et al. 2009).

Whilst barrier function is the primary function of urothelium, it is also well documented that the urothelium is implicated in several mechanosensory functions. Urothelial distension and pressure changes acting upon superficial cells invoke the release of ATP, which has been closely linked to the activation of afferent nerve signalling in the lamina propria and purinergic receptor subtypes are expressed in the urothelium (Ferguson et al. 1997, Vlaskovska et al. 2001, Shabir et al. 2013). Whilst ATP plays an important role in chemical communication within the bladder, other signalling molecules including the ATP break-down product adenosine and nitric oxide have been suggested to have chemical-signalling roles in the urothelium, reviewed in (Winder et al. 2014)

1.1.4 Urothelial Pathologies

Bladder malignancy is the 7th most common cancer in the UK and the 4th most common cancer in men, with most people diagnosed between the ages of 50 and 80 (Cancer Research UK). Transitional Cell Carcinoma (TCC) accounts for approximately 90% of bladder malignancies and is thought to be associated with prolonged exposure of the urothelium to urine-derived carcinogens.

Urinary Tract Infections (UTI) affect more than half of women during their lifetime and are generally caused by uropathogenic *E.coli* (UPEC) bacteria. Interstitial cystitis (IC) is a chronic and painful bladder inflammatory disorder with similar symptoms to UTI, but in the absence of infection. IC mostly affects women, for which a single causal mechanism is unknown; however several studies have implicated a defective urinary barrier (Slobodov et al. 2004, Southgate et al. 2007, Liu et al. 2012).

1.1.5 Urothelial Differentiation

Several groups of proteins are identified as markers of urothelial cytodifferentiation; these include transcription factors which are activated in response to urothelial differentiation cues and drive expression of the programme of genes which contribute to urothelial physiology. Those whose expression is restricted to the superficial cell layer have often been described as markers of terminal differentiation, since this cell layer contains a number of specialist molecular features which are crucial to urinary barrier function, such as uroplakins and tight junction proteins.

1.1.5.1 Uroplakins

Uroplakins are a group of integral membrane proteins which make up the Asymmetric Unit Membrane (AUM) covering the apical surface of much of the

urothelium. The AUM is a hallmark of urothelial differentiation and provides a barrier to the transcellular movement of water and solutes across the apical membrane (Hu et al. 2002). There are five uroplakin proteins, UPK1a, UPK1b, UPK2, UPK3a and UPK3b arranged as 16 nm hexagonal plaques, which were first isolated from bovine bladders (Wu et al. 1990). Deletion of the UPK3a gene results in major changes to urothelial physiology including an increase in transcellular permeability (Hu et al. 2002).

1.1.5.2 Cytokeratins

Cytokeratins (CKs) are intermediate filament proteins found in the cytoskeleton of epithelial cells. The specific cytokeratin profile expressed is a distinguishing feature of epithelial tissue type and differentiation status and in some cases can act as a predictive tool for tumour prognosis. For example in normal urothelium, CK20 expression is confined to the superficial cell layer. Retention of a normal CK20 immunolabelling pattern was found to be predictive of tumour non-recurrence over a 5 year period, whilst full-thickness expression of CK20 was found to be associated with recurrence (Harnden et al. 1995).

Normal urothelial cells *in situ* express a profile of cytokeratins characteristic of both "simple" and stratified epithelia. CK7, CK8, CK18 and CK19 are expressed throughout the urothelium. CK13 is expressed in all but the superficial cell layer, CK17 and CK5 are basally expressed and CK20 is expressed by superficial cells (Southgate et al. 1999).

1.1.5.3 Transcription Factors

Several transcription factors have been identified as key regulators of urothelial cytodifferentiation. One of these is the ligand-activated nuclear receptor PPARγ (Peroxisome Proliferator-activated receptor gamma), which is a key regulator of

adipocyte differentiation. When bound to its heterodimer partner retinoid x receptor α (RXRα), PPARγ binds to specific promoter elements known as peroxisome proliferator response elements (PPREs) in target genes (Blanquart et al. 2003). PPRE binding of the heterodimer induces gene expression of downstream intermediate transcription factors such as FOXA1 and IRF-1 (Varley et al. 2009), which then act downstream to drive the terminal differentiation of human urothelial cells including expression of the uroplakin genes (Varley et al. 2004a, Varley et al. 2004b). The epithelium-specific Ets domain transcription factor ELF3 has also been implicated to promote urothelial cytodifferentiation in a manner which is PPARγ-dependent (Böck et al. 2014). This study also demonstrated that knock-down of ELF3 in urothelial cultures disrupted the expression of FOXA1, as well as another transcription factor which is thought to be essential for the development of the superficial cell layer in mice, GRHL3 (Yu et al. 2009). Whilst the sequence of events surrounding transcriptional factor activation has yet to be fully established for human urothelium, it has been proposed that the transcription factor KLF-5 may play a major regulatory role in the urothelial cytodifferentiation programme (Bell et al. 2011). This study in mice suggests that KLF-5 may function upstream of PPARγ, in the transcription factor hierarchy required for urothelial maturation.

1.1.5.4 Other significant markers of urothelial differentiation

Aquaporins (AQPs) are a group of proteins which selectively allow passage of water down an osmotic gradient (as well as some small neutrally charged solutes). The presence of these water channels in human urothelium has been characterised (Rubenwolf et al. 2009) and provides a basis to support previous work which suggested that the urothelium of some mammalian species is capable of reabsorption in order to modify urine concentration (Negrete et al. 1996). Of particular interest was AQP3, which is thought to be associated with a differentiated urothelial phenotype (Spector et al. 2002, Rubenwolf et al. 2009).

Unpublished data from our laboratory indicates that expression of AQP3 is driven by PPARγ.

Tight junction proteins provide barrier function to the urothelium and are another key set of proteins which are regulated during differentiation to produce a mature, functional urothelium. Their contribution to urothelial physiology is discussed in further detail in section 1.2.3.

1.1.6 Urothelial Cells in vitro

Isolation and subculture of human urothelial cells has proved to be an indispensable tool for studying the cell biology of human urothelial cells. Normal human urothelial (NHU) cells can be isolated from patient biopsies of bladder, ureter or renal pelvis tissue (Southgate et al. 1994). In this method, tissues are placed into a calcium-chelating or "stripping" solution in order to dissociate the urothelial cell layer from the basement membrane. Intact sheets of urothelium are then disaggregated by incubation in collagenase before seeding onto an appropriate substrate for culture in low calcium (0.09 mM) keratinocyte serum-free medium (KSFM) supplemented with recombinant human epidermal growth factor, bovine pituitary extract and cholera toxin which has been demonstrated to improve NHU cell attachment in culture (Southgate et al. 1994). The supplemented KSFM is referred to as KSFMc.

1.1.6.1 Phenotype of normal human urothelial cells in vitro

Upon seeding into primary culture, the differentiated phenotype of NHU cells is rapidly lost in low calcium serum-free growth conditions, whereby the normally quiescent cells adopt a highly migratory and proliferative phenotype, with a population doubling time of approximately 24 hours (Southgate et al. 1994). NHU

cells have a finite lifespan in culture, with senescence normally occurring between 6-12 passages.

In vitro, NHU cells lose markers associated with normal urothelial cell specialisation, such as most uroplakins (with the exception of UP1b), CK20, CK13 and tight junction proteins and show increased expression of CK14 and CK16, indicative of a change to a squamous phenotype (Southgate et al. 1994, Lobban et al. 1998, Varley et al. 2004b). NHU cells do not spontaneously stratify or differentiate upon confluence, but instead grow as monolayer cultures and exhibit reversible contact inhibition of growth as confluence is reached (Southgate et al. 1994). They do however continue to express some markers associated with a basal/intermediate phenotype such as CK7, CK8, CK17, CK18 and CK19.

1.1.6.2 Proliferation of normal human urothelial cells in culture

In low-calcium, serum-free medium, NHU cells display a high growth rate for at least 6 passages before showing signs of senescence. *In vitro* NHU cell growth occurs through autocrine activation of epidermal growth factor receptor (EGFR) signalling (Varley et al. 2005).

1.1.6.3 Stratification of normal human urothelial cells in vitro

NHU cultures can be induced to form a stratified epithelium by adapting the concentration of calcium in the growth medium to near physiological levels (2 mM). This is associated with formation of desmosomes, adherens junctions and the formation of primitive tight junctions, but not cytodifferentiation (Southgate et al. 1994, Southgate et al. 1995). The barrier function as measured by TER remains non-functional in stratified cultures (Cross et al. 2005)

1.1.6.4 Cytodifferentiation of normal human urothelial cells in vitro

Although NHU cells propagated in serum-free low calcium conditions do not exhibit a differentiated phenotype, they can be induced to differentiate in the presence of differentiation cues, irrespective of the urothelial layer the original culture was derived from (basal, intermediate or superficial cells) (Scriven et al. 1997, Wezel et al. 2014).

Cytodifferentiation of NHU cells can be achieved *in vitro*. Studies within the scope of this thesis will focus on two experimental culture systems which have been well characterised. The first (termed "TZ/PD") is an experimental system which involves pharmacologically-driven urothelial cytodifferentiation by activation of the nuclear receptor PPARγ, using the thiazolidinedione compound troglitazone (TZ). With concurrent inhibition of EGFR signalling (using the EGF receptor tyrosine kinase inhibitor PD153035), TZ is highly effective at initiating the urothelial gene expression programme in NHU cultures and results in increased expression of uroplakins, CK13 and tight junction proteins (as well as intermediate transcription factors known to be involved in urothelial differentiation such as FOXA1 and IRF-1) and a loss of CK14 (Varley et al. 2004a, Varley et al. 2006, Varley et al. 2009, Böck et al. 2014). However the TZ-treated cultures fail to stratify and produce a barrier epithelium and differentiation appears to occur on a cellular level rather than producing an integrated functional epithelium. The second method relies on the culture of NHU cells in bovine serum with near physiological concentrations of calcium (termed "ABS/Ca^{2+}"). These cultures express markers associated with terminal differentiation, as with the TZ/PD model, however they also self-organise into a multi-layered urothelium with a functional barrier as demonstrated by high TER values of >3000 Ω.cm^2 (Cross et al. 2005). Whilst the ABS/Ca^{2+} method appears to provide the closest approximation to urothelium in a culture model, the specific details surrounding the reprogramming of NHU cells into a differentiated phenotype are undefined and the specific factors within serum responsible for activating differentiation-promoting transcription factors remain to be determined.

However it seems likely that PPARγ-activation alone is not sufficient to promote tissue organisation and that there may be many factors in serum, such as fatty acids and retinoids, which drive other pathways crucial to urothelial tissue development. A diagram which summarises both methods can be found in chapter 2 (Fig 2.1).

1.2 Cell-cell interactions

Cell-cell interactions are essential for the normal function of cells in most tissues of an organism. In epithelial tissues, cell-cell connectivity is maintained by complexes which form the intercellular junctions; desmosomes, adherens junctions, tight junctions and gap junctions. Desmosomes and adherens junctions provide mechanical strength to epithelial cell contacts. Tight junctions act to control the selective paracellular permeability of the epithelial layer to solutes and ions, whilst gap junctions act to enable cell-cell communication by allowing the passage of signalling molecules between cells. A summary of cell-cell junctions is shown in figure 1.2.

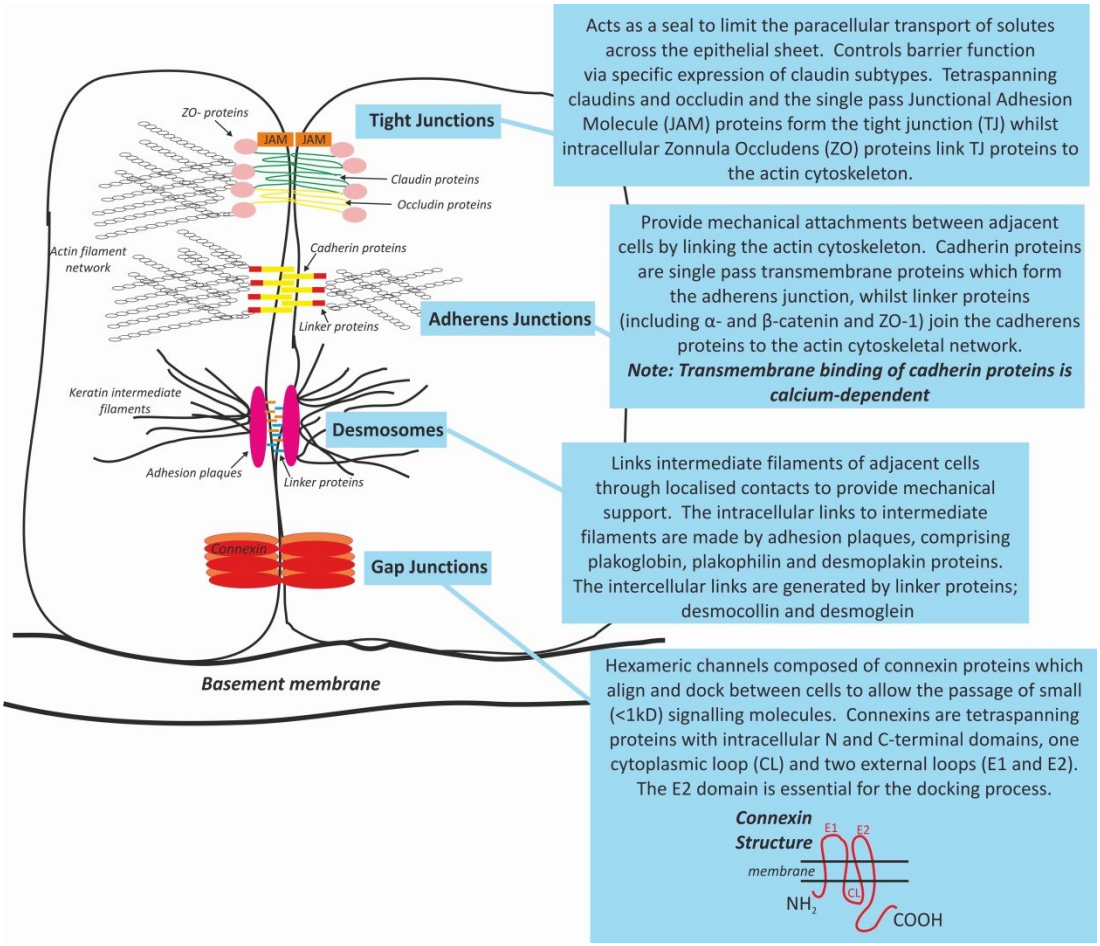

Figure 1.2 Simplified Overview of cell-cell junctions found in typical polarized epithelia.

Four major cell junctional subtypes are illustrated in the order in which these structures would normally be organised in epithelia. The tight junctions are localised to the most apical aspect of the cell-cell junction.

1.2.1 Desmosomes

Desmosomes are strongly adhesive intercellular junctions which allow stratified and differentiated tissues to resist mechanical stress. They contain heterotypic transmembrane proteins and provide mechanical strength by linking the intermediate filament cytoskeleton of adjacent cells at defined spots along the lateral membrane. Their adhesive properties are thought to be dynamic, for example during embryonic development and tissue repair, desmosomal adhesiveness is thought to be of lower affinity, with evidence suggesting that this occurs under the control of protein kinase C (Wallis et al. 2000, Kimura et al. 2007). Desmosomes are comprised of desmoplakin (links the intermediate filaments to the desmosomal adhesion plaque), plakoglobin and plakophilin (which form the desmosomal adhesion plaque) and the desmosomal cadherins, desmocollin and desmoglein (which span the membrane regions), reviewed in (Garrod et al. 2008).

1.2.2 Adherens Junctions

Adherens junctions are cell junctions which (like desmosomes) provide mechanical support to tissues to enable movement of cells in a coordinated manner. Adherens junctions are composed of single pass transmembrane cadherin proteins which homodimerise with cadherins on adjacent cells in a calcium-dependent manner, reviewed in (Meng et al. 2009). The cytoplasmic portion of cadherin proteins interacts with linker proteins including α- and β-catenin and ZO-1 to facilitate actin cytoskeletal binding.

1.2.3 Tight Junctions

1.2.3.1 Function of Tight Junctions

The tight junction (TJ) in epithelia is found at the apical-most region of contact between two cell membranes and serves to provide barrier function to restrict passage of solutes and ions. The TJ's pull together cell membranes on adjacent cells

such that the intercellular space appears to be non-existent on electron micrographs (Farquhar et al. 1963). The TJ serves two major roles, the first, to restrict the paracellular transport of substances across an epithelium providing a barrier or "gate" function, although more recent studies suggest that the tight junction functions to establish a permeability barrier which "limits" rather than prevents paracellular permeation (Angelow et al. 2006). Secondly, TJs function to prevent the free-movement of proteins between the apical and basolateral membrane domains of a cell, thereby establishing polarity and providing what is described as a "fence" function.

Measurement of the TER across different epithelia has demonstrated variability between epithelia, with the highest recorded barrier function of any tissue observed in the urinary bladder (Negrete et al. 1996, Anderson et al. 2009). Whilst it is known that the AUM prevents transcellular permeability of urine across the urothelium, this does not contribute to the high TER observed (Hu et al. 2002). The value of the TER is reflected by the resistance of the tight junction.

Epithelia which display a TER of >500 Ω.cm2 are considered "tight", whereas a TER of below 500 $\Omega.cm^2$ is considered "leaky" (Fromter et al. 1972). The protein components which make up the tight junction are thought to dictate permeability properties.

1.2.3.2 Tight Junction Proteins

Tight junctions have a complex molecular organisation, composed of members of the claudin family, of which there are 24 genes in man, along with occludin, junctional adhesion molecule (JAM) 1, 2 and 3 and the PDZ-containing zonula occludens (ZO) proteins (ZO-1, 2 and 3). Claudins are tetraspanning membrane proteins (with two extracellular loops and intracellular N- and C-terminal domains), which form oligomeric strands. The claudins form the "sealing strands" of the tight junction, pulling together the adjacent membranes which link to the cytoskeleton to create a contractile phenotype. It is believed that the external loop domains

determine the barrier properties afforded by each claudin (Mrsny et al. 2008). The ZO proteins serve to link the claudin proteins to the cytoskeleton and play a critical role in the spatiotemporal organisation of claudins at TJ strands (Umeda et al. 2006). The claudins are thought to be the barrier-defining components of TJs by regulating permselectivity and have been shown to be crucial for the barrier function of mammalian skin (Furuse et al. 2002). It is believed that tissue-specific expression of claudins is important in defining overall tight junction barrier properties and whilst the ZO proteins are required for tight junction stability, they do not play a role in limiting paracellular movement of solutes (Van Itallie et al. 2009, Rosenthal et al. 2010). Claudin 2 is often associated with "leaky" water-transporting epithelia such as found in the proximal tubule of the kidney and a recent study has demonstrated that claudin 2 forms a paracellular water channel (Rosenthal et al. 2010), whilst claudin 3 has been proposed as a sealing component of the TJ. Claudin 3 overexpression has been shown to be associated associated with increased barrier function and reduced permeability in MDCK cells (Milatz et al. 2010).

1.2.3.3 Urothelial Tight Junctions

The development of mature tight junction complexes is of vital importance to urothelial tissue function. Differentiation of NHU cells *in vitro* (using the TZ/PD model described in section 1.1.6.4) and *in situ* studies, have revealed that claudins 3, 4, 5 and 7, as well as occludin and ZO-1 are differentiation-associated (Varley et al. 2006), whilst claudin 1 was downregulated in response to NHU cell differentiation and claudin 6 was absent. The same study demonstrated that NHU stratification (by increasing exogenous calcium to near a near physiological concentration of 2 mM), resulted in an upregulated expression of both occludin and ZO-1 proteins, but not claudins 4, 5 or 7. Another study in immortalised ureteric-derived human urothelial cells cultured in calcium and bovine serum demonstrated the presence of occludin, JAM-1 and ZO-1, 2 and 3 at cell margins (Rickard et al. 2008).

Inspection of TJ protein distribution in urothelial tissue sections revealed that claudin 3 and ZO-1 displayed a restricted expression pattern, between the points of membrane contact at the apical-most aspect of superficial cells (Varley et al. 2006). A detailed analysis of claudin 3 and ZO-1 isoforms in differentiated NHU cells (using the ABS/Ca^{2+} model), demonstrated that claudin 3 is an essential component of the urothelial TJ and is required for barrier development, as well as identifying a "switch" in ZO-1 splice variant expression during differentiation, from ZO-1α^- to the longer ZO-1α^+ isoform (Smith NJ et al. 2015). Interestingly, forced expression of claudin 3 was not enough to induce barrier formation in non-differentiated NHU cells, thus highlighting a more complex interaction of proteins at the TJ is required for barrier function. The individual contribution of other urothelial-associated claudins such as claudins 4 and 5 to barrier function is yet to be studied.

1.2.4 Gap Junctions

In multicellular organisms cell-cell communication within tissues is crucial to enable a community of cells to behave as a tissue, coordinating wound repair and homeostasis. Whilst paracrine signalling permits limited local communication, the results are relatively slow and short-lived when compared with direct cell-cell communication via gap junction (GJ) channels. Gap junctions are the primary means by which cells can directly connect and communicate with one another.

1.2.4.1 Gap Junction Proteins

GJs are composed of connexin (Cx) proteins, six of which combine to form a hemi-channel or connexon which are inserted into the cell membrane. Alignment of two connexons in adjacent cells provides a continuous hydrophilic pore approximately 6-7 Å in radius (Unger et al. 1999) connecting the two cell interiors and permitting the passage of signalling molecules. More recently, three additional

communicating junction proteins known as Pannexins have been identified, however their major function is believed to be as single membrane channels, rather than for direct cell-cell communication (Penuela et al. 2013).

Cxs are a multigene family of tetraspanning proteins with intracellular amino and carboxy groups. Approximately twenty members have been identified in the human genome with cell-type regulated expression. It is common for many connexin family members to be expressed by a single cell type and it unclear whether this is for selectivity purposes or if connexins have overlapping redundant functions.

Cxs are commonly named after their molecular weight (e.g the connexin protein with a molecular weight of 43kD is known as Cx43); however this has proven confusing when comparing Cxs between species, due to modifications in molecular mass. Therefore, gene names are commonly sorted into two major evolutionary subclasses, the α and β forms (GJA and GJB respectively) and minor C, D and E groupings, followed by a number e.g. The gene name for Cx43 is GJA1 (Kumar et al. 1992).

1.2.4.2 The Function of Gap Junctions

GJ channels are dynamic and can flip between open and closed states to mediate the diffusion of small molecules and ions with low molecular mass (generally less than 1kD), including Ca^{2+}, amino acids, nucleotides and the intracellular mediators ATP, cyclic AMP (cAMP) and inositol 1,4,5-triphosphate (IP3), thus providing a mechanism for the movement of molecular information between cells. Intercellular communication via gap junctions has been shown to be critical to many physiological processes such as electrical coupling (Saffitz et al. 2007), embryonic development (Fleming et al. 2000, Eckert et al. 2005), differentiation (Piechocki et al. 2000), apoptosis (Kameritsch et al. 2013) and tissue homeostasis (Li et al. 2010, Scott et al. 2012).

Cxs are known to combine in both homomeric & heteromeric gap junction channels allowing for a further level of control in channel stoichiometry and therefore

selectivity. For example, in murine mammary gland development heteromeric Cx26-Cx32 channels were found to be selectively permeable to cAMP, cGMP and IP_3, but homomeric channels were not (Locke et al. 2004).

1.2.4.3 Connexins and Disease

Insight into the functional roles of Cxs has been revealed by studying a number of human diseases which are caused by mutations or dysregulation in Cx genes. In some cases loss or mutation in a single connexin can result in disease or abnormal development, for example site-specific mutations in Cx26 result in keratitis ichthyosis deafness syndrome (Richard et al. 2002). Additionally Cxs 26 and 30 were ranked among the most upregulated genes in psoriatic lesions when compared to normal skin, even though keratinocytes are known to express at least ten members of the connexin family (Martin et al. 2015), suggesting that Cx26 and Cx30 play crucial and unique functions in human skin (Li et al. 2014). It has been demonstrated that Cx43 plays a role in wound healing of the skin and abnormal Cx43 expression has been linked to the poor rate of skin healing in diabetic chronic wounds (Becker et al. 2012).

Charcot-Marie-Tooth disease is a heterogeneous neuro-genetic disorder, affecting peripheral motor and sensory nerves. It is one of the most common peripheral neuropathies presenting a phenotype which involves distal limb muscle wasting and sensory loss, becoming progressively worse over time. The X-linked form of Charcot-Marie-Tooth disease (CMT1X) is one of the most widely recognised disease states occurring as a result of a Cx defect. Over 400 germline mutations in Cx32 have been described (http://www.molgen.ua.ac.be/cmtmutations/Mutations), spanning the entire coding region resulting in partial or total loss of channel function (Patel et al. 1994, Scherer et al. 1999, Kleopa 2011), as well as in the nerve-specific 5' UTR which prohibits Cx32 expression (Murphy et al. 2011). Several CMT1X patients (both male and female) have been reported with deletions in the entire GJB1 coding sequence (Gonzaga-Jauregui et al. 2010), demonstrating that

loss of Cx32 is not embryonic lethal. This finding is also supported by the study of Cx32 knock-out mice, which have an extremely dysfunctional physiology with peripheral neuropathies consistent with human CMTX disease (Nelles et al. 1996, Scherer et al. 1998), but are not embryonic lethal. Although many cell types express Cx32, peripheral neuropathy appears to be the major clinical manifestation of mutations or loss of GJB1 and in light of the current study it should be noted that urinary tract defects do not appear to occur in these patients. Interestingly, nor has an increase in tumour incidence been reported in these patients, although Cx32 knock-out mice show increased susceptibility to hepatocarcinogenesis (Temme et al. 1997). There is clear potential for partial functional redundancy in many tissues due to co-expression of other connexins which may explain these findings. It is also unlikely that the wide range of mutations observed in CMTX patients is reflective of a complete Cx32 knock-out and the number of reported CMTX cases where Cx32 is deleted is likely too few for an increased incidence of cancers to be detectable (Gonzaga-Jauregui et al. 2010).

There is substantial evidence both *in vitro* using cancer cell line models, as well *in vivo* to support a role for Cxs in tumour suppression (Trosko et al. 1998). For example lack of Cx43 has been associated with breast tumours (Laird et al. 1999) and Cx32 knock-out mice show an increased incidence of hepatocarcinogenesis (Temme et al. 1997), although some findings suggest that some of the tumour suppressive effects of Cxs can be independent of gap junction formation and therefore communication (Moorby et al. 2001).

1.2.4.4 Connexin Biosynthesis and Turnover

Cxs are generally believed to have a very short half-life of approximately four hours and as a result cells are believed to be constantly cycling in Cx biosynthesis and degradation, however some Cxs have been demonstrated to develop more stable gap junction pools (Berthoud et al. 1999). Rapid turnover of gap junctions is thought to promote the dynamic regulation of gap junctional communication and turnover rates have been demonstrated to vary according to Cx type and extracellular pH (Yamaguchi et al. 2003, Berthoud et al. 2004).

Cx43 is the most ubiquitously expressed vertebrate gap junction protein and as a result its life cycle has been studied intensively. Cx43 proteins have been demonstrated to form connexon hemi-channels after exiting the ER in the trans-Golgi network, which then move in vesicles for insertion into the plasma membrane and docking with compatible connexons on adjacent cells (Fig 1.3). The second extracellular loop domain (E2) of connexins has been demonstrated to be essential for docking selectivity and the formation of functional gap junction channels (White et al. 1994, Gong et al. 2013).

It is interesting to note that intracellular connexons are maintained as closed channels until insertion in the membrane, which is thought to prevent any biochemical unbalance from small molecular messengers entering the Golgi. For the same reason, it was originally believed that connexons would remain closed once inserted into the plasma membrane, until docking with a connexon on an adjacent cell. However, an increasing body of research supports a role for the restricted opening of unpaired hemichannels, providing possible paracrine signalling pathways for ions such as Ca^{2+} and ATP (Leybaert et al. 2003, Saez et al. 2005, Evans et al. 2006). In addition it has been demonstrated that under specific conditions of stress such as ischaemia, hypoxia (Clarke et al. 2009), or osmotic stress (Quist et al. 2000), hemichannels may be induced to open, releasing small molecules and ions.

Phosphorylation via mitogen-activated protein kinase activation is thought to play a key role in regulating assembly and function of Cx43 containing gap junctions, (Solan et al. 2007), including hemichannel functions (John et al. 2003). The phosphorylation status of Cx43 can be observed by shifts in band mobility by gel electrophoresis and at least three phosphoforms have been identified: P0, P1 and P2, which can be attributed to key stages in the Cx43 life cycle; P0 being unphosphorylated and present mainly in the trans-Golgi network, P1 being phosphorylated and associated with Cx43 trafficking to the membrane and P2 being heavily phosphorylated and present in functional gap junctions (Solan et al. 2007, Sosinsky et al. 2007). It has been reported that specific phosphorylation of Cx43 by

epidermal growth factor may result in degradation of gap junctions (Leithe et al. 2004). However, whilst phosphorylation may be a prerequisite for degradation of some Cxs, not all require phosphorylation for degradation, which can occur via both proteosomal and lysosomal mechanisms (Berthoud et al. 2004, Laird 2005, Falk et al. 2014) (Fig 1.3).

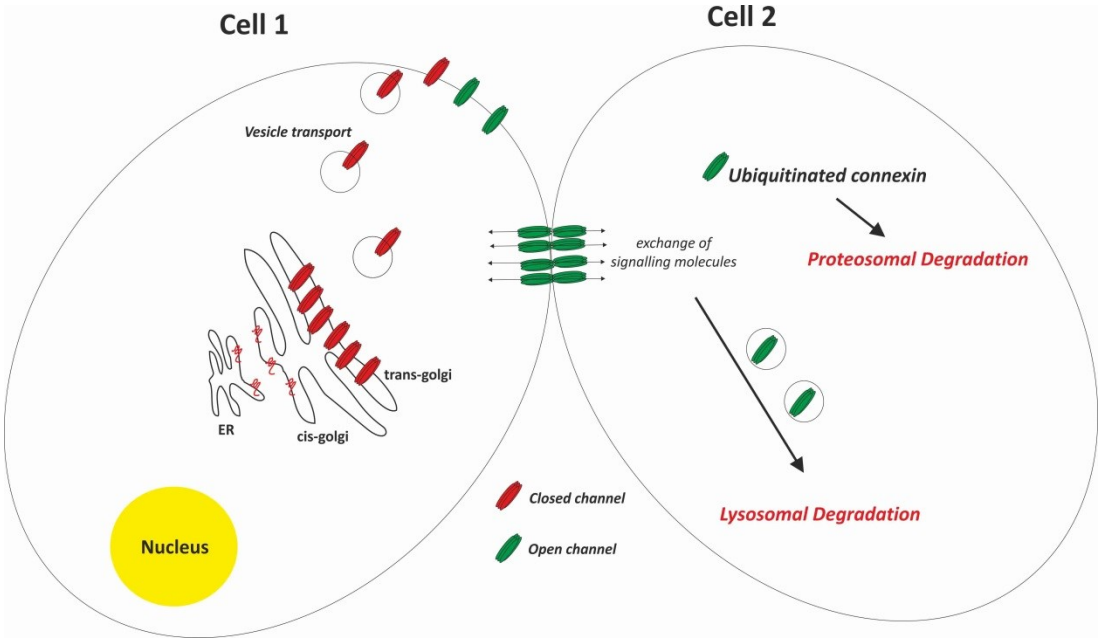

Figure 1.3 Lifecycle of connexins

1.2.4.5 Permselectivity of Gap Junction Channels

The diverse expression patterns of connexins in different tissues may be due to functional differences, with evidence suggesting that gap junctions demonstrate selective permeability for different second messengers and metabolites, based on their connexin composition. In HeLa cells, the G-protein-activated second messenger inositol 1,4,5-triphosphate (IP3), which is known to bind to membrane receptors in the endoplasmic reticulum to promote release of intracellular calcium, has been demonstrated to be more efficient at passing through channels composed of Cx32, than Cx26 (4-fold more efficient) and Cx43 (2.5 fold more efficient)

(Niessen et al. 2000). cAMP demonstrates preferential passage through Cx43 channels, rather than Cx26, Cx32, Cx36, Cx45 and Cx47, which all demonstrate low cAMP permeability in transfected HeLa cells (Bedner et al. 2006). In a layered culture system, transfer of radiolabelled metabolites from donor cells to receiver cells demonstrated a preference for AMP (8-fold), ADP (8-fold) and ATP (300-fold) to pass through Cx43 channels rather than Cx32, however adenosine passed through Cx32 channels 12-fold better than Cx43 channels (Goldberg et al. 2002), suggesting that addition of phosphate groups to adenosine can switch the relative permeability of this messenger molecule. It is clear that different connexins are not simply selective for passage of a single messenger from cell-to-cell, rather they offer passage of signalling molecules with selective efficiency and transfer rates, often based on charge and size (Kanaporis et al. 2011).

1.2.4.6 Connexin Interacting Proteins

It has now been widely demonstrated that connexins have a wide range of functions beyond their role as a communication channel, involving interactions with other proteins at junctional complexes, sometimes referred to as the "junctional nexus" (Duffy et al. 2002). It has been proposed that connexins can form the centre of a "junctional nexus". Cx32 and Cx43 have been demonstrated to influence the expression of over 300 genes, including transcription factors (Iacobas et al. 2007), suggesting that the role of connexins may extend beyond GJIC with influences major regulatory influences on gene transcription.

In addition to influences on gene expression, connexins participate in a huge number of protein-protein interactions. In the same way that tight junctions have been demonstrated to be positioned within the cell membrane anchored to the cytoskeleton, so too have GJ proteins, with several Cxs including Cx30, Cx31.9, Cx32, Cx43 and Cx45 reported to bind to the PDZ domain of ZO-1, thereby stabilising the GJ to the cytoskeleton, reviewed (Herve et al. 2012).

The majority of the literature regarding Cx interactions surrounds Cx43, since it is the most widely expressed connexin and is reported to interact with many proteins including P2 purinergic receptors (Fortes et al. 2004), N-Cadherin (Wei et al. 2005) , β-catenin (Ai et al. 2000), the tight junction proteins claudin 5 (Nagasawa et al. 2006) and ZO-1 (Toyofuku et al. 1998) and calmodulin (Zhou et al. 2007). Due to the close relationship between gap and tight junctional proteins it has been suggested that connexins may play a role in regulating expression of tight junction proteins (Koizumi et al. 2007), but the mechanism by which this occurs has not been identified and it is not clear whether gap junction intercellular communication (GJIC) is critical to tight junction assembly, reviewed in (Dbouk et al. 2009). It does however seem plausible that some connexins may have a secondary role to function within multi-protein complexes for regulation of cell polarity, with influence on the assembly or maintenance of other intercellular junctions, in particular tight junctions.

Interactions between gap junctions and other proteins can be influenced by post-translational modification. Most of the literature surrounding connexin post-translational modifications surrounds Cx43, with at least 14 documented phosphorylation sites at serine or tyrosine residues present in the C-terminal tail (Lampe et al. 2004). Cx32 has been demonstrated to be phosphorylated by PKA, PKC (Elvira et al. 1993), Ca^{2+}/calmodulin-dependent kinase II (Saez et al. 1990) and EGFR (Diez et al. 1998). Connexin phosphorylation events appear to mostly occur in the C-terminal tail with implications on channel gating (including channel closure mediated by a ball and chain mechanism), connexin proteolysis and influence on potential binding partners. For example phosphorylation of Cx43 by Akt can influence its interactions with other proteins (Park et al. 2007).

1.2.4.7 Connexin Expression in the Bladder

There are few studies reporting connexin expression in the bladder. However, the expression of Cx43 has been demonstrated in the lamina propria in a sub-group of cells known as suburothelial myofibroblasts (Fry et al. 2007).

There are a few studies linking connexin expression with urothelial carcinoma, for example high levels of Cx43 expression have been associated with poor prognosis of muscle invasive bladder tumours (Poyet et al. 2015). An immunohistochemical study found that decreased expression of Cx26 was observed in bladder tumours (Gee et al. 2003). Another report which combined experimental and publicly available microarray datasets, from bladder tumours and normal control tissues, identified GJB1 (Cx32) as being one of the most downregulated genes in bladder tumour samples (Zaravinos et al. 2011). Some caution must be taken with interpretation of such data, since bladder tumours collected for microarray analysis can contain varying populations of urothelium, stroma and underlying muscle/fat tissue, therefore linking changes in expression to specific cell types can prove problematic. There are no studies to date reporting the normal expression profile and physiological significance of connexins in human urothelium. At present, there are no studies in which connexin mutations have been linked to urothelial carcinogenesis.

1.3 Wound-healing in epithelial tissues

Differentiated epithelia, including the urothelium contain structural features to provide a specialised barrier. However in order to maintain barrier function, epithelia must be able to rapidly repair when integrity is lost, for example upon mechanical injury and the urothelium has an impressive capacity for self-repair. For this to occur, cells both adjacent to and remote from the wound site must be capable of responding to signals to allow coordinated proliferation and directed migration of healthy cells into the wound space to restore barrier function. There are several key components of cellular behaviour which determine the ability and rate at which cells may migrate into a wound space, including actin cytoskeletal dynamics, cell-cell adhesion and cell-substrate adhesion.

1.3.1 Urothelial regeneration

The urothelium has a high capacity for regeneration following damage. Urothelial destruction may be caused by a number of mechanisms including common bacterial infections, Interstitial Cystitis (IC), Ketamine-induced Cystitis, physical trauma following catheterisation or surgery for removal of urothelial carcinoma. In each case the degree of severity can be variable, from sloughing of a few superficial cells which requires a small level of proliferation to maintain barrier function (Robino et al. 2014), to more acute full-thickness urothelial loss which necessitates rapid migration and proliferation to ensure barrier restoration (Kreft et al. 2005). Whilst repair is extremely efficient, the mechanisms which support regeneration are not limitless. The degree of damage can dictate the ability to regenerate and where damage is considerable, it would be extremely unlikely that a few urothelial cells could regenerate the urothelium to create an effective urinary barrier. In IC patients there is strong correlation between the percentage of denuded bladder mucosa and patient pain, with the most denuded patients on average resulting in more total cystectomies (Leiby et al. 2007).

In vitro studies of NHU cells have shown that upon wounding, the initiating signal for repair is thought to be in the form of an ATP-driven calcium response, which propagates out from the wound edge immediately after damage (Shabir et al. 2008). The calcium wave was followed by increased migration of cells into the denuded space over a period of several hours, though details of the signalling pathways which are activated to drive the migration response to injury are not fully understood. However, it has been demonstrated that TGFβ-receptor signalling is activated in response to wounding of differentiated NHU cultures (Fleming et al. 2012) where it appears to play a key role in migration and repair. Further details of TGFβ signalling in epithelial tissues are discussed in section 1.3.4.

Animal models which mimic selective urothelial damage have provided some insight as to the processes by which barrier function is restored following injury. Damage caused by treatment of rat bladders with protamine sulphate, demonstrated that loss of superficial cells was repaired by a maturation of intermediate cells, which rapidly became terminally differentiated, expressing uroplakins and ZO-1-containing tight junctions (Lavelle et al. 2002). The plasticity of basally-derived NHU cells to regenerate into all three layers of urothelium has recently been demonstrated (Wezel et al. 2014). Superficial and full-thickness wounding of mouse bladder explant cultures confirmed that restoration of tight junctions is one of the earliest events in the bladder wound-healing process, occurring before expression of uroplakins (Kreft et al. 2005). The same study concluded that the proliferative and migratory behaviour necessary to close wounds was mostly performed by basal cells. It has since been demonstrated that immediately after isolation, basally-derived NHU cells have a higher capacity for proliferation than suprabasal-derived cells, but that the growth characteristics of both populations become indistinguishable after a short adaptation period in culture (Wezel et al. 2014). A further study in mice demonstrated that urothelial injury induced by treatment with uropathogenic *E. coli* or protamine sulphate (a cationic peptide which increases urothelial permeability resulting in shedding of urothelial cells), caused a rapid increase in proliferation in the cytokeratin 5-positive

basal cell compartment (Shin et al. 2011). This study also indicates that a paracrine signalling loop operates between the urothelium and stromal cells, in which sonic hedgehog protein is secreted by basal cells following injury, inducing expression of Wnt signals from the underlying stroma, which thereby act upon urothelial cells to drive proliferation.

It has been hypothesised that approximately 10% of rat bladder basal cells are a potential stem cell population, due to long term BrdU label retention (Kurzrock et al. 2008). However, separately isolated basal and intermediate/superficial cells can be sub-cultured and given the correct signalling cues, both populations retain the capacity to differentiate into a multi-layered organised urothelium expressing markers of basal, intermediate and superficial cells, implying that all urothelial cells retain a level of plasticity (Wezel et al. 2014). There are no studies supporting pluripotency in urothelial cells and to date, no studies in which a marker is able to distinguish a subpopulation of urothelial stem cells from the remaining basal cell population. It therefore remains controversial as to whether the urothelium maintains a population of stem cells which could support regeneration; however it would seem likely that the location of these cells would be in the cytokeratin-5 expressing basal cell compartment, should they exist.

1.3.2 The role of Connexins in epithelial wound healing

Remodelling of GJs during wound migration has been frequently observed in skin where expression of up to ten Cxs has been described (Becker et al. 2012). In human skin, the response to injury is thought to involve a rapid down regulation of Cx43 at the leading edge of the wound whilst at the same time a large induction of Cx30 and Cx26 is observed (Brandner et al. 2004). These switches in Cx regulation correlate with a switch to a highly migratory phenotype in keratinocytes, implying that migration does not require a complete absence of cell-cell communication, but rather an absence of Cx43 expression and/or communication. Connexin-mimetic peptides are short peptide sequences which mimetically match the extracellular loops of Cxs. When applied to cells *in vitro* they are capable of blocking connexon

opening and thus intercellular communication, without interfering with Cx expression. Due to similarities in the extracellular domains of connexins, relatively few mimetic peptides exist which are inhibitory to a single connexin; however Gap27 is a mimetic peptide believed to be specific to Cx43 in its effects. Cx-mimetic peptides have been used in several *in vitro* studies to establish the contribution of GJIC, rather than just Cx expression in wound healing. Addition of Gap27 peptide was found to increase the rate of migration in human fibroblasts and keratinocytes suggesting that it is perhaps Cx43-mediated GJIC, rather than just expression which acts to inhibit wound repair (Wright et al. 2009, Wright et al. 2013).

The liver has a remarkable capacity for regeneration, with the dominant gap junction protein known to be Cx32, a commonly used differentiation marker for hepatocyte studies *in vitro* (Kojima et al. 1995). Expression of a dominant-negative form of Cx32 in transgenic mice reduced the rate of liver regeneration, with reduced hepatocyte proliferation following partial hepatectomy (Dagli et al. 2004). However another *in vivo* study in rats indicated that Cx32 may be inhibitory to liver regeneration. Cx32 protein expression, but not transcript, was markedly reduced for up to 30 days during regeneration, following chronic liver injury induced by treatment with hepatotoxic chemicals (Nakata et al. 1996).

1.3.3 The Rho kinase pathway and epithelial wound healing

The Rho family of small GTPases including Rho, Rac and Cdc42 are important signal transducers regulating actin dynamics, cell shape and movement (Fig 1.4 A). During cell migration, slim cytoplasmic projections known as filopodia protrude beyond the leading edge of the cell across the ECM, under the control of cdc42 resulting in actin polymerisation mediated by VASP proteins. The lamellipodium contains an F-actin mesh which acts to propel the cell across the ECM (or substrate) and occurs at the leading edge of motile cells under the control of Rac (Van Aelst et al. 2002). In MDCK cells it has been observed that lamellipodial crawling is dependent on Rac1

activity (Fenteany et al. 2000), where inhibition of Rac1 activity in the first three rows of the leading edge prevented formation of lamellipodia and subsequent wound healing. Rho GTPases are inactive when bound to GDP, but when bound to GTP they activate ROCK, a key regulator of the actin cytoskeleton which has effects on multiple components of cytoskeletal reorganisation (Fig 1.4 A and B). ROCK induces actin filament stabilisation via LIM kinase (LIMK) and also acts to inhibit myosin light chain (MLC) phosphatase, which results in an increase in phosphorylated MLC and the formation of contractile stress fibres. Stress fibres enable dynamic focal adhesions, permitting movement of the cell away from the leading edge (Fig 1.4 A).

In addition to supporting actin reorganisation, Rho GTPases are also though to regulate integrin dynamics as well as being regulated themselves by integrins (Schwartz et al. 2000) and Rho GTPases can also act at cell junctions where they also play a key role in the maintenance of adherens junctions (Watanabe et al. 2009). Cross-talk between the Rho kinase and several other signalling pathways has been identified, including the TGFβ receptor pathway, also known to be a key cell migration regulatory pathway (Clements et al. 2005). Inhibition of TGFβ signalling in endothelial cells was demonstrated to result in a large reduction in Rho A gene expression (Tavares et al. 2006).

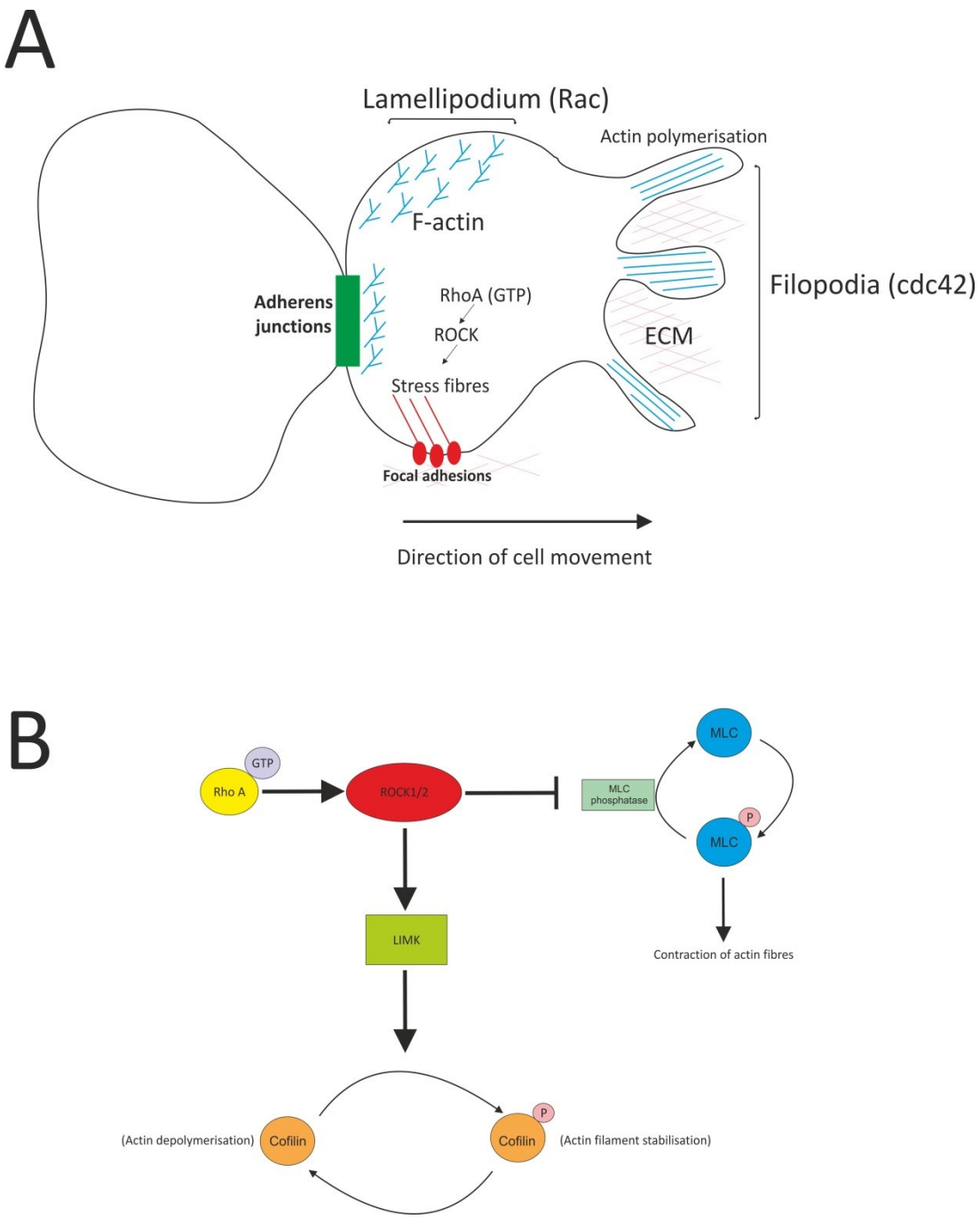

Figure 1.4 Rho Kinase Pathway and Cell Migration

A. Simplified diagram to demonstrate the roles of Rac, cdc42 and RhoA/ROCK in cell movement

B. Simplified overview of the Rho-kinase pathway and regulation of actin dynamics.

1.3.4 TGFβ-receptor signalling and epithelial wound-healing

1.3.4.1 TGFβ signalling mechanism

TGFβ is a cytokine that exists in three isoforms; TGFβ1, TGFβ2 and TGFβ3, which are known to have autocrine, paracrine and endocrine regulatory functions in many cell types and implicated in tissue development and repair, proliferation, differentiation, homeostasis and pathogenesis. As a member of the TGFβ superfamily of ligands, which includes bone morphogenic proteins and growth differentiation factors, TGFβ ligand binds to receptor complexes consisting of TGFβ receptors type I and II. Both receptors have serine/threonine kinase activity and upon ligand binding, the type II receptor phosphorylates and activates the type I receptor, which hydrolyses ATP to directly phosphorylate receptor-regulated SMAD proteins, thus propagating the signal within the cell (Huse et al. 2001). SMAD proteins translocate to the nucleus and act as signal transducers, to induce or repress transcriptional activity of a broad range of downstream genes, some of which are key to regenerative processes such as cell proliferation and migration. Loss of SMAD3 has been shown to delay liver regeneration through reduced hepatocyte proliferation (Kremer et al. 2014).

1.3.4.2 TGFβ signalling in EMT

The diversity of signalling effects brought about by TGFβ are complex and dependent on cell type and biological context. A considerable body of evidence exists to suggest that signalling through TGFβ plays a major role in epithelial-to-mesenchymal transitions (EMT) as reviewed in (Zavadil et al. 2005) and (Heldin et al. 2009). EMT is a process in which polarised epithelial cells adopt a more basic fibroblast-like phenotype and is associated with a loss of cell-cell adhesion, a loss of cell-matrix adhesion and cell migration. EMT is a commonly recognised process associated with tumour metastasis and many developmental processes of which gastrulation is particularly well characterised (Thiery et al. 2009). In some epithelia,

it is also believed that EMT may occur during healing in response to injury, for example during pulmonary fibrosis by alveolar epithelial cells (Kim et al. 2006).

Whether EMT-like behaviour occurs during wound-healing of urothelium is not fully understood, however microarray studies demonstrate that TGFβR/SMAD3 signalling is altered as a consequence of NHU cell differentiation. Evidence suggests that regeneration of differentiated NHU cultures occurs in response to autocrine activation of TGFβR/SMAD3 pathway following wounding (Fleming et al. 2012), however the phenotype of wound-healing NHU cells was not considered in this study and therefore a specific EMT switch has not been identified and whilst TGFβR/SMAD3 signalling is known to participate in EMT-like behaviour, there are other recognised pathways implicated in tissue repair, for which TGFβR/SMAD3 may be involved.

1.3.4.3 cAMP and SMAD regulation

It has been demonstrated in some cell types including fibroblasts and keratinocytes that SMAD-specific gene regulation occurs as a response to changes in intracellular cAMP (Schiller et al. 2003, Schiller et al. 2010). cAMP-dependent activation of PKA induces the release of a catalytic subunit which diffuses into the nucleus where it is thought to phosphorylate cAMP-response element-binding protein (CREB) at serine 133, thereby allowing it to bind with transcriptional coactivators, including P300 and SMAD3 (summarised in figure 1.4). This transcriptional complex binds to conserved cAMP-response elements found within a broad range of genes, including those involved in ECM destruction and synthesis.

1.3.4.4 PPARγ and SMAD regulation

A negative regulation of SMAD3 has been observed in several studies in response to activation of the nuclear hormone receptor PPARγ. Treatment of rats with the

PPARγ agonist Rosiglitazone resulted in decreased levels of phosphorylated SMADS 2 and 3 in subcutaneous adipose tissue (Beaudoin et al. 2014), whilst another PPARγ agonist Pioglitazone, inhibited TGFβ-induced EMT-like behaviour in retinal pigment epithelial cells (Hatanaka et al. 2012). Mouse skin fibroblasts with deleted PPARγ showed an enhanced rate of dermal wound closure compared with wild-type mice (Sha et al. 2012) and PPARγ-null mouse embryonic fibroblasts show constitutive SMAD2/3 phosphorylation and interaction with its transcriptional co-activator P300, with enhanced collagen biosynthesis, even in the absence of exogenous TGFβ (Ghosh et al. 2008). A further study in aortic smooth muscle cells demonstrated a direct binding of PPARγ to SMAD3, resulting in abrogated ECM production and tissue growth following vascular injury (Fu et al. 2001).

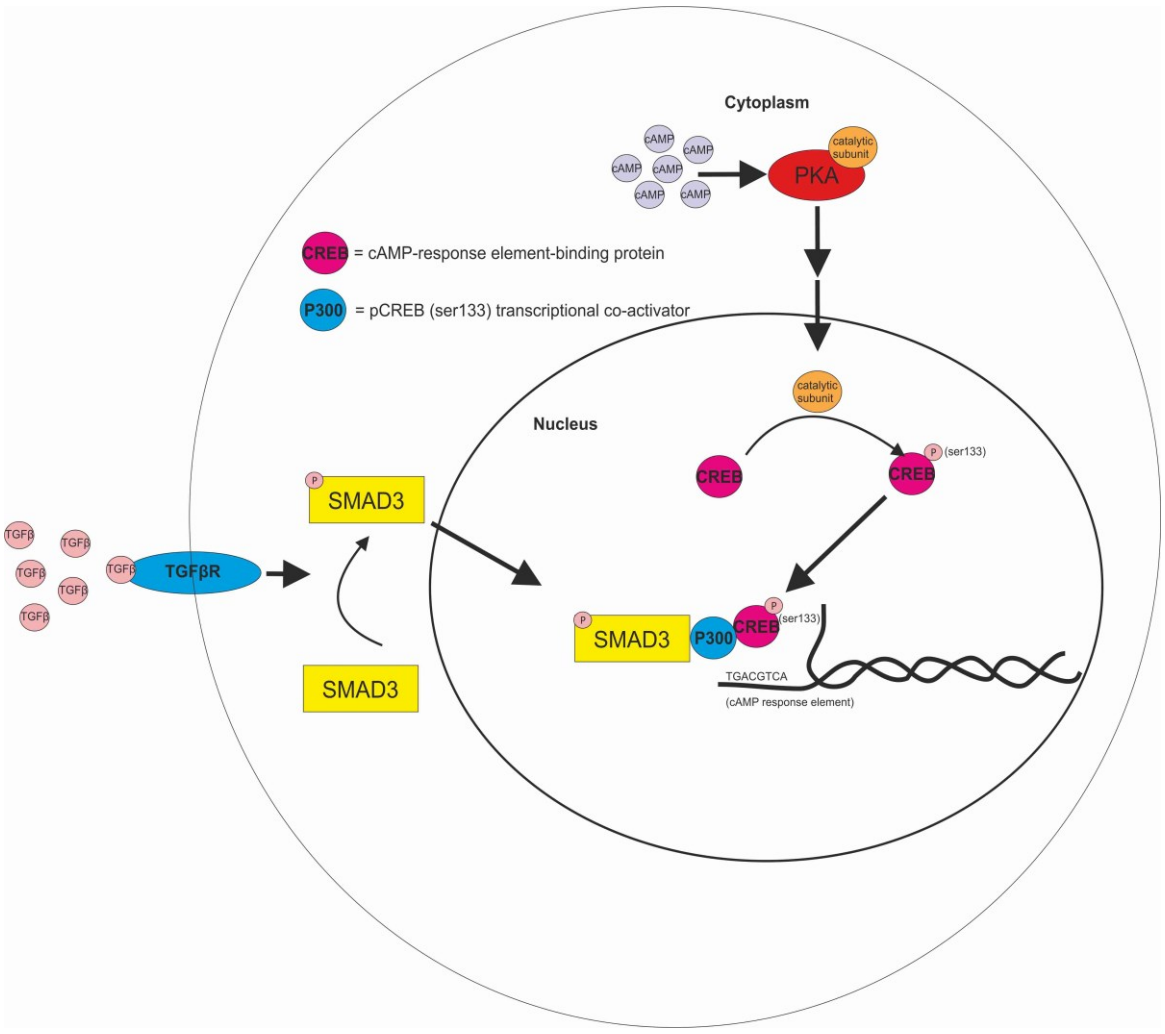

Figure 1.5 Overview of cAMP-dependent SMAD3/CREB gene transcription.

1.4 Thesis Hypothesis and Aims

In order to maintain barrier function, the urothelium is able to switch to a highly migratory state in order to repair damage, which requires that urothelial cells are individually responsive to their environment and can behave in a coordinated manner to respond to regional damage. Direct cell-cell communication is likely to play a key role in maintaining balanced homeostasis and also for generating the field effects necessary to drive a coordinated response to injury.

Whilst the overall importance of gap junction intercellular communication in regulating tissue function and homeostasis is well documented, there is limited knowledge of the properties that specific Cxs offer to tissue function. Elucidating the function of a particular Cx in any given cell type is complex, since most cell types express multiple Cxs which are probably not selective for passage of a single messenger from cell-to-cell. However Cxs do appear to have distinct permeability characteristics, with selective efficiencies and transfer rates and it is likely that their expression in any given tissue will offer permeability characteristics with significant physiological relevance. It has been proposed that in addition to cell-cell communication, some Cxs offer alternative functions in cell signalling events and within large protein complexes for regulation of cell adherence and polarity by influencing the assembly or maintenance of tight/adherens junctions. However, the current knowledge of the fundamental mechanisms underlying the spatial and temporal coincidence of gap and tight/adherens junction proteins is limited.

Whilst the role of some Cxs (in particular Cx43) has been established to be closely linked to the migratory behaviour of cells and tissues during wound-healing, there are no reports which consider a potential role for Cxs in the wound-healing of human urothelium. This may be of critical relevance to maintaining a tight barrier function. In addition there is very little supporting evidence as to how some Cxs

enhance or inhibit wound migration and what migratory cell signalling events and pathways may be affected by the biology of specific Cxs.

The working hypothesis for this project is that specific Cxs will be required for a) urothelial cell differentiation and barrier attainment and b) the ability for urothelial cells to regenerate in response to damage cues.

The overall aims of this work were to use previously characterised *in vitro* systems to assess connexin expression in human urothelium and the contribution of gap junction-mediated intercellular communication to urothelial physiology, including barrier acquisition and wound repair.

Specific objectives were to:

- Characterise connexin family expression in human urothelium to identify connexins which may be closely associated with urothelial physiology and how expression of Cxs may be regulated during the development of a functional differentiated urothelium

- Determine whether Cxs assemble into functional gap junctions in human urothelial cells

- To examine whether specific connexins are involved in the generation of a differentiated urothelial phenotype, including the development of a functional urinary barrier

- To study whether specific Cxs may contribute to the migratory and proliferative behaviour of human urothelial cells in response to wounding and identify potential pathways which may be key to driving such behaviours

2. Materials and Methods

2.1 General

All experimental work was carried out in the Jack Birch Unit or Technology Facility in the Department of Biology, at the University of York. TEM experiments were performed by Meg Stark and DNA plasmid sequencing by Celina Whalley, both in the Technology Facility, University of York.

2.1.1 Suppliers

Suppliers of reagents are indicated within this chapter, either at the first use of the reagent, or in table form for antibodies and drugs. A full list of suppliers is detailed in Appendix 1.

2.1.2 Lab Glassware, Plastic-ware and Accessories

All glassware, glass Pasteur pipettes (Fisher Scientific), disposable microfuge tubes (Sarstedt), pipette tips (Starlab), metal dissection instruments (SLS) and glass multispot slides (C A Hendley) were sterilised by autoclaving at 121 ^{o}C for 20 minutes. Single use plastic-ware, Bijou tubes (Greiner), plastic Pasteur pipettes (SLS), Universal tubes and serological pipettes (Sarstedt) were supplied sterile for single use. Coverslips used for all microscopy work were supplied by SLS (No. 1.5).

2.1.3 Stock Solutions

Recipes for all stock solutions are detailed in Appendix 2. All chemicals were supplied by Fisher Scientific unless detailed otherwise. General lab reagents were prepared using deionised water (dH_2O), reagents for molecular and cell culture techniques were prepared using ultra-pure water from a Purelab (ELGA) ultraviolet purification system. Heat stable solutions were sterilised by autoclaving at 121 ^{o}C

for 20 minutes and non-heat stable solutions were sterilised by filtration through low-protein binding HT-Tuffryn syringe filters with 0.2 µm pore size (VWR).

2.1.4 Antibodies

All primary antibodies used (including source) are listed in Table 2.1. For each application, primary antibodies were optimised by titration on known positive control samples to establish concentrations for use. All antibodies were stored aliquotted at -80 ^{o}C to avoid freeze-thaw cycles and once thawed, aliquots were stored concentrated at 4 ^{o}C or diluted in TBS (Appendix 2) with 0.1 % (w/v) BSA as a protective protein and 0.1 % (w/v) sodium azide as a preservative.

Secondary antibodies used (including relevant conjugate for detection and application purpose) are detailed in Table 2.2. All secondary antibodies purchased were cross-adsorbed against human serum and human IgG. Secondary antibodies were batch-tested using previously optimised primary antibody controls. Neat stocks were stored in a light protective box at 4 ^{o}C and were diluted immediately before use. Any background signal as a result of non-specific secondary antibody binding was assessed by exclusion of primary antibody from the reaction.

2.1.5 Statistical Analysis

All data represented by graphs in this thesis were produced using Microsoft Excel (2010). Data are represented as a mean of all replicates ± standard deviation (SD) where appropriate. Statistical tests performed throughout this thesis were performed using InStat software version 3 (GraphPad). Data were confirmed to be drawn from normal distributions if appropriate. Two-sample T-tests were used when comparing two sample means and one-way analysis of variance (ANOVA) tests were used when comparing more than two sample means (with appropriate post-tests selected). Details of the number of replicates, statistical tests, p-values and levels of significance are detailed in the text (or corresponding figure caption).

Antigen	*Clone/Supplier ref*	*Host*	*Supplier*	*Molecular Weight*
Connexin 32	5F9A9	M	Life Technologies	32kD*
Connexin 32	Ab59924	Rb	Abcam	32kD*
Occludin	71-1500	Rb	Life Technologies	65kD
E-Cadherin	HECD-1	M	Abcam	120kD
ZO-1	1A12	M	Life Technologies	220kD
ZO-1α+	HP9044	Rb	Hycult Biotech	225kD
ZO-2	2874	Rb	Cell Signaling	150kD
ZO-3	D57G7	Rb	Cell Signaling	140kD
Claudin 4	3E2C1	M	Life Technologies	22kD
Claudin 5	4C3C2	M	Life Technologies	24kD
Claudin 7	ZMD.241	Rb	Life Technologies	22kD
β-actin	AC-15	M	Sigma	42kD
CK7	OV-TL12/30	M	Leica	51kD
CK13	1C7	M	Abcam	54kD

Table 2.1 Primary Antibodies.

M = Mouse Rb = Rabbit *Note, connexion 32 dimeric bands were also observed as predicted at approximately 60 kD.

Antigen	*Conjugate*	*Host*	*Supplier*	*Supplier Ref.*	*Application*
Mouse IgG	biotin	Rabbit	DAKO	E0354	IHC
Rabbit IgG	biotin	Goat	DAKO	E0432	IHC
Mouse IgG	Alexa 488	Goat	Life Technologies	A11001	IF
Mouse IgG	Alexa 594	Goat	Life Technologies	A11005	IF
Rabbit IgG	Alexa 488	Goat	Life Technologies	A11008	IF
Rabbit IgG	Alexa 594	Goat	Life Technologies	A11012	IF
Mouse IgG	Alexa 680	Goat	Life Technologies	A21057	WB
Rabbit IgG	IR dye 800	Goat	Tebu Bio	611-132-122	WB

Table 2.2 Secondary Antibodies.

IHC = Immunohistochemistry IF = Immunofluoresence WB = Western Blot

2.1.6 Inhibitors, Agonists, Antagonists and Growth Factors

Pharmacological reagents were prepared by reconstitution in fresh cell culture grade dimethyl sulphoxide (DMSO) or alternative vehicle (described in Table 2.3). Aliquots were stored in light protective boxes at -20 ^{o}C. Drugs/growth factors which had previously been optimised for NHU cell treatment were used at published concentrations and previously untested treatments were tested over a concentration range to determine the effective dosage (see results chapters). Working concentrations are described in Table 2.3

Drug name	*Target*	*Supplier*	*Vehicle*	*Working concentration*
Troglitazone	PPARγ ligand	R&D systems	DMSO	1 µM
PD153035	Inhibitor of the EGFR tyrosine kinase	Merck Millipore	DMSO	1 µM
T0070907	PPARγ antagonist	Cambridge Bioscience	DMSO	1 µM
Heptanol	Uncouples gap junctions	Sigma	n/a (liquid)	1 mM
18α-Glycyrrhetinic acid	Uncouples gap junctions	Sigma	DMSO	5-50 µM
SB431542	Inhibitor of TGFβRI	Sigma	DMSO	10 µM
TGFβ1	Cytokine/growth factor	R&D systems	1 mg/ml BSA in 4 mM HCl	2 -4ng/ml

Table 2.3 Drugs/agonists/antagonists.

2.2 Cell Culture

2.2.1 General

All cell culture work was performed using aseptic technique with work performed in class II laminar air flow safety cabinets with HEPA filters. Work surfaces were cleaned with 70 % (v/v) ethanol before and after use. Cultures were maintained in Heracell™ 240 Incubators (Heraeus®) at 37 ^{o}C in a humidified atmosphere of 5 % CO_2 in air (for buffering of cells cultured in KSFMc) or 10 % CO_2 in air (for all other media types).

Culture medium was replaced on cell cultures every 2 or 3 days following vacuum aspiration of spent medium into a flask containing 10 % (w/v) Virkon® for decontamination.

Centrifugation of cell suspensions was performed in a Sigma 2-6E compact centrifuge (SLS) at 400 x g for 5 minutes. All cell counts were performed by pipetting 20 µl of a single cell suspension in to an "Improved Neubauer" haemocytometer (VWR). Cells were counted in four grids (equivalent to 0.0001cm^3) and the mean cell count was multiplied by 10^4 to give an equivalent cell density per ml of medium.

NHU cell cultures were maintained in Primaria® (BD Biosciences) or Cell$^+$ plastic-ware (Sarstedt), both of which have treated surfaces to promote attachment and growth of primary cells.

Digital photomicrographs were generated by phase-contrast microscopy of cultures on a Nikon Diaphot or EVOS XL Core microscope.

2.2.2 Primary Urothelial Cell Isolation and Sub-culture

2.2.2.1 Tissue Samples

Samples of normal human ureter, bladder and renal pelvis were collected following approval from the relevant local NHS Research Ethics Committee and the University of York Department of Biology Ethics committee. Informed patient consent was obtained as required. Samples were provided by surgeons at St. James's University Hospital and Leeds General Infirmary (Leeds), Pinderfields Hospital (Wakefield), Castle Hill Hospital (Hull), and the Royal Hallamshire Hospital (Sheffield). Patients were selected with no history of urothelial malignancy. Biopsies were collected in 15 ml sterile Transport Medium (Appendix 2) and were stored at 4 ^{o}C (or ambient temperature if delivered by post) until processed (see table 2.4 for details of tissue samples).

2.2.2.2 Normal Human Urothelial (NHU) Cell isolation

Previously described methods for urothelial cell isolation from patient biopsies were adopted to establish primary cultures (Southgate et al. 1994, Southgate J 2002). Samples were dissected in sterile Petri-dishes (Sterilin) using scissors and forceps to remove any excess fat and connective tissue. A small representative sample was dissected with a scalpel and fixed for 24-48 hours in 10 % (v/v) formalin (Appendix 2) for histological assessment (section 2.5). The remaining tissue was incubated in 10 ml Stripper Medium (Appendix 2) for 4 hours at 37 ^{o}C or for 16 hours at 4 ^{o}C, before separation of the urothelial sheets from the underlying stromal tissue using sterile forceps. Sheets were collected by centrifugation, resuspended in 400 units (in 2 ml) collagenase IV (Appendix 2) and incubated for 20 minutes at 37 ^{o}C. Cells were then triturated to encourage a single cell suspension, before centrifugation and seeding at $4x10^4$ cells/cm^2 in Keratinocyte Serum-free Medium (KSFM, Invitrogen), supplemented with 5 ng/ml recombinant human-EGF (Invitrogen), 50 µg/ml Bovine Pituitary Extract (Invitrogen) and 30 ng/ml cholera

toxin (Sigma). This complete KSFM (KSFMc) was used for all NHU cell culture work, unless detailed otherwise.

2.2.2.3 Subculture of Normal Human Urothelial Cell Cultures

At just confluence, NHU cell cultures were passaged by incubating in pre-warmed 0.1 % (w/v) Ethylenediaminetetra-acetic acid (EDTA) in PBS for 3-5 minutes at 37 ^{o}C, until cell contacts were separated and cells began to round up. The EDTA was then replaced with a 0.25 % (w/v) trypsin versene solution in Hank's balanced salt solution (HBSS; Life Technologies) containing 0.02 % (w/v) EDTA. Cultures were incubated at 37 ^{o}C until cells detached from the plastic (approximately 2-4 minutes) and were then collected into KSFMc containing 1.5 mg/ml trypsin inhibitor (from soybean), centrifuged and re-plated at the desired density. NHU cultures were split at a ratio of 1:3 for routine maintenance. For all experimental work, cultures were used between passage 1 and 5. The independent NHU cell lines used in this thesis are detailed in Tables 2.4 a and 2.4b.

Cell Line	*Tissue Derived*	*Donor Age*	*Donor Gender*	*Surgical Procedure*
Y778	Ureter	Unknown	Unknown	Pyeloplasty
Y779	Ureter	Unknown	Unknown	Unknown
Y930	Bladder	65	Male	Prostatectomy
Y1043	Ureter	39	Male	Nephrectomy
Y1054	Ureter	57	Male	Unknown
Y1064	Ureter	3	Male	Ureteric reimplantation
Y1108	Ureter	57	Male	Kidney Transplant
Y1119	Ureter	65	Female	Unknown
Y1153	Ureter	57	Male	Nephrectomy
Y1186	Bladder	79	Male	Prostatectomy
Y1191	Ureter	50	Female	Pyeloplasty
Y1216	Ureter	56	Male	Nephrectomy
Y1221	Ureter	63	Female	Nephrectomy
Y1268	Ureter	74	Female	Nephrectomy
Y1545	Ureter	55	Male	Kidney Transplant

Table 2.4a Origin of NHU cell lines (Non-transduced).

Cell Line	Tissue Derived	Donor Age	Donor Gender	Surgical Procedure
Y1057	Ureter	Unknown	Unknown	Unknown
Y1117	Ureter	64	Female	Unknown
Y1119	Ureter	65	Female	Unknown
Y1151	Ureter	31	Female	Nephrectomy
Y1185	Ureter	45	Female	Unknown
Y1247	Ureter	67	Female	Nephrectomy
Y1270	Ureter	76	Female	Nephrectomy
Y1277	Renal Pelvis	68	Female	Pyeloplasty
Y1284	Ureter	64	Female	Nephrectomy
Y1392	Ureter	60	Male	Kidney Transplant

Table 2.4b Origin of NHU cell lines (Transduction studies).

2.2.2.4 Culture of Transduced Human Urothelial Sublines

NHU cells were transduced with retrovirus to genetically manipulate connexin-32 as described in section 2.9. Transduced cultures were maintained in an identical manner to NHU cells, with the exception that the KSFMc contained a maintenance dose of antibiotic (0.025 mg/ml for G418 and 0.25 µg/ml for puromycin), to maintain selection pressure.

2.2.3 Differentiation of NHU cultures In Vitro

2.2.3.1 Differentiation of NHU cultures by pharmacological activation of PPARγ and inhibition of EGFR signalling

A previously described pharmacological treatment was used to induce cytodifferentiation of human urothelial cells (Varley et al. 2004a, Varley et al. 2004b). NHU cultures were cultured to approximately 70-80 % confluence before replacing the growth medium with KSFMc containing the PPARγ agonist troglitazone at a final concentration of 1 µM and the EGFR inhibitor PD153035 at a final concentration of 1 µM. The troglitazone/PD153035 treatment was maintained for 24h before replacing the growth medium with KSFMc containing 1 µM PD153035 alone and maintaining for a further 6 days, with a single medium change at day 3. Vehicle control cultures were treated with an equivalent concentration of DMSO (without troglitazone or PD153035) to balance for any solvent-driven cellular effects. See summary diagram (Fig 2.1).

2.2.3.2 Differentiation of NHU cultures using 5% bovine serum and physiological calcium

NHU cultures were functionally differentiated using a previously described method which induces a differentiated urothelial phenotype with tight barrier properties (Cross et al. 2005). NHU cultures were grown to approximately 80 % confluence before replacing the growth medium with KSFMc containing 5 % (v/v) batch-tested Adult Bovine Serum (ABS; Harlan Sera-lab) for 4-5 days at 37 ^{o}C. Cultures were then harvested and re-seeded onto Snapwell™ membranes at 5x10^{5} cells per 1.1 cm^{2} membrane (see section 2.8.1) or at a 1:2 ratio into fresh flasks (for protein or RNA lysates), 24-well plates (CA Hendley; time-lapse analysis) or 12-well multi-spot slides (immunocytochemistry) in KSFMc containing 5 % ABS. After 24h, the growth medium was replaced with KSFMc containing 5 % ABS and 2 mM $CaCl_2$ (final concentration). Cultures were then maintained for a further 6 days (unless described otherwise). Control experiments were included in which cells were

maintained in KSFMc alone, or treated with 2 mM calcium alone for a matched time period. For summary diagram see Fig. 2.1.

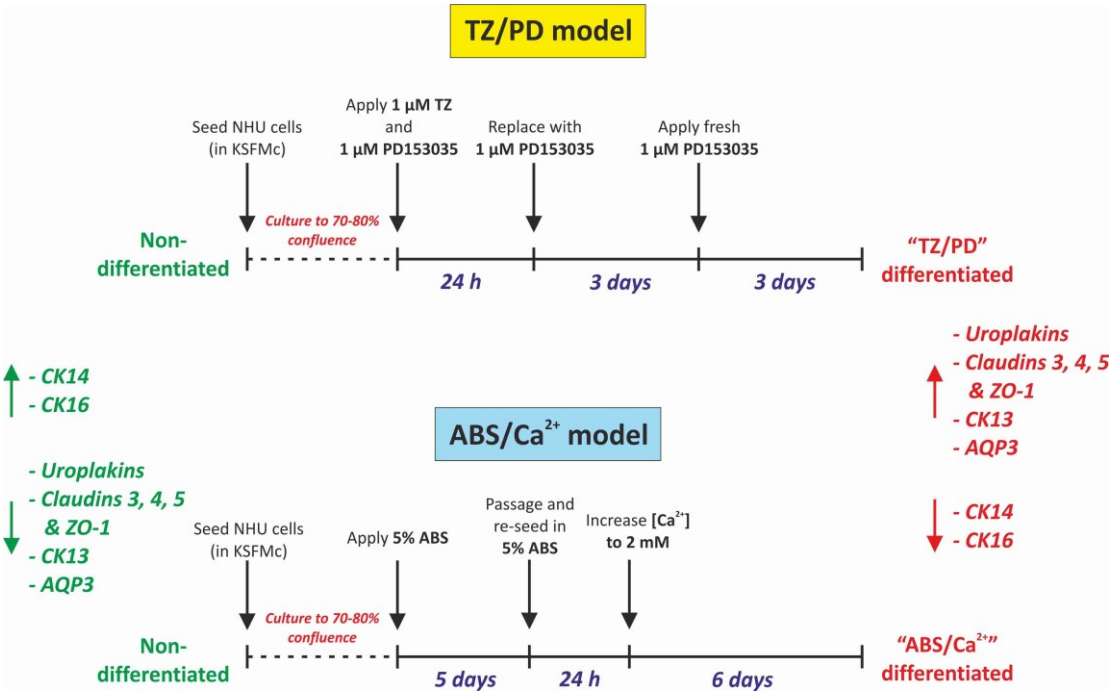

Figure 2.1 Summary of two methods used to induce differentiation of NHU cells in vitro.

Summary of the two in vitro methods used to induce differentiation of NHU cultures as detailed in section 2.2.3. Selected genes which are upregulated or down regulated in non-differentiated and differentiated (both models) NHU cells are indicated (up and down arrows indicate up- or down-regulation respectively).

TZ = the PPARγ agonist, troglitazone. PD = the EGFR inhibitor, PD153035. ABS = Adult bovine serum

Note: The ABS/Ca^{2+} model was the preferred method of differentiation throughout this thesis, since this method supports barrier acquisition, which can be measured by TER. However, the factors in serum which induce differentiation are undefined. The TZ/PD model uses pharmacological activation of PPARγ to initiate the urothelial gene activation pathway in individual cells, however these cells do not self-organise into a multi-layered, barrier-forming epithelium. The TZ/PD model was therefore only used in experiments addressing the specific role of PPARγ to connexin biology.

2.2.4 Culture of Retropack™ PT67 Packaging Cells

The 3T3 fibroblast-derived PT67 cell line (Clontech) has been genetically engineered to stably express the retroviral *gag*, *pol* and *env* genes necessary for retroviral particle production and replication. PT67 cells were maintained in Dulbecco's Modified Eagle's Medium (DMEM) supplemented with 10 % (v/v) Fetal Bovine Serum (FBS; Harlan Sera-lab)) and 1 % (v/v) L-glutamine, in tissue culture flasks (Corning). PT67 cultures were routinely passaged with a split ratio of 1:5, following the same method as for NHU cells (section 2.2.2.3), however the trypsin inhibitor step was not required due to the presence of serum in the growth medium.

Before use for transfection, a stock of PT67 cells was subjected to "HAT" selection, as recommended by the manufacturer, by culture for 5 days in 100nM aminopterin, followed by 5 days in DMEM-HAT medium (30nM hypoxanthine, 1M aminopterin and 20mM thymidine) and then a further 5 days in DMEM-HT medium (30mM hypoxanthine and 20mM thymidine). Following transfection, PT67 cells were continuously maintained in the relevant antibiotic at the selection concentration (as detailed in section 2.9.4).

2.2.5 Cryopreservation and Thawing of Cells

Just confluent cultures were harvested with EDTA and trypsin as described for cell passaging, however following centrifugation, cells were resuspended in cold "freeze-mix" which comprised 10 % (v/v) FBS and 10 % (v/v) DMSO, in the normal culture medium for the cell type. Cells were aliquotted as a 1:3 split ratio into polypropylene cryovials (Sarstedt), with 1 ml freeze-mix used per vial. Vials were placed in an isopropanol freezing chamber (Nalgene) at -80 ^{o}C for 16 h. This allows cells to cool at a steady rate of -1 ^{o}C per minute. The following day cryovials were transferred into a liquid nitrogen dewar for long-term storage.

To thaw cells, cryovials were removed from liquid nitrogen and immediately placed into a water bath at 37 ^{o}C. The thawed freeze-mix was then transferred into 10 ml

growth medium before centrifugation, resuspension in fresh growth medium and plating at the desired density.

2.2.6 Screening for *Mycoplasma spp*.

Cultures were routinely checked for infection by *Mycoplasma spp*. using a DNA staining method to examine cells for extranuclear contamination. Cells were seeded onto 12-well glass slides at a density of $1x10^5$ cells/ml (50 µl/well) and left to attach for 4 h before flooding with medium and incubating overnight. Slides were then washed twice in Phosphate Buffered Saline (PBS; Appendix 2), fixed for 30 seconds in a 1:1 mixture of methanol:acetone and air dried. Slides were incubated with 0.1 µg/ml Hoechst 33258 in PBS, for 5 minutes whilst protecting the slide from light with aluminium foil. Slides were washed once in PBS, air dried and mounted in antifade (Appendix 2) before sealing the coverslip with clear nail polish. Cells were examined for extranuclear DNA, under epifluoresence illumination using an Olympus BX60 microscope.

2.3 Cell Proliferation Assays

The biomass of cell cultures was assessed using AlamarBlue®, a reagent that undergoes a colourimetric change in response to cell metabolism and which can be used to estimate changes in population mass (based on relative change) or number (following comparison against a standard curve). The assay detects reduction of all elements of the electron transport chain and works on the assumption that mitochondrial activity is directly proportional to cell number.

NHU cells were seeded at a density of $2x10^3$ cells/well into Primaria® 96-well plates and allowed to attach for 18 hours overnight in the incubator. The following day, one plate was assayed to establish initial seeding viability (day 0), whilst the growth medium in the remaining plates was replaced, either with fresh KSFMc, or treatment as appropriate and assayed at various timepoints post-treatment. To

determine the relative number of proliferating cells, growth medium was replaced with 200 µl of freshly prepared 10 % (v/v) AlamarBlue® reagent (diluted in pre-warmed KSFMc) in six replicate wells, including empty (no cell) control wells, before returning to the incubator for exactly 4 hours. The absorbance of samples was measured at 570 nm and 600 nm using a Multiskan Ascent 96-well plate spectrophotometer (Thermo Scientific). The absorbance readings were directly proportional to the mitochondrial activity within the cells and were taken to be directly proportional to viable cell number. The percentage reduction of AlamarBlue® was calculated from the absorbance values using the following equation:

$$\text{Percentage Reduction} = \frac{(O2 \times A1) - (O1 \times A2)}{(R1 \times N2) - (R2 \times N1)} \times 100$$

Where:

O1 = molar extinction coefficient (E) of oxidized AlamarBlue® (Blue) at 570 nm, a constant value of 80586

O2= E of oxidized AlamarBlue® at 630 nm, a constant value of 34798

R1 = E of reduced AlamarBlue® at 570 nm, a constant value of 155677

R2= E of reduced AlamarBlue® at 630 nm, a constant value of 5494

A1 = absorbance of test wells at 570 nm

A2 = absorbance of test wells at 630 nm

N1 = absorbance of negative control well (medium plus AlamarBlue® but no cells) at 570 nm

N2 = absorbance of negative control well (medium plus AlamarBlue® but no cells) at 630 nm

2.4 Cell-Cell Communication Assays

2.4.1 Lucifer Yellow / Rhodamine-Dextran method

NHU cells were seeded at $4x10^4$ cells/well (2 cm^2) and cultured to confluence in Primaria® 24-well plates. If required, cultures were treated with drugs or differentiated with troglitazone and PD153035. For the dye-transfer assay, cultures were rinsed twice in PBS before applying 200 µl of KSFMc containing 1 mM lucifer yellow (LY; MW = 457.25 Da) and 0.5 mg/ml rhodamine dextran (RhoD; MW=3000 Da) (both Life Technologies). Both dyes are fixable to lysine residues within the cell and therefore dye-transfer is halted upon formalin fixation. From this stage on, cells were protected from light using aluminium foil.

A single horizontal scratch was performed across each well with a 21 gauge needle to temporarily perturb cell membranes along the scratch region and permit uptake of dye. Cultures were then incubated for exactly 6 minutes in a 37 ^oC incubator to permit dye transfer. Each culture was then washed twice with ice-cold PBS and fixed in 1 ml 10 % (v/v) formalin (Appendix 2) for 10 minutes at ambient temperature before rinsing in PBS. Cells were then incubated with 0.1 µg/ml Hoechst 33258 in PBS, for 5 minutes, rinsed in PBS and stored in 1 ml fresh PBS for imaging. LY, RhoD and Hoechst 33258 labelled cells were visualised along the scratch wound by epifluoresence on an Olympus IX81 motorized inverted microscope. To evaluate the level of gap junctional intercellular communication (GJIC), dye-coupled cells on either side of the scrape line were counted from micrographs taken from 5-10 fields of view per well. Fluorescent images were analysed using TissueQuest v4.0 software (TissueGnostics). Individual cells were identified using the "nuclear mask" function which distinguishes cells based on the Hoechst 33258 stain. The software was then used to perform counts to determine the number of RhoD positive cells (in red) and the number of LY positive cells (in green), after manual setting of a background threshold for each channel. For each field of view the number of LY cells observed per initially-loaded RhoD cell was calculated. Mean values were taken to be proportional to the gap-junction mediated communication capacity of the culture.

2.5 Histological Analysis

2.5.1 Fixation

Tissue specimens or cell sheets were immersed in 10 % (v/v) neutral-buffered formalin (Appendix 2) for 24-48 hrs or 16 h respectively, in 30 ml universal centrifuge tubes at ambient temperature before transferring to 70 % ethanol for storage.

2.5.2 Embedding

Fixed tissue samples or cell sheets were placed into labelled embedding cassettes (CellPath). Very small biopsies or cell sheets were placed into a CellSafe mesh biopsy capsule (CellPath), within an embedding cassette to prevent tissue loss. Labelled cassettes were submerged in fresh 70 % (v/v) ethanol for 10 minutes on an orbital shaker, followed by 10-minute incubations on the orbital shaker with 100 % ethanol (repeated for a total of 3 washes), propan-2-ol (repeated for a total of 2 washes) and finally xylene (repeated for a total of 4 washes), to clear tissues of alcohol and allow wax penetration into the tissue. Tissues were then immersed in liquid paraffin wax (Thermo Scientific) at 60 ^{o}C for 15 minutes, followed by three further 15 minute incubations in fresh liquid paraffin wax, before orienting biopsies in embedding moulds filled with paraffin wax and setting on a cool plate (Raymond A Lamb) at -12 ^{o}C.

2.5.3 Sectioning

5 µM sections were cut using a Leica RM2135 rotary microtome. Sections were floated onto water at 40 ^{o}C to remove creases, before collection onto charged Superfrost microscope slides (Fisher Scientific). Slides were air-dried and stored for up to month at ambient temperature (or 6 months under vacuum), before use for histological staining or immunohistology.

2.5.4 Haematoxylin and Eosin Staining

Tissue sections were de-waxed by incubation in fresh xylene for 1 minute, followed by three further xylene incubations for 1 minute each. Tissues were then rehydrated by submersing in 100 % ethanol for three washes (one minute each), 75 % ethanol for one minute followed by rinsing in gently running tap water for 1 minute. Tissues were then immersed in Mayer's Haematoxylin (Appendix 2) for 2 minutes, before rinsing in running tap water for 1 minute, incubating in Scott's Tap Water (Appendix 2) for 1 minute and then briefly rinsing in tap water before staining tissues with 1 % Eosin solution (Raymond A Lamb) for 30 seconds. Slides were rinsed thoroughly in tap water and then dehydrated in 70 % ethanol for 1 minute, 100 % ethanol for 3 x 1 minute, before clearing in xylene for 2 x 1 minute. Sections were mounted in DPX mountant and a coverslip applied to each slide. Slides were examined by bright field microscopy using an Olympus BX60 microscope.

2.5.5 Transmission Electron Microscopy (TEM)

All TEM analysis was performed by Meg Stark in the Technology Facility. Cell sheets were grown on permeable Snapwell™ membranes and Transepithelial electrical resistance readings were taken (see section 2.8.1 for details). Snapwell™ membranes were released from their detachable supports using a disposable scalpel before placing into a glass vial containing fixative comprising 2.5 % (v/v) glutaraldehyde, 4 % (v/v) formaldehyde in 100 mM phosphate buffer (pH 7.6) for 90 minutes at ambient temperature. Membranes were placed in a solution of 1 % (w/v) osmium tetroxide for 1 h on ice to preserve the lipid composition of the cells and enhance specimen contrast for TEM. Membranes were dehydrated through a series of 25 %, 50 %, 70 %, 90 % and 100 % ethanol for 20 minutes each, followed by 20 minutes in neat 1,2-propylene oxide and then through a series of 1,2-propylene oxide:epon araldite resin (Agar Scientific), at ratios of 25:75, 50:50, 75:25 and finally 100 % resin, for 30 minutes each. Membranes were orientated into fresh 100 % epon araldite resin in a coffin mould and left to set at 60 ^{o}C for 48 h.

Sections cut at 1 µm thickness for light microscopy and mounted onto glass slides and 70 nm for TEM and mounted onto square mesh TEM grids, using a Leica Ultracut UCT microtome. For light microscopy, section were stained with a solution of 0.6 % (w/v) toluidine blue and 0.3 % (w/v) sodium carbonate and mounted in water before applying a coverslip and imaging on Olympus BX60 microscope. For TEM, sections were stained with a saturated solution of uranyl acetate in 50 % (v/v) ethanol for 1 minute, rinsed in dH_20 and stained with Reynold's lead citrate for 30 seconds. TEM was performed on a Technai™ 12 transmission electron microscope (FEI).

2.6 Analysis of gene expression

2.6.1 General

All RNA work was performed on a designated bench and RNAse*Zap*® wipes (Ambion) were used to clean bench, pipettes & gloves before working. DNAse/RNAse-free filter pipette tips (Starlab) and 1.5 ml tubes (Ambion) were used for all RNA and DNA work. For RNA extraction, 15 ml polypropylene tubes and caps (Sarstedt) were treated overnight with a solution of 0.1 % (v/v) diethyl polycarbonate (DEPC) at ambient temperature to remove RNAse activity, before autoclaving to destroy the DEPC and drying.

2.6.2 RNA isolation

Cultures were grown in 25 cm^2 or 75 cm^2 culture flasks or 10 cm (diameter) dishes as required. Following treatments or at the desired confluence or time point, the culture medium was aspirated and cells were solubilised by addition of 2.5 ml (25 cm^2 flask) or 5 ml (75 cm^2 flask or 10 cm dish) TRIzol® Reagent (Life Technologies). Plastic cell scrapers were used to remove any remaining cells from culture flasks and lysates were collected into 15 ml DEPC-treated polypropylene tubes and stored at -70^oC. Lysates were thawed on ice and then incubated at ambient temperature for 5 minutes to allow for complete dissociation of nucleoprotein complexes. 0.2 ml of chloroform was added for each 1 ml of TRIzol® Reagent used and each tube was vortexed for 15 seconds followed by incubation at ambient temperature for 3 minutes to allow phase solubilisation of RNA. Tubes were centrifuged at 12,000 x g for 15 minutes at 4 ^oC to enable phase-separation and the RNA-containing aqueous phase was carefully collected into a fresh DEPC-treated polypropylene tube, avoiding any contamination from the white interphase (DNA containing) and the pink phenol-chloroform phase (protein and lipid containing). RNA was precipitated by addition of 0.5 ml isopropanol for each 1 ml of TRIzol® Reagent used for lysis. Tubes were gently shaken before incubating for 10 minutes at ambient temperature followed by centrifugation at 12,000 x g for 20 minutes at 4 ^oC. The supernatant was removed and 75 % ethanol was added at a volume equal to the

original lysis volume. Tubes were vortexed to remove salt contaminants and centrifuged at 7,500 x g for 5 minutes at 4^{o}C. The ethanol was gently poured off and the RNA pellet air-dried before resuspending in 20 µl (from a 25 cm^2 flask) or 30 µl nuclease free water (from a 75 cm^2 flask or 10 cm dish) and storing at -80 ^{o}C.

2.6.3 DNAse treatment of RNA

To remove any contaminating DNA from RNA samples, a DNase treatment was performed using the DNA-*free*™ kit (Ambion). 1 µl DNase enzyme and 0.1 volume of x10 DNase buffer was added to each sample before gently mixing and incubating at 37 ^{o}C for 30 minutes. The "DNase inactivation reagent" was resuspended by vortexing for 1 minute before adding 5 µl to each RNA sample, which was then incubated for 2 minutes at ambient temperature before centrifugation at 10,000 x g for 1 minute. The DNA-free supernatant was transferred to a new 1.5 ml tube and the RNA concentration and quality was determined using a NanoDrop™ UV spectrophotometer. RNA samples were stored at -80 ^{o}C.

2.6.4 cDNA synthesis

DNAse-treated RNA was reverse transcribed using the SuperScript®II First-Strand Synthesis System (Life Technologies). 50 ng random hexamer primers were annealed to 1 µg RNA at 65 ^{o}C for 10 minutes, before placing on ice and adding a master mix which gave final concentrations of 2.5 mM $MgCl_2$, 10 mM DTT, 1 mM dNTP mix and 1 x "RT buffer". Each reaction was then incubated at 25 ^{o}C for 2 minutes before adding 50 units of SuperScript®II reverse transcriptase enzyme. An enzyme-negative ("RT negative") control was included for each sample to assess for DNA contamination. Reactions were incubated for 50 minutes at 42 ^{o}C and then 15 minutes at 70 ^{o}C to inactivate the reverse transcriptase. The resulting cDNA was stored at -20 ^{o}C (or -80 ^{o}C for long term storage).

2.6.5 Reverse-transcription Polymerase Chain Reaction (RT-PCR)

2.6.5.1 Primer Design

Transcripts for the genes of interest were identified using "Ensembl Genome Browser" and primers were designed to the selected mRNA sequences using Primer3 (v.0.4.0) software. For each gene of interest, protein-coding splice variants were aligned using EMBL-EBI ClustalW2 sequence alignment programme, to select identical regions and primers were designed within these regions using Primer 3 software. Each set of primers were subjected to a search using Primer BLAST software to ensure target specificity. All primer sequences are detailed in Appendix 3. Since expression of some connexin transcripts are rare or tissue-specific, connexin primers were designed within exons to enable use of genomic DNA as a positive control. Other primers were designed either within an exon or spanning two exons, based on optimal annealing predictions from Primer 3.

2.6.5.2 RT-PCR

All RT-PCR reactions were performed using a T100™ Thermal Cycler (Bio-Rad) and the GoTaq® Hot Start Polymerase system (Promega). In 0.2 ml PCR tubes (Star Lab), 1 µl cDNA sample was added to 19 µl PCR master mix comprising 1 x GoTaq® Flexi Buffer, 2.5 mM $MgCl_2$, 0.2 mM of each dNTP (Life Technologies), 10 µM forward and reverse primers and 0.5 units of GoTaq® Hot Start Polymerase enzyme, made up in nuclease-free dH_2O. PCR reactions were performed in the thermal cycler as follows: 5 minutes at 95 ^{o}C, followed by a suitable number of cycles at 95 ^{o}C for 30 sec, optimum annealing temperature for 30 sec and a 72 ^{o}C extension for 30 sec. A final extension step at 72 ^{o}C was performed for 10 minutes. To determine the optimal annealing temperature of each primer set, a temperature gradient PCR reaction was performed using a positive control sample; cDNA from pooled human cell line total RNA (Ambion), where primers flanked intronic regions, or human genomic DNA (Promega), when primers were contained within an exon. A

temperature range of 55-62^{o}C was tested for each primer pair (optimal annealing temperatures are detailed in Appendix 3). RT-PCR reaction controls included were; an RT-negative for each cDNA sample, a non-template (cDNA negative) control and a positive control of genomic DNA or pooled total cDNA, as appropriate. Primers which amplify the house-keeping genes GAPDH or β-actin were included to demonstrate equivalent loading and where necessary, primers which amplify differentiation-associated genes such as Uroplakin IIIa (UPK3a) were included to confirm successful *in vitro* differentiation of NHU cells.

2.6.5.3 DNA Gel Electrophoresis

Gels were prepared by boiling 0.75-4 % (w/v) agarose in a 1 x TBE buffer (Appendix 2). The percentage of agarose in each gel was selected to allow for best resolution based on amplicon length. SYBR® Safe DNA gel stain (Life Technologies) was added to the liquid agarose at a dilution of 1:10,000 before pouring into a gel cast and removing any bubbles which collected using a pipette tip. Gels were set at ambient temperature for at least 30 min before submerging in 1 x TBE in a gel electrophoresis tank. In the first lane of each gel, 5 µl DNA ladder was loaded to allow estimation of amplicon size; using either Hyperladder™ 100 bp (Bioline) where amplicon length was less than 500 bp, or GeneRuler™ 1 kb (Thermo Scientific) for larger products. 10 µl PCR product was loaded in the remaining lanes and gels were run at 100 V for 1 h, before imaging on a GeneGenius gel imaging system with GeneSnap software (Syngene).

2.6.6 Quantitative RT-PCR (qRT-PCR)

Quantitative or real-time PCR measures the accumulation of PCR products as it occurs (i.e. in real time). SYBR® Green I Dye binds only to double-stranded DNA (dsDNA), where it emits a fluorescent signal proportional to the accumulation of PCR product. 1 µl template cDNA was mixed with 300 nM of target gene forward and reverse primers and 15 µl 2 x SYBR® Green PCR master mix (Applied

Biosystems) which contained SYBR® Green I dye, AmpliTaq Gold® DNA polymerase, dNTPs and buffer components (including a passive reference ROX, which did not bind to DNA). Each PCR reaction was loaded in triplicate into a clear optical 96-well reaction plate, which was sealed with an optical adhesive cover (both Applied Biosystems) before centrifugation. Reactions were performed in an ABI Prism® 7900HT Sequence Detection System and analysed with Sequence Detection System software v2.2 (both Applied Biosystems). The thermal profile used was 95 ^{o}C for 10 minutes, followed by 40 cycles of denaturation for 15 seconds at 95 ^{o}C and elongation for 1 minute at 60 ^{o}C. During each cycle the ABI Prism® detected fluorescence of the SYBR® Green I dye which was normalised against the ROX fluorophore to account for any changes in plate fluorescence which were not linked to product amplification. To verify that single products were formed, a final stage "melt-curve" was included to examine the melting profiles of PCR products, which involved three incubations at 95 ^{o}C, 60 ^{o}C and finally 95 ^{o}C for 15 seconds each. For each experiment, controls were performed in triplicate consisting of; an RT-negative for each cDNA sample, a non-template (cDNA negative) control and a positive control of genomic DNA or pooled total cDNA, as appropriate. Primers which amplified the house-keeping gene GAPDH or β-actin were included to check loading and where necessary, primers which amplify the early differentiation-associated gene Aquaporin 3 (AQP3) were included to confirm successful *in vitro* differentiation of NHU cells.

2.7 Protein Analysis

2.7.1 Immunohistochemistry on paraffin wax-embedded sections

Formalin-fixed paraffin-wax embedded sections of tissues or cell sheets (see 2.5) were de-waxed at ambient temperature by incubating twice in fresh xylene for 10 minutes each, followed by two further xylene incubations for 1 minute each. Tissues were then gradually rehydrated by submersing in 100 % ethanol for three washes (one minute each), 75 % ethanol for one minute followed by rinsing in gently running tap water for 1 minute.

To quench endogenous peroxidase activity from red-blood cells, tissue biopsies were incubated in 3 % (v/v) hydrogen peroxide solution for 10 minutes at ambient temperature before gentle rinsing in running tap water for 10 minutes. This step was omitted for labelling cell sheets due to the lack of endogenous peroxidase activity.

Antigen retrieval was performed by placing slides in a Pyrex® dish containing 350 ml of citric acid buffer, pH 6.0, or 350 ml Tris-EDTA buffer, pH 9.0 (Appendix 2). The Pyrex dish was covered in Saran™ food wrap to prevent evaporation and slides were microwaved for 13 minutes at 900 W (to allow for 10 minutes boiling time), before cooling on ice for 10 minutes. Slides were inserted into Shandon Sequenza® slide racks using coverplates, which allowed for the application of reagents which are held over the specimen until displaced by the next reagent or wash buffer. Slides were washed twice in TBS (Appendix 2) wash buffer before applying 100 µl avidin blocking reagent for 10 minutes, followed by briefly washing in TBS and applying 100 µl biotin blocking reagent for 10 minutes (both Vector Labs), to block endogenous biotin-binding sites within the tissue. After briefly rinsing in TBS, 100 µl of 10 % (v/v) serum from the same species that the secondary antibody was generated in (see table 2.2), was applied to each slide for 5 minutes at ambient temperature. Primary antibodies were diluted in TBS before applying 100 µl to each slide and incubating for 16 h at 4 ^{o}C. For each experiment a negative (primary antibody omitted) control was included and a previously tested positive antibody

was used as a method control. Primary and secondary antibodies were titrated on control tissues to optimise the signal to noise ratio and verify specific labelling. After two washes in TBS to remove primary antibody, biotinylated secondary antibodies (table 2.2) diluted in TBS were applied for 30 minutes at ambient temperature before washing twice in TBS. 100 µl of pre-mixed avidin/biotinylated-HRP complex (Vector labs) was applied to each slide for 30 minutes, which was prepared by mixing 40 µl streptavidin, 40 µl biotinylated horseradish peroxidase in 2.5 ml TBS. Slides were washed once in TBS and once in dH_2O, before preparing the 3,3'-diaminobenzidine (DAB) substrate by dissolving Sigmafast™ DAB tablets in 5 ml dH_2O. 200 µl DAB was added to each slide for 10 minutes, before washing in dH_2O. Slides were removed from the Shandon Sequenza® slide rack and counterstaining in Mayer's haematoxylin for 10 seconds (Appendix 2). Slides were then rinsed thoroughly in tap water and dehydrated in 70 % ethanol for 1 minute, 100 % ethanol for 3 x 1 minute, before clearing in xylene for 2 x 1 minute. Sections were then mounted in DPX and coverslips applied. Slides were examined by bright field microscopy on an Olympus BX60 microscope and digital micrographs were collected.

2.7.2 Indirect Immunofluorescence Microscopy

2.7.2.1. Slide Preparation

Sterilised 12-well glass slides (C.A.Hendley Ltd, Essex) were placed in 4-slide quadriPERM® culture dishes (Sarstedt). NHU cells were seeded at $5x10^3$ cells per well (0.38 cm^2) and left to attach at 37 ^oC for 4 hours before flooding with 5 ml KSFMc and left to grow at 37 ^oC overnight. Cells were cultured to the desired density before treating with differentiating or pharmacological agents (as explained in captions). Cells were washed twice briefly in PBS, and fixed either by:

a) Flooding slides for 30 seconds in a 1:1 mixture of methanol and acetone before air-drying. Slides were either used immediately for immunolabelling or wrapped in SaranWrap™ and stored with silica gel desiccant at -20 ^oC.

or

b) Flooding slides for 10 minutes in 10 % formalin in PBSc (Appendix 2). Formalin-fixed slides were washed twice in PBS for 5 minutes and used immediately for immunolabelling or stored in PBS at 4 ^{o}C for up to 1 week. Immediately prior to labelling, slides were permeabilised by incubation in 0.5 % (w/v) Triton™ X-100 in PBS.

Selection of fixative was based on choice of antibody, due to the susceptibility for damage or epitopes masking.

2.7.2.2 Immunocytochemistry

A grease pen (Cell Path) was used to outline each well of the 12-well slide to prevent antibodies from merging. Primary antibody was diluted in TBS containing 0.1 % (w/v) BSA and 0.1 % sodium azide for preservation. 25 µl of primary antibody was applied to each well and incubated at 4 ^{o}C overnight in a humidified chamber. For each experiment a negative (antibody diluent) control was included and anti-CK7 was used as a positive (method) control. After washing 3 times for 5 minutes in PBS on an orbital shaker, slides were incubated with Alexa-488 or 594-conjugated Goat anti-Rabbit IgG or Goat anti-Mouse IgG secondary antibodies (Table 2.2) for 1 hour at ambient temperature. All slides were protected from light from this stage on using aluminium foil. Slides were washed twice in PBS containing 0.25 % (w/v) Tween®20 for 5 minutes on an orbital shaker before counterstaining nuclei with PBS, containing 0.1 µg/ml Hoechst 33258 for 5 minutes. Slides were then rinsed in PBS for 5 minutes and then in dH_2O for 5 minutes before mounting in antifade mountant (Appendix 2). Since the mountant was non-setting, coverslips were sealed with clear nail varnish. Slides were examined by epifluorescent microscopy on an Olympus BX60 microscope.

2.7.3 Immunoblotting

2.7.3.1 Protein extraction

Cells were cultured in 25 cm^2 flasks or 6 cm dishes according to the experimental plan. Cultures were briefly washed twice in ice-cold PBS before lysis under reducing conditions in 2 x SDS sample buffer, supplemented with 0.2 % DTT and 1 x protease inhibitor cocktail set III (Sigma). 100 µl lysis buffer was applied to each culture and lysates were harvested by scraping into ice-cold microfuge tubes using rubber cell scrapers (Sarstedt). Lysates were sonicated on ice for two 10 second bursts, with a 10 second rest on ice in-between, using a sonic probe at 25 W (Jencons) which was cleaned with 70 % ethanol between samples. Samples were incubated on ice for 30 minutes before micro-centrifugation at 25,000 g for 30 minutes at 4 ^{o}C. Supernatants were aliquotted into clean, ice-cold microfuge tubes and either stored at -20 ^{o}C or immediately processed for protein quantification.

2.7.3.2 Protein Quantification

The protein concentration of lysates was measured using a Coomassie® protein assay kit (Pierce). Samples were diluted in 1/12.5 in dH_2O, and 10 µl of each diluted sample was added in duplicate to a 96-well plate. 10 µl aliquots of BSA of known protein concentrations were applied in duplicate to the 96-well plate to generate a standard curve from which unknown protein concentrations could be calculated (BSA supplied at 2 mg/ml from Pierce). To each well, 200 µl of Coomassie reagent was added, taking care not to introduce air bubbles. 96-well plates were shaken for 30 seconds in a Multiskan Ascent® plate reader (Thermo-scientific) and the absorbance of samples was measured at test and reference wavelengths of 570nm and 630 nm respectively against a blank H_2O control. The Ascent software (version 2.6) was used to estimate the protein concentration of samples by comparison with the standard curve.

2.7.3.3 Protein separation by SDS-Polyacrylamide Gel Electrophoresis (SDS-PAGE)

SDS-PAGE is a technique used to separate linear proteins in a gel on the basis of size. Heating of samples in SDS (with addition of reducing agent) disrupts the tertiary structure of proteins (linearises) whilst coating the protein with a uniform negative charge, so that movement through the gel with current applied is based purely on size. SDS protein lysates were prepared for gel separation under reducing conditions to maintain proteins in a reduced state. 15 µg of protein sample was added to 4 x NuPAGE® LDS sample buffer and 10 x NuPAGE® sample reducing agent (each to a final 1 x dilution), in 1.5 ml tubes with addition of dH_2O as required to ensure loading volumes for each well were identical, before heating the mixtures to 70 ^{o}C for 10 minutes to denature proteins and micro-centrifuging briefly to collect. NuPAGE® 4-12 % bis-Tris or 3-8 % Tris-acetate gels were selected for SDS-PAGE, depending on the molecular weight of the protein to be probed, with Tris-acetate gels used for larger proteins (>100 kD). NuPAGE® pre-cast gels contain a "stacker" gel at the top to concentrate proteins to ensure that they collectively enter the running gel. The running gel is manufactured as a gradient gel, to improve band resolution (by ensuring optimal band separation over a wide range of molecular weights). Protein samples were loaded into the pre-cast wells at the top of each gel which was positioned into an XCell SureLock™ electrophoresis tank, containing 800 ml of 1 x NuPAGE® MOPS or Tris-acetate running buffer, with 200 µl NuPAGE® antioxidant added to the inner chamber. All NuPAGE® reagents and electrophoresis equipment was purchased from Life Technologies. Electrophoresis was performed at 200 V (for bis-tris) or 150 V (for tris-acetate) to separate proteins by according to size, for 1 h at ambient temperature. 6 µl Precision Plus Protein™ ladder (BioRad) was added to the first well in each gel to allow for estimation of protein size.

2.7.3.4 Western Blotting

Immobilon®-FL PVDF membranes (Merck-Millipore) were trimmed to size before activating by rinsing in methanol for 30 seconds, washing in dH_2O and equilibrating

in western blot transfer buffer (Appendix 2). A gel-membrane "sandwich" was assembled into an XCell II™ blot module (Life Technologies) with filter paper and blotting pads according to the manufacturer's protocol, ensure that the gel and membrane were fully contacted and taking care not to introduce air bubbles. The inner chamber of the blot module was filled with transfer buffer and the module was positioned in a tank containing tap water which was surrounded by an ice pack to prevent overheating during transfer. Resolved proteins were electro-transferred from gel to membrane at 30 V for 3 h, after which membranes were briefly incubated in a solution of 0.5 % (w/v) Ponceau red in dH_2O and rinsed thoroughly in dH_2O, to enable visualisation of protein bands to check for successful transfer, equal loading and any air bubbles which may have interfered with transfer.

2.7.3.5 Immunolabelling

Non-specific binding by secondary antibodies was minimised by incubating membranes for 1 h at ambient temperature in blocking solution, with 50 % (v/v) Odyssey® blocking buffer (LI-COR) in TBS. Membranes were probed with rabbit or mouse primary antibodies (table 2.1), diluted in 50 % (v/v) Odyssey® blocking buffer in TBS + 0.5 % Tween®20 and incubated for 16 h on an orbital shaker at 4 ^{o}C. After washing in TBS for 4 x 5 minutes, primary antibodies were visualized by incubation with fluorescent dye-labelled secondary antibodies, AlexaFluor 680 goat anti-rabbit or IRDye800-conjugated goat anti-mouse IgG (Table 2.2), diluted in 50 % (v/v) Odyssey® blocking buffer in TBS + 0.5 % Tween®20 . After briefly washing in TBS, membranes were scanned and fluorescent bands directly quantified using the Odyssey infrared imaging system and associated Odyssey software (v1.1; LI-COR). Band intensities were measured using the Odyssey software by drawing boxes around each protein band to calculate densitometry following background subtraction. Densitometry of β-actin protein was measured on the same blot for use as a loading control to normalise protein loading in each lane. Primary antibody dilutions were optimised by titration, using a known positive control lysate Background as a result of non-specific secondary antibody binding was assessed by

incubating with secondary antibody alone prior to the addition of any primary antibody to the membranes to ensure that no labelling was visible.

2.7.3.6 Stripping and re-probing of membranes

If labelling of blots with multiple antibodies was necessary membranes were stripped by incubating for 30 minutes in high pH western blot recycling buffer (Source Bioscience), diluted 1:10 in dH_2O. After stripping, secondary antibody was applied and the membrane was scanned as above to confirm the removal of primary antibodies.

2.7.4 Co-localisation studies by Proximity Ligation Assay (PLA).

Co-localisation of proteins was detected using the Duolink® In Situ PLA assay kit (Olink Bioscience). The assay utilises short complementary oligonucleotide probes attached to anti-mouse and rabbit secondary antibodies which, when in close proximity (<40 nm), can be ligated and form the basis of a rolling circle amplification reaction, into which fluorescent dNTP's are incorporated.

Cells were seeded and grown on glass slides and fixed as described in section 2.7.2.1. A grease pen was used to outline each well of the 12-well slide to prevent merging of antibodies from adjacent wells. 20 µl of primary antibodies (containing one primary antibody raised in mouse and one primary antibody raised in rabbit, table 2.1) were applied to each well, to assess co-localisation. Incubations were carried out in 4-well quadriPERM® slide box (Sarstedt), for 16 hours at 4 ^{o}C in a humidified atmosphere, before carefully removing the antibodies by pipetting and washing slides three times for 5 minutes on an orbital shaker in Duolink® wash buffer A, at ambient temperature. After tapping off excess wash buffer, anti-mouse IgG (minus) and anti-rabbit IgG (plus) PLA probes (each containing complementary oligonucleotide probes), were combined at a dilution of 1/5 in Duolink® antibody

diluent, before applying 20 µl to each well and incubating for 1 hour at 37 ^{o}C in a humidified atmosphere. After removal of excess PLA probes, slides were washed twice for 5 minutes in Duolink® wash buffer A at ambient temperature. PLA probes were ligated (when in close proximity) by addition of 20 µl of the Duolink® ligation solution to each well (containing 1/5 Duolink® ligation buffer and 1/40 Duolink® ligase enzyme diluted in molecular-grade water), which was incubated at 37 ^{o}C for 30 minutes before washing twice for 2 minutes in Duolink® wash buffer A at ambient temperature and tapping off excess wash buffer. To induce the rolling circle amplification reaction, duolink® amplification solution and polymerase were diluted 1/5 and 1/80 respectively in molecular-grade water and 20 µl was applied per well, for 100 minutes at 37 ^{o}C. From this point the slides were protected from light using aluminium foil. The polymerase solution was then removed and slides were washed on the orbital shaker in Duolink® wash buffer B for 10 minutes, counterstained by incubation in 0.1 µg/ml (w/v) Hoechst 33258, diluted in Duolink® wash buffer B for 10 minutes, followed by one wash in dH_2O for 1 minute. Slides were mounted in antifade mountant (Appendix 2). Epifluorescent microscopy was performed on an Olympus BX60 microscope and co-localisation was determined by the presence of fluorescent spots. For each experiment a positive control reaction was included using antibodies raised against ZO-1 and ZO-1α^{+}, since both antibodies bind to the α^{+} variant of ZO-1 and co-localise on the same protein. Negative controls were included in which no primary antibodies were added, or in which primary antibodies for mouse anti-Cx32 and rabbit anti-Cx43 primary were combined (Cx43 is unable to co-oligomerise with Cx32).

2.8 Functional Studies

2.8.1 TER measurements

NHU cultures were seeded onto 0.45 µm permeable Snapwell™ membranes (Fisher Scientific), at $5x10^5$ cells per 1.1 cm^2 membrane (three to six replicate cultures per experimental condition). Cultures were either differentiated with ABS/Ca^{2+} or cultured as non-difefrentiated controls as described in section 2.2.3.2. For each membrane, 0.5 ml medium was added to the inner chamber and 3 ml to the outer chamber. At 24 hrs post-seeding the growth medium was replaced and maintained for 7-14 days with the growth medium changed every other day. Transepithelial electrical resistance (TER) was measured at various time points over the time course, using an EVOM™ voltohmeter (World Precision Instruments). The TER probe was sterilised in Cidex Plus®, 3.4 % (v/v) gluteraldehyde solution (Civco Medical Solutions), for 20 minutes and equilibrated in 7.5 ml growth medium (as used to culture the cells) for 2 x 5 minutes before readings were taken. The electrical resistance of a blank (no cells) membrane was measured and subtracted from the experimental readings to give a resistance reading generated by the cell sheet alone.

2.8.2 Measuring barrier recovery after wounding

Cells seeded onto Snapwell™ membranes and maintained for 7-14 days as described in section 2.8.1. TER measurements were taken immediately prior to wounding NHU cultures (3-6 replicate cultures). To wound, a single horizontal scratch was created across the full width of the Snapwell™ membrane, using a 100 µl sterile pipette tip to generate a scratch approximately 500-750 µm wide. TER measurements of the wounded cultures were recorded immediately post-scratch, before returning cultures to the incubator. TER measurements of each culture were recorded at intervals of 2-4 hours to observe barrier repair.

2.8.3 Analysis of wound-healing in differentiated cultures using time-lapse microscopy

Cultures grown on 24-well plates were wounded with a single horizontal scratch across the full width of the well, using a 100 µl sterile pipette tip to generate a wound approximately 750-1000 µm wide. 24-well plates were placed into an environmental chamber (Solent Scientific) at 37 ^{o}C with 5 % CO_2 (in air) feed for buffering of medium. Wound-repair was monitored in each well by phase-contrast microscopy using an Olymous IX81 motorised microscope. Images were captured every 2 h over a time-course of 36-48 h using CellM image capture software (Olympus). The image analysis software was then used to measure the initial wound area and serial wound-areas during repair to calculate the percentage wound-closure at various time points. Three to six replicate cultures were measured for each experimental condition and the mean percentage wound closure plotted against time.

2.9 Development of Cx32 knock-down and Cx32 overexpressing Wild-type and Dominant Negative (T134A) Human Urothelial Cells

Cx32 shRNA knock-down cultures and Cx32 overexpressing cultures were generated by retroviral transduction of NHU cells with retroviral particles. For overexpressing cultures, two different transductants were generated. Wild-type Cx32 ($Cx32^{WT}$), for which the coding sequence was cloned from differentiated NHU cells, as well as a dominant negative mutant form, in which a single base substitution generated a "closed-channel" phenotype (Beahm et al. 2006). The dominant negative Cx32 ($Cx32^{T134A}$) was generated by site-directed mutagenesis as described below.

2.9.1 Generation of Cx32 shRNA retroviral vectors

Three different short-hairpin RNA (shRNA) sequences were designed to target the Cx32 transcript for degradation. For gene silencing, shRNA sequences were ligated into the *pSIREN-RetroQ* retroviral vector (Clontech). Included in the *pSIREN retro-Q* vector are the following features (figure 2.2):

- 5' and 3' LTRs necessary for transcription
- The RNA packaging signal ψ^+
- A puromycin resistance cassette for selection in eukaryotic cells
- E-coli Amp^r gene for propagation and selection in bacteria
- A site for insertion of shRNA oligonucleotides, flanked by BamHI and EcoRI restriction sited for directional

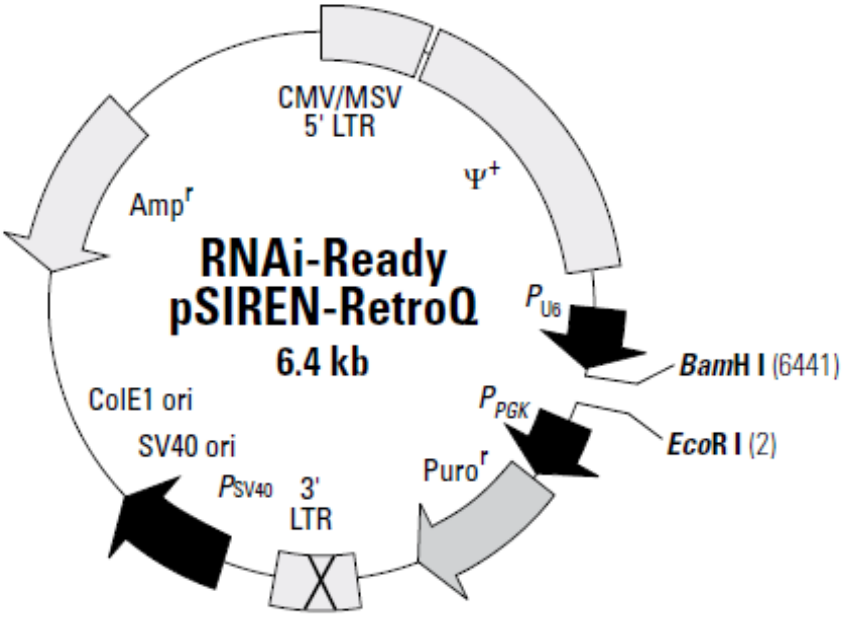

Figure 2.2 Schematic of the pSIREN-RetroQ retroviral vector.

(Image from http://www.clontech.com/images/pt/PT3739-1.pdf)

2.9.1.1 shRNA Oligonucleotide sequence Design

A 269 base pair sequence common to all four human Cx32 transcript variants was used for shRNA design. Two shRNA software packages were used to select three 20-21 base pair target sequences; siRNA target finder (Applied Biosystems) and BLOCK-iT™ RNAi Designer (Life Technologies). shRNA sequence designer software (Clontech) was used to convert the target sequences into short hairpin sequences by addition of the hairpin loop sequence TTCAAGAGA, BamH I and EcoR I restriction site overhangs for directional vector insertion, RNA Pol III terminator sequence (a run of 6 thymidine residues) and an additional Mlu1 restriction site immediately downstream of the terminator sequence to confirm the presence of the cloned insert. Target sense and antisense sequences are detailed in table 2.5 and were purchased from Eurofins Genomics.

Cx32 shRNA id	Full shRNA oligonucleotide (5' – 3') (Sense strand)
shRNA 1	gatccAATGAGGCAGGATGAACTGGATTCAAGAGATCCAGTTCATCCTGCCTCATTTTTTTTACGCGTg
shRNA 2	gatccAACTGGACAGGTTTGTACACCTTCAAGAGAGGTGTACAAACCTGTCCAGTTTTTTTTACGCGTg
shRNA 3	gatccGCCGGCATTCTACTGCCATTTTCAAGAGAAATGGCAGTAGAATGCCGGTTTTTTACGCGTg

Table 2.5 shRNA oligonucleotides.

Specific Cx32 target sequences are underlined

2.9.1.2 Annealing shRNA Oligonucleotides

Each shRNA oligonucleotide sequence was resuspended in nuclease-free water to a concentration of 100 µM. Top and bottom strands were mixed in a 1:1 ratio (to give a 50 µM concentration of double stranded oligonucleotide) and heated in a thermal cycler for 30 seconds at 95 ^{o}C (to remove secondary structure) followed by annealing (hybridisation) for 2 minutes at 72 ^{o}C, 2 minutes at 37 ^{o}C and finally 2 minutes at 25 ^{o}C before storing on ice.

2.9.1.3 Ligation of double-stranded Oligonucleotides into pSIREN-RetroQ

Annealed oligos were ligated into RNAi-Ready pSIREN-RetroQ vectors by incubation of the following ligation mixture at ambient temperature for three hours:

1 µl diluted, annealed oligonucleotide (0.5 µM) or nuclease-free water (negative control), 2 µl linearised pSIREN-RetroQ vector (25 ng/µl), 1.5 µl 10x T4 DNA ligase buffer (Promega), 1 µl T4 DNA ligase (3 U/µl; Promega) and 9.5 µl nuclease-free water.

2.9.1.4 Transformation of Chemically Competent E-coli

2 µl of ligated vector mixture was added to 50 µl XL-1 Blue (*Escerichia Coli*) chemically competent cells (Stratagene) in Falcon 2059 polypropylene tubes. Vials were tapped gently to evenly distribute and incubated for 30 minutes on ice. A negative cell-only control was included. Cells were transformed by heat-shock for 30 seconds in a water bath at 42 ^{o}C before immediately returning to ice. 250 µl SOC medium (Life Technologies) was added to promote membrane repair and the mixture was shaken at 250 rpm for 60 minutes at 37 ^{o}C. 5-50 µl from each transformation was plated onto LB-agar plates (Appendix 2) containing 100 µg/ml ampicillin, for 16 hours at 37 ^{o}C.

2.9.1.5 Amplification of Plasmid DNA

Five single, isolated colonies were selected from each plate and used to inoculate 5 ml LB-liquid cultures (Appendix 2) containing 100 µg/ml ampicillin, for 16 hours at 37 ^{o}C with shaking at 250 rpm.

2.9.1.6 Glycerol Stocks

For long-term storage of transformed bacteria, glycerol stocks were prepared by mixing 750 µl cell suspension (section 2.9.1.5), with 250 µl sterile 80 % (v/v) glycerol in dH_2O into a cryovial (Sarstedt) and storing at -80 ^{o}C. To recover cells from a frozen glycerol stock, a small "stab" of frozen stock was streaked onto LB-agar

plates containing 100 µg/ml ampicillin and plates were incubated at 37 ^{o}C overnight, before amplifying plasmid DNA as described in section 2.9.1.5.

2.9.1.7 Purification of Plasmid DNA

Plasmid DNA was purified using a spin-column system which captures plasmid DNA on a spin column, following bacterial cell lysis. Bacterial cells were pelleted from 5 ml liquid cultures (section 2.9.1.5) by centrifugation at 1100 x g for 10 minutes and the supernatant was discarded. Plasmid DNA was extracted and purified using the "QIAprep® Spin Miniprep Kit" according to manufacturer's recommendations (Qiagen). Bacterial cells were resuspended in 250 µl of buffer "P1" (resuspension solution) containing RNase A (to remove RNA) and transferred into a microcentrifuge tube. 250 µl of lysis buffer "P2" was added and the reaction which contains SDS to induce cell lysis. The reaction mixture was gently mixed by inverting the tubes several times over a 5 minute period (at ambient temperature). 350 µl neutralisation solution buffer "N3" was added and cell debris/chromosomal DNA was pelleted by centrifugation at 9500 x g for 10 minutes. The clear supernatant was added to the QIAprep® spin column and centrifuged at 9500 x g for 60 s to bind plasmid DNA to the column. After a wash step in 750 µl "buffer PE" the purified plasmid was eluted in a clean 1.5 ml microcentrifuge tube by addition of 50 µl nuclease-free water followed by centrifugation at 9500 x g for 1 minute. The plasmid DNA concentration was determined using a NanoDrop™ UV spectrophotometer.

2.9.1.8 Screening plasmid DNA for shRNA insertion

Purified plasmid DNA was tested for successful shRNA insertion by restriction analysis of the Mlu1 restriction site, positioned downstream of the terminator sequence in the shRNA. Each restriction digest was set up in nuclease-free 1.5 ml microcentrifuge tubes, containing: 1 µl Mlu1 enzyme (10 units) and 2 µl 10x restriction enzyme buffer (both New England Biolabs) with 5 µl miniprep plasmid

DNA and 12 µl nuclease-free water. In control digests restriction enzyme was replaced with nuclease-free water. Digests were incubated at 37 ^{o}C for 3 hours before running on a 1 % (w/v) agarose gel (section 2.6.5.3).

The pSIREN-RetroQ vector does not contain an internal Mlu1 restriction site, therefore successful shRNA insertion was confirmed in plasmid DNA from the difference in migration into the gel between the faster migrating uncut plasmid DNA (control digest) and the slower migrating linear cut DNA (Mlu1 digest).

2.9.2 Generation of Cx32^{WT} overexpression vector

For overexpression studies the full-length coding sequence of Cx32 was cloned from differentiated NHU cells and ligated into the multiple cloning site of the *pLXSN* retroviral overexpression vector (Clontech). Included in the *pLXSN* vector are the following features (figure 2.3):

- 5’ and 3’ LTRs necessary for transcription
- The RNA packaging signal ψ^{+}
- A neomycin (G418) resistance cassette for selection in eukaryotic cells
- E-coli Amp^{r} gene for propagation and selection in bacteria
- A multiple cloning site with EcoRI, HpaI, XhoI and BamHI restriction sites

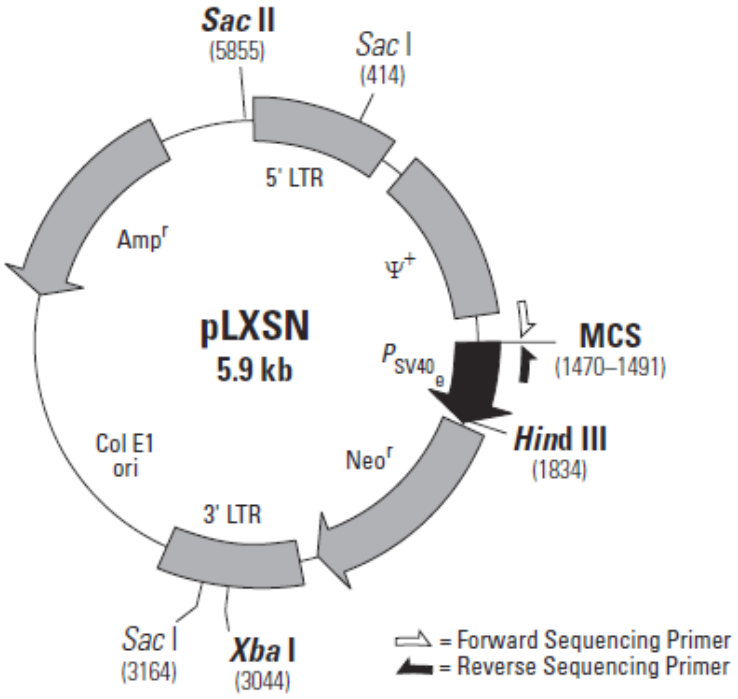

Figure 2.3 Schematic of the pLXSN retroviral vector.

(Image from www.clontech.com/products/cat/HTML/1076.shtml*).*

2.9.2.1 Primer design for Cx32 cloning

Primers were designed to flank the full length protein coding sequence of Cx32, with the forward primer containing the first 24 nucleotides of Cx32 and the reverse the last 21 nucleotides, since this gave a very similar annealing temperatures for the two primers. An EcoRI restriction site was added to the forward primer and a BamHI site to the reverse, to enable directional cloning into pLXSN and it was verified that neither restriction sites were present within the Cx32 coding sequence using restriction digest prediction software (RestrictionMapper v3.0). To aid initiation of translation, a Kozak sequence (ACC) was inserted to the forward primer immediately prior to the start codon and to preserve the restriction sites, 6 extra bases (all A's) were added to the primers upstream of the restriction site. The resultant cloning primers were purchased (Eurofins Genomics) with the following

sequences (restriction sites are underlined, Cx32 cloning components are in capital letters):

Fwd 5'-3': aaa aaa gaa ttc acc ATG AAC TGG ACA GGT TTG TAC ACC

Rev 5'-3': aaa aaa gga tcc TCA GCA GGC CGA GCA GCG GTC;

2.9.2.2 PCR amplification of Cx32 cDNA

Cx32 was amplified from cDNA extracted from Y1151 NHU cells, following differentiation with 5 % ABS and 2 mM Ca^{2+}. The "Expand High Fidelity PCR System" was used (Roche), in which the polymerase has proofreading activity to ensure high fidelity. Each PCR reaction contained 0.3 µM forward and reverse primers, 0.2 mM of each dNTP (Life Technologies), 5 % DMSO, 1 X Expand PCR buffer, 0.375 µl Expand Taq polymerase and 1 µl cDNA diluted in nuclease-free water to a final reaction volume of 25 µl. Duplicate PCR reactions were performed in the thermal cycler as follows: 2 minutes initial denaturation at 94 ^{o}C, followed by 35 cycles of denaturation at 94 ^{o}C for 30 sec, 61 ^{o}C annealing for 30 sec and a 72 ^{o}C extension for 60 sec. A final extension step at 72 ^{o}C was performed for 7 minutes. One of the completed PCR reactions was examined in a 1 % agarose gel as described in section 2.6.5.3, to verify a single band product of 852 base pairs, once verified, the remaining reaction was processed for purification.

2.9.2.3 Purification of PCR products

Amplicon was purified from the PCR reactions (section 2.9.2.2) using a QIAquick® PCR purification kit (Qiagen), which purifies and concentrates PCR products up to 1 kb in size. The 25 µl PCR reaction mixture was combined with 125 µl buffer PB and loaded on to a QIAquick column which was centrifuged for 60 seconds at 9500 x g, in a table-top microcentrifuge to bind DNA. To wash, 750 µl of PE wash buffer was added to the column and centrifuged for 60 seconds at 9500 x g, before discarding the flow through and centrifuging again for 30 seconds at 13,000 rpm to remove residual wash buffer. QIAquick columns were then placed into clean 1.5 ml

microcentrifuge tubes and the DNA eluted by adding 50 µl nuclease free water to the column and centrifuging for 1 minute at 13,000 rpm. The DNA concentration was determined using a NanoDrop™ UV spectrophotometer.

2.9.2.4 TA cloning into the expression vector pGEM®T Easy

The pGEM®T Easy expression vector was used for sub-cloning of the Cx32 PCR product. The vector contains the following features (see figure 2.4):

- T7 and SP6 RNA polymerase transcription initiation sites
- Ampicillin-resistance gene for colony selection
- 3' Thymidine overhangs for TA-cloning of PCR products

Cx32 PCR product was ligated into the pGEM®T Easy cloning vector by incubation of the following ligation mixture at 4 ^{o}C for 16 h; 3 µl PCR product (or nuclease-free water background control), 1 µl pGEM®T Easy vector (50 ng), 5 µl 2x rapid T4 DNA ligase Buffer (Promega), 1 µl T4 DNA ligase (3 U/µl; Promega).

E-coli were transformed with the Cx32-pGEM®T Easy ligation mixture and plasmid DNA was amplified and purified as described in sections 2.9.1.4 to 2.9.1.7.

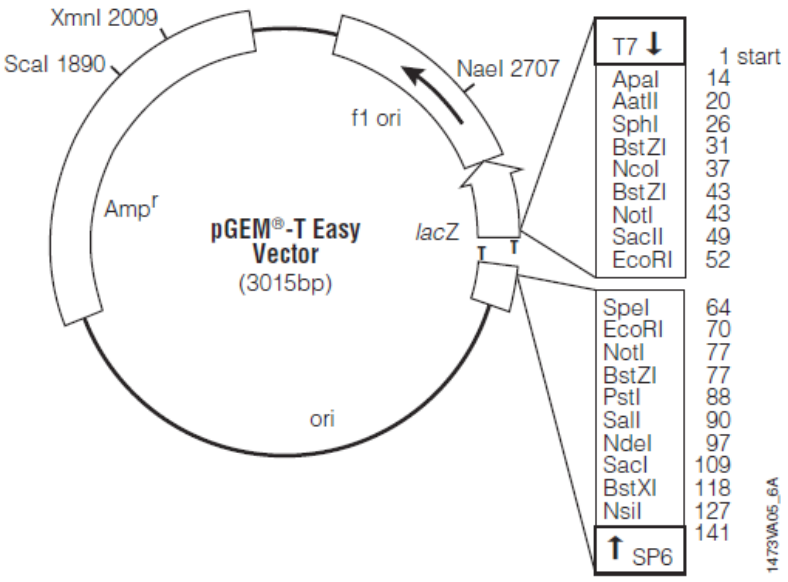

Figure 2.4 pGEM®T Easy Vector Map.

(Image from: http://www.promega.com)

2.9.2.5 Screening Plasmid DNA for Insertion of Cx32 by sequencing

To assess the presence and sequence fidelity of Cx32 in pGEM®-T easy following ligation, 300 ng purified plasmid DNA was sequenced using an Applied Biosystems 3130XL Genetic Analyser, with sequencing primers specific to regions within the T7 and SP6 RNA polymerase binding sites found up- and downstream of the multiple cloning site in pGEM®-T easy (fig 2.4). Sequencing was performed by Celina Whalley in the Technology Facility. The resulting sequencing data was analysed using Chromas software (v1.45), comparing both sense and antisense strands with the published Cx32 coding sequence (from Ensembl).

2.9.2.6 Restriction Digests for Subcloning of Cx32 into the pLXSN Overexpression Vector

Restriction digests were set up to cut Cx32 from the pGEM®-T Easy vector and to linearise the pLXSN vector for subcloning. 5 µl purified plasmid DNA (either pLXSN or pGEM®-T Easy-Cx32) was combined with 0.5 µl EcoRI restriction enzyme, 2 µl 10x EcoRI buffer, 0.2 µl BSA (all Promega) and 12.3 µl nuclease-free H_2O in 1.5 ml microcentrifuge tubes and incubated for 3 h at 37 ^{o}C. Digest reactions were "cleaned" to remove digest enzyme and buffers as detailed in section 2.9.2.3. DNA was eluted in 17 µl nuclease-free H_2O and a second digest was performed by adding 0.5 µl BamHI enzyme, 2 µl 10 x BamHI buffer and 0.2 µl BSA (all Promega) to the eluate and incubating for 3 h at 37 ^{o}C. Digested pLXSN and pGEM®-T Easy-Cx32 products were loaded into a 0.75 % agarose gel and electrophoresis was performed at 90 V for 1 h to separate bands (as described in section 2.6.5.3), using a wide gel comb to enable all DNA to be loaded onto the gel. Linearised pLXSN and Cx32 bands were then excised during brief viewing on a UV transilluminator, using a clean disposable scalpel for each band.

2.9.2.7 DNA Purification by Gel Extraction

Excised bands were placed into a 1.5 ml nuclease-free microfuge tube and weighed. DNA was purified from gel fragments using a QIAquick® Gel extraction Kit (Qiagen). 300 µl buffer QG was added to each tube per 100 mg gel present and the gel slices were dissolved by incubation at 50 ^{o}C for 10 minutes. The resulting solution was then diluted 1:1 with isopropanol and mixed, before loading onto a QIAquick spin column and centrifuging for 1 minute at 13,000 rpm in a bench-top centrifuge to bind DNA to the column. The flow-through was discarded and the DNA was washed by adding 750 µl Buffer PE to the column and centrifuging again for 1 minute, before discarding the flow through. Elution of DNA was performed by placing the column into a clean microfuge tube and adding 20 µl nuclease-free water, before centrifuging for 1 minute. The final DNA concentrations were determined using a NanoDrop™ UV spectrophotometer.

2.9.2.8 Subcloning of Cx32 into the pLXSN Overexpression Vector

The Cx32 coding sequence was ligated into pLXSN by combining 30 ng purified, linearised pLXSN plasmid with 13 ng purified Cx32 DNA with 1.5 µl 10 x T4 DNA ligase buffer and 0.5 µl T4 DNA ligase (both Promega), in a total volume of 15 µl and incubating for 16 h at 4 ^{o}C. pLXSN-Cx32 plasmid DNA was amplified and purified as described in sections 2.9.1.4 to 2.9.1.7. Insertion of the correct Cx32 sequence and orientation was verified by sequencing as described in section 2.9.2.5.

2.9.3 Generation of the Dominant Negative Cx32^{T134A} overexpression vector

In addition to generating the Cx32-pLXSN overexpression vector, a second mutant overexpression vector was generated, Cx32^{T134A}-pLXSN. This dominant-negative form of Cx32 is non-functional with a channel-closed phenotype, but retains the ability to be correctly synthesised and trafficked into Cx32 gap junctions (Beahm et al. 2006). A single base-pair mutation was performed, altering the Threonine in position 134 to an Alanine (T134A mutant) to generate the desired mutant. To achieve this, site directed mutagenesis (SDM) was performed using a Single-Primer Reactions In Parallel (SPRINP) technique described below, in a technique adapted from a previous study (Edelheit et al. 2009), see figure 2.6.

2.9.3.1. SDM Primer design

Primers were designed using Primer X software (*www.bioinformatics.org/primerx)* to produce a single base-pair substitution, in which the bases to be mutated were in the centre of both primers (highlighted below). The T134A mutation was performed by converting the sense sequence from ACC to GCC (underlined below). Primers were ordered from MWG Eurofins.

Fwd (5'-3') GGACACTGTGGTGGGCCTATGTCATCAGC

Rev (5'-3') GCTGATGACATAGGCCCACCACAGTGTCC

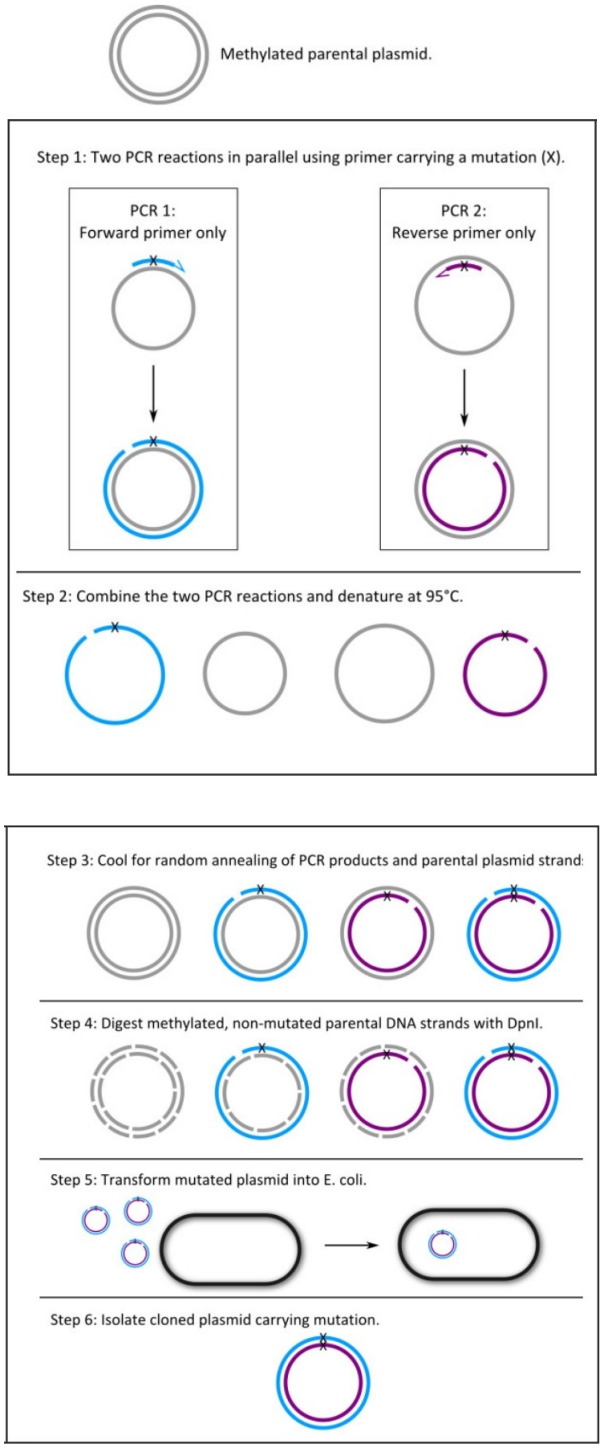

Figure 2.5 Flow chart of the single-primer site-directed mutagenesis method.

Image adapted from Edelheit et al. (2009). The parental plasmid is shown in grey and the two PCR synthesised strands are shown in blue and purple. The letter x marks the position of the mutation.

2.9.3.2. Site-directed mutagenesis

Wild-type Cx32 cDNA was cloned into the pGEM®-T Easy expression plasmid as described in 2.9.2. Purified plasmid DNA was isolated from XL1-Blue cells (Stratagene), which have a dam^+ (wild-type) genotype encoding Dam methylase. This was necessary since the method requires methylated parental DNA to provide a distinction between parental and newly synthesised (mutant) DNA strands.

Forward and reverse primer reactions were set up in parallel (separate tubes) to prevent binding of the forward and reverse primers which would otherwise reduce the yield of successful transformants. PCR reactions were set up using Expand High Fidelity PCR system (Roche) as described in table 2.6 using a Biorad T100™ thermal cycler. After an initial denaturation step of 94 ^oC for 2 minutes, PCR was performed for 30 cycles with a denaturation step of at 94 ^oC for 40 s, primer annealing at 65 ^oC for 40 s and template extension phase at 72 ^oC for 4 minutes. A final 10 minute extension phase was included at 72 ^oC.

Reaction products were then combined to give a total reaction volume of 50 µl and the reaction was heated to 95 ^oC for 5 minutes in the thermal cycler to separate the PCR products from the template strands, followed by slow cooling to 37 ^oC (1 min at 90 ^oC, 1 min at 80 ^oC, 30 s at 70 ^oC, 30 s at 60 ^oC, 30 s at 50 ^oC, 30 s at 40 ^oC and held at 37 ^oC), to promote random annealing of parental strands and PCR products.

Component	*Reaction 1*	*Reaction 2*
Cx32-pGem®T plasmid DNA	500 ng	500 ng
Forward primer	300 nM	-
Reverse Primer	-	300 nM
dNTPs	200 nM	200 nM
Expand High Fidelity Buffer (10x) with 15 mM $MgCl_2$	1X	1X
Expand High Fidelity Enzyme	1.3 Units	1.3 Units
Nuclease-free water	19.875 µl	19.875 µl
Reaction Volume	25 µl	25 µl

Table 2.6 Site-directed mutagenesis PCR reaction components.

Forward and reverse reactions were set up in parallel separate tubes (Reactions 1 and 2) and PCR performed with forward and reverse primers which incorporate the mutated base.

2.9.3.3. Digestion of Parental DNA strands

The combined reaction mixture was divided between two PCR tubes (25 µl per tube) and a restriction digest was performed on one of the 25 µl aliquots to digest methylated parental strands by addition of 15 units DpnI enzyme, 0.1 µg/ml acetylated BSA and 1X DpnI restriction enzyme buffer (all Promega) for 16 h at 37 ^{o}C. The second aliquot was also set up as a non-digested control (by replacing the DpnI enzyme with nuclease-free water). The resulting DNA fragments were purified using a PCR clean-up column (section 2.9.2.3) to remove digested nucleotides and enzyme reagents, before running on a 1 % gel by electrophoresis (section 2.6.5.3) to confirm the removal of methylated DNA leaving only nicked-plasmid DNA (non-methylated).

2.9.3.4 Plasmid Transformation and isolation

Mutated plasmid DNA was transformed into E.coli for amplification and nick-repair, before purification (sections 2.9.1.4 to 2.9.1.7). Sequencing in both forward and reverse directions (as described in 2.9.2.5), was performed to confirm whether the cDNA carried the desired mutation and to check that the cDNA did not carry any other mutation. The digested $Cx32^{T134A}$ fragment was subcloned into the pLXSN overexpression vector (sections 2.9.2.6 - 2.9.2.8).

2.9.4 Transfection of Retroviral Vectors into the RetroPack™ PT67 Packaging Cell Line

All retroviral work (transfections and transductions) was performed in a Biosafety Level 2 safety cabinet with containment level 2 working practices.

Viral gag, pol and env genes necessary for particle formation and replication are stably integrated into the genome of RetroPack™ PT67 cells (Clontech) and are maintained by HAT selection (section 2.2.4). When transfected with a retroviral vector, PT67 cells produce high-titre replication-incompetent viruses, which may be collected and used to infect target cells.

PT67 cells were maintained in T25 culture flasks in DMEM (GIBCO) supplemented with 10 % FBS and 1 % L-glutamine in a humidified atmosphere at 37 ^{o}C and 10 % CO_2 in air. All tranfections were performed using Effectene® reagent (Qiagen). Transfection medium was generated by adding 5 µg plasmid DNA to 150 µl buffer EC and 40 µl enhancer and incubating for 5 minutes at ambient temperature. 50 µl of Effectene® transfection reagent was added and the mixture was vortexed briefly before incubating for 10 minutes at ambient temperature. This mixture was then added to 5 ml growth medium and used to transfect packaging cells. At approximately 60 % confluence, medium was aspirated from the PT67 packaging cells and replaced with the transfection mixture before returning the culture to the incubator for 16 hours. The transfection mixture was removed from the cells and replaced with growth medium and after a further 24 hours, cells were passaged at a

split ratio of 1:3 and subjected to antibiotic selection in growth medium containing 0.5 mg/ml G418 (for pLXSN vector) or 4 µg/ml puromycin (for pSIREN-RetroQ vector). Mock-transfected cells (lacking retroviral vectors) were generated as control cultures for antibiotic selection. Empty-vector pLXSN and control shRNA-pSIREN-RetroQ (Clontech) were transfected as vector controls. Following transfection, packaging cells were maintained in growth medium containing antibiotic at a reduced maintenance concentration of 0.05 mg/ml G418 or 0.25 µg/ml puromycin (as appropriate) to retain selection pressure.

2.9.5 Retroviral Transduction of NHU Cells

The growth medium was aspirated from T75 flasks containing 100 % confluent cultures of PT67 cells transfected with empty or recombinant plasmids and replaced with 10 ml of antibiotic-free medium consisting of equal volumes of DMEM:RPMI with 5 % FBS and 1 % L-glutamine for 16 hours. Virus was harvested by removing the culture medium from the packaging cells and passing through a 0.45 µM Acrodisc® syringe filter to remove cell debris. To enhance retroviral infection the virus-containing medium was supplemented with 8 µg/ml Polybrene (hexadimethrine bromide, Sigma). Growth medium was removed from 50-60 % confluent NHU cultures and replaced with the virus-containing medium before returning the cultures to the incubator for 6 hours, before replacing medium with KSFMc. 48 hours post-infection, NHU cells were passaged 1:3 and subjected to antibiotic selection in growth medium containing 0.1 mg/ml G418 (for pLXSN vector) or 0.5 µg/ml puromycin (for pSIREN-RetroQ vector). Mock-transduced cultures (lacking retroviral vectors) were generated as control cultures for antibiotic selection. Following transduction, cells were maintained in growth medium containing the relevant antibiotic to prevent out-growth from non-transfected cells.

One to two weeks post-transduction, the growth medium was replaced with antibiotic-free complete medium. After an overnight incubation, this medium was harvested and used to infect NHU cells using the above transduction protocol and selected in antibiotic to test for the absence of retroviral production. Transduced

NHU cells were then returned to level 1 containment and routinely cultured in the relevant antibiotic to maintain selection pressure.

3. Characterisation of Connexin Expression and Distribution in Human Urothelial Cells *In vitro* and *In vivo*

The biological requirements of different tissues will likely necessitate differences in the capacity of GJIC and connexin expression. Distribution of connexins is extremely variable amongst epithelia and further, compartmentalisation of expression is observed within stratified epithelia (for example in skin and gut), suggesting that selective compartments for communication are set up. An assessment of Cx expression in human urothelium has not previously been reported.

3.1. Aims

The overall aims of this chapter were to use previously characterised in vitro systems to assess connexin expression in human urothelium. More specifically:

- To define the connexin genes expressed by normal human urothelial cells *in vitro* using well characterised culture systems to replicate non-differentiated and differentiated cell phenotypes *(section 3.3)*
- To determine the expression of specific connexin genes in human urothelium *in situ (section 3.3)*
- To examine the expression of specific connexin proteins whose function may contribute to a differentiated urothelial phenotype using two *in vitro* models to mimic urothelial differentiation *(section 3.4)*
- To examine the distribution of specific connexin proteins of interest in native urothelium *(section 3.5)*
- To predict potential transcriptional regulators of connexin expression following differentiation *in vitro (section 3.6)*
- To determine if expressed connexins assemble into functional gap junctions in human urothelial cells *(section 3.7)*

3.2. Experimental Approach

RT-PCR was used to assess transcript expression of each of the known human connexin genes in non-differentiated NHU cells (grown in KSFMc) and NHU cells differentiated using the two methods: ABS/Ca^{2+} and TZ/PD described in detail in section 2.2.3). Differentiation was verified by expression of uroplakin 3a *(UPK3a)* or aquaporin 3 *(AQP3)* transcripts. Transcript expression of specific connexins of interest was also studied in freshly isolated (P0) urothelium.

On the basis of this data, the spatio-temporal regulation of Cx32 expression during NHU cytodifferentiation *in vitro* was examined by quantitative RT-PCR (RTqPCR), immunocytochemistry and western blot analyses of NHU cells differentiated using both methods. Western blot and immunocytochemistry analysis of Cx32 was performed using a monoclonal antibody which recognises the C-terminal domain of both monomeric and dimeric Cx32 products.

The PPARγ-dependency of Cx32 gene and protein expression was studied using T0070907, a specific and potent inhibitor of PPARγ which binds covalently to the ligand binding region (at cysteine 313), inducing a conformational change which irreversibly blocks the recruitment of transcriptional cofactors. The dose of T0070907 selected for use was previously titrated in our laboratory and was demonstrated to specifically block expression of PPARγ-driven genes in NHU cells in a dose dependent manner (Varley et al. 2006). For quantitative RT-PCR studies, *AQP3* gene expression was used to confirm induction of differentiation (Rubenwolf et al. 2012) and for immunoblot analysis, the tight junction protein claudin 5 was used (Varley et al. 2006).

Immunohistochemistry of Cx32 in native human bladder and ureter was performed to establish whether distribution of Cx32 within the multi-layered urothelium was associated with differentiation stage *in situ*.

A transcription factor prediction binding database (JASPAR) was used to predict potential regulators of Cx32 expression during NHU cell differentiation, with search parameters limited to transcription factors that have been previously demonstrated to promote urothelial cytodifferentiation in human and mouse (Varley et al. 2004b, Varley et al. 2009, Bell et al. 2011, Böck et al. 2014).

Finally, the functionality of gap junctions in non-differentiated and differentiated NHU cultures was examined using a method to examine intercellular communication by transfer of labelled dyes between cells, known as the Scrape-Load Dye-Transfer (SLDT) method.

SLDT method

This technique provides a useful screening tool for determining the presence/absence of functional gap junctions. A membrane-impermeable low-molecular weight dye (such as lucifer yellow, MW=457.2 Da) is added to the culture medium before scratching a confluent cell culture with a scalpel. The membranes of cells along the scratch wound are temporarily damaged, but rapidly reseal, thereby introducing dye into the cells. If cells are communication competent, the dye will be transferred to neighbouring cells. Concurrent loading with a high molecular weight dye (rhodamine-dextran, MW=4 kDa) is used to verify that dye-transfer of lucifer yellow is via gap junctions; as rhodamine-dextran is unable to pass through the relatively narrow channels (Fig 3.1). Dye transfer occurs within minutes and both dyes are lysine fixable which allows the assay to be terminated at fixed time-points after scraping, for analysis by fluorescence microscopy.

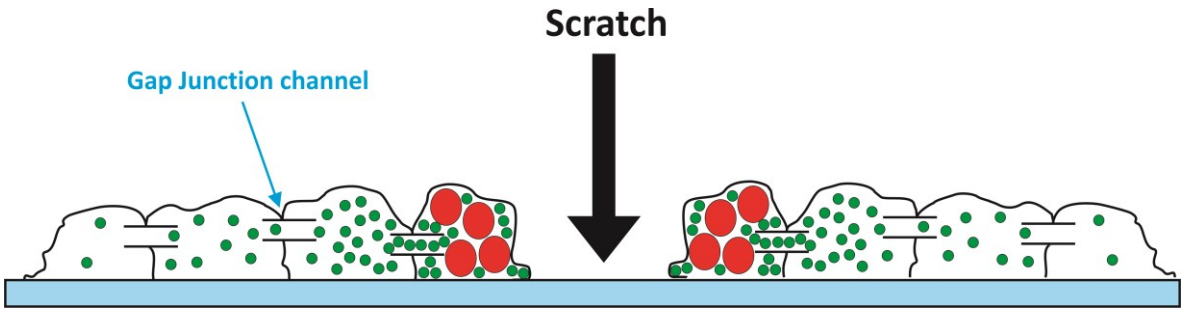

Figure 3.1 Schematic to demonstrate theory of scrape-load dye-transfer.

Cell monolayers are scraped in the presence of lucifer yellow (shown in green, gap junction permeable) and rhodamine-dextran (shown in red, gap junction impermeable).

SLDT was optimised for NHU cells by adapting a basic method as detailed in methods section 2.4 (el-Fouly et al. 1987). Assessment of ABS/Ca^{2+}-differentiated cultures by SLDT was not performed due to the technically challenging nature of performing cell counts with highly stratified cultures; therefore the TZ/PD method of differentiation was selected for SLDT studies, since they retain a monolayer aspect.

Results

3.3 Expression of Connexin Genes in Normal Human Urothelial Cells *in vitro* and *In Situ*

3.3.1 RT-PCR Screen to Assess Expression of Connexin Genes in Proliferating and Differentiated NHU Cell Cultures

An RT-PCR screen of two independent ureteric NHU cell lines harvested in proliferating (non-differentiated) and differentiated (using the ABS/Ca^{2+} method) states, confirmed that of nineteen human connexin genes assessed, eight were expressed by cultured NHU cells (Fig 3.2). Those expressed were: Cx26, Cx30, Cx30.3, Cx31.1, Cx31.9 Cx32, Cx43, and Cx45.

Cx25, Cx30.2, Cx31, Cx36, Cx37, Cx40, Cx40.1, Cx47, Cx50, Cx59 and Cx62 were not expressed. Successful attainment of differentiation was confirmed by an increase in the expression of *UPK3a* transcript. Cx32 and Cx31.9 transcripts were upregulated in response to differentiation. Five of the eight connexins expressed belonged to the β-subclass group of connexins.

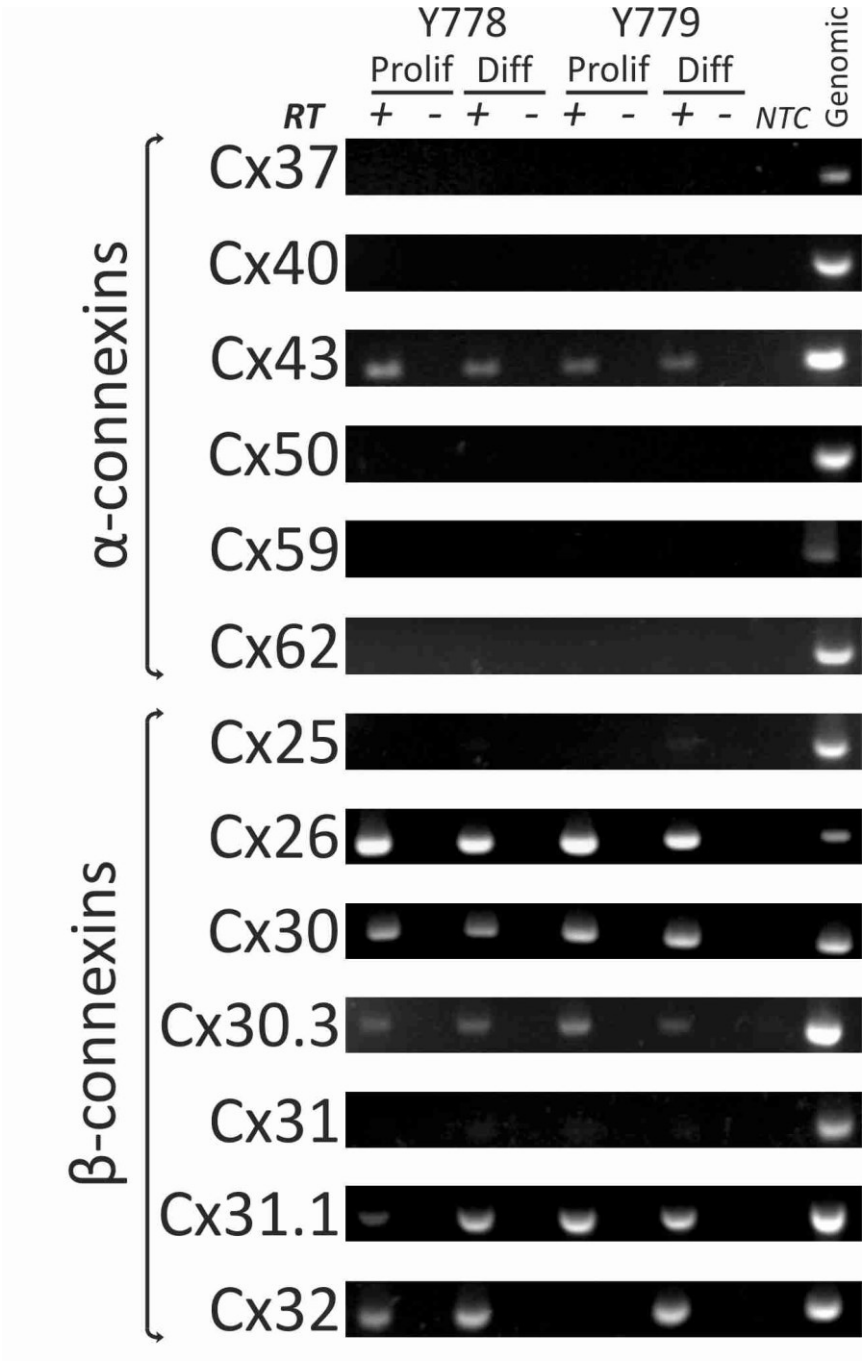
Y778
Y779
Prolif
Diff
Prolif
Diff
RT
+ - + - + - + -
NTC
Genomic
α-connexins
Cx37
Cx40
Cx43
Cx50
Cx59
Cx62
β-connexins
Cx25
Cx26
Cx30
Cx30.3
Cx31
Cx31.1
Cx32

Continued

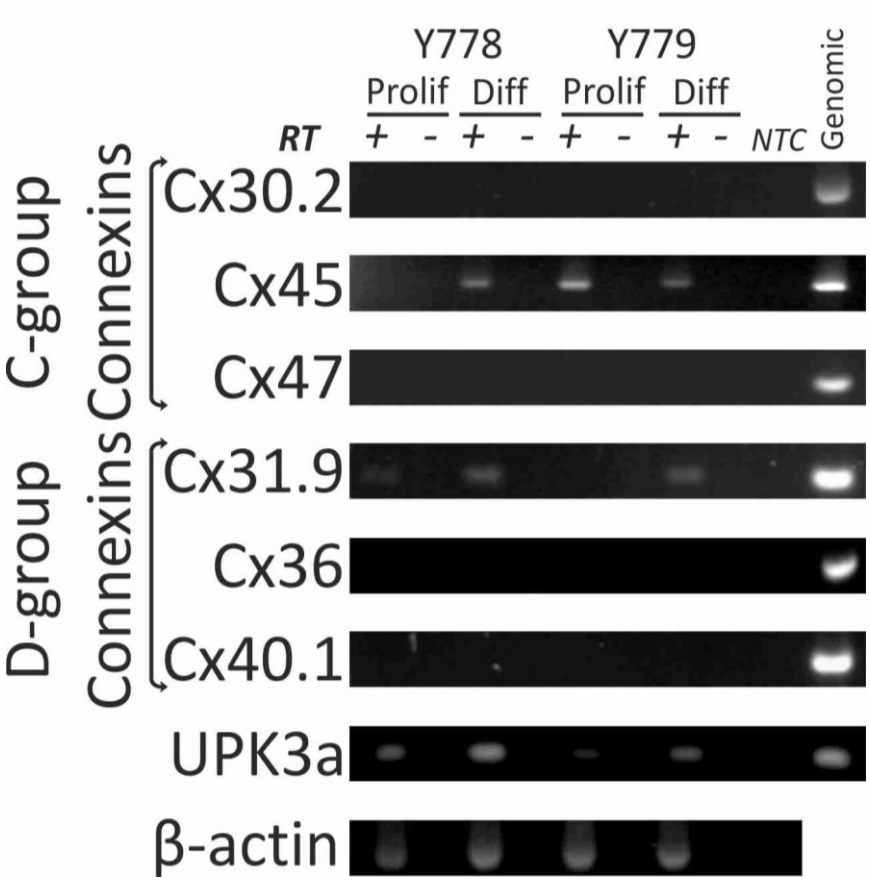

Figure 3.2 RT-PCR Screen to Assess Connexin Expression in Proliferating and Differentiated NHU cell cultures. RNA was extracted from ureteric-derived Y778 and Y779 NHU cells cultured in KSFMc (Prolif) or following differentiation in 5% ABS and 2 mM Ca^{2+} (Diff). RT-PCR was performed to amplify 19 human connexin gene products. For presentation the connexin genes are split into α, β, C and D subclasses. Reaction controls included an RT-negative for each RNA sample (RT-), a no-template water control (NTC), a β-actin loading control and a Uroplakin IIIa (UPK3a) control to confirm urothelial differentiation status. Human genomic DNA was used as a positive control since all primers (with the exception of β-actin) were designed to amplify gene products confined within an exon (and common to all splice variants). Products result from 28-31 PCR cycles.

3.3.2 RT-PCR Screen to Assess Expression of Connexin Genes *In Vitro* and *In Situ*

To characterise the expression of the eight connexins with identified expression in NHU cells, RT-PCR was performed to study transcript expression in freshly isolated urothelium (P0), as well as in cultured NHU cells isolated from a donor bladder sample (Y930). Phase contrast micrographs of Y930 NHU cultures taken immediately before harvesting for RNA extraction showed that when grown in KSFMc, cells grew as a monolayer culture with a pavement-like morphology and phase-bright cell borders typical of an epithelial culture, which was retained as cells reached confluence (Fig 3.3A). Growth in 2 mM [Ca^{2+}] induced stratification and an apparent alignment of more cuboidal cells within the culture, whilst differentiation by culture in 5% ABS and 2 mM [Ca^{2+}] resulted in a complex heterogeneous population of spindly and stratified cells. Concurrent activation of PPARγ with TZ and inhibition of EGFR signalling by PD153035 resulted in a culture containing compact, tear-shaped cells with occasional organisation into rosette structures (Fig 3.3A arrow). Both methods used to induce differentiation (ABS/Ca^{2+} and TZ/PD) resulted in an induction of *UPK3a* gene expression, which was weakly expressed in freshly isolated NHU cells and not detected in stratified or non-differentiated cultures, irrespective of degree of confluence (Fig 3.3B).

Expression of connexin genes is summarised in table 3.1. An increase in the confluence of non-differentiated cultures did not appear to have an impact on connexin gene expression.

Results of particular interest were:

- Cx26 and Cx31.1 appeared to be expressed as a result of cell culture, whereas they were minimally expressed in freshly isolated urothelium.
- Cx45 was expressed in proliferating and stratified cultures, but expression was non-detectable in freshly-isolated (P0) urothelium and minimally detected in both sets of differentiated cultures (ABS/Ca^{2+} and TZ/PD).
- Cx26, Cx30 and Cx43 were constitutively expressed in freshly isolated urothelium and in NHU cultures regardless of growth conditions.
- Cx31.9 expression was weakly associated with a differentiated NHU cell phenotype, being minimally expressed in P0 and ABS/Ca^{2+}-differentiated cultures only
- Cx32 expression was associated with a differentiated phenotype, with expression observed in cultures differentiated by both methods, as well as in freshly isolated urothelium.

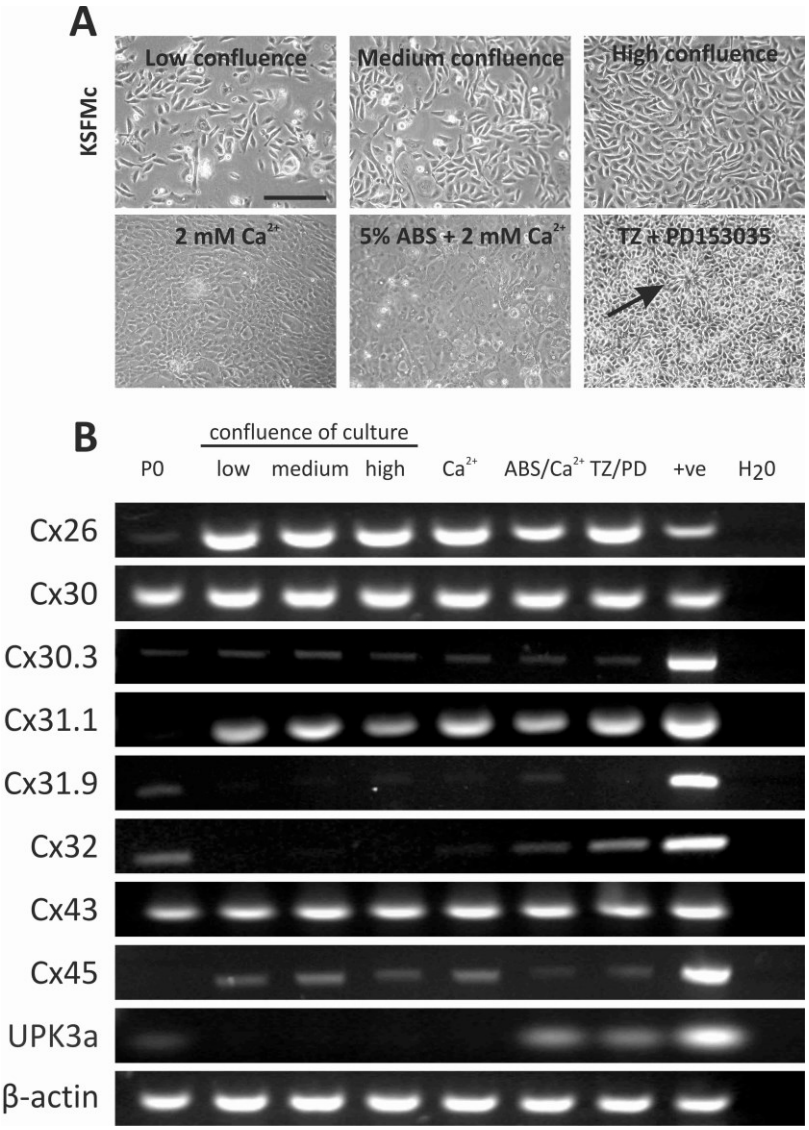

Figure 3.3 RT-PCR to Assess Connexin Expression in NHU Cell Cultures and Freshly Isolated Urothelium.

(A) - RNA was collected from bladder-derived Y930 NHU cell cultures (P4), following growth in KSFMc to low (<50%), medium (60-70%) and high (90-100%) confluence, in medium with 2 mM [Ca^{2+}] for 5 days or following induction of differentiation in either 5% ABS with 2 mM [Ca^{2+}]or TZ/PD. Phase contrast images were taken from each culture immediately prior to lysis (A). Arrow indicates the presence of rosette structures in cultures differentiated with TZ and PD153035. Scale bar = 200 µm

(B) - RT-PCR was performed to amplify gene products from eight connexins of interest (Cx26, 30, 30.3, 31.1, 31.9, 32, 43 and 45) in these cultures as well as from Y1043 (ureteric) freshly isolated (P0) urothelium. UPK3a transcript expression was assessed to confirm

induction of differentiation and β-actin was included as a loading control. PCR controls included genomic DNA control (+ve) and a no-template water control (H_2O).

		Confluence					
	P0	**low**	**medium**	**high**	**Stratified**	**Diff** ***(ABS/Ca^{2+})***	**Diff** ***(TZ/PD)***
Cx26	+	+++	+++	+++	+++	+++	+++
Cx30	+++	+++	+++	+++	+++	+++	+++
Cx30.3	+	+	+	+	+	+	+
Cx31.1	-	+++	+++	+++	+++	+++	+++
Cx31.9	+	-	-	-	-	+	-
Cx32	++	-	-	-	+	++	++
Cx43	+++	+++	+++	+++	+++	+++	+++
Cx45	-	++	++	++	++	+	+

Figure 3.1 Summary Table of Connexin Transcript Expression

Expression of connexion transcripts by freshly isolated NHU Cells (P0), non-differentiated NHU cultures (of low, medium and high confluence), stratified NHU cultures (grown in 2 mM [Ca^{2+}]) and NHU cultures differentiated using ABS/Ca^{2+} and TZ/PD methods are indicated as follows: - (no expression), + (weak expression), ++ (expressed), +++ (strongly expressed).

3.3.3 Assessment of Cx32 Gene Expression in Response to NHU Cell Differentiation *In Vitro*

RTqPCR analysis of three independent donor NHU cell lines (Y930, Y1054 and Y1108) confirmed the previous finding that Cx32 expression was significantly induced following a 6 day induction of differentiation *in vitro*. When compared to non-differentiated cultures (grown in KSFMc), mean Cx32 expression was 14-fold higher when cells were differentiated by ABS/Ca^{2+} and 58-fold higher by TZ/PD (Fig 3.4A). Increased *AQP3* expression confirmed successful induction of differentiation (Fig 3.4B).

To verify that differentiation-induced Cx32 expression was PPARγ-dependent in the, NHU cells (Y1153) were cultured in TZ/PD in the presence of the PPARγ antagonist, T0070907 for up to 72h. At each time-point assessed, Cx32 expression was plotted as fold-change relative to the 6 h vehicle control cultures (to enable the increase in Cx32 during the differentiation time-period to be assessed, see Fig 3.4C). In TZ/PD cultures, mean Cx32 gene expression was increased by 24-fold at 24 hours and 174-fold by 72 hours. A small induction of Cx32 (3.5 fold) was observed at 6h in cultures containing TZ/PD suggesting induction of Cx32 is initiated early following PPARγ activation.

T0070907 inhibited TZ/PD-induced Cx32 gene expression by 85% and 57% at 48 and 72 hours, respectively. Throughout the 72 h experiment, the expression of Cx32 was found to be significantly higher in TZ/PD cultures, than in parallel cultures with T0070907 or vehicle-only controls. However, expression in both vehicle control and T0070907-treated cultures did increase during the time course. At each time point assessed, Cx32 expression in TZ/PD cultures with T0070907 was not significantly different to vehicle control cultures, suggesting that the PPARγ antagonist completely abolished the induction of Cx32 expression observed in TZ/PD cultures.

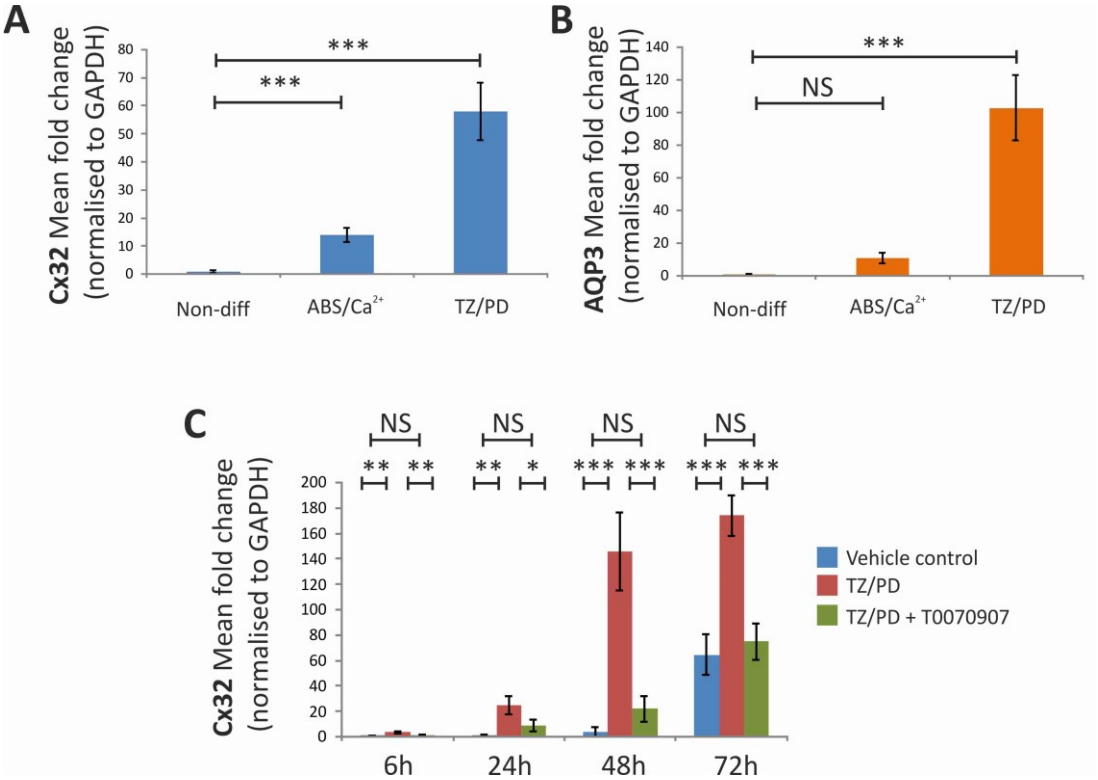

*Figure 3.4 RT-qPCR analysis of Cx32 expression in non-differentiated and differentiated NHU cultures. RNA was extracted from NHU cell lines grown in KSFMc for 6 days (Non-diff) or differentiated following the ABS/Ca^{2+} or TZ/PD methods for 6 days. Quantitative analysis of Cx32 transcript (A) was assessed alongside AQP3 (B) to confirm differentiation status. Mean expression is plotted as fold-change relative to non-differentiated cultures, after normalisation to GAPDH. In (C), NHU cells were pre-treated with the PPARγ antagonist T0070907 (5 µM) or vehicle for 3 h, before supplementing with 1 µM troglitazone (TZ) and 1 µM PD153035. RNA was collected for analysis at 6 h, 24 h, 48 h and 72 h post-treatment. At each time point a DMSO vehicle control was included. Cx32 quantitative RT-PCR was performed and expression was normalised to the housekeeping gene GAPDH. Values represent Cx32 expression fold-change relative to the 6 h vehicle control. One way ANOVA tests were performed with a Tukey-Kramer multiple comparisons post-test. NS = not significant, *** = P<0.001 ** = P<0.01 * = P<0.1*

Data for A & B are pooled mean values from three independent donor NHU cell lines (Y930, Y1054 and Y1108); Data in C are three technical replicates from a single donor cell line (Y1153).

3.4 Protein Expression of Connexin 32 in Normal Human Urothelial Cells I*n Vitro*

3.4.1 Cx32 Protein Expression following NHU Cytodifferentiation using ABS/Ca^{2+} and TZ/PD Methods

Cx32 immunoblotting revealed the presence of two clear bands in NHU cell cultures differentiated with both TZ/PD and ABS/Ca^{2+} methods, one at the estimated molecular weight of 32kD and a second dimeric product, at approximately 50kD (Fig 3.5A). The weaker band at 32kD was present in non-differentiated cells and was not further induced following differentiation.

A large induction of dimeric Cx32 was observed in cultures differentiated with TZ/PD. In cells cultured in TZ alone or PD alone, expression levels of the dimer were weak compared to the combined treatment. Claudin 5 protein expression was used to confirm differentiation and was found to be enhanced when cells were cultured in both TZ and PD, with low level expression in the solo treatments and no observable protein expression in vehicle control cells.

Dimeric Cx32 was induced upon differentiation with 5% ABS and 2 mM [Ca^{2+}], with no expression of the 50 kD band in proliferating cultures (grown in KSFMc). Induction of claudin 5 protein expression confirmed differentiation.

By indirect immunofluorescence, Cx32 protein expression was extremely weak in non-differentiated cells and DMSO control cells, with expression confined to perinuclear regions within the cytoplasm of cells (possibly ER/Golgi associated), with no evidence of localisation at intercellular junctions (Fig 3.5B). When cells were cultured in TZ/PD for 6 days, Cx32 expression was heterogeneous across the culture, with some negative patches and large islands where expression was

intense and localised to cell junctions (Fig 3.5B). In cultures differentiated in ABS/Ca^{2+}, expression was observed throughout the entire culture with distinctive cell junction labelling and some punctate cytoplasmic expression.

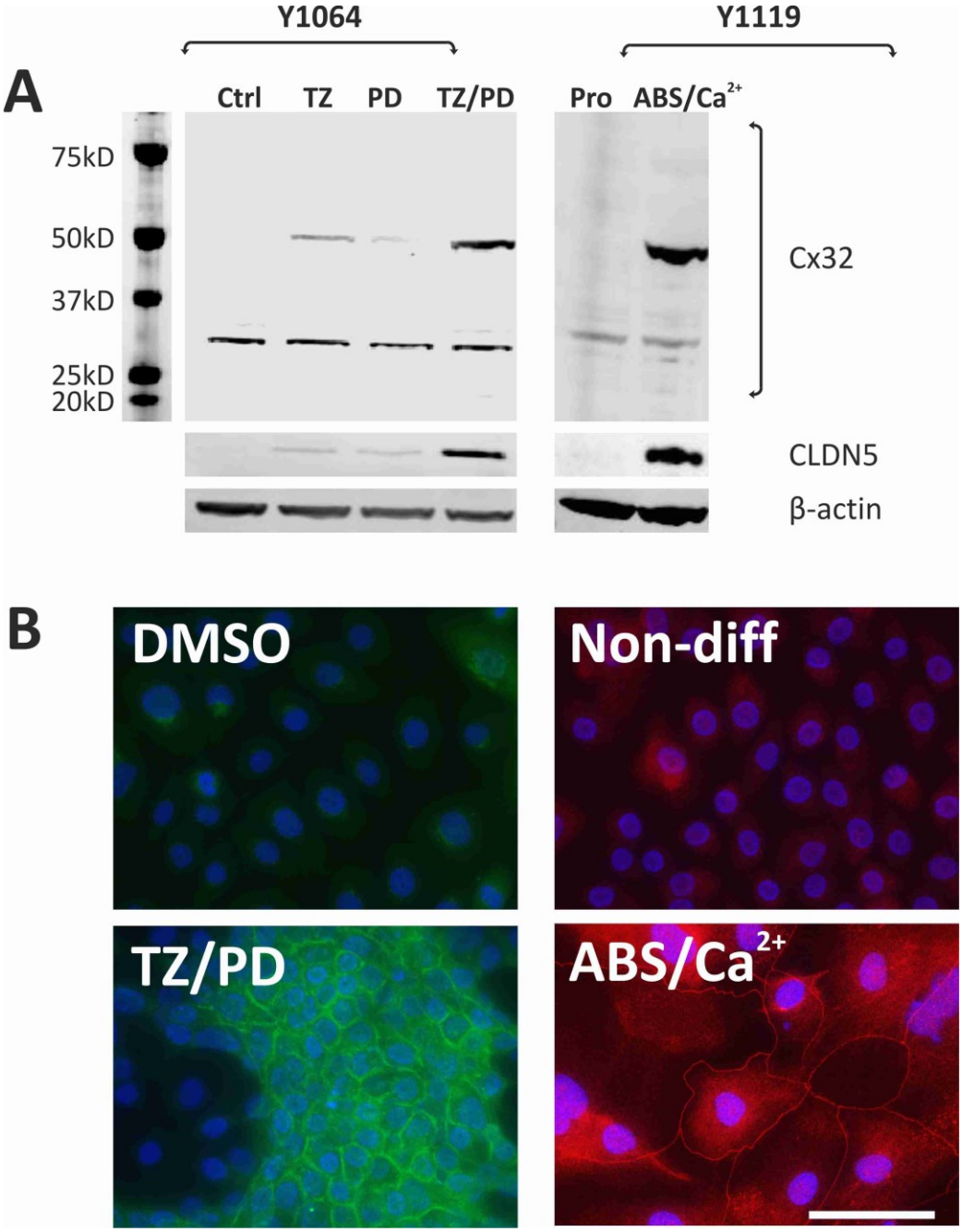

Figure 3.5 Immunoblot and Immunofluoresence Analysis of Cx32 Expression in Differentiated and Non-differentiated NHU cultures. (A) Cx32 immunoblotting from two NHU cell lines. Y1064 cells were treated with 1 µM troglitazone (TZ) and 1 µM PD153035 (PD), either as combined or solo treatments for a period of 6 days with a parallel vehicle control culture (Ctrl). Y1119 cells were grown in 5% ABS and 2 mM Ca^{2+} to induce differentiation for 6 days. A parallel culture of non-differentiated (confluent) was harvested before addition of serum as a control (Non-diff). Western blot membranes were also probed with antibodies against claudin 5 (CLDN5), to confirm differentiation and β-actin to demonstrate equivalent loading. The protein ladder image was extracted from a different

fluorescent channel. (B) Cx32 immunofluorescence labelling of non-differentiated and differentiated NHU cells using both the TZ/PD and ABS/Ca^{2+} culture systems. Parallel cultures as described in (A) were set up on glass slides and fixed for indirect immunofluorescence after 6 days. Nuclei were counterstained (blue) with Hoechst 33258. Scale bar = 50 µm

Note: Red and green immunolabelling are the consequence of using secondary antibodies conjugated to different fluorochromes.

3.4.2 Defining the Specific Effects of PPARγ activation on Cx32 Protein Expression in NHU Cultures.

To verify that the induction of Cx32 protein expression was PPARγ-dependent, NHU cultures (Y1153) were treated with troglitazone and PD153035 in the presence of the PPARγ antagonist T0070907 for up to 72 h. Cx32 immunoblotting confirmed the presence of a weak band at 32kD in all cultures regardless of treatment, in keeping with previous findings (section 3.2.1); however in this cell line the 32kD band appeared as a weak doublet (Fig 3.6A). The presence of Cx32 at 50kD was first observed in TZ/PD cultures at 48 h post-treatment and was also observed at 72 h, however when TZ/PD cultures were supplemented with the PPARγ antagonist T0070907, dimeric Cx32 expression was absent and equivalent to vehicle control cultures. In TZ/PD treated cultures, claudin 5 expression confirmed induction of differentiation and was first observed weakly at 24 h, with a more striking expression at 48 h and 72 h. The PPARγ antagonist T0070907 attenuated the induction of claudin 5 observed in TZ/PD cultures.

Cx32 protein was immunolocalised to patchy islands of cells in cultures treated for 72 h with TZ/PD, where it was localised to cell borders (Fig 3.6B). Cell junction immunolabelling of Cx32 was not seen where cultures contained T0070907, where only weak cytoplasmic labelling was observed.

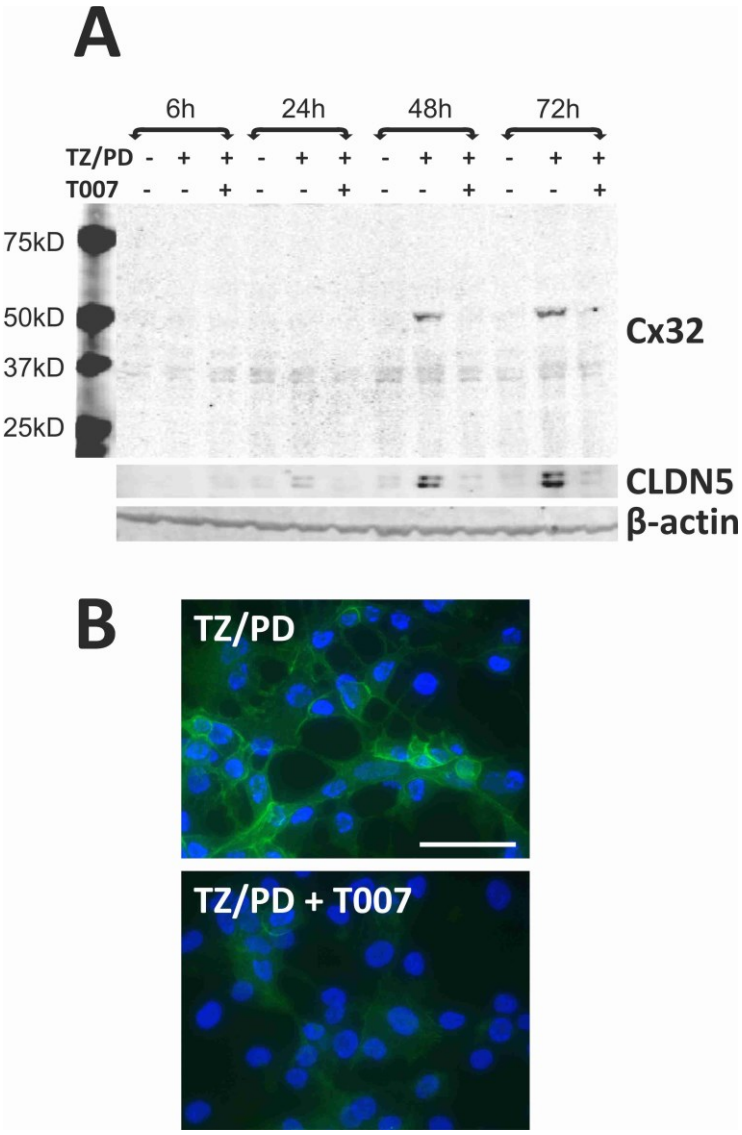

Figure 3.6 Immunoblot and Immunofluoresence Labelling of Cx32 in Response to PPARγ Activation or Inhibition. Y1153 (P3) NHU cells were pre-treated with the PPARγ antagonist T0070907 (5 µM) (T007) or DMSO vehicle control for 3 h before supplementing with 1 µM Troglitazone (TZ) and 1 µM PD153035 (PD). (A) Whole cell lysates were collected for analysis at 6 h, 24 h, 48 h and 72 h post-treatment. A DMSO vehicle control was included at each time point. The same membranes were also probed with antibodies against claudin 5 (CLDN5) to assess differentiation and β-actin to verify equivalent loading. The protein ladder image was extracted from a different fluorescent channel. (B) Y1153 (P3) NHU cells grown on glass slides were treated with 1 µM TZ and 1 µM PD153035, in the presence of the PPARγ antagonist T0070907 (5 µM) or vehicle control. Cultures were fixed 72 h post-treatment and Cx32 indirect immunofluorescence was performed. Nuclei were counterstained (blue) with Hoechst 33258. Scale bar = 50 µm

3.4.3 Characterisation of Cx32 Protein Localisation during NHU Cell Differentiation with ABS/Ca^{2+}

Protein expression of Cx32 was examined over the 11 day process of differentiation following the ABS/Ca^{2+} procedure (indicated in Fig 3.7A). In cultures grown only in KSFMc (day 0), a weak, cytoplasmic distribution was observed throughout all cells, with no Cx32 labelling at cell junctions (Fig 3.7B). Pre-treatment of cultures with 5% ABS for 3 days resulted in an increase in Cx32 expression with heterogeneous patches of membrane labelling for Cx32. When cultured in growth medium containing both 5% serum and 2 mM [Ca^{2+}], bright membrane labelling was observed for Cx32 throughout the culture with large amounts of cytoplasmic labelling. At the final time point assessed for differentiation, i.e. following 6 days culture in ABS/Ca^{2+}, the Cx32 protein localisation was mostly visible at the cell membranes, with reduced cytoplasmic labelling compared to earlier time points. The pattern of expression of Cx32 at cell junctions was very similar to that of the differentiation-associated tight junction protein claudin 5 during the differentiation time course, which was detected at tight junctions after 3 days growth in 5% ABS and expression was further enhanced at tight junctions and within the cytoplasm of cells following the switch to ABS/Ca^{2+}. Expression of the structural tight junction protein ZO-1 was extremely patchy after 3 days in ABS, but after calcium supplementation was observed very clearly at cell-cell junctions throughout the culture.

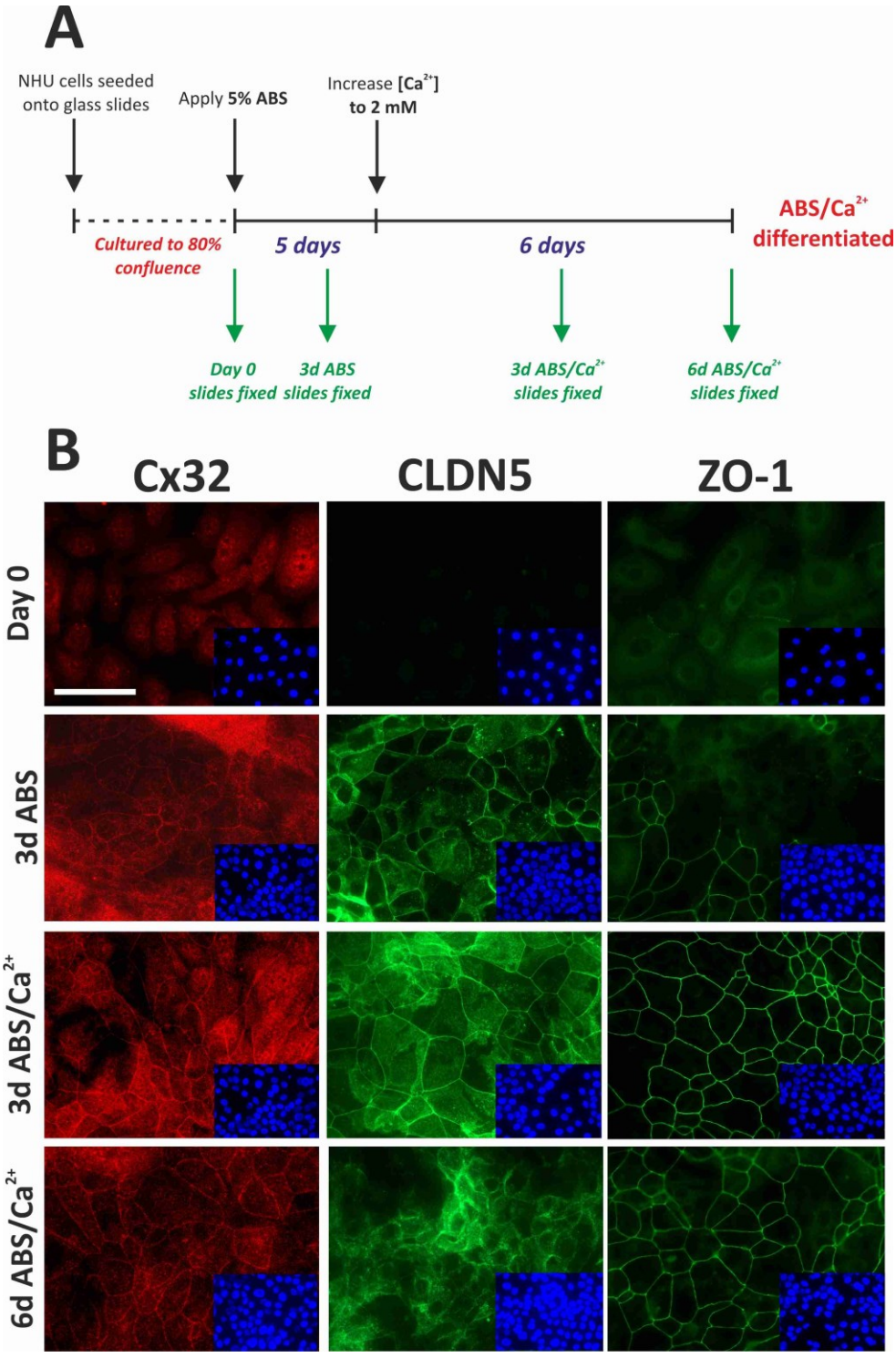

Figure 3.7 Immunofluoresence Analysis of Cx32 Expression During Differentiation of NHU Cells following the ABS/Ca2+ method. Y1191 (P3) NHU cells were grown to just confluence on glass slides in KSFMc and fixed at the time points indicated in A during the ABS/Ca^{2+} differentiation process. Slides were immunolabelled with primary antibodies against Cx32, and the tight junction proteins claudin 5 (CLDN5) and ZO-1 (B). Insert images show nuclei stained with Hoechst 33258. Scale bar = 50 µm

3.5 Protein Expression of Connexin 32 in Native Human Urothelium

Immunohistochemical labelling of Cx32 in normal human bladder and ureter, demonstrated that labelling was reproducibly distinct between the superficial and intermediate/basal cell layers of human urothelium (Fig 3.8). In the basal and intermediate cell compartments, Cx32 labelling was weakly cytoplasmic and membrane-associated, whilst intense Cx32 expression was observed in the basolateral membrane underlying the most-specialised superficial cells.

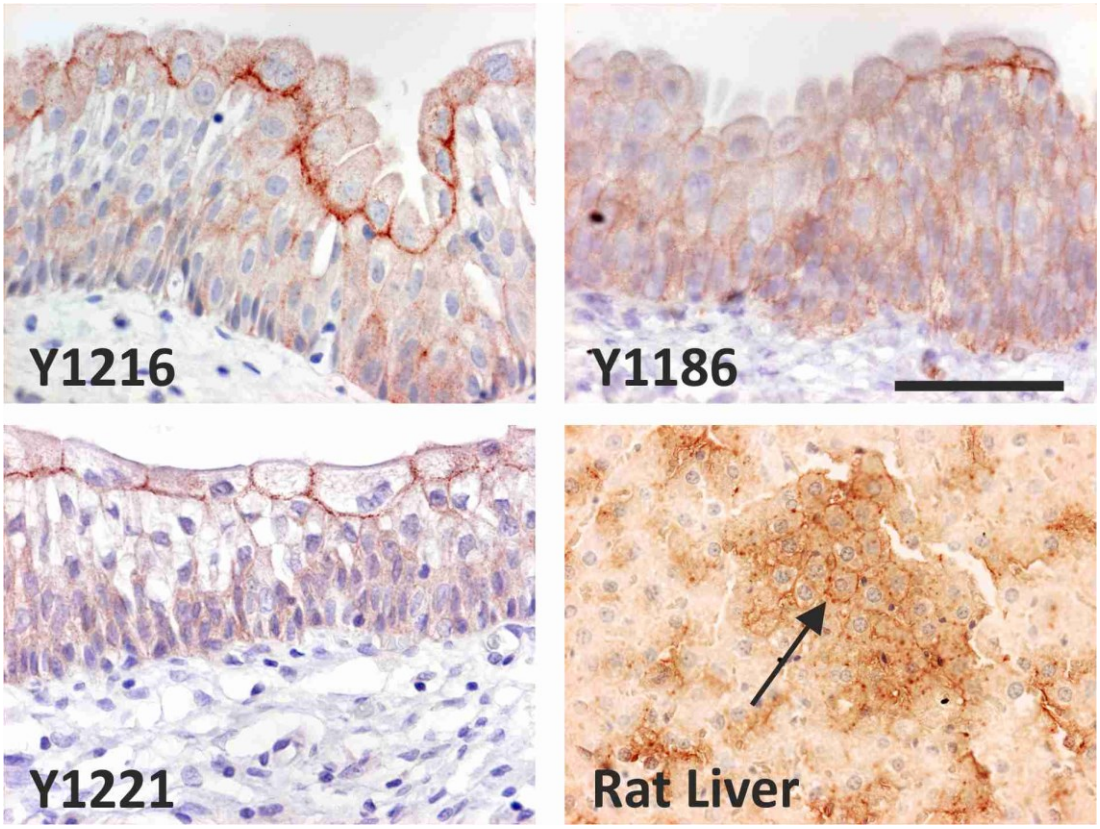

Figure 3.8 Immunohistochemical Labelling of Cx32 in Normal Human Urothelium.

Antibody labelling of Cx32 in normal human ureter (Y1216 and Y1221) and bladder (Y1186). Note: Rat liver was used as a positive control to optimise the primary antibody (as recommended by the antibody manufacturer), since the epitope for which the antibody was raised is identical in rat Cx32. Note islands of membrane labelling within the rat liver (arrow). Scale Bar = 50 µm

3.6 Identification of Potential Transcription Factor Binding Sites within the Cx32 Promoter Region

A bioinformatics analysis of predicted transcription factor binding motifs in the 5000 bp sequence upstream of the Cx32 (*GJB1)* transcriptional start site (using JASPAR datasets), revealed the presence of potential high affinity binding sites for FOXA1 and KLF5 (see table 3.2). Transcription factors with the highest predicted scores from those searched (relative score of greater than 0.95), were FOXA1, with and KLF5; the closest predicted binding site to the start codon was KLF5 which was found to be immediately adjacent to the start codon.

Predicted binding domains for IRF-1, GATA3 and PPARγ were also sought as part of the analysis. A PPAR-response element (PPRE) was not identified within the region selected for analysis; nor was predicted transcriptional start sites for IRF-1 or GATA3. The search was limited to predict binding sites for transcription factors implicated in the urothelial differentiation, however multiple high-affinity predicted binding sites for the transcription factors SP1 and SOX10 were also identified (three predictions for SP1 and 12 for SOX10). This was included as a control search, since both SP1 and SOX10 have previously been implicated in Cx32 transcriptional regulation (Piechocki et al. 2000, Bondurand et al. 2001).

Model Name	Relative Score	Start (bp)	End (bp)	Predicted site sequence
KLF5	**0.97**	**3128**	**3137**	**CCCCCACCCA**
FOXA1	**0.95**	**4186**	**4200**	**TCTCTGTTTACCTTA**
KLF5	**0.96**	**4990**	**4999**	**GTCCCTCCCC**

Table 3.2 Potential KLF5 and FOXA1 binding sites identified within the 5000 bp sequence upstream of the Cx32 start codon. The 5000 bp sequence immediately upstream of the Cx32 (GJB1) start codon was used to perform a motif search in the JASPAR database for predicted TF binding sites. The profile score threshold was set to 95% to ensure only extremely high sensitivity predictions were generated. The search included selected transcription factors implicated in urothelial development and differentiation (PPARγ, FOXA1, IRF-1, KLF5 and GATA3; the predictive tool did not contain algorithms for GRHL3 and ELF3). Note: only KLF5 and FOXA1 gave matches, as indicated by the similarity score (relative score calculated by JASPAR where the highest score of 1.0 represents 100% identity).

3.7 Functional Assessment of Gap Junctional Communication in NHU Cultures

Gap junction dye-transfer of Lucifer-yellow (LY, mw = 457 Da) in NHU cell cultures demonstrated that both non-differentiated cultures (Fig 3.9A) and those differentiated using the TZ/PD method to induce differentiation (Fig 3.9B) were capable of dye-transfer via gap junctions. Cell counts revealed that for every cell initially loaded with dye following scratching (assessed by uptake of rhodamine-dextran), the mean number of cells which were subsequently positive for LY after 6 minutes was 8 and 6 (to the nearest whole number), for non-differentiated and differentiated cultures respectively (Fig 3.9C). Pre-treatment of cultures with the gap junction inhibitors heptanol or 18α-glycyrrhetinic acid, resulted in a reduction in dye-transfer capacity of both non-differentiated and differentiated cultures. This reduction was not statistically-significant with heptanol treatment; however addition of 18α-glycyrrhetinic acid resulted in a highly significant reduction in the number of dye-transmitted cells.

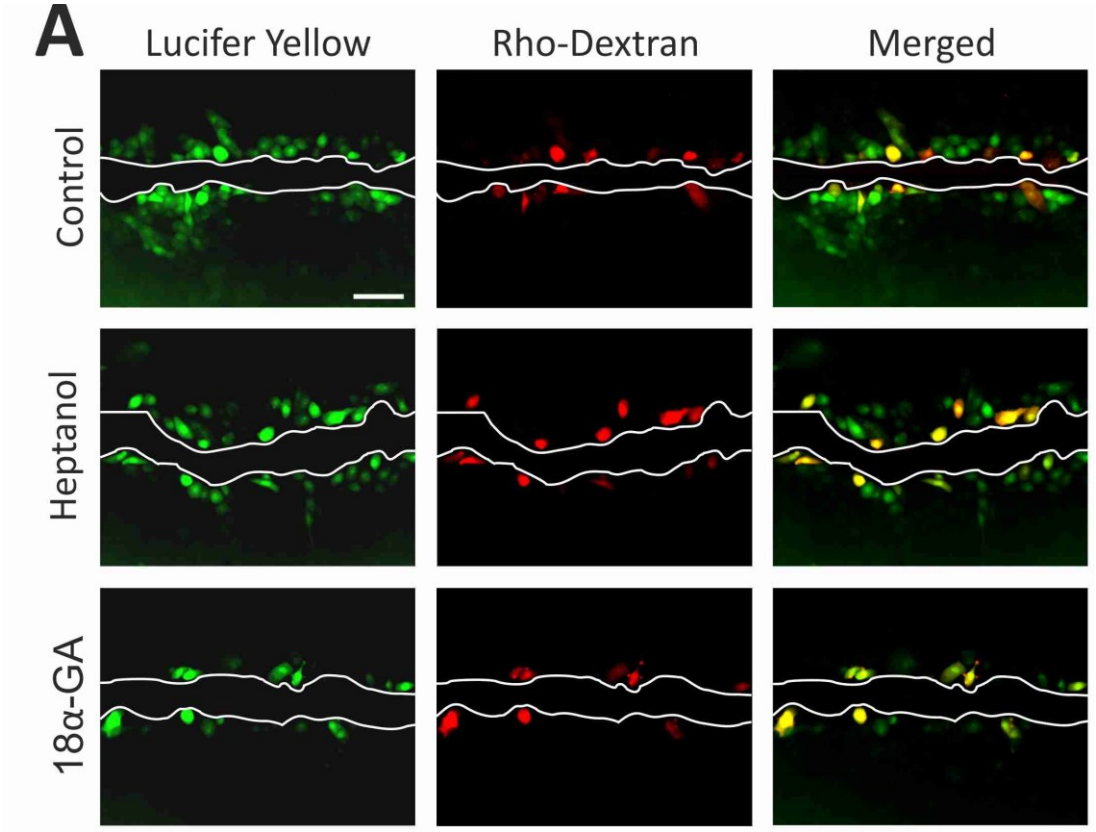

Figure 3.9A Gap Junction Mediated Dye-Transfer in control NHU Cultures.

Y1268 (P3) NHU cells were cultured for 6 days prior to pre-treatment for 30 minutes with the gap junction inhibitors heptanol (1 mM) or 18α-glycyrrhetinic acid (18αGA; 5 µM), or DMSO (vehicle control). Cultures were scrape-loaded in the presence of the gap junction permeable Lucifer-yellow dye (green) and the gap junction impermeable rhodamine-dextran fluorescent dye (red). After 6 minutes, the dye-transfer was halted by formalin fixation and dyes were visualised by fluorescent microscopy to determine the extent of GJIC. Representative images are shown (one region from five). Merged overlaid images are also shown. White lines indicate the approximate scratch boundaries.

Scale bar = 50 µm

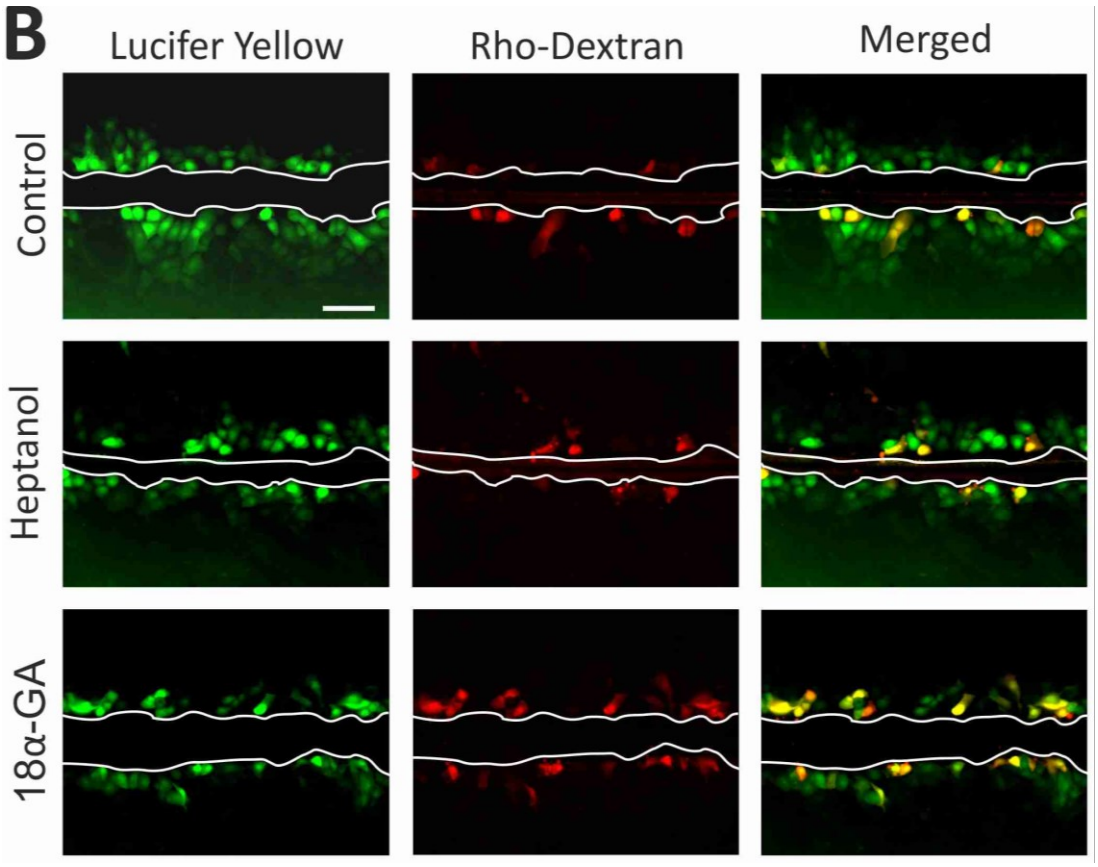

Figure 3.9B Gap Junction Mediated Dye-Transfer in TZ/PD differentiated NHU Cultures.

Y1268 (P3) NHU cells were cultured for 6 days in TZ/PD prior to pre-treatment for 30 minutes with the gap junction inhibitors heptanol (1 mM) or 18α-glycyrrhetinic acid (18αGA; 5 µM), or DMSO (vehicle control). Cultures were scrape-loaded in the presence of the gap junction permeable Lucifer-yellow dye (green) and the gap junction impermeable rhodamine-dextran fluorescent dye (red). After 6 minutes, the dye-transfer was halted by formalin fixation and dyes were visualised by fluorescent microscopy to determine the extent of GJIC. Representative images are shown (one region from five). Merged overlaid images are also shown. White lines indicate the approximate scratch boundaries.

Scale bar = 50 µm

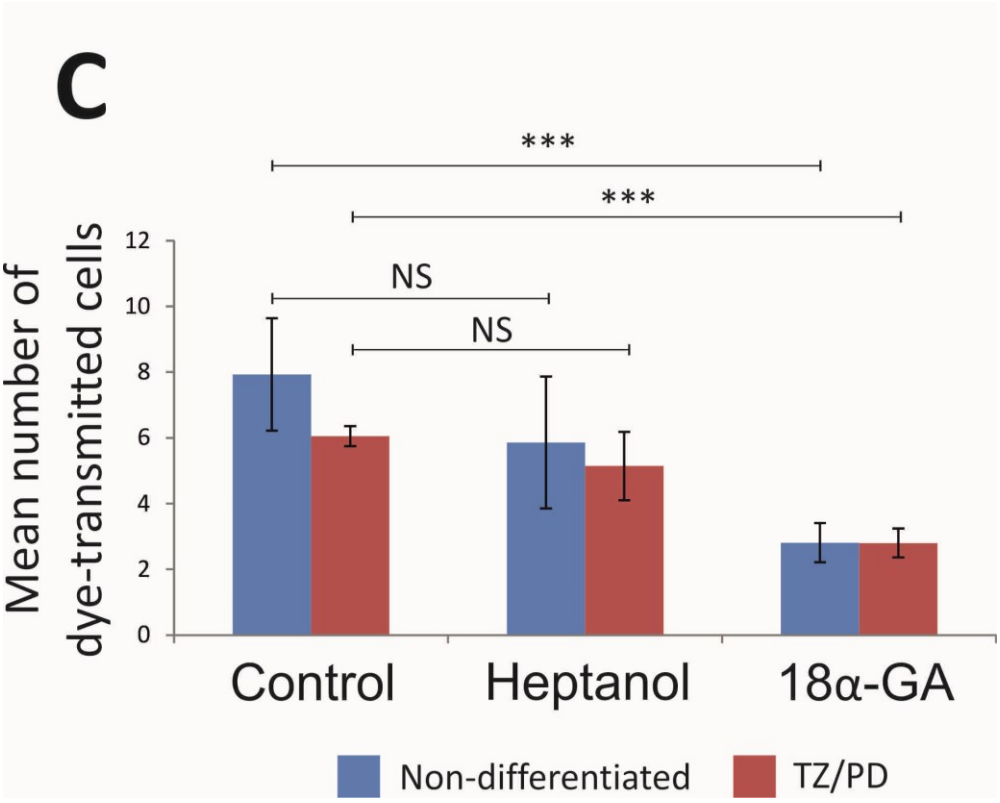

Figure 3.9C Assessment of Gap Junction Mediated Dye-Transfer in NHU Cultures.

Y1268 (P3) NHU cells were treated for 6 days with DMSO (A) or TZ/PD (B). Cultures were pre-treated for 30 minutes with the gap junction inhibitors heptanol (1 mM) or 18α-glycyrrhetinic acid (18αGA; 5 µM), or DMSO control. Cultures were scrape-loaded in the presence of Lucifer-yellow and rhodamine-dextran fluorescent dyes. After 6 minutes, the dye-transfer was halted by formalin fixation and visualised by fluorescent microscopy and cell counts performed. The number of cells containing the gap junction permeable dye Lucifer yellow, were normalised to the number of initially loaded (rhodamine-dextran) cells to give a mean number of LY dye-transmitted cells (per initially loaded cell), at 5 contiguous areas across each scratch.

**** P value <0.001 considered extremely significant*

NS = not significant (One way ANOVA)

3.8 Discussion

This data has revealed the expression of multiple connexin genes in human urothelium and NHU cell cultures. Whilst several of these connexins (Cx26, Cx30, Cx30.3 and Cx43) are constitutively expressed both *in situ* and *in vitro* regardless of differentiation status, others (Cx31.9 and Cx32) appear to be distinctly associated with a differentiated NHU cell phenotype. Due to the close association with urothelial differentiation using both ABS/Ca^{2+} and TZ/PD models, Cx32 was selected for follow up studies for this research project. However, this is not to discount the clear potential interest for studying other connexins in the urothelium, including those not linked to a differentiated state such as Cx26, Cx30, Cx30.3 and Cx43. Whilst the non-differentiated and differentiated NHU cell lines where used as a screening tool to select candidate connexins worthy of further study here, the gene expression of all connexins in freshly isolated urothelium was not performed here. There may be other connexins expressed *in situ* for which the differentiation models lack expression which would be useful to include for future studies. A summary of this gene expression data, along with other representative tissues and cell types which express each connexin is summarised in table 3.3.

Cx31.9 may be extremely relevant to the differentiated phenotype of urothelium, especially given that expression was only observed with the ABS/Ca^{2+} model of differentiation (in which tissue stratification and barrier function is observable), but not the TZ/PD model. *In situ* expression was also observed in freshly isolated, uncultured NHU cells (P0), which is of particular interest since Cx31.9 is rarely expressed in other tissues (and not in other epithelia).

Cx45 was the only connexin where expression appeared to be associated with loss of differentiated phenotype. Cx45 knock-out mice are embryonically lethal; possibly because Cx45 is essential for the early stages of cardiogenesis (Kumai et al. 2000). However, other than studies which document the expression of Cx45 in

human keratinocytes (Di et al. 2001) and corneal epithelium (Yuan et al. 2009), there is little evidence to support a functional role for Cx45 in epithelial tissues, or to indicate why Cx45 expression may be reduced in response to differentiation cues in urothelium.

There are very few studies describing connexin expression in the urothelium however previous studies have shown expression of two of the most frequently studied human connexins; Cx26 and Cx43. In studies of cultured human urothelial cells, expression of Cx26 and Cx43 mRNA was detected and loss of Cx26 expression was observed in human bladder cancer cell lines (Grossman et al. 1994) and bladder tumour tissue biopsies (Gee et al. 2003). In rat bladder, Cx26 and Cx43 were found to be expressed in the urothelium in a punctate labelling pattern (Sunagawa et al. 2015) and in mouse urothelium, Cx26 was described as restricted to the basal cell compartment (Lorentz et al. 2012).

This is the first systematic characterisation of connexin family expression in urothelium and demonstrates that urothelial cells alter their connexin expression upon differentiation to produce specific channels. Dye-transfer studies indicated that functional channels exist in both non-differentiated (confluent) and differentiated NHU cultures.

It should be noted however that RT-PCR was selected as a gene expression screening tool for the connexins, for which there are technical caveats due to it being a fixed end-point method, such as limiting reagent concentrations after the exponential phase of the reaction. Therefore subtle changes in abundance cannot be presumed accurate and although useful as a crude screening tool, quantitation was required for further analysis of gene abundance in the follow-up Cx32 experiments.

Connexin	*Expression in urothelial cultures*	*Bladder expression in situ*	*Representative tissues and cell types**
Cx25	no	nd	
Cx26	Yes – ND and D	Yes (P0)	Breast, cochlea, placenta, hepatocytes, skin, pancreas, kidney, intestine
Cx30	Yes – ND and D	Yes (P0)	Brain, cochlea, skin
Cx30.2	no	nd	Brain, spinal cord, Schwann cells
Cx30.3	Yes – ND and D	Yes (P0)	Skin, Kidney
Cx31	no	nd	Cochlea, placenta, skin
Cx31.1	Yes – ND and D	no	Skin
Cx31.9	Yes – D only	Yes (P0)	Vascular smooth muscle
Cx32	Yes – D only	Yes (P0)	Hepatocytes, Schwann cells
Cx36	no	nd	Neurons, pancreatic β-cells
Cx37	no	nd	Endothelium, granulosa cells, lung, skin
Cx40	no	nd	Endothelium, lung, myocardium, skin
Cx40.1	no	nd	Heart, Kidney, Liver, Pancreas
Cx43	Yes – ND and D	Yes (P0)	Bone, cartilage, colon myocardium, skin, spleen, thyroid, tonsil (among many others)
Cx45	Yes – ND and D	no	Myocardium, neurons, skin, smooth muscle cells
Cx47	no	nd	Brain, spinal cord
Cx50	no	nd	Lens
Cx59	no	nd	Retinal cells
Cx62	no	nd	Retinal cells

Table 3.3 Connexin genes and their expression in human cells and organs.

Data in red are summarised from the present study, all other data is derived from previous studies with major sites of expression selected. ND = non-differentiated urothelial cultures. D = urothelial cultures differentiated by adaptation of culture conditions (Varley et al. 2004b, Cross et al. 2005). P0 = freshly isolated (uncultured) urothelial cells from human bladder. nd = no data (Gene expression was not examined in these freshly isolated samples due to lack of expression in urothelial cultures).*

**data derived from multiple sources (Di et al. 2001, Nielsen et al. 2003, Sohl et al. 2003, Oyamada M 2005, Laird 2006, Sohl et al. 2010).*

Since it is understood that different connexins form selective channels offering distinct permeability characteristics (Goldberg et al. 2004), it is a possible that in urothelium, expression of multiple connexins may support a range of physiological functions, some of which may or may not be overlapping. It has been proposed that several connexins have alternative roles within multi-protein complexes for regulation of cell polarity, with influence on the assembly or maintenance of tight/adherens junctions (Herve et al. 2012). It is therefore possible that although some urothelial connexins may be involved in cell-cell communication, other connexins may have an alternative communication-independent role.

The unique differentiation-restricted expression of Cx32 transcript in both freshly-isolated NHU cells, as well as in NHU cultures differentiated using two independent cell culture methods, suggests that Cx32 may play a prominent functional role during urothelial cytodifferentiation or in the homeostasis of the mature urothelium. However, data presented in this chapter does not identify a potential role, nor allow for speculation as to whether the role of Cx32 in urothelium might be dependent or independent of Cx32-mediated cell-cell communication.

Patients with X-linked Charcot-Marie-Tooth disease (CMTX) demonstrate that partial or total loss of Cx32 channel function is not lethal, but does lead to progressive peripheral nerve neuropathy linked to a highly specific role of Cx32 in Scwann cells (Patel et al. 1994, Scherer et al. 1999, Kleopa 2011). Moreover, there are no apparent urinary tract defects reported in these patients as may be predicted in light of the present study, nor are there reports of liver dysfunction or enhanced hepatocarcinogenesis as might be predicted since Cx32 is a major liver gap junction and a marker of hepatocyte differentiation (Piechocki et al. 2000). This suggests that the function of Cx32 in liver and bladder is either non-essential for tissue function or there may be potential for redundancy from other connexins. It is likely a complex situation since CMTX patients are found with a huge degree of variability in mutations and their effects on channel function, from partial to total

loss. The number of patients with total Cx32 gene deletion appears to be very few and therefore liver and/or urinary tract symptoms may not be reported as significant (Gonzaga-Jauregui et al. 2010). There is added complexity in that transcriptional regulation of Cx32 differs between Schwann cells and liver (Piechocki et al. 2000, Murphy et al. 2011), each being expressed from separate Cx32 splice variants (differing only in the 5' UTR's). Although, given that the majority of CMTX patients have mutations in the coding sequence for Cx32 (rather than in the UTR), there is little evidence to suggest that this should explain the lack of liver and/or bladder pathologies in these individuals.

Specific PPARγ antagonism blocked the inducibility of Cx32 during TZ/PD differentiation of NHU cells *in vitro*. This suggests that it is highly likely that Cx32 expression in human urothelium is regulated under the influence of PPARγ, as is the case with a range of other proteins identified as "markers" of urothelial cytodifferentiation (see section 1.1.6.4). Specific PPARγ antagonism was not considered in cultures differentiated using the ABS/Ca^{2+} method and therefore regulation of Cx32 expression by PPARγ using this method of differentiation cannot be supported. As with the PPARγ-regulated aquaporin 3, induction of Cx32 expression was more effective in cultures differentiated with TZ/PD than those differentiated following the ABS/Ca^{2+} method, thus further providing evidence for a strong influence of PPARγ on the expression of Cx32. It should be noted from immunoblotting data that it is a requirement that EGFR signalling is inhibited for maximal PPARγ-driven Cx32 expression. Inhibition of EGFR-signalling in the absence of differentiation did induce a small amount of dimeric Cx32 expression, however not to the same extent as when PPARγ was activated. This in itself is of potential interest, since a study in rat hepatocytes has reported that EGFR can phosphorylate Cx32 at tyrosine residues (Diez et al. 1998). However the biological significance of this finding is not known, although Diez *et al.* speculate that it may play a role in assembled channel stoichiometry and thus channel function. Since little is known about the exact mechanism by which bovine serum induces urothelial cytodifferentiation *in vitro*, it is not possible to determine the relative contribution that PPARγ activation may play in driving Cx32 expression in the

ABS/Ca^{2+} method of differentiation, when compared with using troglitazone to directly ligand-activate PPARγ. Future studies using a specific PPARγ antagonist in ABS/Ca^{2+} differentiated cultures may provide further understanding.

Sequence analysis did not identify a high-affinity PPRE within the promoter region of Cx32, increasing the likelihood that the PPARγ-mediated induction of Cx32 is indirect. Although caution must be taken not to over-interpret the findings of transcription factor binding predictor tools, the predicted presence of a high-affinity FOXA1 binding site 800bp upstream of the Cx32 start codon might be an encouraging starting candidate in unravelling the mechanisms of Cx32 regulation in urothelial cells. The promoter region of FOXA1 does contain a high-affinity PPRE and FOXA1 has previously been shown to act downstream of PPARγ, as an intermediary transcription factor driving expression of other markers of urothelial cytodifferentiation, including *UPK2* (Varley et al. 2009). However, FOXA1 has not previously been described as a regulator of Cx32 gene expression. The transcription factor *SOX10* has been shown to directly regulate human Cx32 in Schwann cells of peripheral nervous system and mutations in the SOX10 binding region of the Cx32 promoter (position -526bp), have been identified in a subset of patients with the Cx32-linked form of Charcot-Marie-Tooth disease (Bondurand et al. 2001, Houlden et al. 2004). Cx32 is the predominant gap junction protein expressed in liver and is a commonly used marker of hepatocyte differentiation, as well as being a key mediator of cell-cell communication throughout the liver (Patel et al. 2012). Studies in rat hepatoma cells have identified Sp1 and two putative HNF-1 binding regions (at -187 and -736), within the Cx32 promoter region as being crucial to Cx32 expression (Piechocki et al. 2000).

Observation of monomeric and dimeric Cx32 products was observed by immunoblotting, which is consistent with the theory that Cx32 is commonly resolved in monomeric and dimeric form by SDS-PAGE (Green et al. 1988, VanSlyke et al. 2000, Scherer et al. 2005, Fowler et al. 2009). A detailed study using five

independent Cx32 antibodies for immunoblotting in Cx32 wild-type and knock-out mice neatly demonstrated this phenomenon (Nagy et al. 2003). Three monoclonal and two polyclonal Cx32 antibodies were used; raised to epitopes present in both the cytoplasmic loop and the C-termianl domain of Cx32. Nagy *et al*. demonstrated two Cx32 products at approximately 30-32 kD and 50-52 kD in Cx32 wild-type mice, which were absent in knock-out mice; this was a consistent finding with all five antibodies (including the antibody used in the present study). A third band at approximately 90 kD was observed with four of the five antibodies tested, however this was not lost in Cx32 knock-out mice and therefore was presumed to be non-specific. An additional study demonstrated dimeric Cx32 products with multiple Cx32 antibodies which were absent in Cx32 K/O mice (Nagy et al. 2003). There are possible explanations for why Cx32 may resolve in monomeric and dimeric forms and one study reports a shift in immunoreactivity to only a monomeric form when samples are reduced in 50 mM DTT (Tang et al. 2009). These are more stringent conditions than followed in standard protein preparation methods for SDS-PAGE, where DTT concentrations are commonly in the 1-10 mM range (2 mM used in the current study), suggesting that disulphide bonds formed when connexins dimerise require strong reducing conditions for separation. It has been demonstrated that Cx32 GJ channel assembly involves dimeric and tetrameric intermediates (Ahmad et al. 2001) and therefore with specific SDS-PAGE conditions it tetramers may also be present, however these were not detected in the conditions used in the current project. Given that Cx32 GJ assembly involves dimeric intermediates, it seems unlikely that the observation of the Cx32 immunoreactive 50-52 kD band is the product of a strong interaction between Cx32 interacting and another protein of similar size (although not impossible). Therefore given the supporting literature the term “dimeric” was used throughout in the present study.

In differentiated NHU cultures two specific bands at approximately 32kD and 50 kD were observed, however the dimeric band was not observed in non-differentiated cultures. The presence of dimeric Cx32 bands following induction of differentiation coincided with increased membrane-associated Cx32. This may indicate that the

dimeric band observed on immunoblots represents assembled Cx32 junctional complexes at the membrane, or partially assembled connexons prior to membrane insertion. Under differentiating conditions, inhibition of PPARγ blocked both the expression of Cx32 dimeric products and also membrane-associated Cx32; suggesting that PPAR activation not only regulates overall Cx32 expression, but also induces the development of membrane-associated Cx32 channels. The presence of monomeric Cx32 products in non-differentiated cultures along with a small amount of cytoplasmic Cx32 labelling suggests a likely low level basal Cx32 expression is expressed by NHU cells even in the absence of differentiation. This is supported by the quantitative RT-PCR data which demonstrated some increase in Cx32 expression over time in non-differentiating growth conditions (treated with DMSO as a vehicle control), although to a much lesser extent than when differentiation was induced with TZ/PD. It is highly possible that this increase in Cx32 expression over time is due to an increased culture confluence, however non-quantitative RT-PCR analysis of non-differentiated NHU cultures of increasing cell density (in the absence of DMSO as a vehicle control), did not result in an apparent upregulation of Cx32. This may be due to the threshold of sensitivity associated with viewing RT-PCR amplicon products by gel-electrophoresis, although an alternative explanation may implicate DMSO treatment with enhanced Cx32 gene expression, since DMSO has been previously recognised as a differentiation-enhancing agent (Chetty et al. 2013).

In situ, urothelium is organised into basal, intermediate and superficial cell layers, with each compartment expressing specialist proteins appropriate for function. The superficial cells are often described as terminally-differentiated, based on their high degree of specialisation towards barrier function, such as the expression of the uroplakins, which generate a transcellular barrier to urine (Hu et al. 2002) and terminal tight junctions which support barrier function (Varley et al. 2006, Smith NJ et al. 2015). Since PPARγ plays a key role in driving expression of many proteins expressed superficially in the urothelium, it was noteworthy to find that Cx32 protein was most strongly expressed by the most terminally differentiated

superficial cell layer of urothelial cells *in situ*. The positioning of membrane-bound Cx32 within the basolateral membrane of superficial cells may infer a potential role in allowing passage of specific signalling molecules between the superficial cell zone and the intermediate/basal cell layers, or a potential role in the final stages of differentiation or repair following loss of superficial cells (for example due to infection).

In NHU cultures differentiated following the ABS/Ca^{2+} method, a tight barrier (as measured by TER) is known to develop following supplementation of ABS pre-treated cultures with near-physiological concentrations of calcium (Cross et al. 2005). The timing of Cx32 protein expression at the cell membrane was observed to be approximately coincidental with that of the tight junction proteins claudin 5 and ZO-1. Some assembly was observed in cultures treated with bovine serum alone; however expression was enhanced and more consistent across the entire culture after calcium concentrations were increased. This indicates that Cx32 expression is temporally and spatially similar to the development of urothelial tight junctions during the process of barrier development.

In summary, data presented here indicates that several connexins are expressed in human urothelium; singled out to be of particular interest was Cx32, due to its close correlation with terminal differentiation of this tissue under the influence of the nuclear receptor and transcriptional regulator PPARγ. It remains to be determined whether functional Cx32 gap junctions are essential to the physiology of human urothelium. Work presented in the final two chapters will address the hypothesis that Cx32 plays a critical role in the balance between generation of a tight urothelial barrier and the switch to regeneration during wound healing.

4. Defining the Role of Cx32 in Urothelial Differentiation

Previous studies have linked specific connexin expression to tissue differentiation, in some cases with implications on cell polarity and development of tight junctions. Data presented in results chapters 3 has identified Cx32 as a gap junction protein which is highly up-regulated during urothelial cell differentiation, indicating potential relevance to the differentiated urothelial cell phenotype. This chapter will focus on the specific role of Cx32 and its associated cell-cell communication, in one particular aspect of urothelial biology: the generation of a tight epithelial barrier.

4.1 Aims

Specific objectives were to:

- generate Cx32 knock-down and Cx32 overexpressing (wild-type and pore-closed dominant-negative) human urothelial sub-lines *(section 4.3)*
- characterise the morphology, growth rates and gap junction-mediated communication of Cx32 knock-down and Cx32 overexpressing (wild-type and dominant-negative) transduced cells *(section 4.4)*
- assess the differentiation capacity and barrier function of Cx32 knock-down and Cx32 overexpressing (wild-type and dominant negative) NHU cells following induction of differentiation using the ABS/Ca^{2+} method *(Section 4.5)*
- assess the histology and tight junction ultrastructure of differentiated urothelial constructs in Cx32 knock-down and Cx32 overexpressing (wild-type and dominant negative) NHU cells, compared with control cultures *(section 4.6)*
- evaluate the potential physical association of Cx32 with the urothelial tight junction *(section 4.7)*

4.2 Experimental Approach

Cx32 shRNA knock-down, Cx32 (wild-type) overexpressing and Cx32 (dominant negative) overexpressing sub-lines were developed from NHU cells, using retroviral gene transfer technology. Full-length Cx32 cDNA was cloned from differentiated NHU cells and was used to generate the dominant-negative mutant by site-directed mutagenesis. Full method details of retroviral vector preparation and transfection into packaging cells are detailed in chapter 2.9.4.

The dominant-negative form of Cx32 was generated by a single point mutation which eliminates functionality without interfering with gap junction formation, as described by Beahm *et al.* (2006), see figure 4.1. The mutated channel ($Cx32^{T134A}$) is reported to be correctly synthesised, trafficked and inserted into the plasma membrane where it is able to dock with partner connexons on adjacent cells; however passage of signalling molecules through the channel is disabled, enabling the identification of cellular behaviours which are entirely communication-dependent, rather than just dependent on physical expression.

Retroviral particles were collected from the growth medium of the transfected PT67 packaging cell line and used to transduce proliferating NHU cells before subjecting the cells to antibiotic selection. Immunoblotting and immunocytochemistry techniques were used to confirm Cx32 knock-down or overexpression, using an antibody which recognises the C-terminus of Cx32; identical in both wild-type and mutated $Cx32^{T134A}$. RT-PCR was performed to assess Cx32 transcript expression following shRNA gene silencing.

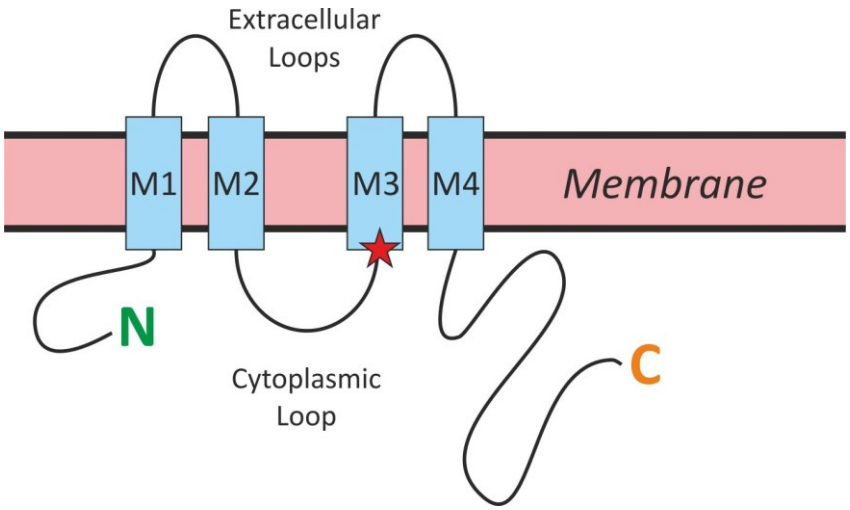

Figure 4.1 Schematic of Cx32 Pore-closed Mutant.

A single point mutation in a threonine (position 134) at the cytoplasmic end of the third transmembrane helix (approximate location is indicated by the star symbol), is described to eliminate functionality without interference with gap junction formation (Beahm et al. 2006). This threonine is strictly conserved among the α- and β-connexin subgroups.

Transduced NHU sub-lines were observed by phase-contrast microscopy for morphological changes before and after differentiation with ABS/Ca^{2+}. Growth capacities of all transduced cultures were assessed in cultures grown in KSFMc using an AlamarBlue® assay, to determine the effects of Cx32 expression and associated cell-cell communication on NHU cell proliferation.

Dye-transfer techniques were used to determine the effects of Cx32 gene silencing and overexpression of wild-type ($Cx32^{WT}$) and dominant negative Cx32 ($Cx32^{T134A}$) on functional gap junction mediated cell-cell communication. This was particularly important since no antibody specific to the mutated T134A Cx32 was available, therefore dye-transfer studies served to confirm dominant negative function. In all dye-transfer studies, transduced cells were cultured in troglitazone and PD153035, to induce a differentiated phenotype (and Cx32 expression) in a monolayer, to facilitate fluorescent cell counts.

TER measurements were recorded to determine the functional role of Cx32 for barrier attainment in transduced NHU cultures. To determine the effects of Cx32 manipulation on differentiation capacity, western blot analysis of each transductant during differentiation with ABS/Ca^{2+} was performed, to study the expression of other differentiation-associated markers such as tight junction proteins, CK13 and E-cadherin. Transmission electron microscopy (TEM) was performed on differentiated NHU constructs to assess the tight junction integrity in Cx32 knock-down and overexpressing $Cx32^{WT}$ and $Cx32^{T134A}$ transductants.

A flow diagram to summarise the experiments performed with Cx32 modified sub-lines is shown in figure 4.2 and the individual sub-lines generated are summarised in table 4.1.

A proximity ligation assay was performed on differentiated (non-transduced) NHU cells, to assess potential direct tight junction protein interactions with Cx32. The assay involves use of two primary antibodies raised in different host-species to label two proteins for which an interaction is unknown. Ligation of labelled oligonucleotides attached to specific secondary antibodies occurs when the proteins of interest are in close proximity (<40 nm) resulting in a fluorescent signal. The technique allows for localised detection of interacting protein pairs (Soderberg et al. 2006, Jarvius et al. 2007). For further details see methods section 2.7.4.

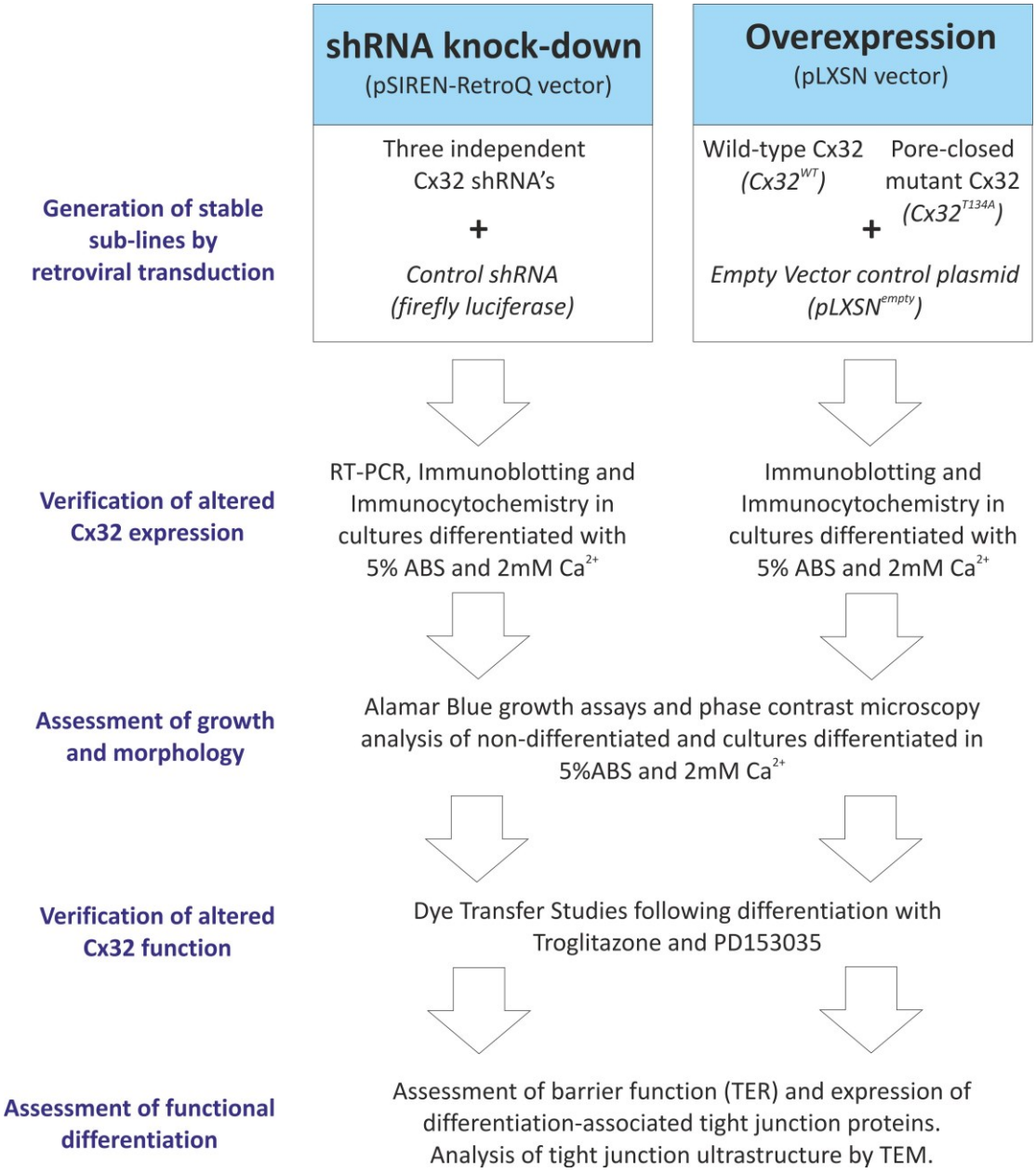

Figure 4.2 Summary flow diagram of experiments performed with Cx32 modified NHU sub-lines.

Cell Line	Tissue Of Origin	Donor Age/Sex	Genetic Manipulation
Y1185	Ureter	45/F	Cx32 shRNA (1,2,3) and control shRNA
Y1117	Ureter	64/F	Cx32 shRNA (1) and control shRNA
Y1057	Ureter	unknown	Cx32 shRNA (1) and control shRNA
Y1119	Ureter	65/F	Cx32 shRNA (1) and control shRNA
Y1151	Ureter	31/F	Cx32 shRNA (1) and control shRNA
Y1270	Ureter	76/F	pLXSN (empty, Cx32-WT and Cx32-T134A)
Y1284	Ureter	64/F	pLXSN (empty, Cx32-WT and Cx32-T134A)
Y1277	Renal Pelvis	68/F	pLXSN (empty, Cx32-WT and Cx32-T134A)
Y1247	Ureter	67/F	pLXSN (empty, Cx32-WT and Cx32-T134A)

Table 4.1 Cell lines manipulated by retroviral transduction.

Results

4.3 Generation of Cx32 Knock-down and Overexpressing Human Urothelial Sub-lines

4.3.1 Generation of Cx32 shRNA and $Cx32^{WT}$ and $Cx32^{T134A}$ overexpressing vectors

A Mlu1 restriction digest on purified plasmid DNA confirmed that the three independent Cx32 shRNA sequences were successfully ligated into the retroviral vector pSIREN-RetroQ (Fig 4.2). shRNA reactions containing the Mlu1 enzyme ran more slowly through the gel than control reactions without Mlu1 enzyme, indicating linearization. Control empty pSIREN-RetroQ vector was not linearised by Mlu1.

Generation of the $Cx32^{WT}$-pLXSN overexpression vector was confirmed by sequencing. After mutating the wild-type Cx32 coding sequence by site-directed mutagenesis, a Dpn1 digest confirmed the presence of newly synthesised plasmid DNA (Fig 4.3 A) and sequencing results confirmed that 1 out of the 4 single bacterial colonies from which plasmid was purified, successfully contained the T134A mutation (Fig 4.3 B).

Full plasmid map details for pSIREN-RetroQ and pLXSN are provided in the methods chapter (section 2.9).

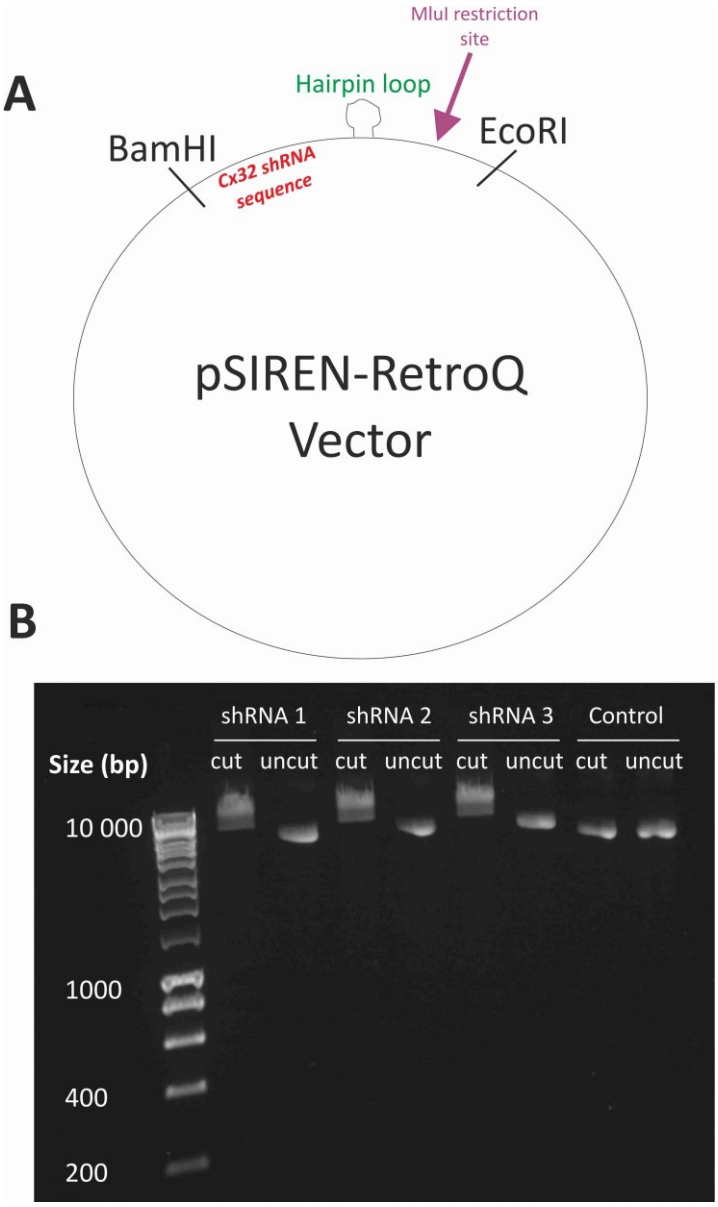

Figure 4.2 Schematic of shRNA Vectors and Mlu1 Restriction Digest to Verify Cx32 shRNA Inserts.

To verify that the pSIREN-RetroQ vector contained Cx32 shRNA inserts, a Mlu1 restriction digest was performed on purified plasmid DNA. The three shRNAs were designed to be inserted directionally between BamHI and EcoRI restriction sites (A). Each shRNA contained a Mlu1 restriction site downstream of the hairpin loop (not found in the vector backbone). shRNA digests containing the Mlu1 enzyme resulted in a product that was retarded on the gel indicating linearization (B).

Figure 4.3 Sequence Confirmation for DNA Plasmids following Site-directed Mutagenesis.

(A) Cx32 (wild-type plasmid) was subjected to site-directed mutagenesis using primers to incorporate the single base change. The resulting plasmid DNA PCR products were incubated with DpnI restriction enzyme to digest methylated parental (non-mutated) plasmid to leave only mutated plasmid, as illustrated by reduced intensity of band at 4 kb(*). Following Dpn1 digest, additional smaller DNA fragments were observed (**). These are predicted to be incomplete PCR products from the site-directed mutagenesis, or partially DpnI-digested parental plasmid according to Edelheit et al. 2009.

(B) Purified plasmids containing "mutated" Cx32 DNA were sequenced following bacterial expansion to identify successful site-directed mutagenesis. Of four sequenced plasmids, one contained the desired T134A mutation as circled in red (ACC mutated to GCC at nucleotide position 400).

4.3.2 Generation of retroviral transfected PT67 packaging cell lines

Following transfection of the PT67 packaging cells with the pSIREN-RetroQ shRNA or pLXSN overexpression vectors, antibiotic selection was effective in removing non-transfected cells from the cultures. Phase contrast micrographs of packaging cells transfected with pSIREN-RetroQ or pLXSN vectors are presented in figures 4.4

and 4.5 respectively. Mock-transfected control cultures were killed by the antibiotic selection within 3 days for shRNA-transfected cells grown in puromycin and 5 days for pLXSN-transfected cells grown in G418.

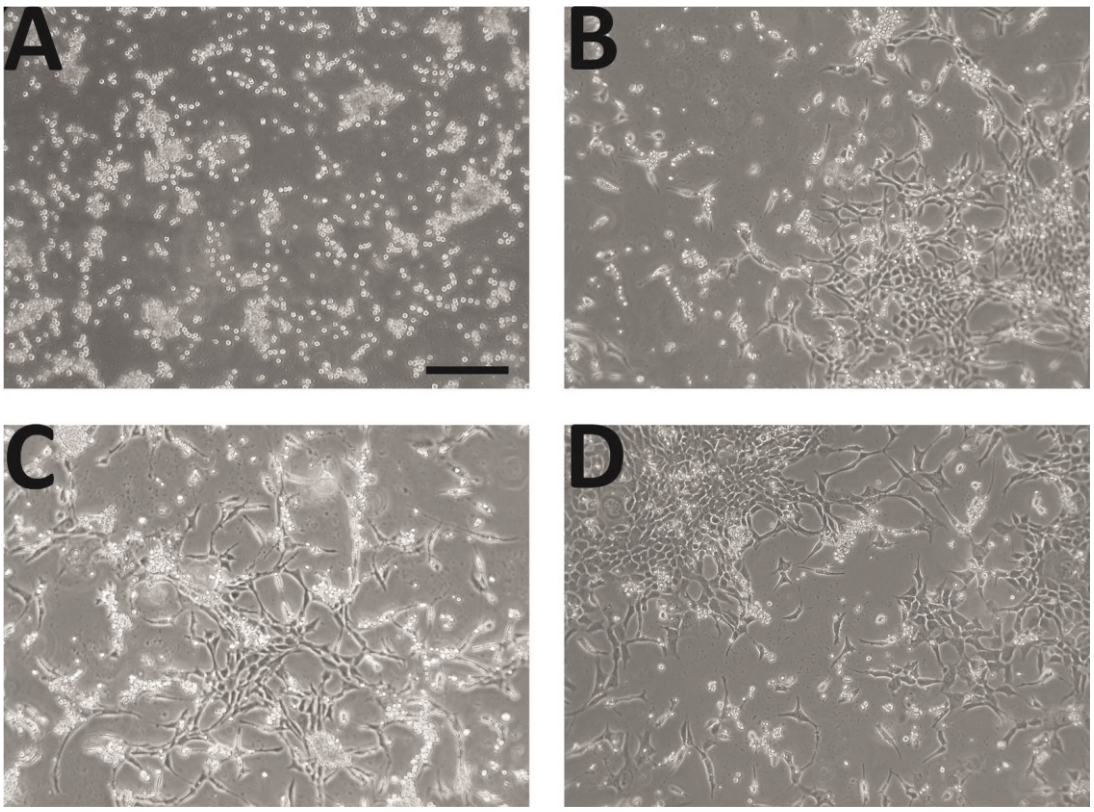

Figure 4.4 Phase Contrast Micrographs of Cx32 shRNA Transfected PT67 Cells Following Antibiotic Selection.

PT67 cells were transfected with pSIREN-RetroQ vector containing Cx32 shRNAs 1, 2 and 3 (B-D respectively) and selected in puromycin. A mock-transfected control was included to demonstrate the effectiveness of the antibiotic on non-transfected cells (A). Images were taken 3 days after growth in 4 µg/ml puromycin.

Scale bar = 200 µM

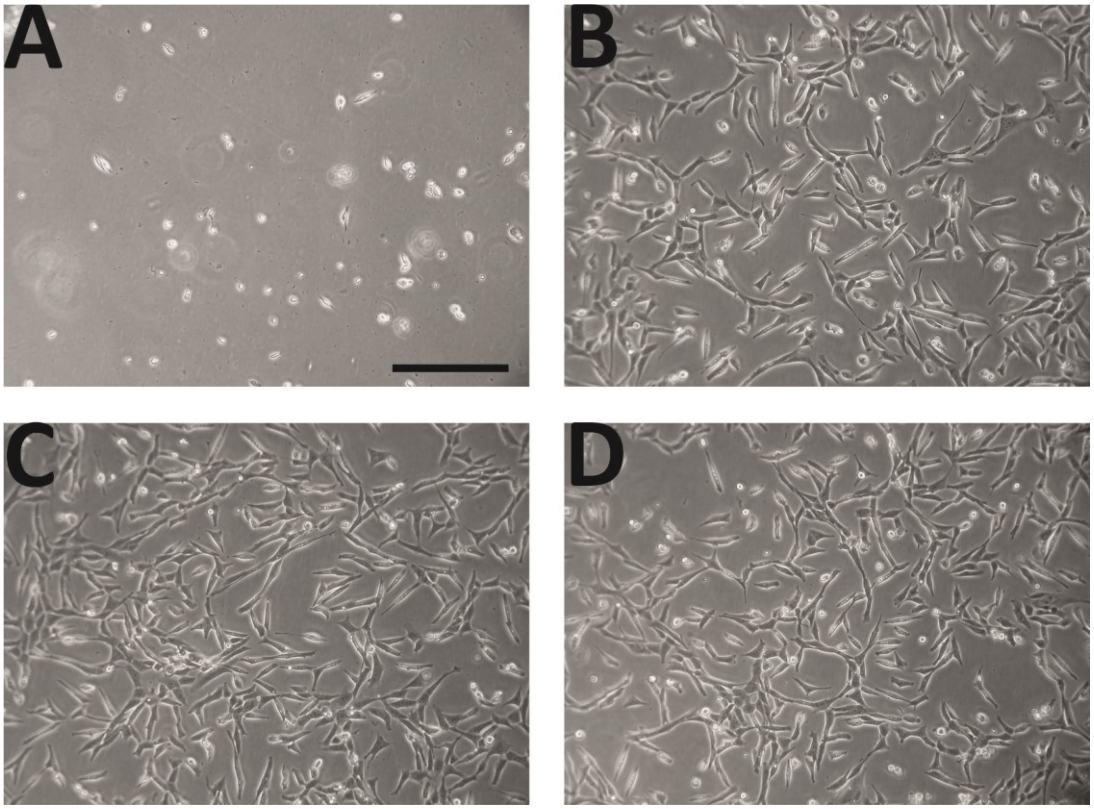

Figure 4.5 Phase Contrast Micrographs of pLXSN Transfected PT67 Cells Following Antibiotic Selection.

PT67 cells were transfected with pLXSN^{empty} (B), pLXSN-Cx32^{WT} (C) and pLXSN-Cx32^{T134A} and then selected in 0.5 mg/ml G418. A mock-transfected control was included to demonstrate the effectiveness of the antibiotic on non-transfected cells (A). Images were taken after 5 days growth in antibiotic.

Scale bar = 200 µM

4.3.3 Generation of stable Cx32 shRNA knock-down sub-lines

Following retroviral transduction complete death of mock-transduced NHU cells occurred after 5 days in puromycin, whilst the successfully transduced NHU cells were actively proliferating indicating successful antibiotic selection (Fig 4.6). The transduction efficiency was estimated to be similar for control and Cx32 shRNA cells; however transduction efficiencies between three independent NHU cell lines were variable, with estimated transduction efficiencies ranging between 30 and

70%. The appearance of Cx32 shRNA cells grown in KSFMc was morphologically indistinguishable from control shRNA cultures; cells grew as a monolayer with an epithelial pavement-like morphology.

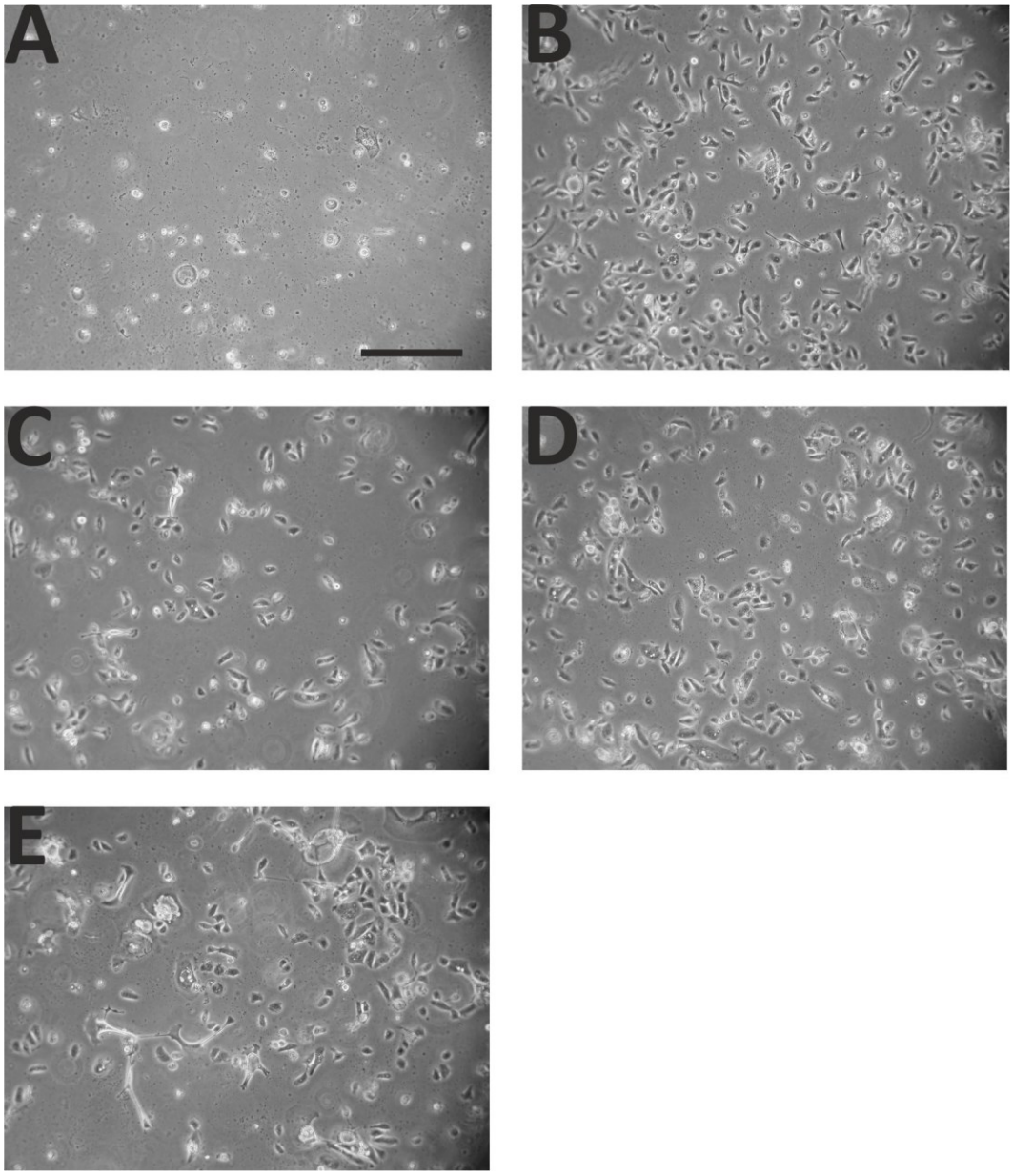

Figure 4.6 Phase Contrast Micrographs of Representative Cx32 shRNA Transduced NHU Cells Following Antibiotic Selection.

Y1185 (P1) NHU cells were transduced with retroviral particles containing control shRNA (B) and Cx32 shRNAs 1, 2 and 3 (C-E respectively) and then selected in 1 µg/ml puromycin. A mock-transfected control was included to demonstrate the effectiveness of the antibiotic on non-transfected cells (A). Images were taken 5 days after antibiotic treatment.

Scale bar = 200 µm

4.3.4 Verification of Cx32 shRNA knock-down in NHU transductants

RT-PCR analysis of Cx32 transcript demonstrated an observable knock-down in expression in Cx32 shRNA cells grown in either 5% serum or cells differentiated in ABS/Ca^{2+}, compared to control shRNA cells (Fig 4.7 A). Expression of Cx32 was not detected by RT-PCR in control or Cx32 shRNA cells grown in either KSFMc (undifferentiated) or 2mM [Ca^{2+}] (stratified).

Cx32 protein expression in differentiating cultures was analysed by immunoblotting to verify successful protein knock-down (Fig 4.7 B). Following 5% ABS pre-treatment, the calcium concentration in cultures was increased to 2mM and protein lysates of control shRNA and Cx32 shRNA (1), (2) and (3), were collected after 3 or 6 days. Bands were analysed by densitometry following normalisation to the loading control β-actin, which revealed that after 3 days the expression of the dimeric product of Cx32 was reduced by 58%, 31% and 41% in each of the three shRNA transductants respectively, compared to the scrambled control shRNA cells. By day 6 post differentiation, protein knock-down was less pronounced, with expression of dimeric Cx32 product knocked down by 34% in Cx32-shRNA (1) cell lysates and in shRNAs (2) and (3), expression was 2% or 9% higher (respectively) than scrambled control cells.

Monomeric Cx32 product was knocked-down to a lesser extent than dimeric, with a reduction of 36%, 15% and 25% in shRNA (1), (2) and (3) respectively after 3 days compared with control shRNA cells. By 6 days post-differentiation, monomeric Cx32 product was reduced by only 12% in shRNA (1) compared with control shRNA cells, however there was a 53% increase in Cx32 shRNA (2) and no change in Cx32 shRNA (3) when compared to control shRNA cells.

An additional band at approximately 100 kD was observed in these blots; previous studies with Cx32 knock-out mice using the same antibody suggest that it is non-specific since the same band was observed in lysates from Cx32 knock-out mice (Nagy et al. 2003). It was therefore not analysed in this study.

Cx32 shRNA (1) gave the most effective knock-down of Cx32 protein and was therefore selected for use in all subsequent shRNA experiments, unless otherwise stated.

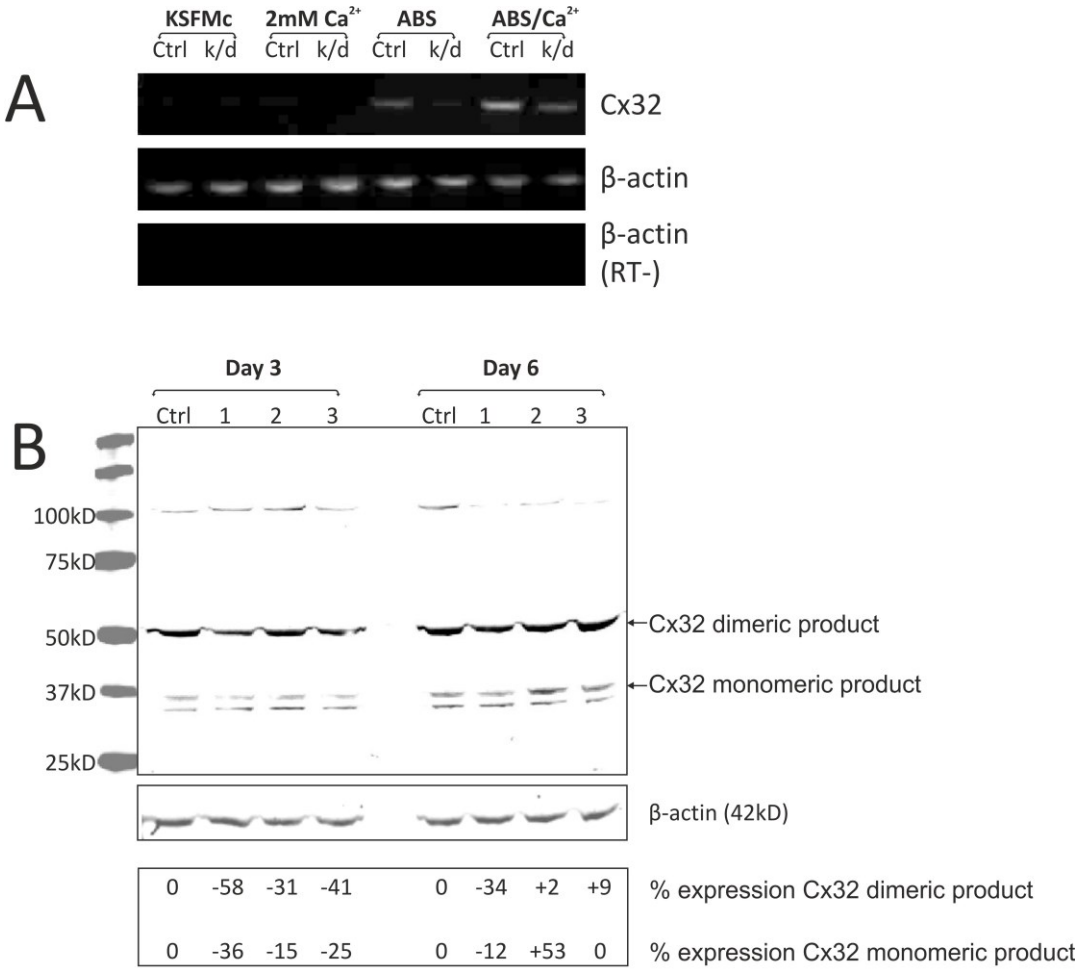

Figure 4.7 Verification of Cx32 Knock-down in Retroviral Transduced NHU Cultures.

(A) Expression of Cx32 transcript was examined in Y1185 Cx32 shRNA-1 transduced NHU (k/d) and control shRNA (Ctrl) cell cultures, grown for 5 days in KSFMc, 2 mM [Ca^{2+}] or 5% ABS, or differentiated following the ABS/Ca^{2+} method for 6 days. Cx32 expression was analysed by RT-PCR and β-actin was included as a normalisation control. A negative control β-actin PCR was performed in which the reverse transcriptase was omitted.

(B) Cx32 protein expression in Y1185 NHU cells transduced with control shRNA (Ctrl) or three independent Cx32 shRNAs (1-3) after 3 or 6 days grown in differentiating conditions following the ABS/Ca^{2+} method. Whole cell lysates were processed for western blotting and labelled with antibodies against Cx32 or β-actin as a loading control. Cx32 monomeric and dimeric products are indicated. Both bands were assessed by densitometry after normalisation to β-actin and expression of each band is indicated relative to control shRNA expression.

4.3.5 Subcellular localisation of Cx32 in control shRNA and Cx32 shRNA transduced NHU cultures

Expression of Cx32 in ABS/Ca^{2+} differentiated NHU control shRNA cultures was cytoplasmic with clean continuous Cx32-labelling observed along the intercellular cell membranes of the majority of cells (Fig 4.8). In Cx32 shRNA knock-down cells, membrane labelling was sparse when compared to control shRNA cells although the majority of cells contained some cytoplasmic labelling.

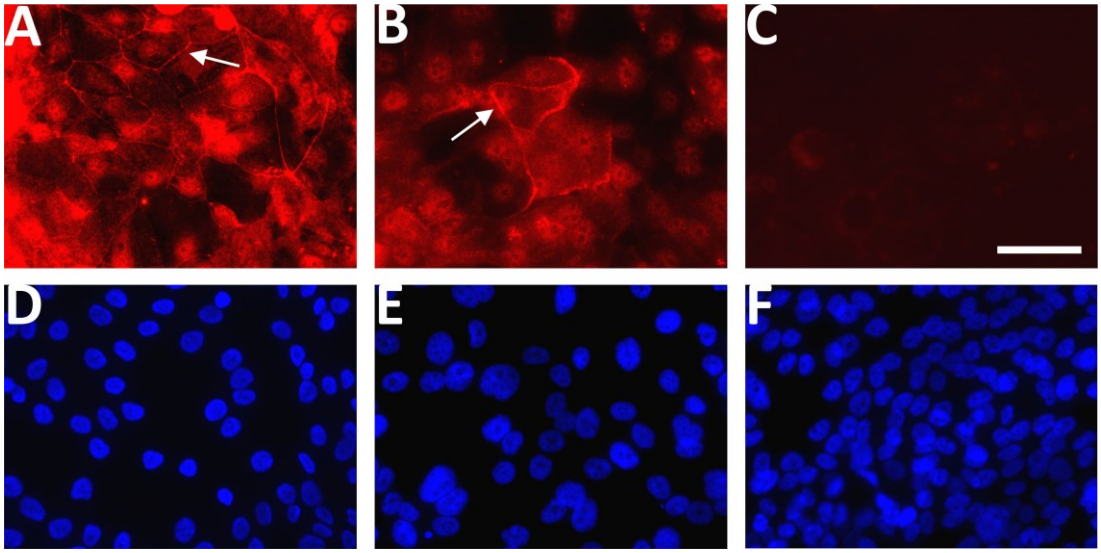

Figure 4.8 Cx32 Immunocytochemistry in Cx32 shRNA Transduced NHU Cultures.

Cx32 immunolabelling in Y1185 ABS/Ca^{2+} differentiated NHU cells transduced with either control shRNA (A) or Cx32 shRNA 1 (B). Arrows indicate membrane labelling.

C = negative control, D-F = Corresponding Hoechst 33258 images.

Scale bar = 50 µm

4.3.6 Generation of Cx32-overexpressing wild-type and T134A dominant-negative mutant sub-lines

After harvesting viral particles from the packaging cells, NHU cells were retrovirally transduced with pLXSN^{empty}, pLXSN-Cx32^{WT} or pLXSN-Cx32^{T134A} and selected with G418 to kill any non-transduced cells. Mock transduced NHU cultures were included to verify the effectiveness of the G418 selection. Complete death of the mock-transduced cells occurred after 4 days in G418, whilst the successfully transduced NHU cells were growing back (Fig 4.9). The effectiveness of each transduction varied between experiments, with estimated efficiencies between 40 and 60% based on the population of cells which survived antibiotic treatment.

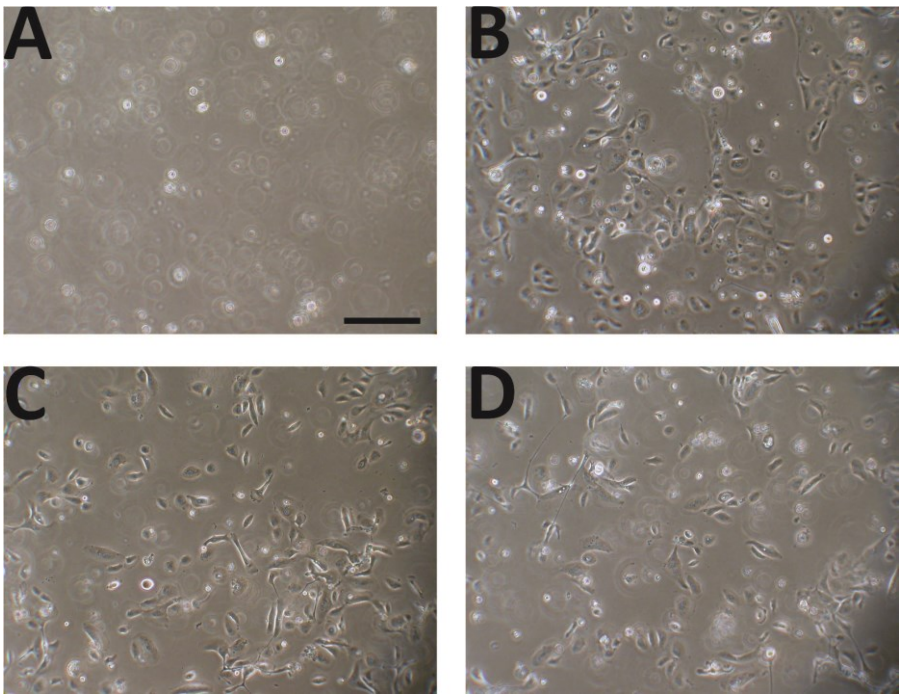

Figure 4.9 Phase Contrast Micrographs of Representative pLXSN Transduced NHU Cultures following Antibiotic Selection.

Y1270 NHU cells were transduced with pLXSN^{empty} (B), pLXSN-Cx32^{WT} (C) and pLXSN-Cx32^{T134A} (D) and then selected in 0.1 mg/ml G418. A mock-transfected control was included to demonstrate the effectiveness of the antibiotic on non-transduced cells (A). Images were taken 4 days after antibiotic treatment.

Scale bar = 200 µm

4.3.7 Verification of $Cx32^{WT}$ and $Cx32^{T134A}$ overexpression in transduced NHU cultures

In control ($pLXSN^{empty}$) cells, expression of dimeric Cx32 was induced following differentiation using the ABS/Ca^{2+} method, with very little monomeric Cx32 protein observed regardless of culture conditions (Fig 4.10 A). Expression of monomeric and dimeric Cx32 bands were strongly upregulated in both wild-type and mutant Cx32 overexpressing cells. In overexpressing cells, Cx32 protein expression was substantially increased as differentiation progressed. Densitometry analysis of Cx32 bands after 6 days culture in ABS/Ca^{2+} revealed an increase in monomeric Cx32 by 40- and 29-fold in Cx^{WT} and $Cx32^{T134A}$ cells respectively, and dimeric Cx32 by 10-fold in both $Cx32^{WT}$ and $Cx32^{T134A}$ (Fig 4.10 B).

In addition to monomeric and dimeric protein products, immunoblotting with $Cx32^{WT}$ and $Cx32^{T134A}$ cell lysates demonstrated expression of many additional bands and some band smearing was observed. The extra protein products were associated with Cx32 overexpression, increased in intensity during cell differentiation and were not observed in control ($pLXSN^{empty}$) cells. This included a 13kD product which is the size of the C-terminal tail recognised by the Cx32 antibody. The 13kD product was particularly abundant in non-differentiated cells and cells treated with 5% ABS, with a small amount observed in differentiated cells.

4.3.8 Subcellular localisation of Cx32 in overexpressing $Cx32^{WT}$ and $Cx32^{T134A}$ transduced NHU cells

Intensity of Cx32 by immunocytochemistry was increased in $Cx32^{WT}$ and $Cx32^{T134A}$ transductants when compared to pLXSN empty vector control cells (Fig 4.11). In $Cx32^{WT}$ and $Cx32^{T134A}$ overexpressing cells, strong punctate Cx32 expression was observed in large cytoplasm vesicles, whereas cytoplasmic Cx32 expression was weak and diffuse in empty vector control cells with smaller vesicles observed.

Areas of continuous membrane labelling were observed in all cells, however large patches of cells in both $Cx32^{WT}$ and $Cx32^{T134A}$ overexpressing cultures contained thick brightly labelled plaques of Cx32 which appeared to be membrane-associated and were not observed in control cells (Fig 4.11 D).

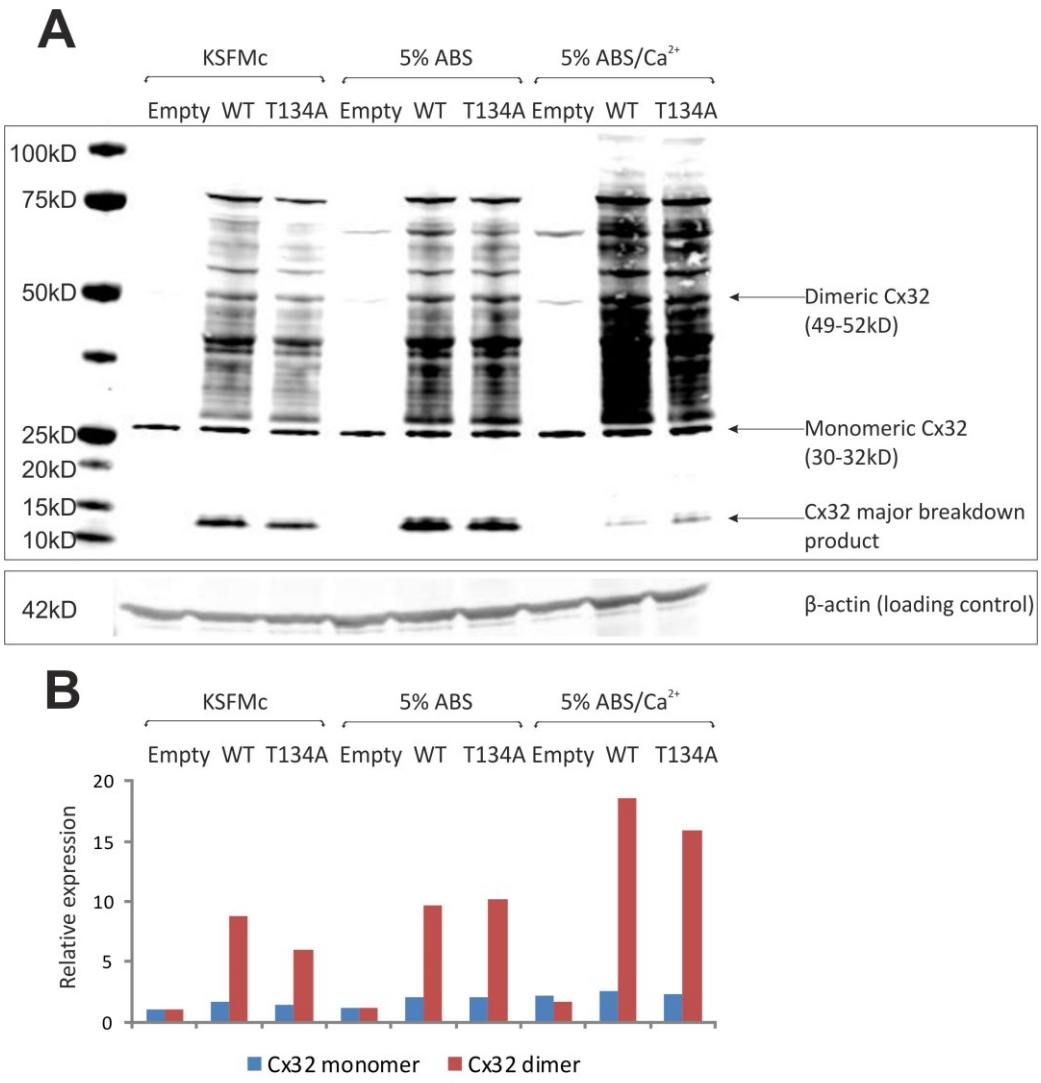

Figure 4.10 Western blot analysis of pLXSN transduced Y1270 NHU cells.

NHU cells were transduced with $pLXSN^{empty}$, $pLXSN\text{-}Cx32^{WT}$ and $pLXSN\text{-}Cx32^{T134A}$ and differentiated using the ABS/Ca^{2+}method. Whole cell lysates were collected during the differentiation time course (in KSFMc, after 5 days in 5% ABS and after 6 days in ABS/Ca^{2+}) and 12 µg protein was processed for immunoblotting. Monomeric, dimeric and breakdown products are indicated on the western blot image (A). Densitometry analysis was performed and after normalisation to β-actin, expression of monomeric and dimeric Cx32 bands were plotted, in each case relative to non-differentiated (KSFMc) $pLXSN^{empty}$ cells (B).

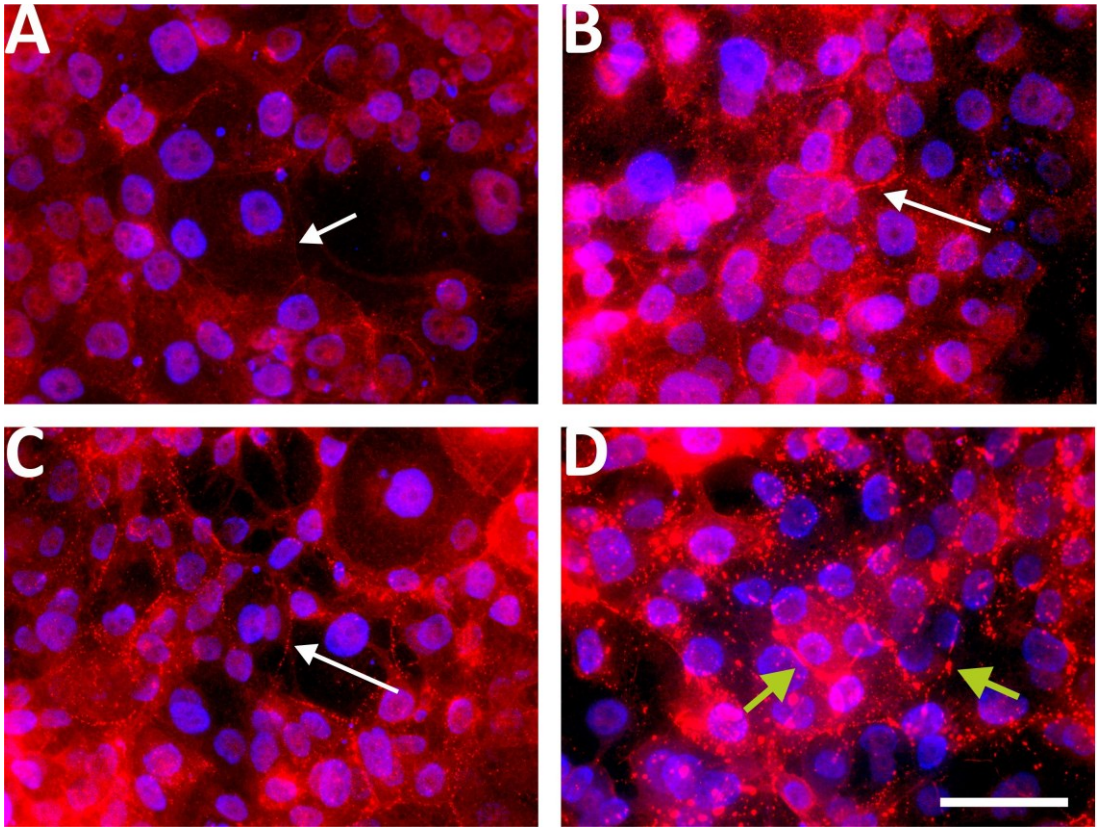

Figure 4.11 Immunocytochemistry of Cx32 in pLXSN-transduced NHU Cultures following Differentiation in ABS/Ca^{2+}.

pLXSN-transduced Y1270 NHU cells were seeded onto glass slides and differentiated following the ABS/Ca^{2+}method prior to fixation. Immunofluoresence of Cx32 immunolabelling in pLXSN^{empty} (A), pLXSN-Cx32^{WT} (B) and pLXSN-Cx32^{T134A} (C & D) cells is shown. Continuous membrane labelling (white arrows, A to C) and large membrane plaques (green arrows, D) are indicated. Large membrane plaques were observed in both Cx32^{WT} and Cx32^{T134A} cultures, but not pLXSN^{empty} transduced cells.

Scale bar = 50 µm

4.4 Assessment of Growth and Morphology of Cx32 Knock-down and Overexpressing Human Urothelial Cell Lines

4.4.1 Assessment of growth in Cx32 shRNA Knock-down NHU cells.

Growth rates in Cx32 and control shRNA transduced NHU cells grown in KSFMc (3 independent cell lines, Y1057, Y1119 and Y1185) were determined by Alamar Blue® assay (Fig 4.12). Cx32 shRNA cells were growth-inhibited compared with control shRNA cells, but this effect was variable between cell lines and most pronounced early in the exponential growth phase (approximately 4-5 days post-seeding) where the percentage reduction of Alamar Blue® was significantly different in all three cell lines. However, overall growth trends over the 11 day time period were comparable between Y1057 control and Cx32 shRNA cells (Fig 4.12 A), whereas Cx32 shRNA cells demonstrated reduced growth rates compared to control shRNA cells in both Y1119 and Y1185 cell lines (Fig 4.12 B & C).

4.4.2 Assessment of growth in $Cx32^{WT}$ and $Cx32^{T134A}$ overexpressing transduced NHU cells

The biomass of pLXSN-transduced (empty vector, $Cx32^{WT}$ and $Cx32^{T134A}$) NHU sub-line cultures was determined by Alamar Blue® assay which was performed up to 9 days after seeding in KSFMc (Fig 4.13). Cultures displayed normal growth patterns regardless of plasmid insert, with exponential growth occurring between days 3 and 7 after seeding.

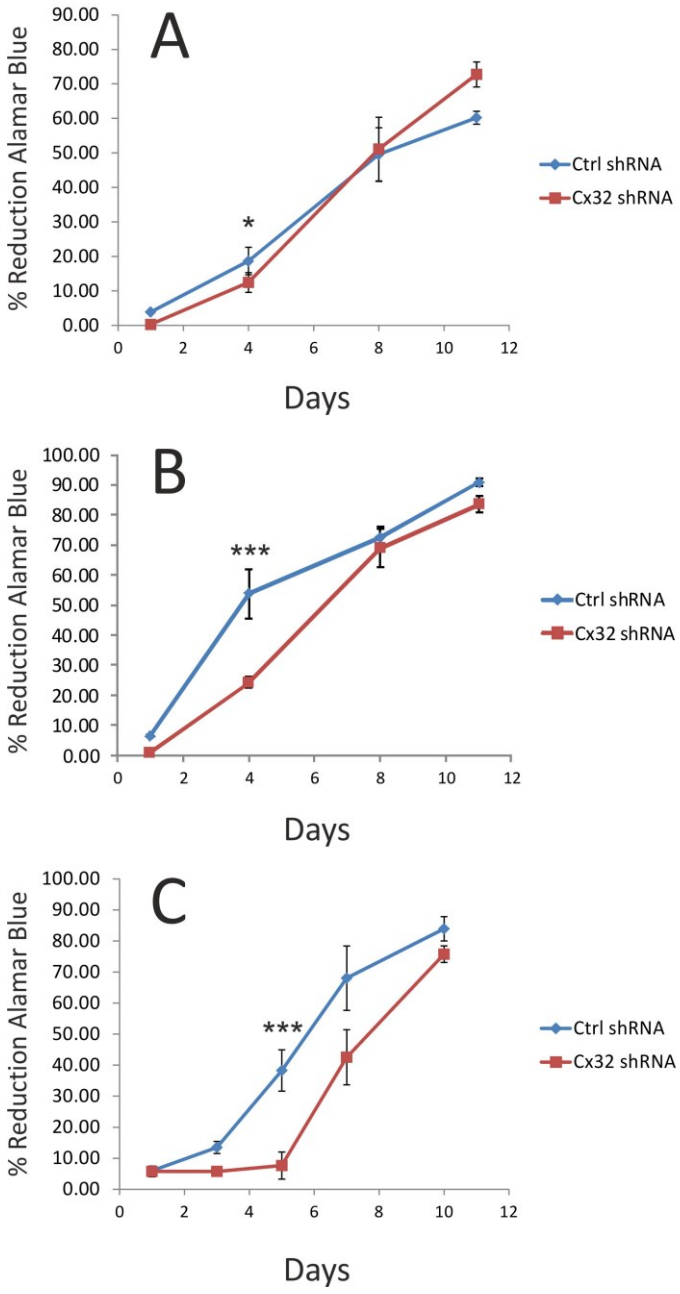

Figure 4.12 Assessment of Growth in Cx32 shRNA Knock-down NHU Cultures.

Alamar Blue® assays were performed on Y1057 (A), Y1119 (B) and Y1185 (C) NHU cell lines, transduced with control shRNA or Cx32 shRNA retroviral vectors. Percentage reduction of Alamar Blue® over a 10 or 11 day period was plotted to demonstrate growth of cells grown in KSFMc. Each data point is the average of six replicates ± SD.

*Two-tailed P-values: *P=0.01 ***P<0.001.*

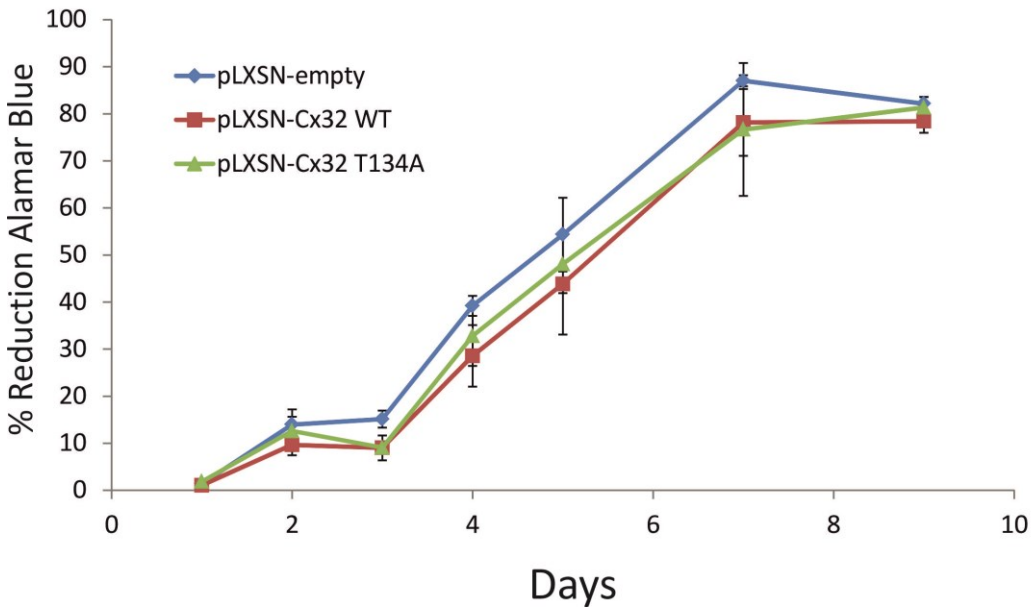

Figure 4.13 Assessment of Growth in Cx32 Wild-type and Dominant Negative Cells.

Alamar Blue ® assays were performed on Y1247 NHU cells transduced with pLXSN-empty vector, pLXSN-Cx32^{WT} and pLXSN-Cx32^{T134A} retroviral overexpression vectors. Percentage reduction of Alamar Blue® was plotted over a 9 day period to demonstrate growth of cells grown in KSFMc. Each data point is the average of six replicates ± SD.

4.4.3 Assessment of morphology of Cx32 knock-down and overexpressing $Cx32^{WT}$ and $Cx32^{T134A}$ cells following differentiation in ABS/Ca^{2+}

Examination of Cx32 shRNA cells after differentiation in ABS/Ca^{2+} for 6 days revealed that they were similar in appearance to control cells, with a heterogeneous population of spindly and stratified cells characteristic of a differentiated phenotype (Fig 4.14 A-C). Some cells contained phase-bright borders. Cx32 overexpressing cells ($Cx32^{WT}$ and $Cx32^{T134A}$) were very similar in morphology to empty-vector control cells (Fig 4.14 D-F). All pLXSN-transduced cultures exhibited heterogeneous morphologies with large numbers of spindly cells, some containing large vacuoles and a number of small rounded cells with phase-bright borders.

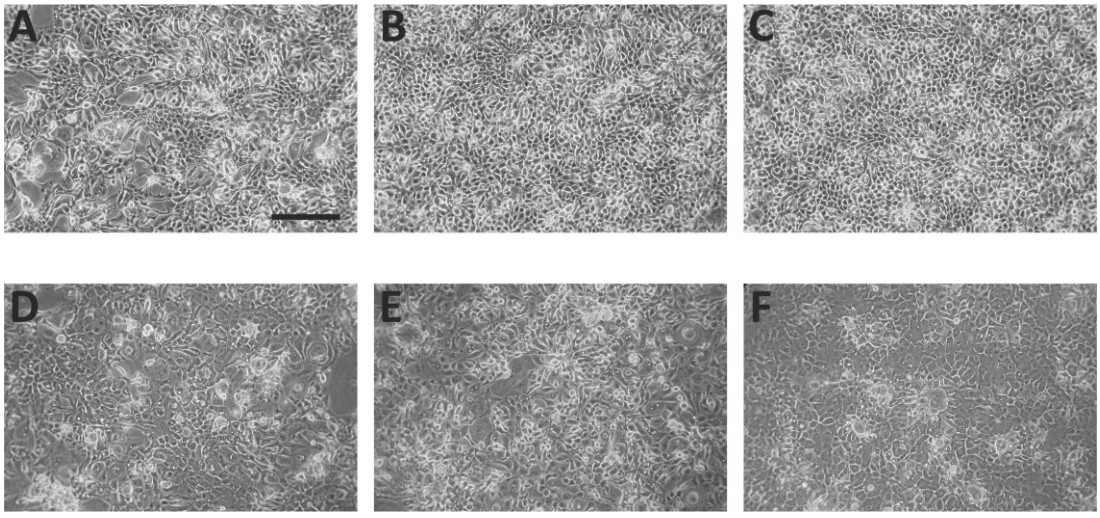

Figure 4.14 Phase Contrast Micrographs of Cx32 shRNA Knock-down, $Cx32^{WT}$ and $Cx32^{T134A}$.

Overexpressing NHU Cultures following Differentiation in ABS/Ca^{2+} Phase contrast micrographs of mock (A), control shRNA (B) and Cx32 shRNA (C) transduced NHU cells (Y1185 at P4) and Y1270 NHU cells transduced with pLXSN-Empty Vector (D), pLXSN-$Cx32^{WT}$ (E) and pLXSN-$Cx32^{T134A}$ (F) at P4. Following transduction and successful selection of NHU cultures, cells were differentiated according to the ABS/Ca^{2+} protocol.

Scale bar = 200 µm

4.4.4 Effects of Cx32 knock-down and overexpression on gap junction mediated intercellular communication

Quantitative assessment of Lucifer yellow dye-transfer was performed in Cx32 shRNA knock-down and in $Cx32^{WT}$ and $Cx32^{T134A}$ overexpressing cells, following differentiation with the TZ/PD method to study the extent of functional GJIC in each transduced cell line.

In Cx32 shRNA cells, Lucifer yellow dye-transfer was significantly reduced when compared with control shRNA cells (Fig 4.15). In shRNA control cells the mean number of lucifer yellow containing cells was 8.8 ± 2.6 (sd) for every cell initially scratch loaded (as observed by Rhodamine dextran), whereas the mean number of Lucifer yellow containing cells in Cx32 shRNA cultures was 4.5 ± 1.5 (sd).

Quantitative assessment of $Cx32^{WT}$ overexpressing cells revealed that there was a highly significant increase in the number of dye-receiving cells following scratching, when compared to pLXSN empty vector control cells and $Cx32^{T134A}$ dominant negative cells (Fig 4.16). There was also a significant reduction in dye-transfer in $Cx32^{T134A}$ dominant negative cells, compared to empty vector and $Cx32^{WT}$ cells suggesting inhibition of GJIC when the mutant channel was over expressed, indicative of a dominant negative influence. In $Cx32^{WT}$ overexpressing cells, the mean number of Lucifer yellow dye-transmitted cells was 10.1 ± 3.5 (sd) for every cell initially loaded with Rhodamine dextran, whereas the mean number of Lucifer yellow containing cells in $Cx32^{T134A}$ overexpressing cells was 1.1 ± 0.2 (sd) and in control $pLXSN^{empty}$ cells 2.1 ± 1.0 (sd).

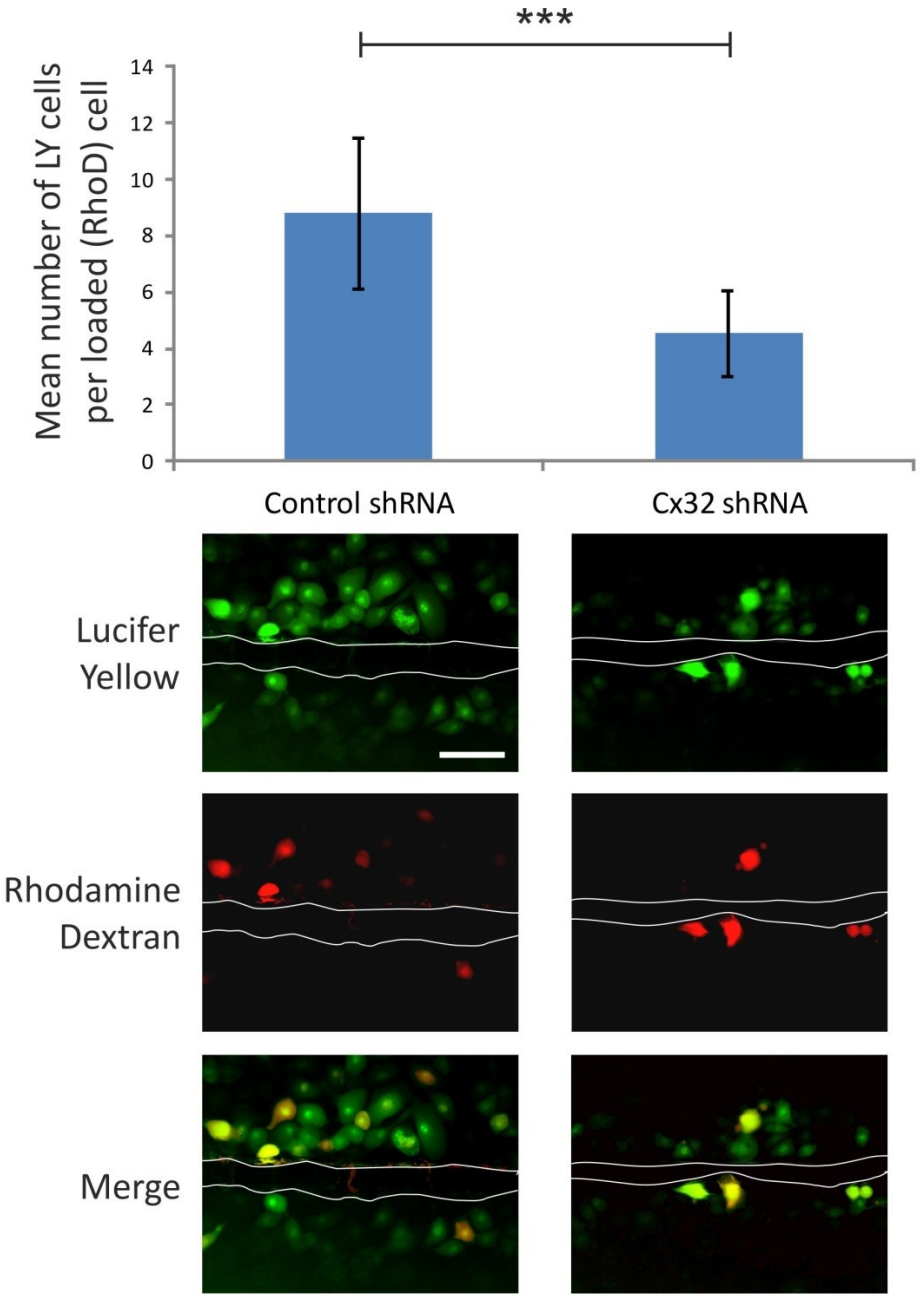

Figure 4.15 Lucifer Yellow Scrape-load Dye-transfer in Cx32 Knock-down Cultures.

Y1117 Cx32 shRNA and control shRNA transduced NHU cultures were differentiated following the TZ/PD method for 6 days. Cultures were scratched in the presence of Lucifer yellow and Rhodamine-dextran fluorescent dyes to load cells during temporary membrane perturbation. The number of cells containing the gap junction-permeable dye Lucifer yellow, were normalised to the number of initially loaded (rhodamine dextran) cells at 10 continuous areas across each scratch. White lines indicate the approximate scratch boundaries. Scale bar = 50 µm

****P value < 0.001, considered extremely significant (Unpaired t-test)*

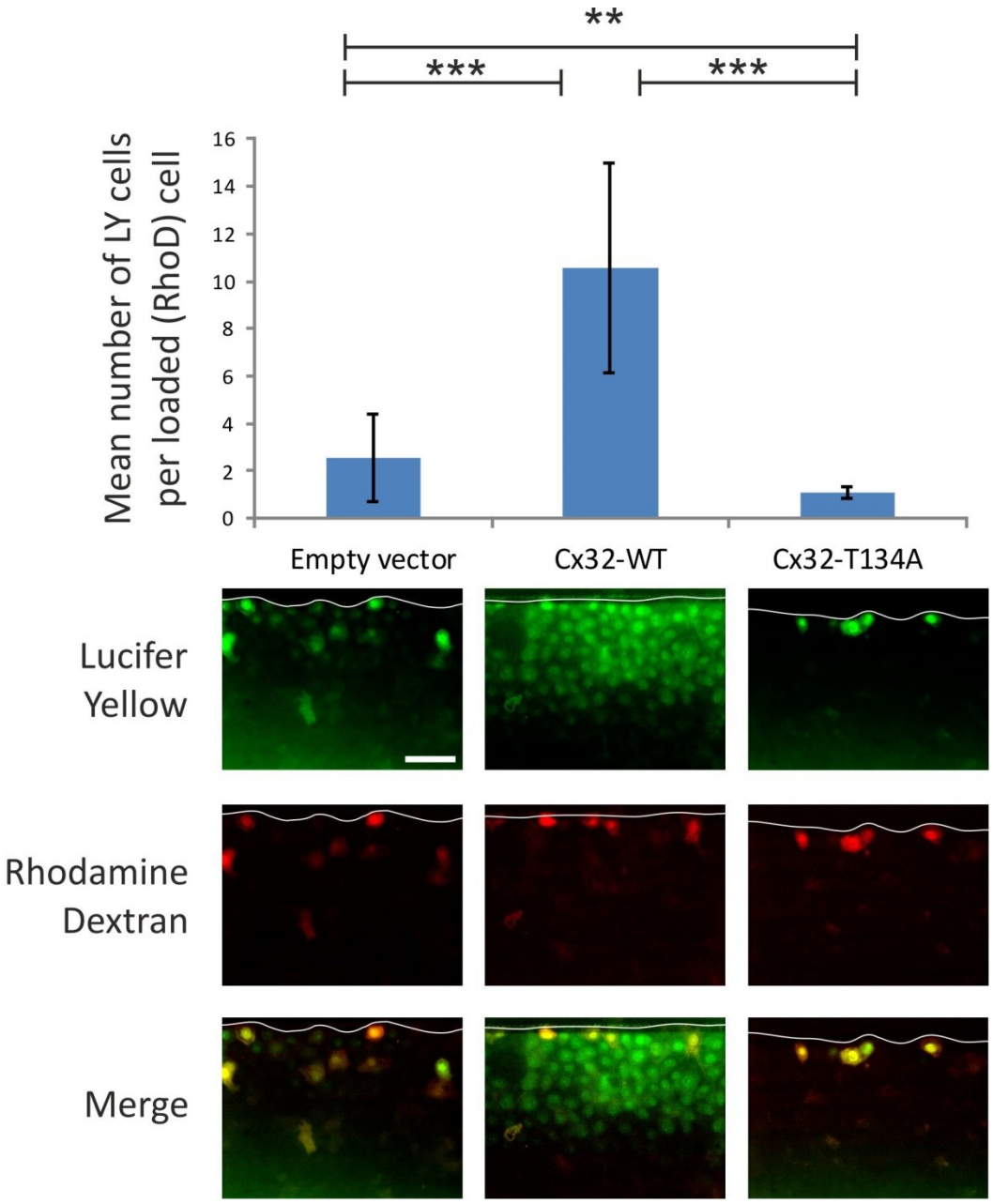

Figure 4.16 Lucifer Yellow Scrape-load Dye-transfer in $Cx32^{WT}$ and $Cx32^{T134A}$ Transduced Cultures.

pLXSN-empty, $Cx32^{WT}$ and $Cx32^{T134A}$ transduced NHU cultures (Y1270) were differentiated following the TZ/PD method for 6 days, before scratching to load cells in the presence of fluorescent dyes. The number of cells containing Lucifer yellow were normalised to the number of initially loaded (Rhodamine dextran) cells at 10 regions of interest across each scratch. White lines indicate the approximate scratch boundaries. Scale bar = 50 µm

**** P value <0.001 considered extremely significant **P<0.01 considered very significant (One way ANOVA)*

4.5 Assessment of Barrier Function and Differentiation Capacity of Cx32 Knock-down and Overexpressing Human Urothelial Cell Lines

4.5.1 Assessment of barrier function in Cx32 shRNA knock-down cultures

In Cx32 shRNA transduced cells, barrier development as measured by TER was delayed following differentiation with ABS/Ca^{2+}, when compared to control shRNA transduced cells or mock-transduced NHU cells (Fig 4.17 A). The effect was apparent with all three Cx32 shRNA sequences. After 6 days in differentiating conditions the mean TER values of mock-transduced and control shRNA cultures were 2500 Ω.cm^2 ± 75 (sd) and 2490 Ω.cm^2 ± 437 (sd) respectively, compared with Cx32 knock-down cultures for which the mean TER values were 212 Ω.cm^2 ± 4 (sd), 168 Ω.cm^2 ± 6 (sd), and 186 Ω.cm^2 ± 10 (sd) for Cx32 shRNA (1), (2) and (3) respectively. However, a tight barrier did eventually develop in all Cx32 shRNA cells between days 10 and 13 after induction of differentiation.

Although the rates of barrier development during differentiation of independent donor samples was variable, the compromised barrier development following Cx32 gene silencing was reproducible in three independent cell lines transduced with control shRNA and Cx32 shRNA (Fig 4.17 B). After 6 days in differentiating conditions, all three cell lines examined had significantly lower TER values following Cx32 shRNA knock-down, than control shRNA cells.

4.5.2 Assessment of barrier function in $Cx32^{WT}$ and $Cx32^{T134A}$ transduced NHU cultures

To examine the relationship between Cx32-mediated cell-cell communication and barrier development, TER was examined in wild-type and mutant Cx32 overexpressing cell lines during differentiation in ABS/Ca^{2+}. Transduced cell lines from three independent donors were investigated (Fig 4.18 A). Although there were some significant TER differences between empty vector, $Cx32^{WT}$ and $Cx32^{T134A}$ transductants, particularly in the Y1277 cell line, there were no clear and consistent differences in TER which could be confirmed across multiple cell lines at both 3 and 6 days during differentiation.

Variability in barrier development was clear between the three cell lines, one of the cell lines tested (Y1270) gave a tight barrier which exceeded 1500 Ω.cm^2 after 3 days in differentiating conditions, whilst the other two cell lines (Y1284 and Y1277) were still below 500 Ω.cm^2 at a comparable time point during differentiation, confirming that barrier attainment across different donor cell lines occurs at a variable rate.

The relationship between gap junction-mediated intercellular communication and barrier development of NHU cells was further examined in non-transduced NHU cells, undergoing differentiation in the presence of the generic gap junction communication inhibitor 18α-glycyrrhetinic acid (Fig 4.18 B).

Barrier development (as measured by TER) was not compromised by the addition of 18α-GA. 3 days after seeding cells in ABS/Ca^{2+}, the mean TER of NHU cells treated with 5 µM or 50 µM 18α-GA was 1937 Ω.cm^2 and 2223 Ω.cm^2 respectively (n=6), compared to 2355 Ω.cm^2 for vehicle control cultures. Mean TER values increased to

>3900 Ω.cm^2 by day 6 and no significant difference was observed between 18α-GA treated and control cultures.

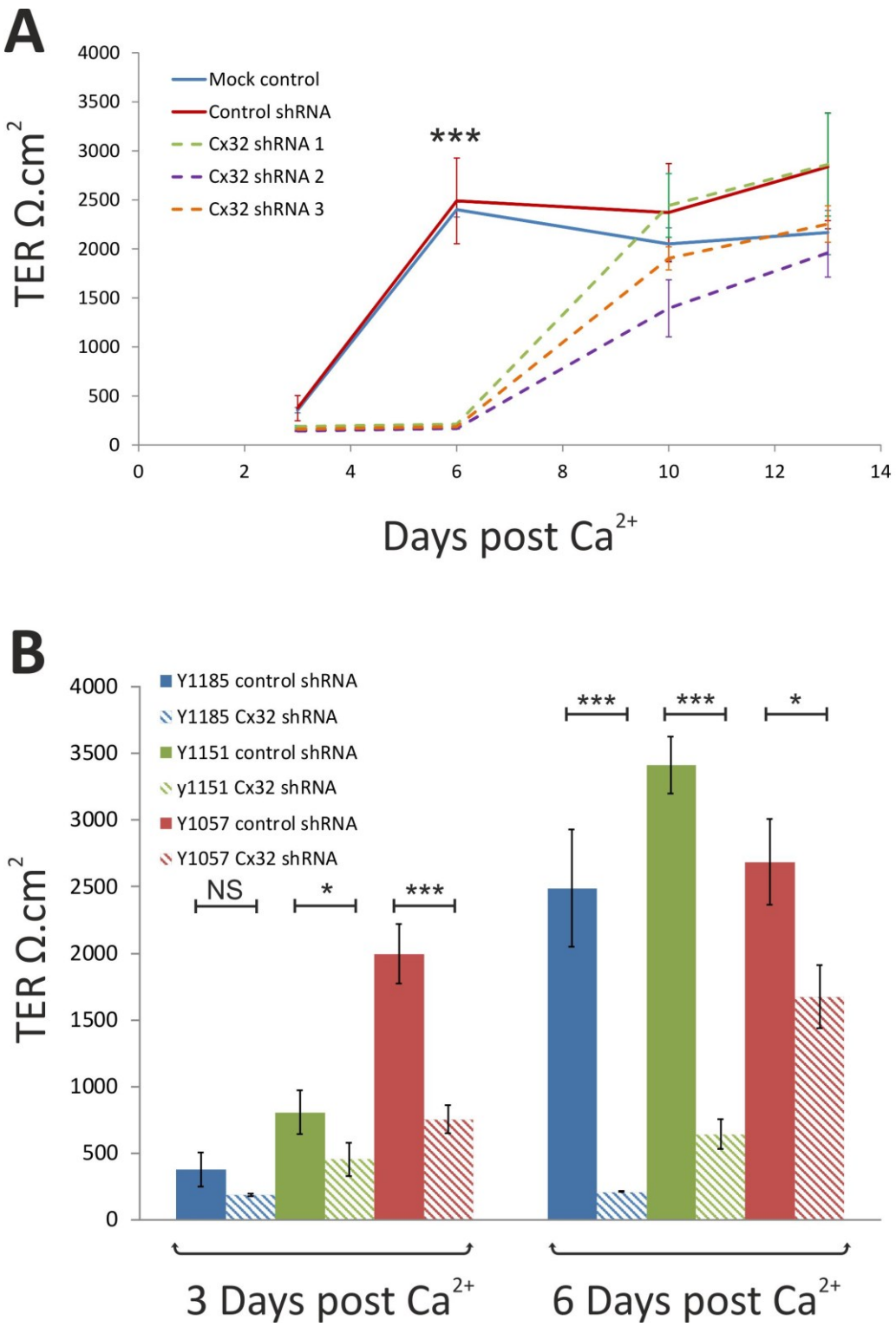

Figure 4.17 Effect of Cx32 shRNA Knock-down on NHU Cell Barrier Development.

*(A) Barrier function of Cx32 shRNA knock-down NHU cells (Y1185, P4) was determined by measurement of TER in ABS/Ca^{2+} differentiating conditions at 3, 6, 10 and 13 days following addition of 2 mM calcium. Mean TER values of control shRNA and mock-transduced NHU cells are represented by solid lines, whilst the TER of three Cx32 shRNA transductants (three independent Cx32 shRNA sequences) are represented by dashed lines. Data show the mean of four replicate cultures ± SD (***P<0.001 T-test comparing the mean TER for the Control shRNA with the mean value TER of Cx32 shRNA at day 6 post addition of Ca^{2+}).*

*(B) Barrier function as measured by TER in three independent cell lines (Y1185, Y1151 and Y1057), transduced with control or Cx32 shRNA retroviral vectors and grown on permeable Snapwell™ membranes. Mean TER values are plotted after 3 or 6 days culture in ABS/Ca^{2+} differentiating conditions. Data show the mean of 4-6 replicate cultures ±SD (*** P<0.001 *P<0.05 NS = not significant (P>0.1). T-test comparing the mean TER for control shRNA with the mean TER of Cx32 shRNA).*

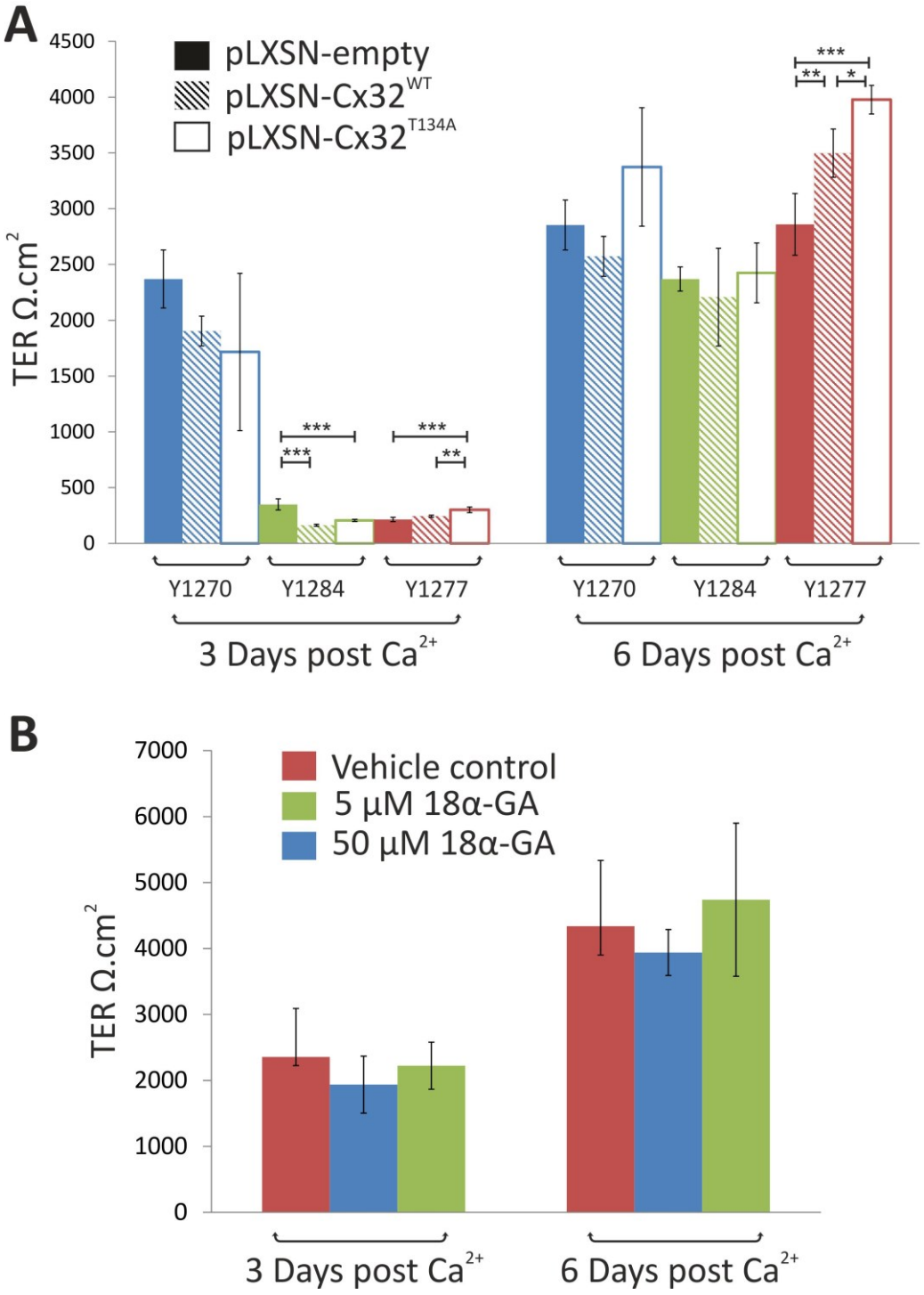

Figure 4.18 Effect of Cx32-mediated GJIC on the Barrier Development of Differentiated NHU Cultures.

(A) Barrier function of Y1270, Y1284 and Y1277 NHU cells overexpressing wild-type or pore-closed mutant Cx32, determined by measurement of TER in cells grown in ABS/Ca2+ on permeable Snapwell™ membranes. Mean TER values (±SD) are plotted at days 3 and 6 post-differentiation in pLXSN-empty vector control cells (solid bar),

*pLXSN-Cx32WT cells (dashed bar) and pLXSN-Cx32T134A cells (white bar). Data show the mean TER of 3 to 6 replicate cultures ± SD (One way ANOVA P values of ***=P<0.001, **=P<0.01 and *=P<0.1 indicate significance with Tukey-Kramer post-test. Where a P-value is not indicated, data was considered not significant).*

(B) Barrier function as measured on by TER plotted on days 3 and 6 during differentiation of Y1335 NHU cultures in ABS/Ca2+. Cells were grown on permeable Snapwell™ membranes and treated with 5µM or 50µM 18α-glycyrrhetinic acid (18α-GA) or DMSO vehicle control for the duration of the experiment. Data show the mean TER of 6 replicate cultures ±SD (One-way ANOVA P values of >0.3 at day 3 and >0.5 at day 6, considered not significant).

4.5.3 Phenotypic Assessment of Cx32 shRNA knock-down cells during differentiation.

Control and Cx32 shRNA cells were seeded at equivalent cell densities and differentiated following the ABS/Ca^{2+} method. Whole cell lysates were collected during the differentiation time course; from cultures before addition of serum (untreated), after culture in serum for 1 or 3 days and at days 1, 3 and 6 after increasing the calcium concentration to [2 mM] (as summarised in 4.19A). This allowed for a time-dependent assessment of proteins associated with urothelial differentiation and tight barrier development such as claudins and Zonula Occludens proteins.

Cx32 shRNA expression in NHU cells resulted in Cx32 protein knock-down (Fig 4.19 B), however as observed previously (see Fig 4.7), the knock-down in protein became less pronounced as differentiation proceeded. Monomeric Cx32 was expressed throughout the differentiation procedure, with knock-down in expression observed at early time-points (day 0 and after 1 day in ABS). Dimeric Cx32 protein was upregulated following the switch to ABS/Ca^{2+}, with knock-down observable at days 1 and 3 post addition of 2 mM calcium. The effects of Cx32

shRNA knock-down on expression of selected markers of urothelial differentiation are summarised below.

Claudin 4

Claudin 4 was expressed following treatment of cells with 5% ABS and the expression of both proteins increased as differentiation progressed. Claudin 4 expression was reduced in Cx32 knock-down cells when compared to control shRNA cells, this was particularly apparent before the addition of calcium but continued throughout (Fig 4.19 B-D).

Claudin 5

A large decrease in Claudin 5 expression was observed in Cx32 shRNA cells, compared to control shRNA cells throughout the full 6 day differentiation period, with expression knocked down by approximately 75% after 1 day in ABS and 50% after 6 days in ABS/Ca^{2+}.

Claudin 7

Claudin 7 was expressed in non-differentiated cells, although expression did increase during differentiation. The effects of Cx32 knock-down on claudin 7 were not consistent, since at day 0 a slight increase in expression was observed in Cx32 shRNA cells; this was reduced compared to control cells after 1 day in ABS but for the remainder of the differentiation time-course claudin 7 expression was comparable between control and Cx32 shRNA cells.

E-Cadherin

E-cadherin was first observed after the addition of ABS to the cultures and expression was increased after the switch to ABS/Ca^{2+}. In Cx32 shRNA cells, E-cadherin expression was reduced compared to control cells, until after 3 days in ABS/Ca^{2+} when levels became comparable between control and Cx32 shRNA cells.

Cytokeratin 13

CK13 expression was increased during differentiation with very little/no expression in non-differentiated cultures, however expression levels were highest in control cells at day 1 in ABS/Ca^{2+}, after which expression declined during the latter part of the time course. Expression of CK13 was reduced in Cx32 shRNA cells until 1 day in ABS/Ca^{2+}, after which the expression of CK13 was found to be higher in Cx32 knock-down cells than control cultures.

ZO-1

Both ZO-1α^- and ZO-1α^+ splice variants of ZO-1 were expressed in differentiating NHU cells as indicated by the double band recognised by the ZO-1 antibody. In Cx32 knock-down cells a decrease in ZO-1α^- was observed early in the differentiation time course compared to control cells, however by day 6 in ABS/Ca^{2+} there was more ZO-1α^- observed in Cx32 shRNA cells than control cells. Expression of the ZO-1α^+ splice variant was reduced in Cx32 knock-down cells throughout the differentiation experiment.

ZO-2

ZO-2 expression was observed throughout the differentiation time-course with some induction of expression after 1 day and 3 days in ABS. This induction of ZO-2 was more apparent in control shRNA cells than Cx32 shRNA cells after 1 day in ABS,

but after this time point the expression of ZO-2 was comparable between the two transduced cell lines.

ZO-3

ZO-3 expression was not induced in cells until growth conditions were switched to ABS/Ca^{2+}. The induction of ZO-3 expression was delayed in Cx32 shRNA cells, as observed by reduced ZO-3 expression after 1 day in ABS/Ca^{2+} compared to control shRNA cells.

Occludin

Occludin expression was upregulated during differentiation of control shRNA cells and was found to be reduced in Cx32 shRNA cells after 1 day in ABS, but comparable to control shRNA cells at later time points. Overall, occludin expression was highest after 1 day in ABS/Ca^{2+} and a decline in expression was observed after 6 days culture in ABS/Ca^{2+}.

4.5.4 Localisation of selected tight junction proteins in Cx32 shRNA cells

Expression of ZO-1 and ZO-3 were examined by immunocytochemistry in Cx32 shRNA cultures after differentiation in ABS/Ca^{2+} for 6 days. In control shRNA cells both ZO-1 and ZO-3 were expressed at cell borders in most cells across the culture where expression highlighted a largely intact network of tight junctions (fig 4.20). In Cx32 shRNA cells, expression of both ZO-1 and ZO-3 were observed, however distribution at cell borders was patchy and sparse. Cytoplasmic labelling for both ZO-1 and ZO-3 was at a similar intensity in Cx32 shRNA cultures and control shRNA cultures.

4.5.5 Phenotypic assessment of wild-type and mutant Cx32 overexpressing cells following differentiation.

$Cx32^{WT}$, $Cx32^{T134A}$ and pLXSN-empty vector control cells were seeded at comparable cell densities and whole cell lysates were collected from non-differentiated cultures grown in KSFMc, after culture in 5% serum for 5 days and in differentiated cultures grown according to the ABS/Ca^{2+} method.

Forced expression of wild-type and mutant Cx32 resulted in the overexpression of monomeric and dimeric Cx32 protein products (Fig 4.21). The increase in Cx32 protein products was more apparent in differentiated cultures for all three transductants, compared with non-differentiated cultures; however in this cell line (Y1270), very little monomeric Cx32 was expressed in control $pLXSN^{empty}$ cells. The overexpression of Cx32 did not appear to impact on the protein expression levels of claudins 4 and 5 or occludin, all of which were upregulated following addition of serum to the cultures.

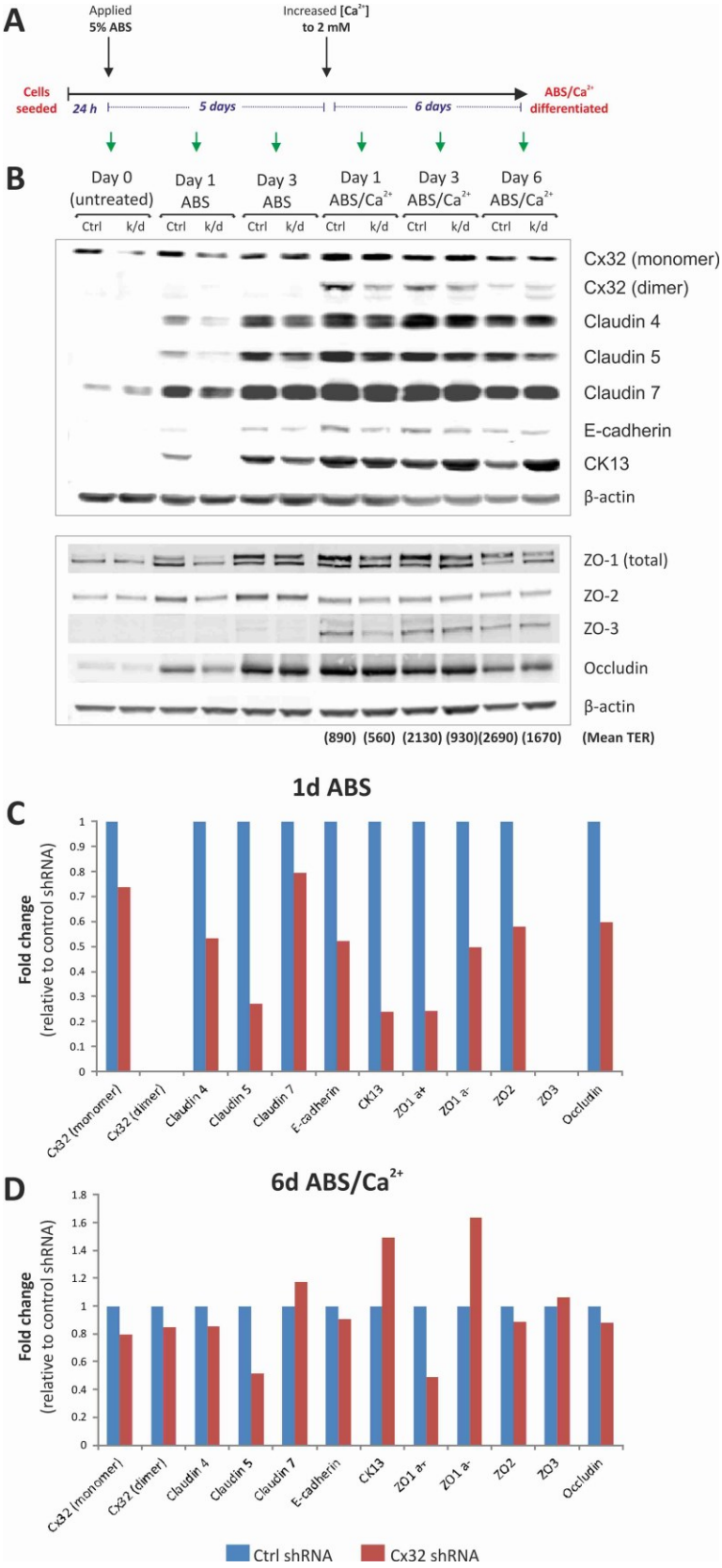

Figure 4.19 Western Blot Analysis of Cx32 shRNA Cultures During Differentiation in ABS/Ca^{2+}.

Y1151 NHU cells expressing either Cx32 shRNA (k/d) or control shRNA (Ctrl) were seeded and pre-treated with 5% serum for 5 days, followed by 5% *ABS and 2 mM* Ca^{2+} *for 6 days, as summarised in (A). Whole cell lysates were harvested before treatment (day 0) and after 1 or 3 days in ABS or 1, 3 or 6 days in ABS/*Ca^{2+} *and processed for immunoblotting with anti-Cx32, Claudin 4, Claudin 5, Claudin 7, E-cadherin, Cytokeratin 13 (CK13), ZO-1, ZO-2, ZO-3, Occludin and β-actin (loading control) antibodies (B). For ZO-1, the upper band represents the ZO-1*α^{+} *variant and the lower band the ZO-1*α^{-} *variant. Parallel cultures were seeded on permeable Snapwell™ membranes after 5 days ABS pre-treatment. Mean TER values of 6 replicate cultures are indicated in brackets below.*

Densitometry analysis of each band formed and (after normalisation to β-actin) was plotted as fold-change relative to control shRNA from cultures after 1 day grown in 5% ABS (C) or 6 days in 5% ABS and 2 mM Ca^{2+} *(D).*

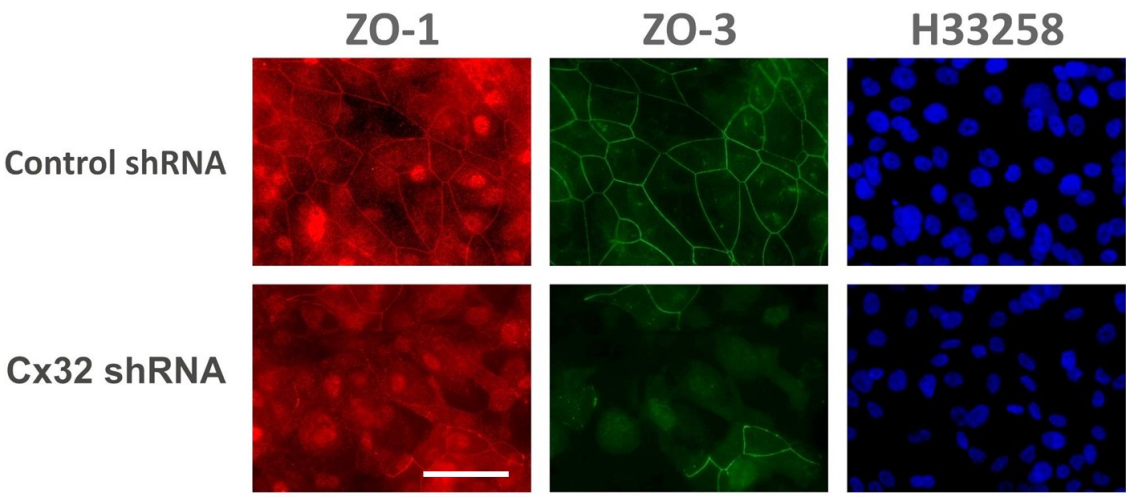

Figure 4.20 Immunocytochemistry of ZO-1 and ZO-3 in Cx32 shRNA Transduced Cultures following Differentiation in ABS/Ca^{2+}.

Y1185 transduced cells were seeded onto glass slides and differentiated with 5% ABS and 2mM Ca^{2+} for 6 days prior to fixation. Immunofluoresence of ZO-1 and ZO-3 immunolabelling in control and Cx32 shRNA cells is shown. Cell nuclei were counterstained with Hoechst 33258 (H33258). Scale bar = 50µM

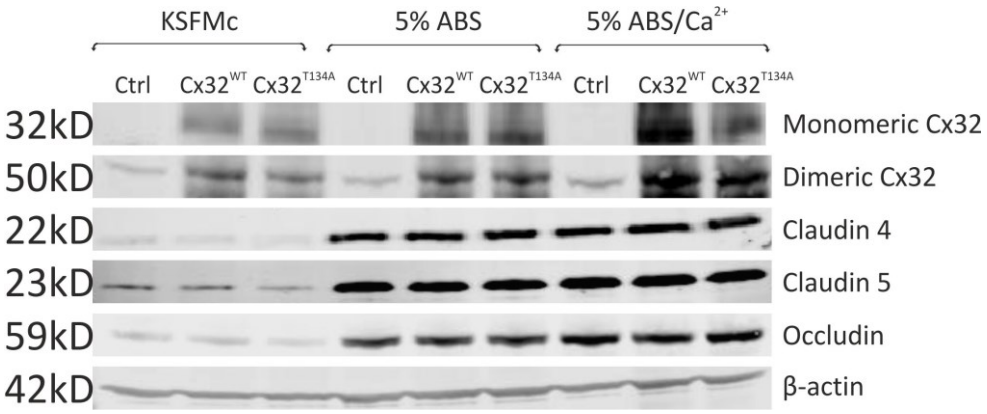

Figure 4.21 Immunoblot Analysis of Cx32 Overexpressing Cultures During Differentiation in ABS/Ca^{2+}.

Y1270 NHU cells transduced with overexpressing pLXSN-$Cx32^{WT}$, $Cx32^{T134A}$ or control pLXSN-empty vector control plasmid were seeded and grown to 80% confluence. Whole cell lysates were harvested from non-differentiated (KSFMc) cells, cells grown in 5% ABS for 5 days or cells differentiated according to the ABS/Ca^{2+} method and processed for immunoblotting with anti-Cx32, Claudin 4, Claudin 5, Occludin and β-actin (loading control) antibodies.

4.6 Assessment of Histology and Ultrastructure of Cx32 Knock-down and Overexpressing Differentiated Human Urothelial Cell Lines

4.6.1 Analysis of histology and ultrastructure of Cx32 shRNA cell sheets after differentiation in ABS/Ca^{2+}

The barrier function of transduced NHU cells (Y1117) was assessed by TER, before fixation and processing for transmission electron microscopy. TER measurements for control shRNA and Cx32 shRNA cells were 2000 Ω.cm^2 and 533 Ω.cm^2 respectively, at day 6 post-differentiation in ABS/Ca^{2+}. The histological appearance of toluidine blue-stained control and Cx32 shRNA cell sheets grown on permeable membranes were similar (Fig 4.22 A and B). Each membrane was overlaid with an intact sheet of cells approximately 3 cells thick with occasional vacuoles observed between cells.

Apical tight junctions were observed in all electron micrographs of control shRNA cells which reproducibly appeared as protein dense (dark), clearly-defined tight junction strands, aligned between the apical-most aspect of cell contact (Fig 4.22 C-K). The particle distance across the width of the tight junction strands was measured to be approximately 15 nm.

Tight junction-regions in Cx32 shRNA transduced cells were extremely variable (Fig 4.22 L-T). Some areas of apical cell-cell contact did not contain defined protein-dense strands, but rather wider, indistinct areas of protein with a blurred appearance (Fig 4.22 L, M, O, R). Other regions contained apparent tight junction strands which were distinct, but shorter than those observed in control shRNA cells (Fig 4.22 N and O). Some tight junction strands were comparable to those observed in control shRNA cells (Fig 4.22 P and S), whilst other areas completely lacked a junction with wide spaces between the cells (Fig 4.22 T).

4.6.2 Analysis of histology and ultrastructure of wild-type and mutant Cx32 overexpressing cell sheets after differentiation in ABS/Ca^{2+}

The barrier function of pLXSN transduced NHU cell cultures (Y1284) were assessed by TER before fixation and processing for TEM analysis; measurements were 1500 Ω.cm^2, 1450 Ω.cm^2 and 1430 Ω.cm^2 for control empty-vector, $Cx32^{WT}$ and $Cx32^{T134A}$ overexpressing cells respectively at day 6 post-differentiation in ABS/Ca^{2+}. The histological appearance of toluidine blue-stained cell sheets grown on permeable membranes was similar between all three transductants (Fig 4.23 A-C). Each cell sheet was approximately 3 cells thick with occasional vacuoles observed between cells. In $Cx32^{T134A}$ cells, toluidine blue uptake was variable and many purple spots were observed within the cytoplasm of cells.

Apical tight junctions were observed in electron micrographs of all transductants with some variability in protein density surrounding tight junction regions; however the overall majority of tight junction strands were clearly-defined and protein dense (dark), with tight alignment between the apical-most aspect of cell contact (fig 4.23 D-I).

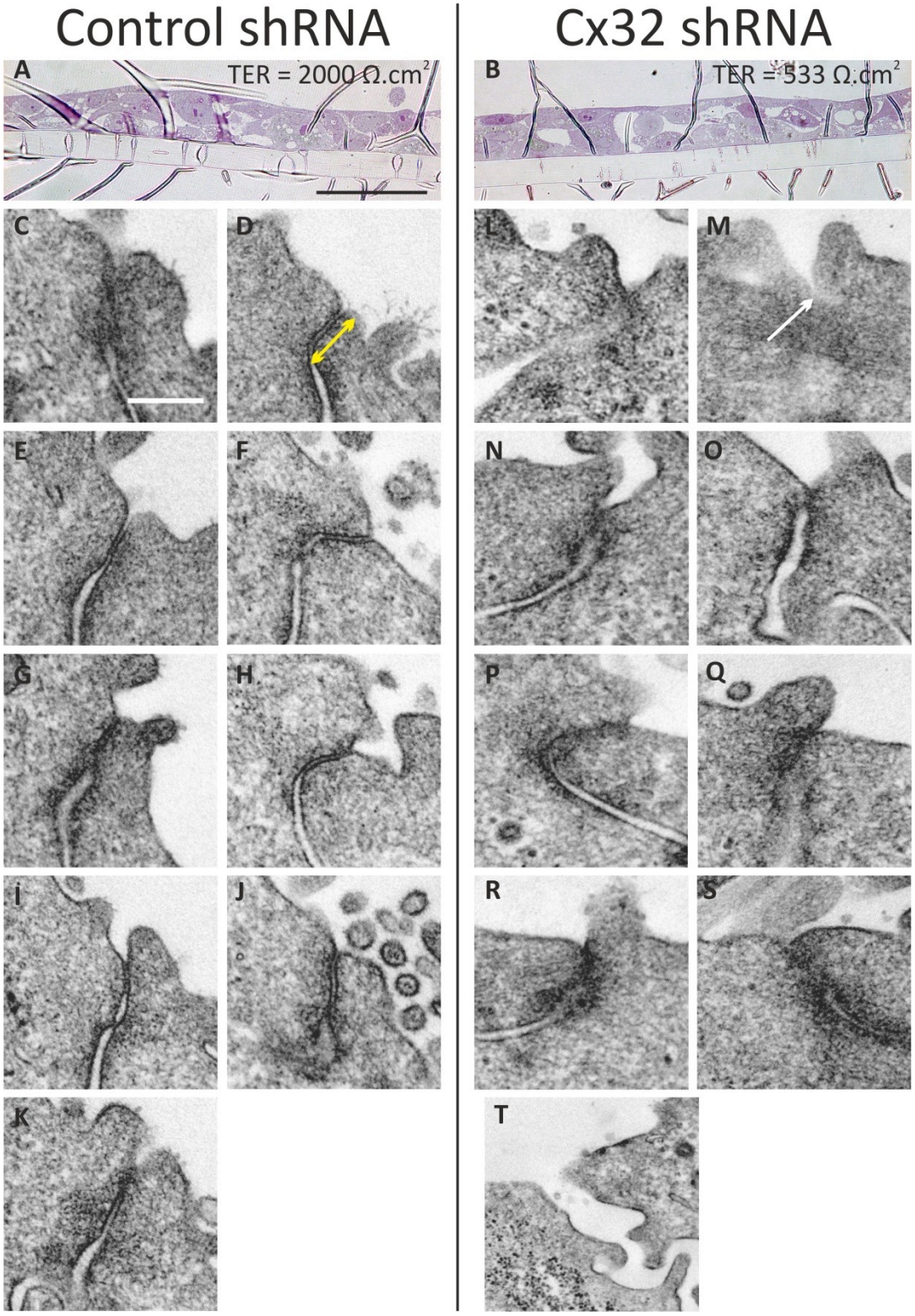

Figure 4.22 Transmission Electron Micrographs of Terminal Tight Junctions in Cx32 shRNA Differentiated Cell Constructs.

Light microscopy images of resin embedded ultrathin (0.1 µm) sections of control shRNA (A) or Cx32 shRNA (B) transduced NHU cell sheets (Y1117), stained with Toluidine Blue after

differentiating on permeable Snapwell™ membranes for 6 days following the ABS/Ca^{2+} method. TER values for each construct are indicated. Six replicate cultures were differentiated; the cell sheet with the TER reading closest to the mean was selected for transmission electron microscopy analysis. Thick ruckled areas can be observed in the resin sections. Transmission electron micrographs were taken of the apical-most tight junctions in control shRNA (C-K) and Cx32 shRNA (L-T) differentiated cells. Yellow arrow indicates a well-defined tight junction strand (D) and the white arrow indicates a non-developed junction between two apical cells (M). Note: all apical tight junctions assessed in control shRNA cells contained well defined tight junction strands (C-K), whereas tight junction regions in Cx32 shRNA cells were either less defined (L, N, O, P, Q, R, S), or non-developed (M and T).

Light microscopy scale bar (black) = 50 µm

TEM scale bar (white) = 250 nm

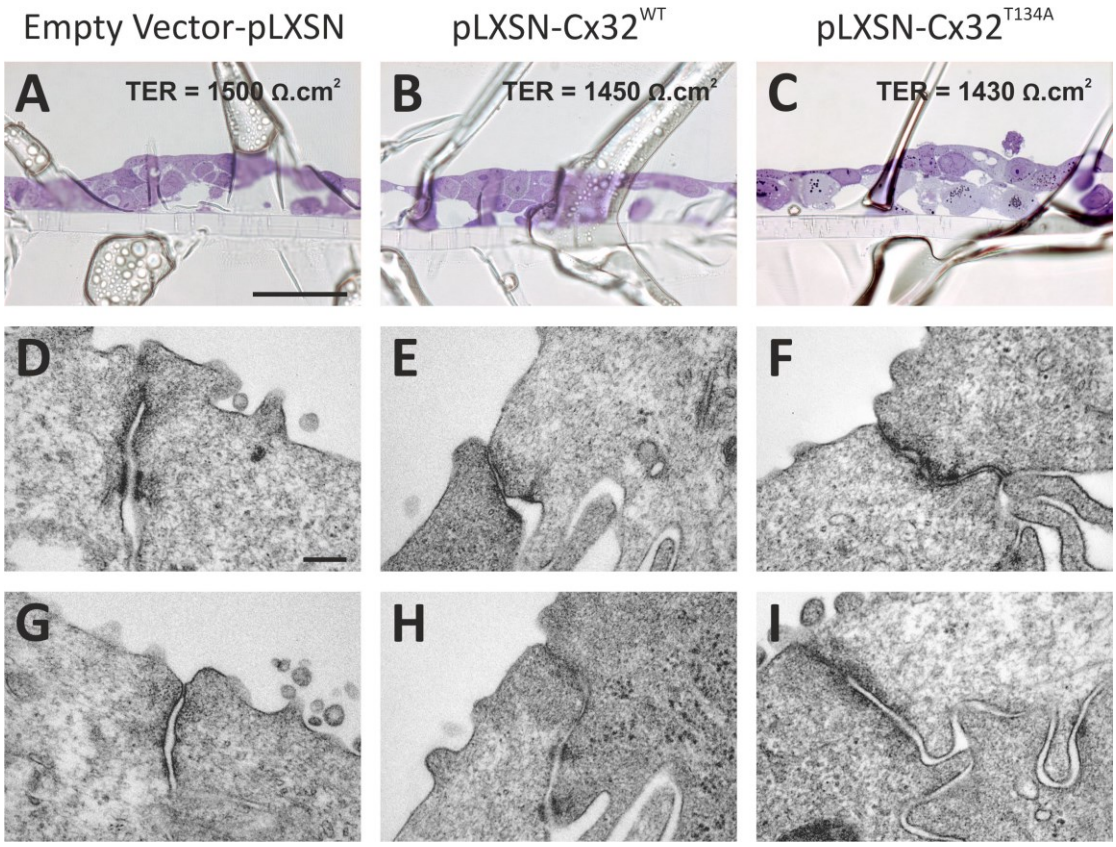

Figure 4.23 Transmission Electron Micrographs of Terminal Tight Junctions in Cx32 Overexpressing Wild-type and T134A Mutant NHU Constructs.

Light microscopy images of resin embedded ultrathin (0.1 µm) sections of control empty-vector pLXSN (A) pLXSN-Cx32^{WT} (B) and pLXSN-Cx32^{T134A} (C) transduced NHU cell sheets (Y1284), stained with Toluidine Blue after differentiation on permeable Snapwell™ membranes for 6 days following the ABS/Ca^{2+} method. TER values for each construct are indicated. Four replicate cultures were differentiated; the cell sheet with the TER reading closest to the mean was selected for transmission electron microscopy analysis. Thick ruckled areas can be observed in the resin sections. Transmission electron micrographs were taken of tight junctions regions in pLXSN-empty (D & G), pLXSN-Cx32^{WT} (E & H) and pLXSN-Cx32^{T134A} (F and I) differentiated cells. Well defined tight junction strands were observed in apical tight junction regions for all three transductants.

Light microscopy scale bar = 50 µm

TEM scale bar = 200 nm

4.7 The Association of Cx32 with Urothelial Tight Junction Proteins

4.7.1 Assessment of Cx32 interaction with tight junction proteins

Cx32 protein interactions were examined in ABS/Ca^{2+} differentiated urothelial constructs using a Proximity Ligation Assay (PLA). Areas with fluorescent spots were observed throughout the cell sheets when antibody combinations for Cx32/Occludin and Cx32/ZO-2 were applied to cell sheets indicating a potential interaction between Cx32 and these two tight junction proteins (Fig 4.24). Cx32 did not appear to co-localise with ZO-3, since distinct fluorescent spots were not observed. As a positive control, primary antibodies for the known interacting tight junction proteins ZO-1 and ZO-3 were applied to human ureter and bright areas of fluorescent spots were observed, in particular at the apical-most region of the urothelium.

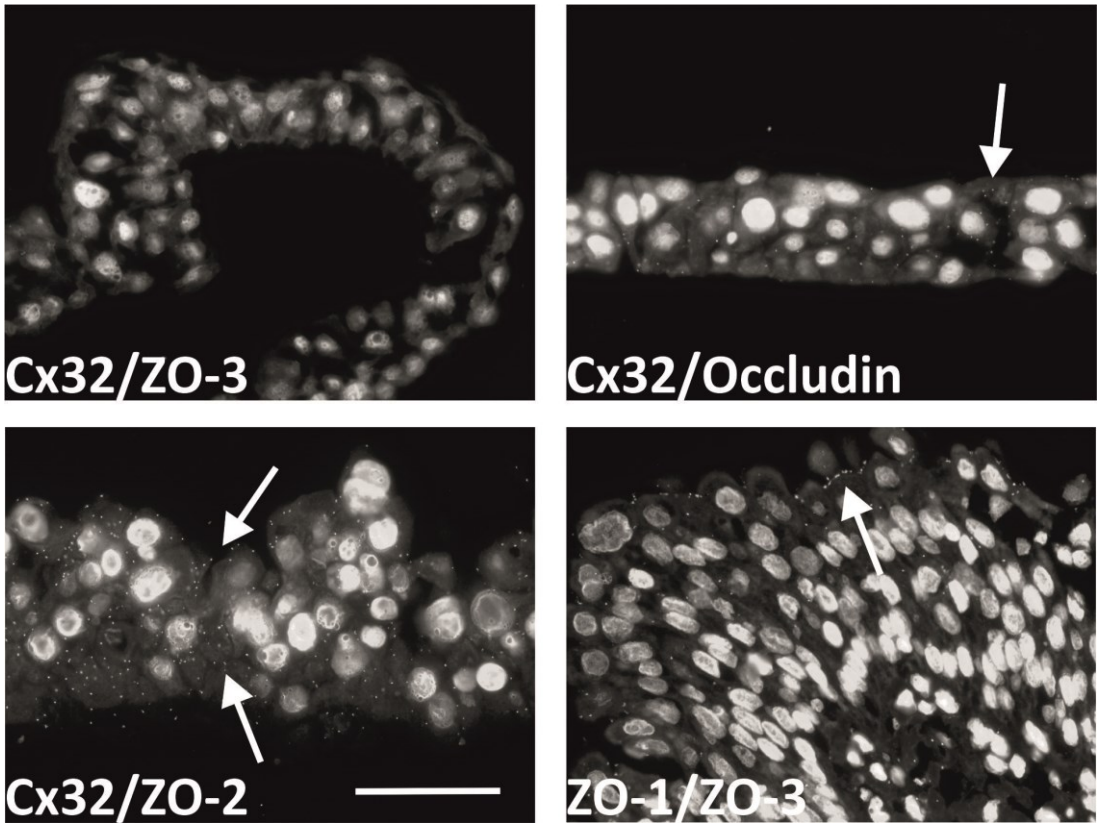

Figure 4.24 Proximity Ligation Assay to Evaluate Cx32 Co-localisation with Tight Junction Proteins in Differentiated Urothelial Constructs.

Y1151 (non-transduced) NHU cells were differentiated according to the ABS/Ca^{2+} method for 6 days on Snapwell™ permeable membranes, prior to fixation in 10% formalin and paraffin-embedding. A fluorescent proximity-ligation assay (Duolink®) was performed on de-waxed 5 µM sections with primary antibody combinations as indicated on each image. Cells were counterstained in Hoechst 33258. White spots indicate areas of antibody interactions (arrows). The known interaction of ZO-1 and ZO-3 was used as a positive control on a section of human ureter (Y1216).

Scale bar = 50 µm

	Summary of findings
Cx32 shRNA knock-down	• Cx32 knock-down cultures were generated which gave functional reduction in gap junction-mediated intercellular communication • Cx32 expression was knocked-down in these cultures, but the reduction in protein expression became less pronounced as differentiation proceeded over time • Morphologically, Cx32 knock-down cells were similar to controls with a minor reduction in growth rate of non-differentiated cells • Normal barrier development of differentiated NHU cells was inhibited as a consequence of Cx32 shRNA knock-down • Tight junction protein expression was affected by Cx32 knock-down and the ultrastructure of tight junctions was abnormal
Cx32 overexpression (wild-type and dominant negative)	• Cx32 overexpressing cultures were generated. A functional reduction in gap junction-mediated intercellular communication was observed when the pore-closed mutant was expressed and an increase in functional communication was observed in wild-type overexpressing cultures. • Cx32 protein was overexpressed successfully in undifferentiated and differentiated cells. • Morphologically Cx32 overexpressing cultures were similar in appearance to control cells with similar growth rates • Overexpression of wild-type and mutant forms of Cx32 did not affect barrier function. • Tight junction expression and ultrastructure appeared normal in all overexpressing cells
NHU cells	• Treatment of NHU cells with a general gap junction inhibitor did not affect barrier development • In differentiated cells, Cx32 potentially co-localised with Occludin and ZO-2, but not ZO-3

Table 4.2 Summary of Findings from Chapter 4.

4.8 Discussion

The primary function of the urothelium is to line the urinary tract and prevent toxins from re-entering the body after urine production by the kidneys; therefore a tight barrier function is essential to bladder physiology. It is considered that the urothelium serves as the tightest barrier epithelium in the human body (Negrete et al. 1996); with terminal tight junctions, the most apical components of intercellular junctional complexes, playing a fundamental role in barrier attainment (Anderson et al. 2009).

In vitro, terminal tight junction complexes have been shown to develop during urothelial cytodifferentiation *in vitro* under the influence of the nuclear receptor PPARγ (Varley et al. 2006). Regulated expression of specific claudin proteins, including claudins 3, 4, 5 and 7, form the basis of the primary seal-forming fibrils in urothelium and concurrent expression of zonnula occludens proteins plays a likely role in maintaining structural support for these tight junctions, by linking the cytoplasmic face of tight junction complexes to the actin cytoskeleton (Varley et al. 2006, Smith NJ et al. 2015). Previous reports have suggested that a compromised urothelial barrier, demonstrated by decreased expression of claudins, ZO-1 and occludin, may contribute to benign disease states including interstitial cystitis and painful bladder syndrome (Slobodov et al. 2004, Southgate et al. 2007, Lee et al. 2014).

4.8.1 Cx32 and barrier function of NHU cultures

Data presented here provides direct evidence that the gap junction protein Cx32 performs a distinct role in urothelial barrier acquisition. Inhibition of Cx32 expression by RNA interference with three independent Cx32 shRNAs, resulted in a striking delay in barrier formation when NHU cells were differentiated in culture. This was associated with a time-delay in expression and assembly of tight junction proteins, as well as abnormalities in the ultrastructure of the resultant terminal

tight junctions, as assessed by TEM. A complete knock-out of Cx32 was not achieved by RNA interference and Cx32 protein expression did increase in Cx32 shRNA cultures during the differentiation period. The accumulation of dimeric Cx32 in these knock-down cultures was slower than in control cells but did eventually reach comparable expression levels. This may indicate the formation of a stable membrane pool with low turnover, which eventually reaches a maximum expression level necessary for function. It is not possible to speculate as to whether a complete Cx32 knock-out in NHU cultures would ablate barrier function and the development of tight junction complexes altogether, or whether Cx32 expression enhances the rate of barrier development but is not essential to the final barrier outcome. It is possible that the role of Cx32 in barrier development could be compensated by other connexins. The urothelia in Cx32 knock-out mice and patients with Cx32-linked Charcot-Marie-Tooth disease have not previously been reported to be defective, however this could be an interesting avenue for future study.

4.8.2 Connexin/tight junction interactions

It is believed that the primary function of gap junctions is for communication; to allow individual cells within a tissue to behave in a co-ordinated manner. However, gap junctions are often found to be located within tight junction complexes and it has been proposed that several connexins have a secondary role to function within multi-protein complexes for regulation of cell polarity, with influence on the assembly or maintenance of tight/adherens junctions (reviewed in Herve *et al.* 2012). This role is supported by evidence from thyroid epithelial cells, where co-expressed connexins were found to differ in their membrane locations, with Cx43 being located within tight junction regions and Cx32 in the lateral membrane domain (Guerrier et al. 1995). It is interesting to note that although thyroid follicles co-express both Cx32 and Cx43, when thyrocytes are cultured as a monolayer they lose expression of Cx32, which they then regain when *in vitro* conditions are adapted to promote the formation of 3D follicles (Tonoli et al. 2000). This may be

comparable to the expression of Cx32 in NHU cells, where monolayers of undifferentiated cells do not express Cx32, however differentiated stratified cell sheets do. Co-immunoprecipitation studies with cultured mammary epithelial cells have described interactions between Cx43 and Cx32 with ZO-2 and alpha- and beta-catenins (Talhouk et al. 2008). Cx43 was shown to be crucial for tight junction development in Sertoli cells (Li et al. 2010).

The epithelium of the intestine is, like urothelium, a key barrier epithelium where tightly regulated paracellular transport is paramount for function. It has been reported that Cx26 interacts with occludin in polarised sheets of intestinal epithelial cells (Nusrat et al. 2000).

Cx32 expression has been associated with the expression of tight junction proteins in primary cultured rat hepatocytes, where Cx32 (but not Cx26) co-immunoprecipitates with occludin, claudin 1 and ZO-1 (Kojima et al. 2001). Immortalised mouse hepatocytes lacking Cx32 were transfected with human Cx32 and northern blot analyses demonstrated a concurrent induction of occludin and claudins 1 and 2 (Kojima et al. 1999). In addition Cx32 was found to co-immunoprecipite with occludin in these cells.

Current knowledge of the temporal coincidence of gap and tight junction proteins indicates that a role for Cx32 interacting at the urothelial tight junction is entirely plausible. The proximity-ligation assay (PLA) data presented in this study is evidence of direct interactions between Cx32/ZO-2 and Cx32/occludin (but not Cx32/ZO-3). A recent study using PLA technology in WIF-B9 hepatocytes demonstrated that Cx32 and claudin 2 are co-localised and that this interaction is disrupted by the presence of cadmium (Boucherie et al. 2013). Cadmium is a highly toxic environmental pollutant and a known human and animal carcinogen. Is has been held responsible for tumour formation in several organs including the prostate, lungs and testes (Bertin et al. 2006) and has very recently been linked to urothelial carcinogenesis as a result of occupational cadmium exposure (Colt et al. 2014, Garcia-Perez et al. 2015). Boucherie and colleagues speculate that the

interaction between claudin 2 and Cx32 is crucial for hepatocyte barrier function, although they did not present evidence of any barrier defect as a direct result of cadmium treatment in the study.

4.8.3 Tight junction assembly in NHU cultures

In the present study, the timecourse of Cx32 and tight junction protein expression demonstrated that development of the urothelial tight junction is a multi-step process involving timed appearance of protein constituents. Expression of dimeric Cx32, and ZO3 were markedly enhanced following the switch to physiological calcium concentrations, coinciding with barrier development. The presence of tight junction proteins by immunoblotting does not necessarily imply functional assembly at the cell junction, however immunocytochemistry demonstrated that assembly of both ZO-1 and ZO-3 were compromised in Cx32 knock-down cultures at day 6 post-differentiation (along with a compromised barrier function). This might indicate that functional expression of ZO-3 or Cx32 performs a critical final step in the construction of a functional tight junction.

4.8.4 Cx32 assembly in NHU cultures

Overexpression of Cx32 (both wild-type and mutated) in NHU cell cultures resulted in a large number of bands by immunoblotting which were not observed in cells transduced with the vector alone. Monomeric and dimeric Cx32 bands were identified; however there were many higher molecular weight bands which may represent a large pool of whole or partially assembled/broken down connexons. Further work into Cx32 turnover in NHU cells may shed further light on the stability of Cx32 in these cultures (in both normal and Cx32 overexpressing states). Proteosome inhibitors (e.g. MG132) or inhibitors of intracellular protein transport (such as Brefeldin A or temporarily reducing the temperature of cultures), would be useful tools for this. The antibody used in this study reacts with the C-terminal domain of Cx32 and the band observed at approximately 13 kD has previously been reported to be due to the loss of the C-terminal tail during Cx32 breakdown (Rahman et al. 1993). This, together with the observed increase in cytoplasmic

labelling of Cx32 in overexpressing cultures suggests that at least some of the overexpressed Cx32 is being broken down by the cell and may be present in a state of partial assembly/disassembly. However, large membrane plaques of Cx32 at cell borders in overexpressing cultures, along with an increase in dimeric Cx32 expression, suggests that there is a significant increase in assembled Cx32 at gap junction plaques as a result of the overexpression. Dye-transfer studies further support the finding that much of the overexpressed Cx32 is functional in gap junction plaques, since overexpression of $Cx32^{WT}$ significantly enhanced dye-transfer, whilst the dominant negative mutant $Cx32^{T134A}$ overexpression blocked dye-transfer when compared to control (non-overexpressing) cultures.

4.8.5 Cx32 pore-closed dominant-negative mutant

This is the first investigation in which the T134A mutation in the third transmembrane helix of Cx32 has been demonstrated to function in a dominant negative fashion, although it has previously been predicted (Beahm et al. 2006). In studies involving several other connexins (Cx26, Cx43 and Cx50), Beahm *et al*. demonstrated that mutation of this conserved thronine does not impede the synthesis or trafficking of connexins, insertion into gap junctions or docking with partner connexons on adjacent cells; however they observed a completely non-communicating channel which mimicked a pore-closed state, with an approximate reduction in pore size of 17% at the edge of the pore, as examined by cryo-electron microscopy. This threonine residue is strictly conserved in α- and β-connexin subgroups (but not γ-connexins) and was demonstrated to block functionality of homomeric and hereromeric channel combinations. Channels comprising 50% wild-type and 50% mutated connexin demonstrated total loss of function demonstrating the powerful dominant-negative effect of the mutation. Although the T134A mutation was specifically predicted by Beahm *et al*. to block function of Cx32 channels, it was not demonstrated as part of the study, however it was independently documented to be the most cytoplasmic pore-lining residue in Cx32 (Skerrett et al. 2002). Interestingly, patients with CMTX disease have been

identified with mutations spanning the entire third transmembrane helix of Cx32, including those residues immediately adjacent to T134A, however the T134A mutation has not been reported in CMTX patients, which led Beahm *et al*. to speculate that mutations in this residue might be embryonically lethal in man. However, Cx32 knock-out mice are known to give birth to live young, although with an extremely dysfunctional physiology (Nelles et al. 1996, Scherer et al. 1998). In addition, a small number of CMTX patients with a complete deletion of the coding sequence for Cx32 have since been identified, which suggests that embryonic lethality is unlikely (Gonzaga-Jauregui et al. 2010).

The exact mechanism which results in the lack of functionality in this T134A mutant is not fully understood. Cryo-EM demonstrated that the pore size is reduced in the mutant pore, by approximately 17% compared with wild-type pores (Beahm et al. 2006). However, it is unknown if this occurs at the cytoplasmic or extracellular surface and it may be possible that the constriction on diameter is even greater within the pore. It has since been demonstrated in Cx26 that the channel features a wide cytoplasmic opening which then narrows into a funnel structure within the central pore region (Maeda et al. 2009). Since the mutant connexins retain the ability to form oligomers, traffic and dock successfully there is a possibility that this mutation may have influences on channel gating, although the mechanism supporting the permanently closed state is not clear. Several studies have described the effects of cytoplasmic pH, calcium concentration and junctional voltage (Vj) on gap junction open/closed states (reviewed in (Oshima 2014)). In addition there is a "plug-gating" model which supports the idea that a hydrogen bond network set up by the six connexin N-termini may be collapsed to regulate channel closure when necessary (Maeda et al. 2009). A further "ball and chain" model reports channel opening/closing as a result of the flexible C-terminus "clumping" into a ball and physically blocking the channel pore mouth, with evidence for calcium-dependent confirmation changes in the C-terminal domain of Cx43 (Delmar et al. 2004, Liu et al. 2006). However, the T134A mutation described here lies in the third transmembrane domain, close to the cytoplasmic loop, making pore-closure due to "ball and chain" or "plug gating" unlikely, although the effects

of the mutation on neighbouring amino acids and the overall inter-helical interactions within the pore may be complex.

4.8.6 Cx32 channel communication and barrier function

The T134A mutant was of particular use in the current study, since by stable overexpression of $Cx32^{T134A}$ or $Cx32^{WT}$, it was possible to infer whether or not behaviours attributable to Cx32 in NHU cells were mediated by intercellular communication, rather than just presence. $Cx32^{T134A}$ mutant NHU cultures did not exhibit a defect in barrier generation, whereas Cx32 knock-down cells did, inferring that the role of Cx32 in urothelial barrier development is independent of Cx32 mediated cell-cell communication, but dependent on Cx32 expression. This is further evidenced by the finding that inhibition of cell-cell communication using the generic gap junction inhibitor 18α-GA, did not interfere with barrier development.

However, an *in vitro* study in porcine blood-brain barrier endothelial cells demonstrated that Cx40 and Cx43 co-immunoprecipitated with occludin, ZO-1 and claudin 5 at tight junctions (Nagasawa et al. 2006); and that disrupting cell-cell communication with the gap junction inhibitor 18β-glycyrrhetinic acid inhibited barrier function in these cells (as measured by TER), suggesting that intercellular communication mediated by Cx40 and/or Cx43 might be necessary for barrier development in some cell types. In addition, in epithelial cells from the intestine Cx26 expression was found to be tightly linked to tight junction expression and use of the gap junction inhibitor 18β-glycyrrhetinic acid inhibited barrier function in these cells (Morita et al. 2004). Conversely Cx26 expression, but not mediated intercellular communication was observed to contribute to expression and function of tight junctions in human airway epithelial cells (Kojima et al. 2007). Interactions of connexins with tight junction proteins may be cell-type and/or species specific and evidence suggests that tight junctions may be in part controlled by connexins mediated through both communication-dependent and independent mechanisms.

Given that Cx32 knock-down resulted in a defective barrier development in NHU cell cultures, it might have been predicted that Cx32 overexpression could act to enhance the rate of barrier development. This was not observed, implying that although Cx32 is required for barrier development, its expression alone is not sufficient to instigate barrier formation or an enhancement in the expression of tight junction proteins. This may support a role for Cx32 as an integral component of the tight junction complex in urothelial cells, where expression is essential to the stabilisation of other proteins at the tight junction complex, but that Cx32 is not responsible for the recruitment of these proteins. The interactions between tight/gap junction proteins are highly complex and it may be reasonable to assume that loss of any one of these components could destabilise the tight-junction and thus deplete barrier formation.

It should be noted that differences in the rate of barrier development were observed in the three transduced cells lines selected for the Cx32 shRNA and also Cx32 overexpression studies. This is particularly evident with the Y1277 overexpressing cell line, which was the only non-ureteric NHU cell line (renal pelvis derived) and gave a rapid tight barrier, in comparison to the other ureteric cell lines. It is plausible that the tissue source of the NHU cells may be linked to the rate of barrier development. However, a large number of studies in which barrier function is measured over time have been performed in our lab and variability in NHU barrier development rate is common (data not shown here). This is one of the caveats of working with patient-derived samples and does not detract from the ability to draw conclusions based on the appropriate controls (control shRNA or empty vector in this case).

4.8.7 Cx32 and differentiation of NHU cultures

In addition to a compromised barrier function and delayed tight junction expression, Cx32 knock-down cultures demonstrated a loss of two markers associated with urothelial cytodifferentiation: cytokeratin 13 and E-Cadherin. This may indicate potential for a compromised differentiated phenotype in cultures lacking Cx32 expression. A more detailed analysis of differentiation-associated proteins including terminal markers of differentiation (such as uroplakins and CK20) as well as transcriptional regulators of differentiation in NHU cells did not form part of this study, but could for the basis of future studies to further unravel the role for Cx32 in urothelial cytodifferentiation.

4.8.8 Summary of findings

In summary, the results shown here suggest that Cx32 expression is essential for the barrier function of this epithelial tissue and that it is likely to be stably associated with proteins at the urothelial tight junction complex. It is unclear whether the contribution of Cx32 to urothelial physiology is purely structural at the tight junction and independent of gap junction intercellular communication, or whether it serves a further role supporting the differentiation and homeostasis of the urothelium. Work presented in the final results chapter will focus on the contribution of Cx32 to the regenerative phenotype in urothelium.

5. Defining the role of Cx32 in Urothelial Wound Repair

Data presented in results chapters 3 and 4 identified Cx32 as a gap junction protein which was highly up-regulated during human urothelial cytodifferentiation where its expression, but not channel-mediated communication, was demonstrated to be closely linked to the generation of functional tight junctions and a tight barrier.

This final chapter will consider a further significant aspect of urothelial biology: the ability to regenerate and maintain a functional barrier in response to insult or injury.

The rate at which a subpopulation of cells migrates into a damaged region is central to tissue healing. Analysis of wound healing in many *in vitro* and *in vivo* systems has revealed a complex association between connexin expression and the coordination of wound healing (Becker et al. 2012). Connexin-mediated cell-cell communication may be required for relaying damage signals to initiate wound-repair in some systems, however in others, the expression of connexins is thought to be inhibitory to wound migration, for example connexins 31 and 43 are thought to inhibit epidermal wound closure (Kretz et al. 2003). As a further complication, it is emerging that connexins may play a key role in cell adhesion (Yang et al. 2011) and cell cycle-mediated events (Dbouk et al. 2009), both of which may affect the efficiency at which a tissue may repair damage to injury.

5.1 Aims

The focus of this chapter was to examine the specific role of Cx32 and Cx32-mediated cell-cell communication in the repair and regeneration of urothelial barrier function, using the differentiated *in vitro* urothelial cell system (ABS/Ca^{2+}) described in earlier chapters.

Specific objectives were to:

- study the role of Cx32 and associated cell-cell communication in coordinating the rate of migration during urothelial wound healing (section 5.1).

- identify signal transduction pathways which may be involved in coordinating cell migration in wound healing as a response to intercellular communication through Cx32 channels (section 5.2).

- examine the phenotype of differentiated NHU cells during urothelial wound repair, with specific focus on the polarity and proliferation status of cells at the leading edge of migration (section 5.3).

5.2 Experimental Approach

To study the relevance of Cx32 and associated cell-cell communication to wound healing of differentiated NHU cells, a scratch-wound analysis of Cx32-modified cultures was performed. Retroviral transduction and details of cell lines generated are detailed in chapter 4. Cx32 shRNA knock-down or Cx32 overexpressing (wild-type and dominant negative) cultures were used to perform this analysis. As described in previous chapters, the dominant-negative mutant form of Cx32

(T134A) is correctly synthesised, trafficked and inserted into the plasma membrane; however passage of signalling molecules through the channel is disabled, enabling the impact of Cx32-mediated communication (rather than just expression) to be assessed in wound healing assays.

Transduced cells were differentiated using the ABS/Ca^{2+} method, before scratching with a sterile pipette tip to generate a wound of 750-1000 µm wide across the culture. Time-lapse microscopy was used to image the wound area and establish wound-healing healing rates, by measuring the relative decrease in the denuded area over time in an environmental chamber (see fig 5.1).

To further verify the relationship between Cx32 and urothelial wound healing, parallel cultures grown on Snapwell™ permeable membrane supports were differentiated to develop a tight barrier and wounded using the same technique, after which the restoration of barrier function was monitored by measuring the TER at regular intervals post-wounding, until a tight barrier was achieved.

On the basis of these experiments candidate signalling cascades that may promote or inhibit epithelial wound migration were interrogated. Overexpressing Cx32 wild-type, Cx32-T134A (dominant negative, pore-closed mutant) and control empty vector transduced NHU cells, were scratched multiple times following ABS/Ca^{2+} differentiation. These cultures were lysed for immunoblotting to enable analysis of proteins which may be modified as a result of signalling cascades which may influence NHU cell migration (Fig 5.2). Immunofluoresence on parallel wounded cultures was also performed to study protein localisation. Two pathways closely associated with epithelial cell migration were examined:

a) The Rho-kinase pathway, known to be a key effector of cell shape and movement, via ROCK 1 and 2 proteins. ROCK 1 and 2 are known to exert downstream effects on cytoskeletal organisation by altering the phosphorylation status of the actin polymerisation/depolymerisation factor cofilin (Rho kinase pathway summarised in Fig 1.3).

b) The canonical TGFβ-receptor (TGFβR) mediated cell signalling pathway was also studied. TGFβR signalling is known to be positively associated with a wound-healing phenotype in differentiated NHU cell cultures, where it has been shown to promote migration in a process that involves direct phosphorylation of the cytoplasmic mediator SMAD3 by activated TGFβRI (Fleming et al. 2012).

On the basis of these results, further study of the TGFβR pathway in Cx32-modified cultures was performed. The rate of migration of Cx32-modified cultures during wound repair was studied following addition of a) exogenous TGFβ1 ligand and b) the TGFβRI tyrosine-kinase inhibitor, SB431542. A single ligand (TGFβ1) and inhibitor (SB431542) were selected on the basis that they had previously been demonstrated to activate and inactivate TGFβR signalling (respectively) at previously defined concentrations (Fleming et al. 2012). RT-PCR analysis of TGFβ ligand and receptor genes was performed in non-wounded Cx32-modified cultures and during wound-healing, to determine if Cx32-mediated effects on migration rate were associated with expression changes of TGFβ ligand or receptor genes. To further elucidate whether ligand released from differentiated NHU cells acts in a paracrine manner to drive TGFβ/SMAD3-mediated cell migration following wounding, conditioned medium from $Cx32^{WT}$ and $Cx32^{T134A}$ cell cultures was harvested from non-wounded and wounded cultures. This conditioned medium was applied to non-transduced (proliferating) NHU cells, which were lysed and assessed for SMAD3 activation by immunoblotting with an antibody which recognises phosphorylated SMAD3 (ser 423/425).

Immunofluorescence labelling of the SMAD3 transcriptional co-activator CREB (cAMP response element binding protein) and its PKA-activated form pCREB (ser133) were studied in Cx32-modified cultures, to examine possible changes in protein expression and or intracellular localisation, which may be linked to changes in migratory behaviour as a consequence of Cx32 channel status.

Examination of PPARγ protein expression in Cx32-modified cultures was also studied, since in some biological systems, PPARγ has been demonstrated to negatively regulate phosphorylation of SMAD3 (activation), by a physical interaction between SMAD3 and PPARγ (Fu et al. 2001).

The wound-healing phenotype of differentiated (non-transduced) NHU cells was studied by immunoblotting and immunocytochemistry during wound repair, to determine whether migration of cells at the wound edge was associated with a loss of urothelial polarity or adhesion.

Finally, the effects of Cx32 channel status on the proliferative capacity of differentiated NHU cells was determined by the study of Ki67, a cellular marker associated with proliferation. Expression of Ki67 was determined in non-wounded and wounded $Cx32^{WT}$ and $Cx32^{T134A}$ cultures by RT-PCR and immunocytochemistry.

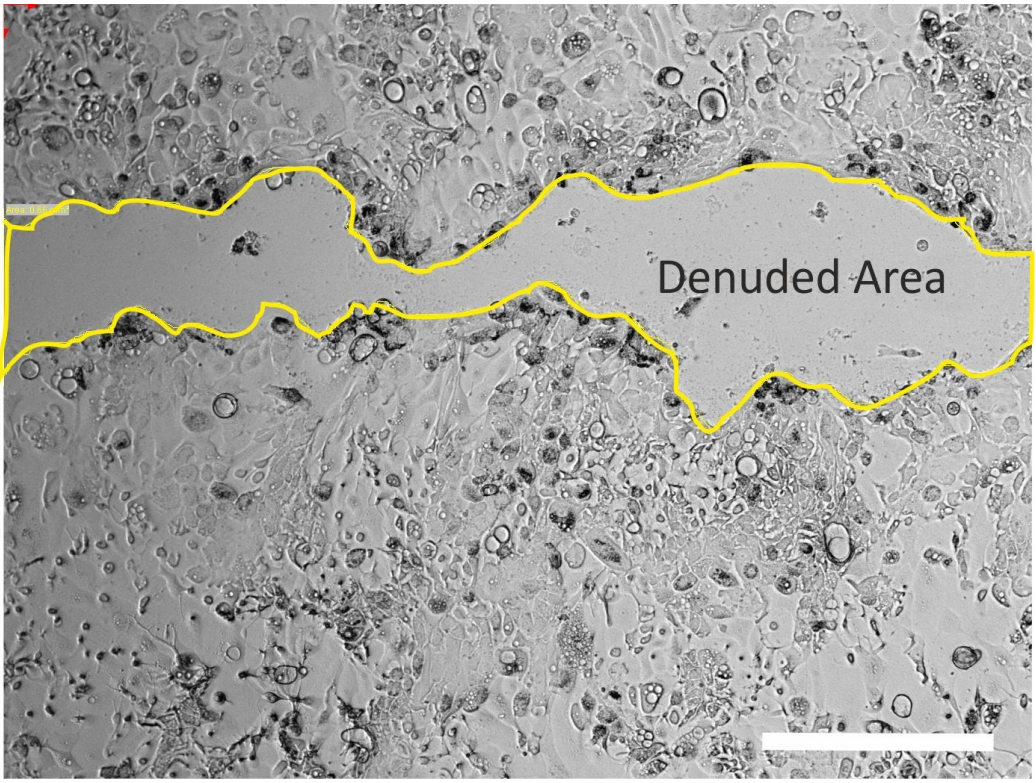

Figure 5.1 Analysis of Differentiated NHU Transductants during Wound Healing.

Example image to demonstrate wound healing analysis. Confluent NHU cultures were differentiated by the ABS/Ca^{2+} method and scratched across the centre of the culture to generate a wound approximately 750-1000 µM wide. The denuded area was imaged every 2 h and for each time point, the wound area was calculated by using the Cell^{M} software to outline the wound edge (shown in yellow). The extent of repair was calculated as a percentage, relative to the original wound. Six replicate cultures were wounded for each experimental condition.

Scale bar = 500 µM

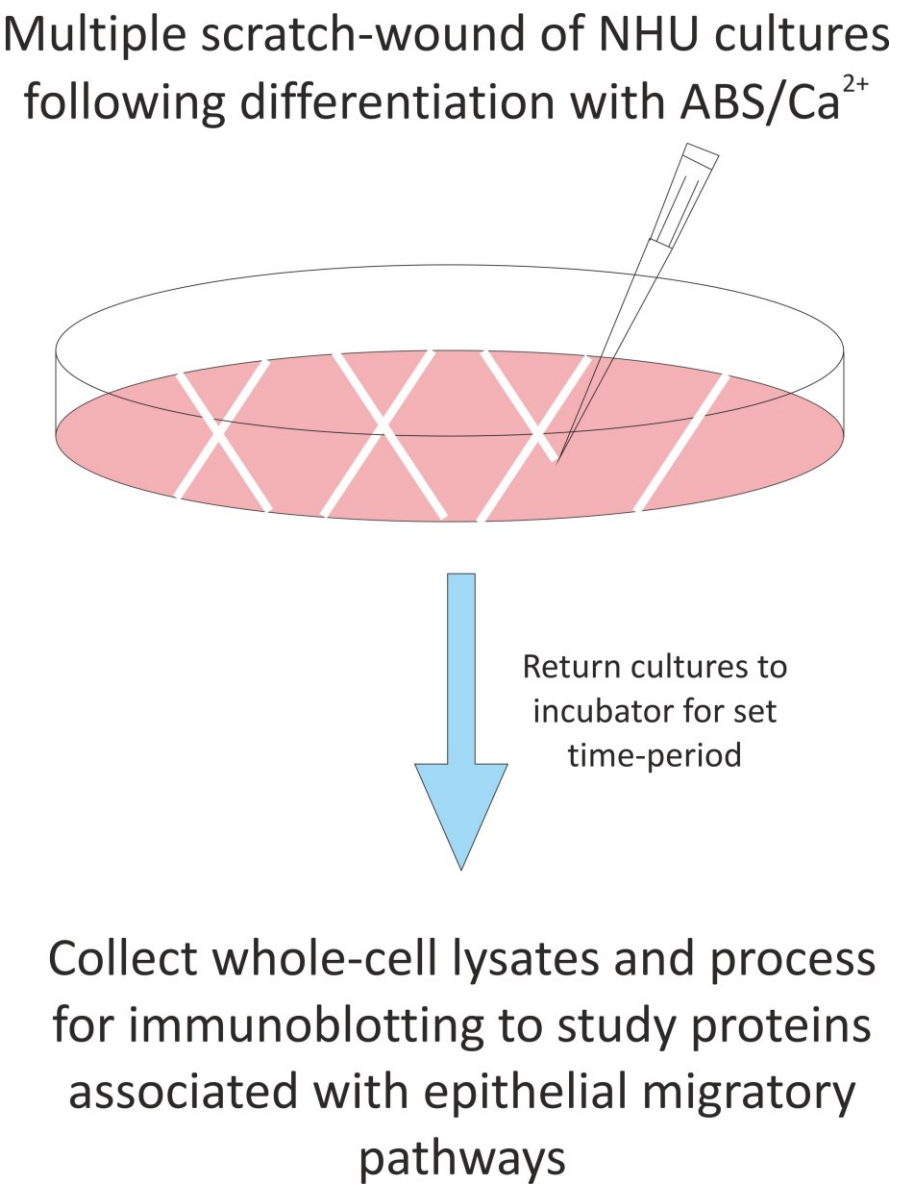

Figure 5.2 Analysis of Protein Expression in Wounded NHU cultures.

Transduced NHU cells were differentiated following the ABS/Ca^{2+} method in 6 cm culture dishes and scratched eight times by hand with a sterile pipette tip, following a grid guideline positioned under the dish. After incubation for a fixed number of hours, whole-cell lysates were harvested to study proteins by immunoblotting during the wound-healing process. Cultures were not washed immediately after scratching, to ensure that any factors released by the damaged cells were maintained in the growth medium for influence on migrating cultures. However, cell debris was washed away with ice cold PBS immediately prior to cell lysis.

Results

5.3 The Effects of Cx32 on the Rate of Wound Healing of Differentiated NHU Cell Cultures

5.3.1 The effects of Cx32 knock-down on the wound healing rate of differentiated NHU cell cultures

After scratch-wounding, time-lapse microscopy analysis revealed that control shRNA cultures (Y1151, P4) took longer to heal than parallel Cx32 shRNA knock-down cultures. Six replicate control cultures took 22-24 h to fully heal (Fig 5.3A), whilst Cx32 shRNA cultures took 12-14 h for 100% healing to occur. The mean time taken for a 50% closure (Wc50) was significantly different between the transductants, with a Wc50 of 13 h for control shRNA cultures and 7.6 h for Cx32 shRNA cultures (Fig 5.3B). Examination of cultures by phase contrast microscopy revealed that control and Cx32 shRNA cultures were similar in appearance immediately following wounding, containing a heterogeneous population of spindly and stratified cells, characteristic of a differentiated phenotype (Fig 5.3C). However, 10 hours after wounding, the appearance of Cx32 shRNA cells close to the wound edge was altered, with an elongated appearance, aligned in the direction of forward movement as if being pulled or stretched forward towards the wound site (Fig 5.3C, red arrow).

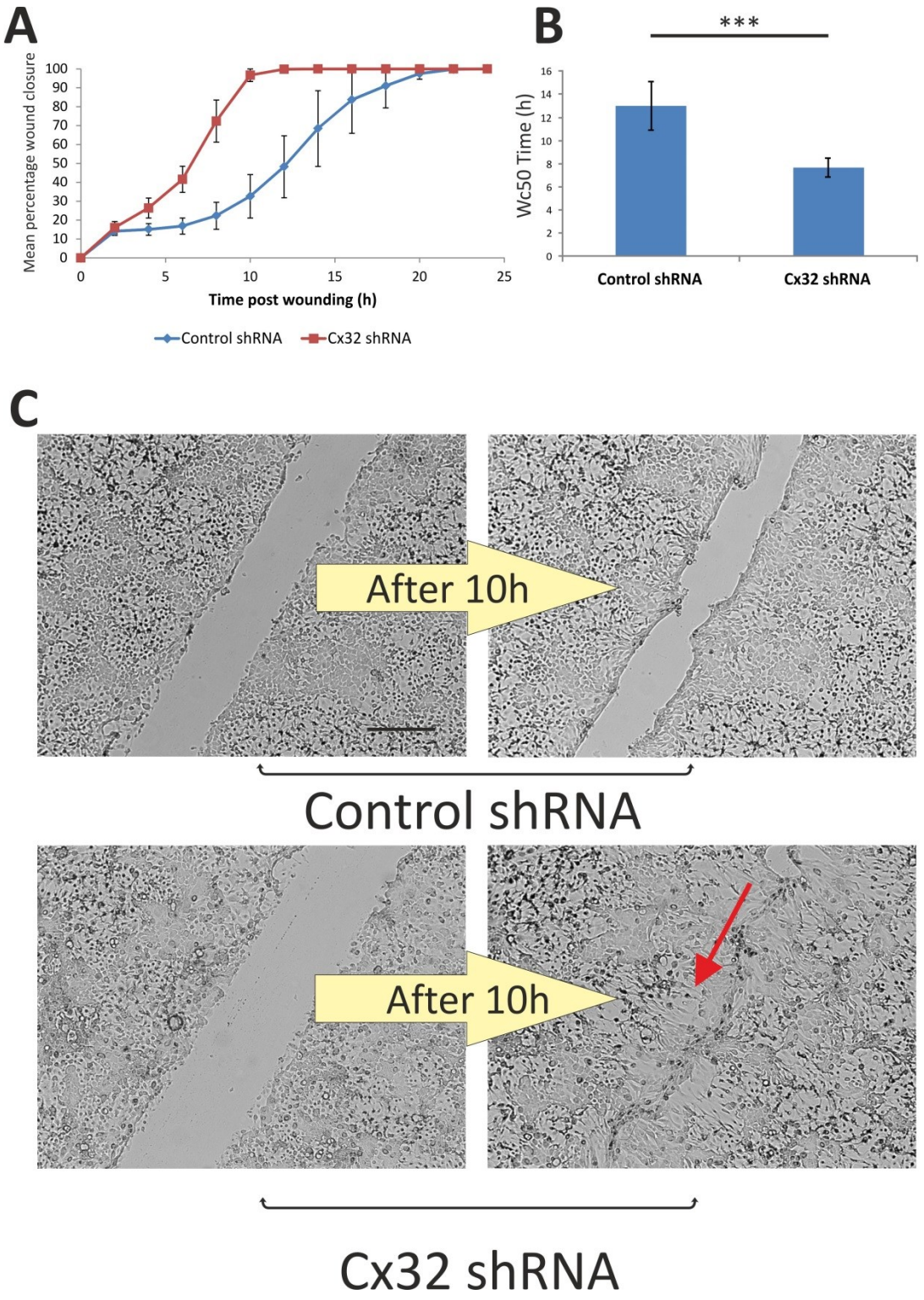

Figure 5.3 Wound Healing Analysis of control and Cx32 shRNA Cell Cultures.

(A) Cultures of Y1151 (P4) control shRNA and Cx32 shRNA transduced cells were induced to differentiate following the ABS/Ca^{2+} procedure. A single scratch (750-

1000 µM wide) was generated in 6 replicate cultures which were imaged in an environmental chamber every 2 hours. The mean percentage closure of the wound space was plotted against time to demonstrate the rate of wound healing.

(B) The mean time point at which the wound was 50% closed (Wc50). Data from closure of 6 replicate cultures. All error bars shown are ± Standard Deviation.

****P-value =0.0002 considered extremely significant (Unpaired t-test).*

(C) Representative bright field images of Y1151 control or Cx32 shRNA cells immediately after wounding and at 10h post-wounding. Note: red arrow indicates regions where cells showed an elongated appearance.

Scale bar = 500 µM

5.3.2 The effects of Cx32 knock-down on the restoration of barrier function after wounding

Restoration of barrier function after wounding was measured in control and Cx32 shRNA cultures by scratch-wounding of differentiated (ABS/Ca^{2+}) cell sheets grown on Snapwell™ membranes and measuring the TER immediately after wounding, and then at regular intervals during wound repair. Immediately prior to wounding, mean TER measurements of control and Cx32 shRNA cultures were 2565 Ω.cm^2 (± SD =348) and 2478 Ω.cm^2 (± SD = 351) respectively. Mean TER measurements were reduced to 381 Ω.cm^2 and 330 Ω.cm^2 for control and Cx32 shRNA cultures respectively, immediately following scratch-wounding (Fig 5.4) and TER values for both remained <500 Ω.cm^2 for 3 h post-scratching, with no significant difference observed between the two cell types. However, from 5 h post-scratching, barrier recovery was considerably more rapid in Cx32 shRNA cultures than control shRNA cultures, with a significant difference in barrier function at 5, 7 and 9 h post-wounding. By 24 h post-wounding, mean TER values in control shRNA cultures had increased to a similar value as observed in Cx32 shRNA cells (difference between control and Cx32 shRNA cultures at 24 h was not significant).

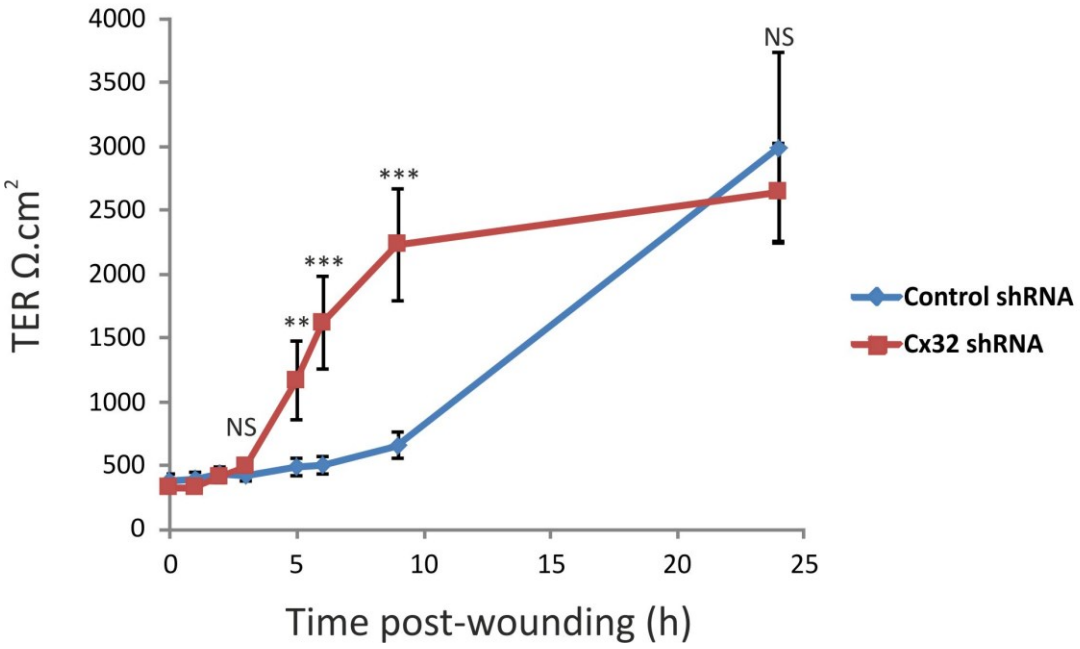

Figure 5.4 Recovery of Transepithelial Electrical Resistance in Cx32 shRNA Cultures Following Wound Damage.

Y1151 (P4) control shRNA and Cx32 shRNA cells were seeded onto Snapwell™ permeable membranes and differentiated for 10 days by the ABS/Ca^{2+} method. A single scratch (750-1000 µM wide) was generated in 6 replicate cultures and TER values were measured at intervals over a 24 h period. Mean TER values were plotted against time to demonstrate the rate of barrier repair. All error bars shown are ± Standard Deviation.

*NS = not significant. **P<0.001 ***P<0.0001 (Unpaired t-test)*

5.3.3 The effects of $Cx32^{WT}$ and $Cx32^{T134A}$ overexpression on the wound healing rate of differentiated NHU cell cultures

After scratch-wounding, time-lapse microscopy analysis revealed differences in the rate of wound-healing between differentiated cultures of empty-vector control, $Cx32^{WT}$ and $Cx32^{T134A}$ transduced cells. Measurement of mean wound-healing rates from two independent cell lines revealed that $Cx32^{WT}$ overexpressing cells were slowest to heal and the dominant negative overexpressing cells ($Cx32^{T134A}$) were fastest, with control empty-vector cell cultures healing at an intermediate rate (Fig 5.5 A & C). In both cell lines tested (Y1270 and Y1392), analysis of $Cx32^{WT}$ and $Cx32^{T134A}$ cultures revealed a significant difference in the number of hours taken for the wounded cultures to heal by 50% (Wc50) (Fig 5.5 B & D). In Y1270 cells, the difference in Wc50 time between control (empty vector) and $Cx32^{WT}$ or $Cx32^{T134A}$ cultures was not significant (Fig 5.5 B). In Y1392 cells, a significant difference in Wc50 time was observed between control and $Cx32^{WT}$ cells, but this was not significant between control and $Cx32^{T134A}$ cells (Fig 5.5 D).

5.3.4 The effects of $Cx32^{WT}$ and $Cx32^{T134A}$ overexpression on the restoration of barrier function after wounding.

Restoration of barrier function after wounding was measured in differentiated empty vector control, $Cx32^{WT}$ and $Cx32^{T134A}$ overexpressing cultures, by measuring the TER during wound repair. Mean TER measurements were reduced to $<500\ \Omega.cm^2$ immediately following scratch-wounding (Fig 5.6) and TER values in all three transduced cultures remained low ($<500\ \Omega.cm^2$) for 6 h post-scratching, with no significant difference observed between the three data sets. However, from 8 h post-scratching, barrier recovery was substantially more rapid in pore-closed $Cx32^{T134A}$ cultures than empty-vector control cultures and conversely, $Cx32^{WT}$ cultures displayed a much slower rate of barrier recovery than control cultures, with an extremely significant difference in barrier function between all three

cultures observed at 24 h post-scratch. By 48 h post-wounding, TER values in all three cultures had reached a plateau such that the difference in mean TER was no longer significant.

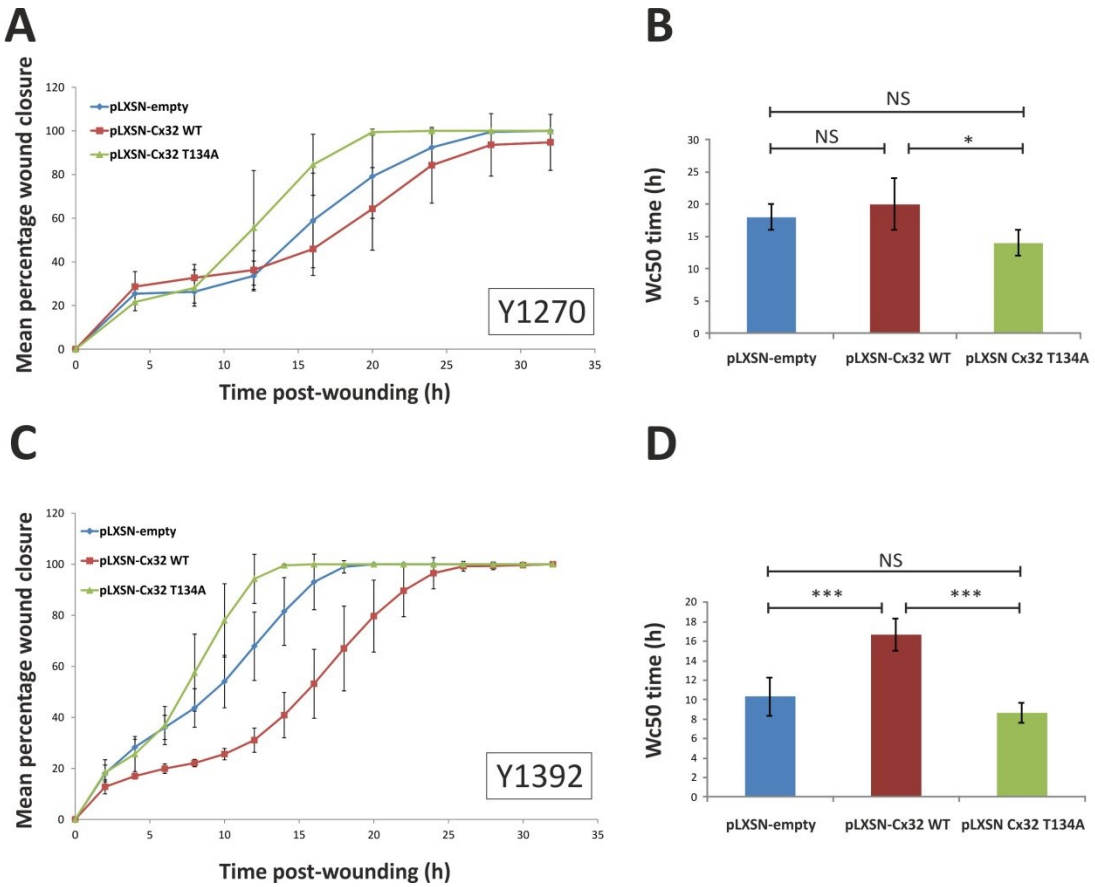

Figure 5.5 Wound Healing Analysis of Cx32^{WT} and Cx32^{T134A} Overexpressing Cultures.

Y1270 (P4) and Y1392 (P4) NHU cells transduced to overexpress wild-type or pore-closed Cx32 (pLXSN-Cx32^{WT} and pLXSN-Cx32^{T134A}) were differentiated in 24-well plates following the ABS/Ca^{2+} procedure. pLXSN-empty vector transduced cells were included as a control. A single scratch wound (750-1000 µM wide) was generated in 6 replicate cultures which were imaged in an environmental chamber for 34 h. The mean percentage closure of the wound space was plotted over time to demonstrate rates of wound healing in both cell lines respectively (A and C). B & D represent the mean time point at which the wound was 50% closed (Wc50). Data from closure of 6 replicate cultures. All error bars shown are ± Standard Deviation.

*NS = not significant *P<0.05 ***P<0.001 (One way ANOVA with Tukey-Kramer multiple comparisons post-test).*

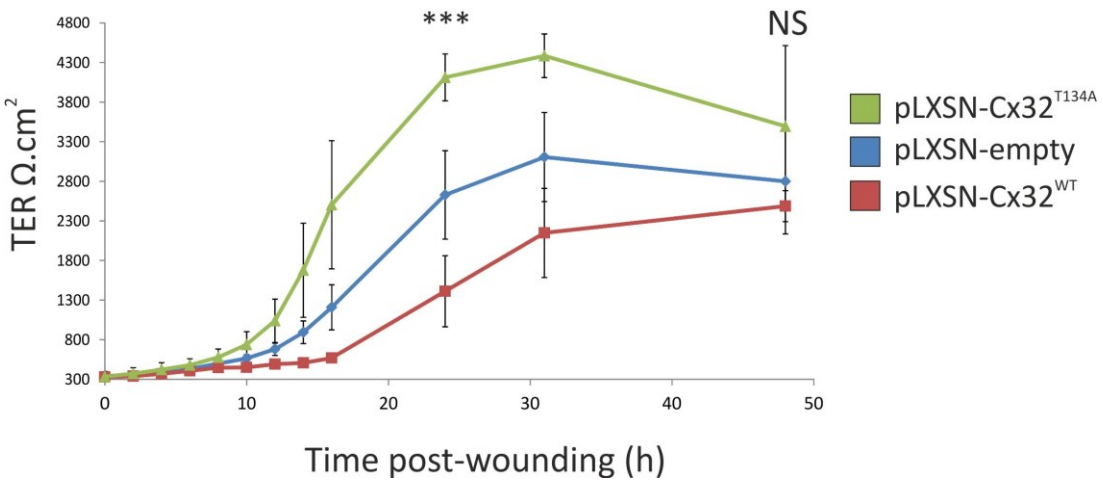

Figure 5.6 Recovery of Transepithelial Electrical Resistance in Cx32 Overexpressing Cultures Following Scratch Wound Damage.

*Y1270 (P4) cells transduced with pLXSN-empty, pLXSN-Cx32^{WT} and pLXSN-Cx32^{T134A} retroviral vectors were seeded onto Snapwell™ permeable membranes and differentiated with ABS/Ca^{2+} for six days. A single scratch (750-1000 µM wide) was generated in 6 replicate cultures for each group and TER values were measured immediately after scratching and then at intervals over a 48 h period. The mean TER was plotted against time to demonstrate the rate of barrier repair. All error bars shown are ± Standard Deviation. ***P<0.0001 (extremely significant) for comparisons of the three transductants. (Empty versus WT, WT versus T134A and empty versus T134A) NS = not significant. (One-way ANOVA with Tukey-Kramer multiple comparisons post-test).*

Note: Mean TER values for empty vector, Cx32^{WT} and Cx32^{T134A} prior to scratch wounding (at day 6) were 2853 Ω.cm^2 (± 260 SD), 2573 Ω.cm^2 (± 134 SD) and 3373 Ω.cm^2 (± 704 SD) respectively.

5.4 Examining the Adverse Effects of Cx32-mediated Communication on Migratory Signalling Events in Differentiated NHU Cell Cultures

5.4.1 Examination of rho-kinase pathway proteins in wounded $Cx32^{WT}$ and $Cx32^{T134A}$ cultures by immunoblotting

Y1277 (P4) cells transduced with pLXSN-empty, pLXSN-$Cx32^{WT}$ and pLXSN-$Cx32^{T134A}$ retroviral vectors were differentiated following the ABS/Ca^{2+}method, before repeat scratching as detailed in Fig 5.2. Immunoblotting of lysates collected at 1 h and 6 h post-wounding (with non-wounded control), confirmed that Cx32 overexpression was retained during wound healing of cultures (Fig 5.7). Expression of the biologically-inactive phosphorylated form of RhoA (ser188), was observed in all cultures, whether wounded or not and was not changed between $Cx32^{WT}$ and $Cx32^{T134A}$ cultures. Downstream expression of ROCK1 was not altered in any of the cultures. Identification of a band specific for ROCK2 was difficult, due to a triple band which appeared at the predicted 160 kD molecular weight, although clear changes in any of the three bands between the cultures were not observed. Downstream expression of cofilin (actin depolymerising) and its phosphorylated form (ser 3; actin-stabilising) were also unchanged at the protein level. β-actin immunoblotting confirmed equivalent loading.

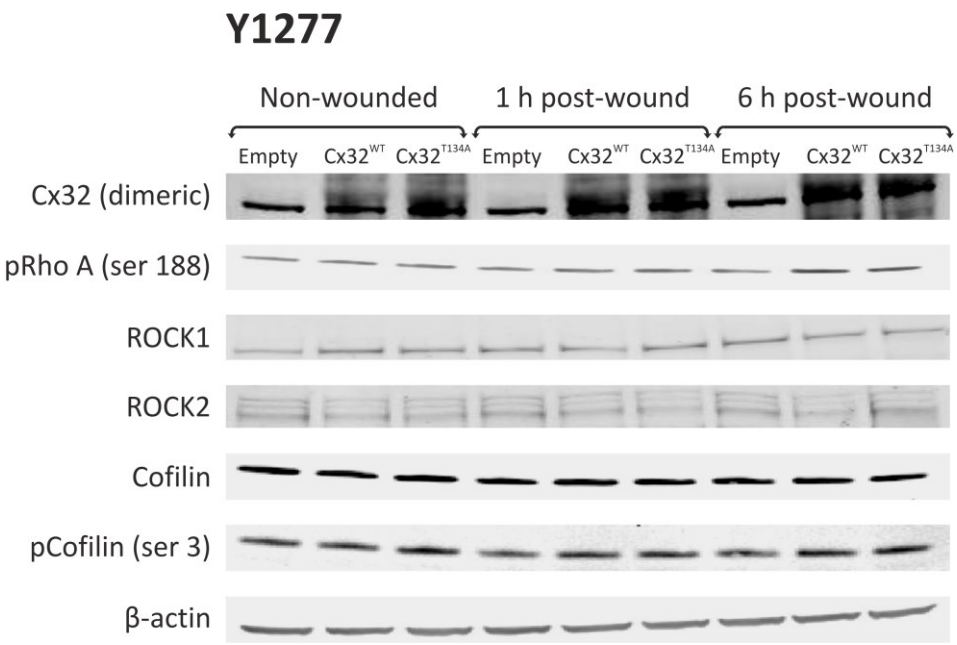

Figure 5.7 Immunoblotting of Wounded Cx32^{WT} and Cx32^{T134A} Overexpressing Cultures for Rho-kinase Signalling Pathway Proteins.

Y1277 (P4) cells transduced with pLXSN-empty, pLXSN-Cx32^{WT} and pLXSN-Cx32^{T134A} retroviral vectors were seeded onto 6 cm culture dishes and differentiated following the ABS/Ca^{2+} procedure. Whole cell lysates were harvested from non-wounded cultures and cultures at 1 h and 6 h post-wounding (see Fig 5.2). Immunoblotting was performed using antibodies to label Cx32, p-Rho A (ser 188), ROCK1/2, cofilin and p-cofilin (ser 3), as well as β-actin (loading control).

5.4.2 Examination of rho-kinase pathway proteins in wounded Cx32^{WT} and Cx32^{T134A} cultures by indirect immunofluorescence

Examination of ROCK1 and ROCK2 expression in both Cx32^{WT} and Cx32^{T134A} cells at 2 h and 8 h after wounding was weakly cytoplasmic, with some weak membrane-associated labelling, in particular towards the wound margin (Fig 5.8 A & B). In Cx32^{T134A} cells only, a small number of cells with exceptionally bright ROCK1 and

ROCK2 labelling at pronounced borders was observed (Fig 5.8 arrows), at both 2 h and 8 h post-wounding. However, these cells were unusually large compared to other cells and very rare within the culture. They were found both adjacent and remote to the wound edge. Cofilin was expressed distinctly at cell borders with weak cytoplasmic labelling in both $Cx32^{WT}$ and $Cx32^{T134A}$ cells, with no clear difference in expression between the two cell types at 2 h or 8 h post-wounding (Fig 5.8 C).

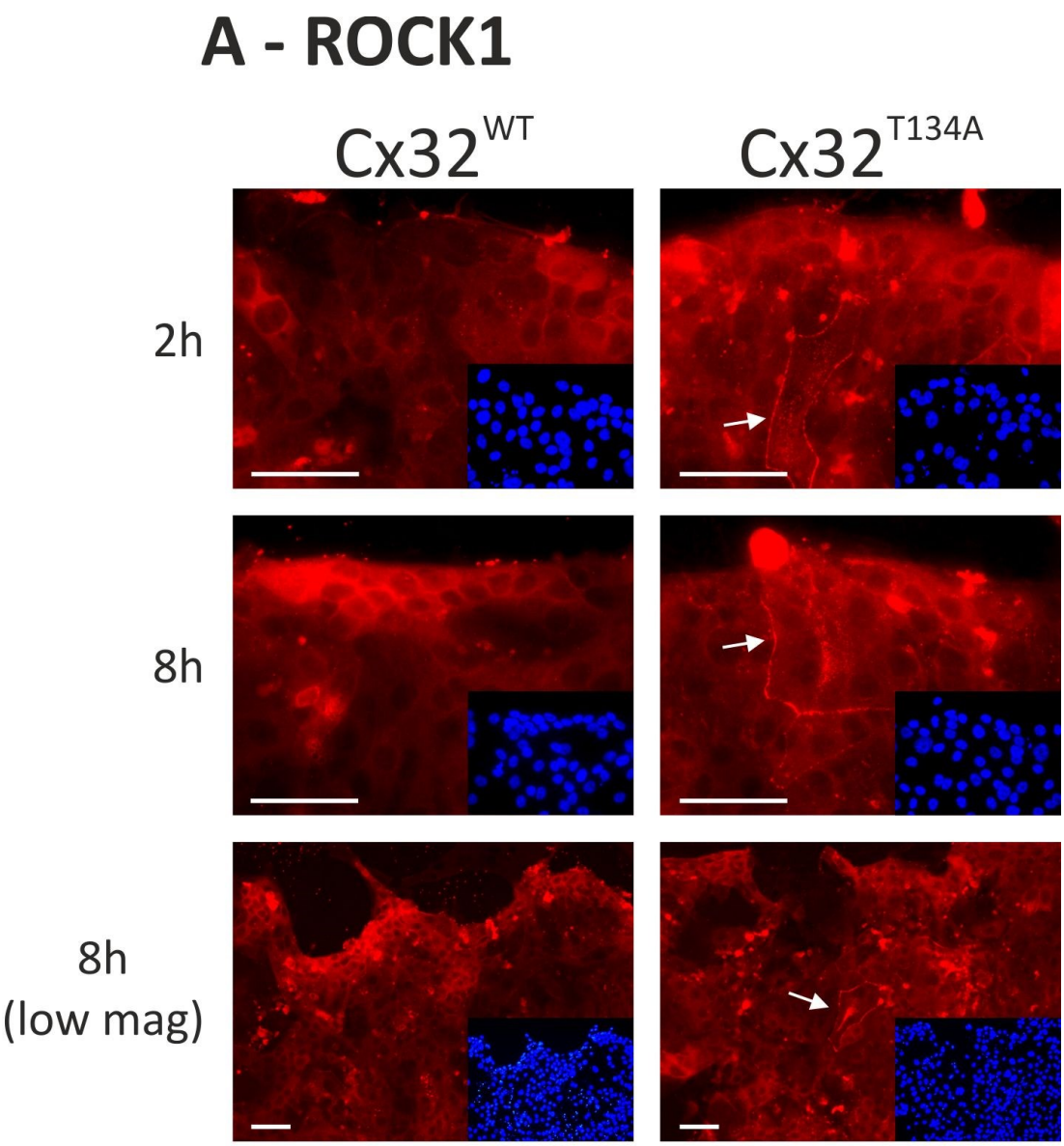

Fig 5.8 A

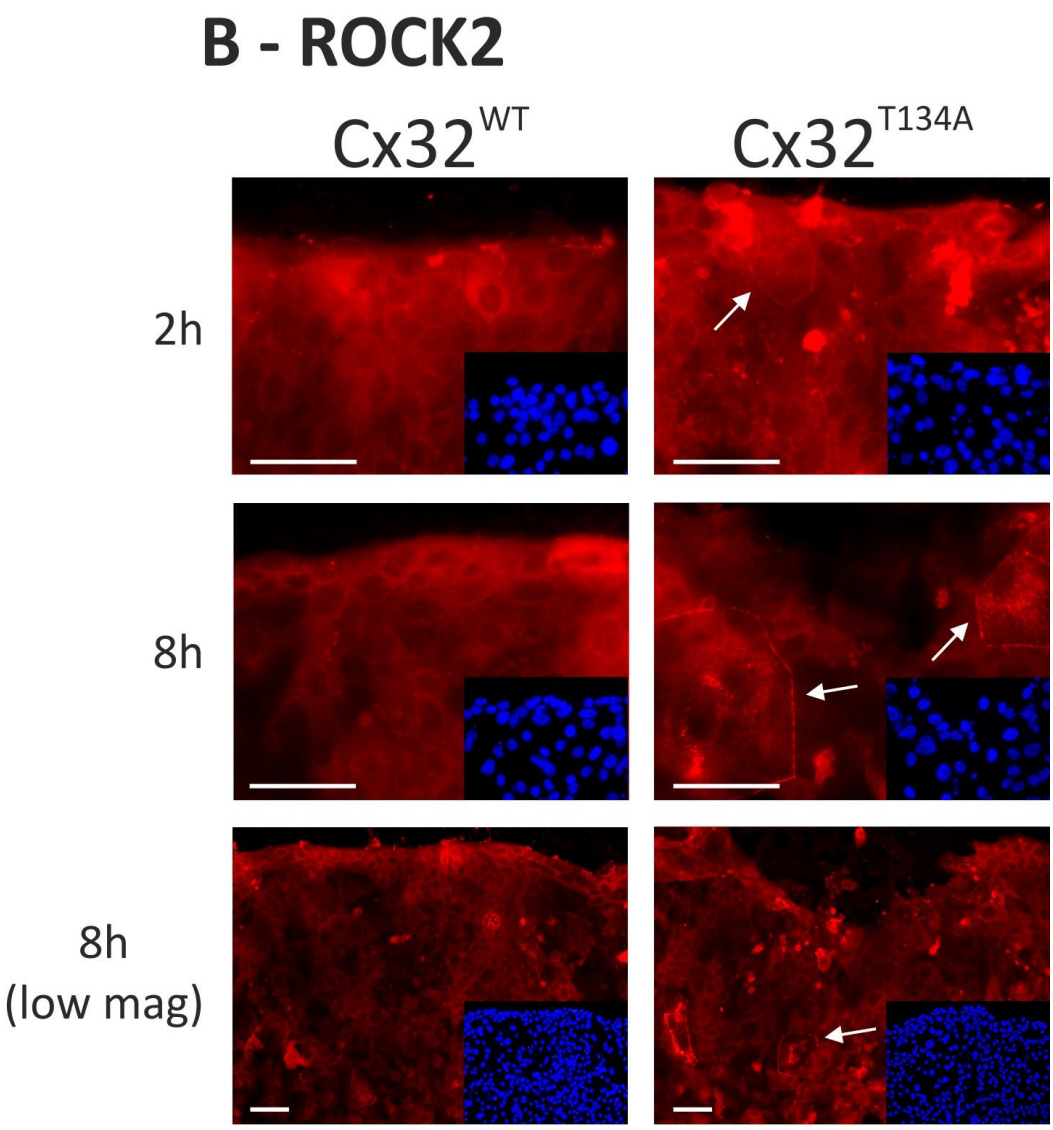

Fig 5.8 B

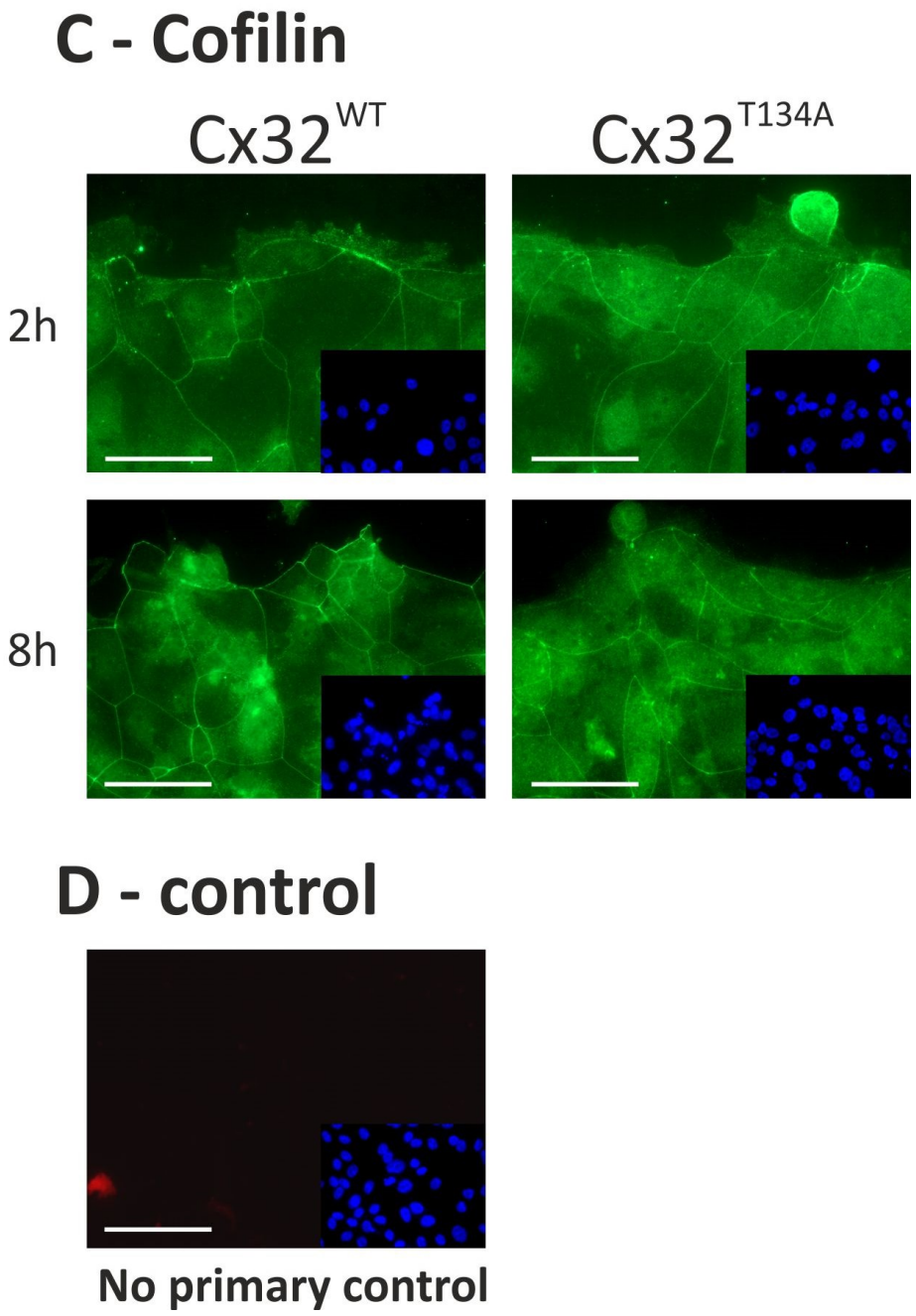

Figure 5.8 Immunofluoresence Labelling of Wounded Cx32^{WT} and Cx32^{T134A} Cultures to Examine Protein Localisation of ROCK and Cofilin.

Y1392 NHU cells transduced with Cx32^{WT} and Cx32^{T134A} overexpression vectors were differentiated following the ABS/Ca^{2+} method on glass slides. Cultures were scratched to generate a wound approximately 750-1000 µm wide and allowed to heal for 2 h or 8 h before fixing. Indirect immunofluorescence was performed using

anti- ROCK1 (A), ROCK2 (B) and cofilin (C) antibodies (or no primary negative control (D)). Fluorescence microscopy images were taken along the wound edge.

Hoechst 33258 images for each region are shown in the corner of each image and arrows depict bright border labelling of ROCK1 and 2.

Low mag = low magnification. Scale bar = 50 µm

5.4.3 Assessment of the TGFβ signalling pathway in wounded $Cx32^{WT}$ and $Cx32^{T134A}$ cultures by immunoblotting and immunocytochemistry of activated SMAD3.

To determine whether differences in TGFβ signalling might account for changes in wound-healing rates between $Cx32^{WT}$ (pore open) and $Cx32^{T134A}$ (pore closed) cultures, expression of activated SMAD3 (pSMAD3) was examined. Y1392 (P4) and Y1277 (P4) cells transduced with pLXSN-empty, pLXSN-$Cx32^{WT}$ and pLXSN-$Cx32^{T134A}$ retrovirus were differentiated following the ABS/Ca^{2+} method, before repeat scratching as detailed in Fig 5.2. Immunoblotting of lysates collected at 1 h and 6 h post-wounding (with non-wounded control), confirmed that in both cell lines, $Cx32^{WT}$ cells had a reduced pSMAD3 expression compared to cultures of empty vector or $Cx32^{T134A}$ cells (Fig 5.9). In Y1392 cells, this reduction in pSMAD3 expression was more pronounced at 6 h post-wounding, as determined by densitometry. However, even in non-wounded cells, pSMAD3 expression was reduced in both cell lines compared with $Cx32^{T134A}$ and empty-vector control cells. β-actin immunoblotting confirmed equivalent loading.

By immunocytochemistry, expression of pSMAD3 was nuclear and profoundly decreased in $Cx32^{WT}$ cultures following scratching, when compared with pLXSN-empty vector control cells. Expression was more intense towards the wound margin in $Cx32^{WT}$ and empty vector control cultures, whereas in $Cx32^{T134A}$ cultures, expression was intensely nuclear throughout (Fig 5.10). Images were taken at 8 h

post-wounding and the decreased rate of wound migration in Cx32^{WT} cells was apparent by the large wound area observed after fixation.

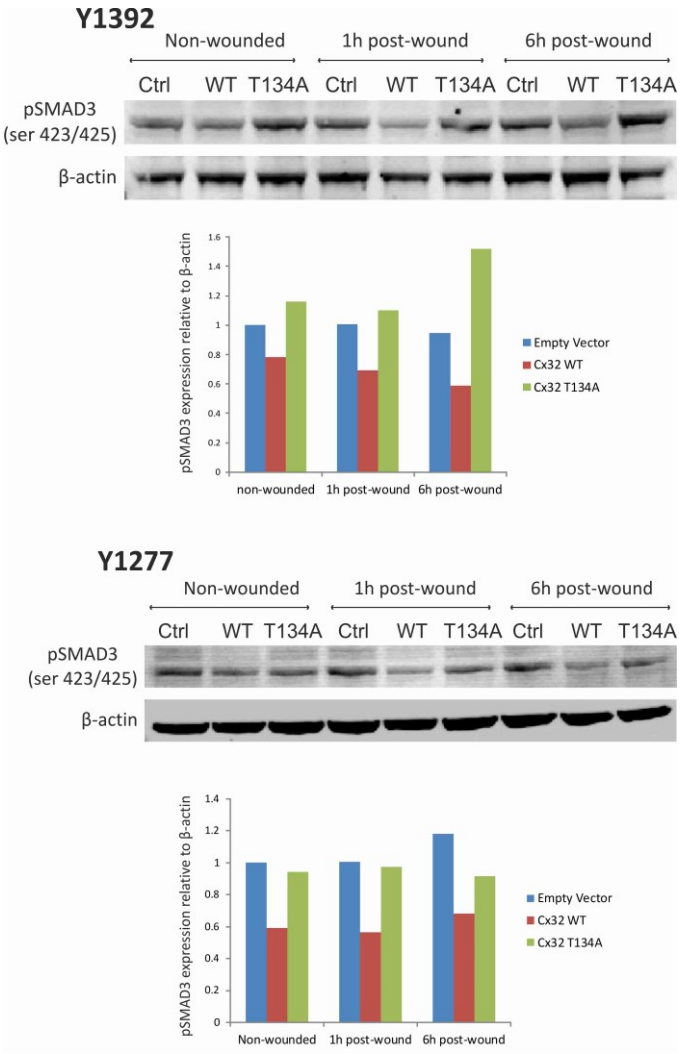

Figure 5.9 pSMAD3 Immunoblotting of Wounded Cx32^{WT} and Cx32^{T134A} Overexpressing Cultures.

Y1392 (P4) and Y1277 (P4) cells transduced with pLXSN-empty, pLXSN-Cx32^{WT} and pLXSN-Cx32^{T134A} retrovirus were seeded onto 6 cm culture dishes and differentiated for 7 days following the ABS/Ca^{2+} procedure. Whole-cell lysates were harvested from non-wounded cultures and cultures at 1 h and 6 h post-wounding with a pipette tip (see Fig 5.2). Immunoblotting was performed using antibodies to detect pSMAD3 and β-actin (loading control). Densitometry analysis was performed and relative expression (after normalisation to β-actin) plotted, as shown below each blot.

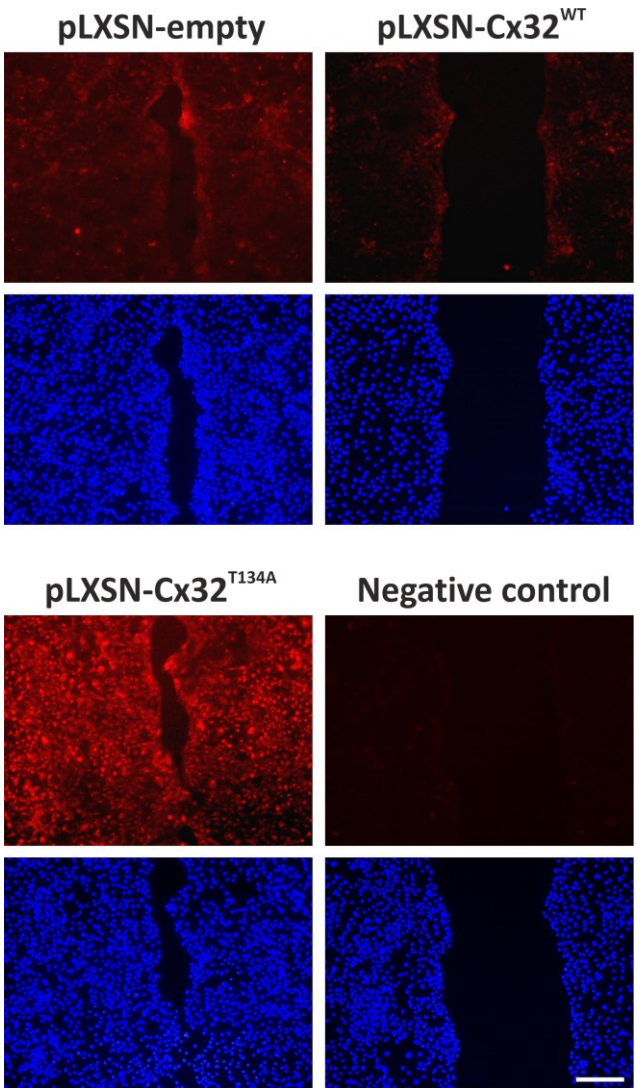

Figure 5.10 pSMAD3 immunolabelling of wounded $Cx32^{WT}$ and $Cx32^{T134A}$ overexpressing cultures.

Y1270 NHU cells transduced with control empty-vector, $Cx32^{WT}$ and $Cx32^{T134A}$ overexpression vectors were differentiated with ABS and Ca^{2+} on glass slides for 7 days. Cultures were scratched to generate a single wound approximately 750-1000 µm wide and allowed to heal for 8 h before fixing. Indirect immunofluorescence was performed using an anti-pSMAD3 antibody (or no primary negative control). Fluorescent microscopy images were taken along the wound edge of pSMAD3 (top row) or the Hoechst 33258 nuclear counterstain (bottom row). Scale bar = 200 µm

Note: the wound margin observed in $Cx32^{WT}$ cultures at 8 h is markedly wider than in $Cx32^{T134A}$ or empty vector control at the same time point, since wound healing was retarded in $Cx32^{WT}$ cultures.

5.5 Examination of TGFβ/TGFβRI Mediated Cell Migration in Cx32-modified Cultures

5.5.1 Wound-healing rates in Cx32-modified cultures in the presence of exogenous TGFβ1

The rate of wound-healing was examined in ABS/Ca^{2+} differentiated $Cx32^{WT}$ and $Cx32^{T134A}$ transduced cultures (Y1284), with or without the addition of exogenous TGFβ1 (Fig 5.11). When compared with vehicle control cultures, addition of 2 ng/ml TGFβ1 did not affect the rate of wound repair. At 18 h post-wounding, no significant difference was observed in the mean percentage wound closure between control cultures and those cultures which contained 2 ng/ml TGFβ1 (Fig 5.11 A). *Note, the concentration of TGFβ1 was previously titrated for effectiveness (Fleming et al. 2012).* However, in both treatment sets, an extremely significant difference was observed in the mean percentage wound closure between $Cx32^{WT}$ and $Cx32^{T134A}$ cultures observed at 18 h. Addition of 4 ng/ml TGFβ1 significantly accelerated the rate of wound migration in both $Cx32^{WT}$ and $Cx32^{T134A}$ cultures (Fig 5.11 B). At 18 h post-wounding, vehicle control cultures had healed by an average of 60% and 84% in $Cx32^{WT}$ and $Cx32^{T134A}$ cultures respectively, whereas cultures treated with 4 ng/ml TGFβ1 had healed by 76% and 99% respectively. As previously observed, a significant difference was observed in the mean percentage wound closure between $Cx32^{WT}$ and $Cx32^{T134A}$ cultures, regardless of treatment with TGFβ1 or vehicle control.

5.5.2 Investigating wound-healing rates in Cx32-modified cultures in the presence of the TGFβR tyrosine kinase inhibitor SB431542.

The rate of wound-healing was examined in $Cx32^{WT}$ and $Cx32^{T134A}$ transduced cultures (Y1277), with or without the addition of SB431542 (Fig 5.12). Addition of 10 μM SB431542 had a pronounced and significant effect on the wound-healing

rates of both in $Cx32^{WT}$ and $Cx32^{T134A}$ cultures. Measurement of wound areas at 18 h post-wounding revealed that $Cx32^{WT}$ and $Cx32^{T134A}$ cultures were healed by 59% and 90% respectively in vehicle control-treated cells, whereas parallel cultures treated with SB431542 were healed by 18% and 35% respectively indicating that inhibition of TGFβRI tyrosine kinase activity reduced wound healing rates in both $Cx32^{WT}$ and $Cx32^{T134A}$ cultures. As previously observed, a significant difference was observed in the mean percentage wound closure between $Cx32^{WT}$ and $Cx32^{T134A}$ cultures, regardless of treatment with SB431542 or vehicle control.

5.5.3 Investigating gene expression of TGFβ and TGFβ-receptors in wounded and non-wounded Cx32-modified cultures

RT-PCR, performed with cDNA generated from $Cx32^{WT}$ and $Cx32^{T134A}$ cultures following ABS/Ca^{2+} differentiation revealed that both TGFβ1 and 2 were expressed (Fig 5.13 A). There was no clear difference in expression between $Cx32^{WT}$ and $Cx32^{T134A}$ cells, although a reduction in TGFβ1 transcript expression was noted in both cultures following wounding, compared with non-wounded cultures. Although expressed in both non-wounded and wounded $Cx32^{WT}$ and $Cx32^{T134A}$ cultures, no change in transcript of TGFβR 1 or 2 was observed between the two transduced cell lines and no change was observed following wounding.

5.5.4 Examination of SMAD3-activation by paracrine factors released from Cx32-modified cultures

Medium was harvested from non-wounded and wounded $Cx32^{WT}$ and $Cx32^{T134A}$ cultures and applied to cultures of non-transduced NHU cells to determine if paracrine factors released by $Cx32^{WT}$ or $Cx32^{T134A}$ cells were capable of activation/suppression of SMAD3. SMAD3 activation was examined using an anti-pSMAD3 antibody and immunoblotting revealed that treatment of NHU cells with conditioned medium from $Cx32^{WT}$ or $Cx32^{T134A}$ cultures did not alter the activation of SMAD3 compared to NHU cells treated with comparable, non-conditioned medium (Fig 5.13 B). Controls behaved as expected: following stimulation with exogenous TGFβ1, amounts of pSMAD3 were strongly enhanced. Baseline expression of pSMAD3 was abrogated by addition of the TGFβR tyrosine kinase inhibitor SB431542.

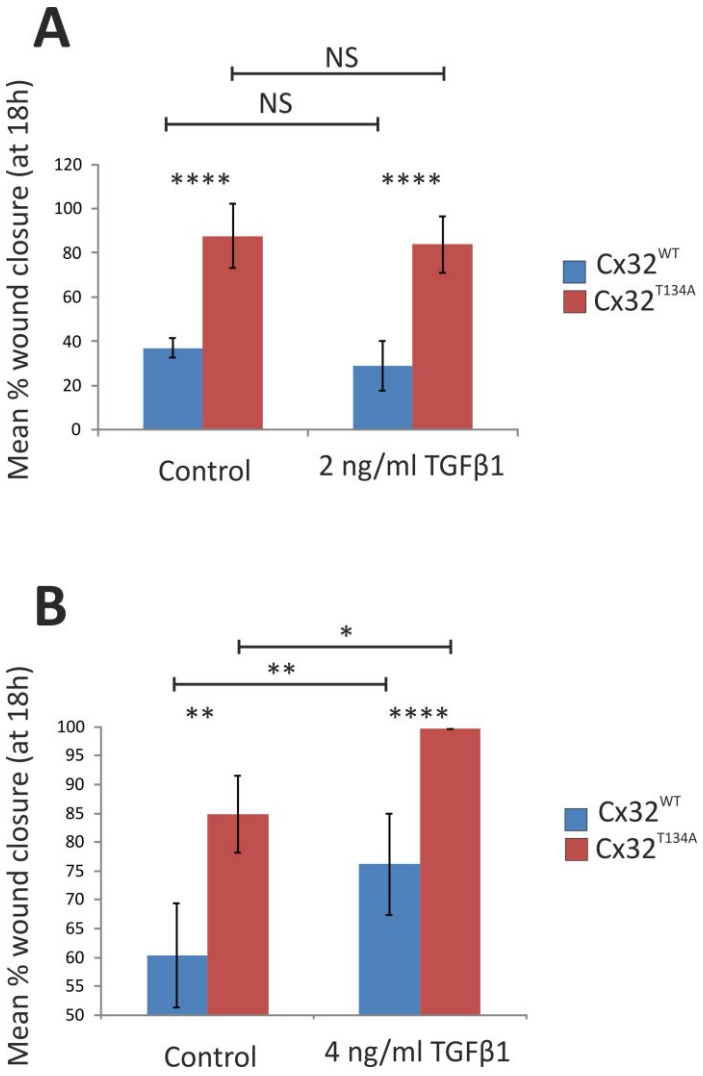

Figure 5.11 Wound-healing of $Cx32^{WT}$ and $Cx32^{T134A}$ Overexpressing Cultures in the Presence of Exogenous TGFβ1.

Y1284 (P4) NHU cells overexpressing $Cx32^{WT}$ and $Cx32^{T134A}$ were induced to differentiate following the ABS/Ca^{2+} procedure in 24-well plates. Cultures were pre-treated with 2 ng/ml (A) or 4 ng/ml TGFβ1 (B) for 3 h before scratching. A single scratch wound (750-1000 µM wide) was generated in each of six replicate cultures which were incubated in an environmental chamber for 18 h before imaging. Graphs show mean percentage wound closure at 18h for vehicle control or TGFβ1-treated cultures. All error bars shown are ± Standard Deviation.

*NS = not significant. **** (P <0.0001) extremely significant. ** (P <0.01) very significant. * (P<0.1) considered significant (One way ANOVA with Tukey-Kramer multiple comparisons post-test).*

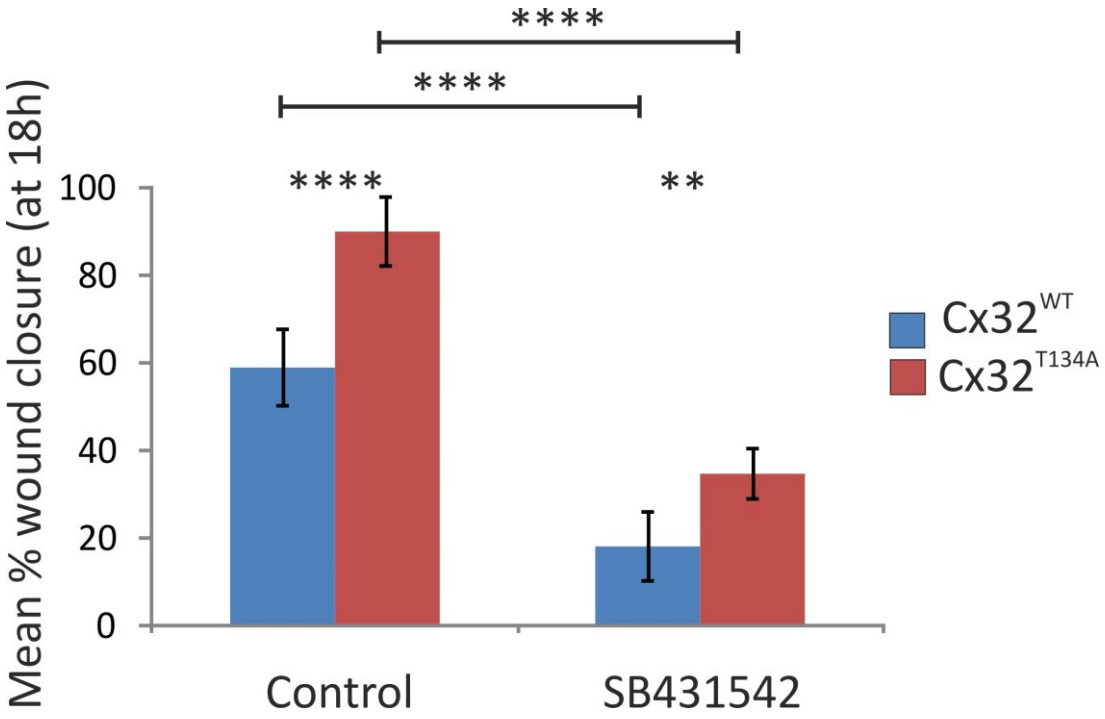

Figure 5.12 The Effects of TGFβRI Inhibition on Wound-healing of $Cx32^{WT}$ and $Cx32^{T134A}$ Overexpressing Cultures.

Y1277 (P4) NHU cells overexpressing $Cx32^{WT}$ and $Cx32^{T134A}$ were induced to differentiate following the ABS/Ca^{2+} procedure in 24-well plates. Cultures were pre-treated with 10 µM SB431542 for 3 h before scratching. A single scratch wound (750-1000 µM wide) was generated in 6 replicate cultures which were incubated in an environmental chamber for 18h before imaging. Graphs show mean percentage wound-closure at 18h for vehicle control or SB431542-treated cultures. All error bars shown are ± Standard Deviation.

***** (P <0.0001) extremely significant. ** (P <0.01) very significant. (One way ANOVA with Tukey-Kramer multiple comparisons post-test).*

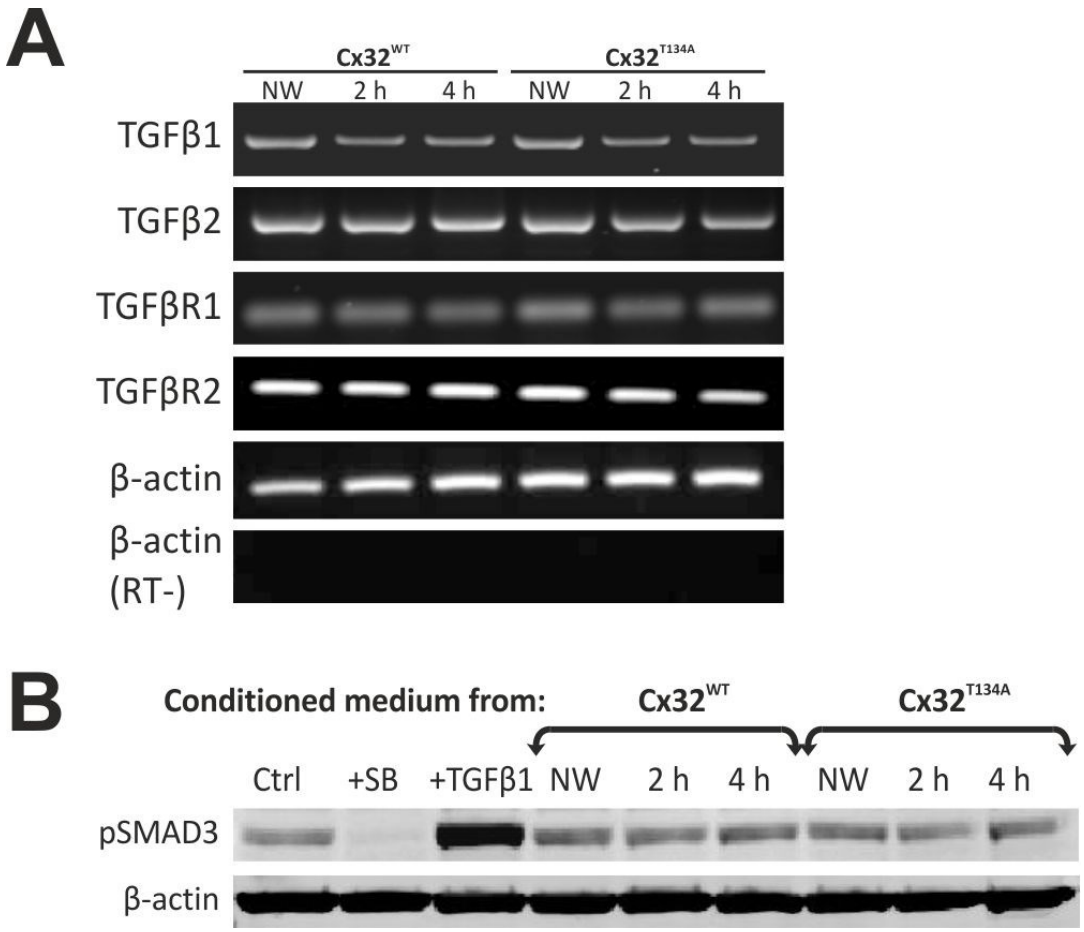

Figure 5.13 TGFβ/TGFβR Expression and Activity in Cx32^{WT} and Cx32^{T134A} Overexpressing Cultures.

A – Y1284 (P4) NHU cells overexpressing Cx32^{WT} and Cx32^{T134A} were induced to differentiate following the ABS/Ca^{2+} procedure in 6-well plates. After 7 days, RNA was harvested from non-wounded (NW) cultures and cultures at 2 h and 4 h post-wounding with a sterile pipette tip. RT-PCR was performed using primers to amplify TGFβ (1 and 2) and TGFβR (1 and 2) from each culture. Reaction controls included: β-actin (to demonstrate equivalent loading) and a reverse transcription negative (RT-) control (to rule out amplicon/genomic contamination).

B – Conditioned medium was harvested from Cx32^{WT} and Cx32^{T134A} cultures used in (A) immediately prior to RNA extraction and used to treat proliferating (50% confluent), Y1545 NHU cells for 3 h at 37 ^{o}C. Lysates were harvested for immunoblotting with pSMAD3 (ser423/425) and β-actin loading control antibodies. Control treatments included non-conditioned ABS/Ca^{2+} (Ctrl) and culture medium containing 10 μM SB431542 (+SB) or 4 ng/ml TGFβ1 (+TGFβ1).

5.5.5 Examination of active SMAD3 and CREB protein localisation inwounded $Cx32^{WT}$ and $Cx32^{T134A}$ cultures

Activated SMAD3 (pSMAD3) was strongly expressed in differentiated NHU cells overexpressing mutant $Cx32^{T134A}$, both adjacent to and remote from the wound edge (Fig 5.14), confirming previous observations (Fig 5.10). pSMAD3 expression was predominantly nuclear with some weak cytoplasmic expression. In $Cx32^{WT}$ cells, pSMAD3 expression was extremely weak, with very occasional positive nuclear labelling. Expression of pSMAD3 in control (empty vector) cells was less intense than in $Cx32^{T134A}$ cells; occasional positive nuclei were observed and expression was enhanced in a small population of cells along the wound-edge where both nuclear and cytoplasmic labelling was abundant. Expression of the SMAD3 transcriptional coactivator CREB and its cAMP-dependent, PKA-activated form pCREB (ser133) were strongly expressed in the nuclei of $Cx32^{WT}$, $Cx32^{T134A}$ and empty vector cells, with no difference observed between the three transductants. Expression of both proteins was consistent whether adjacent or remote from the wound edge.

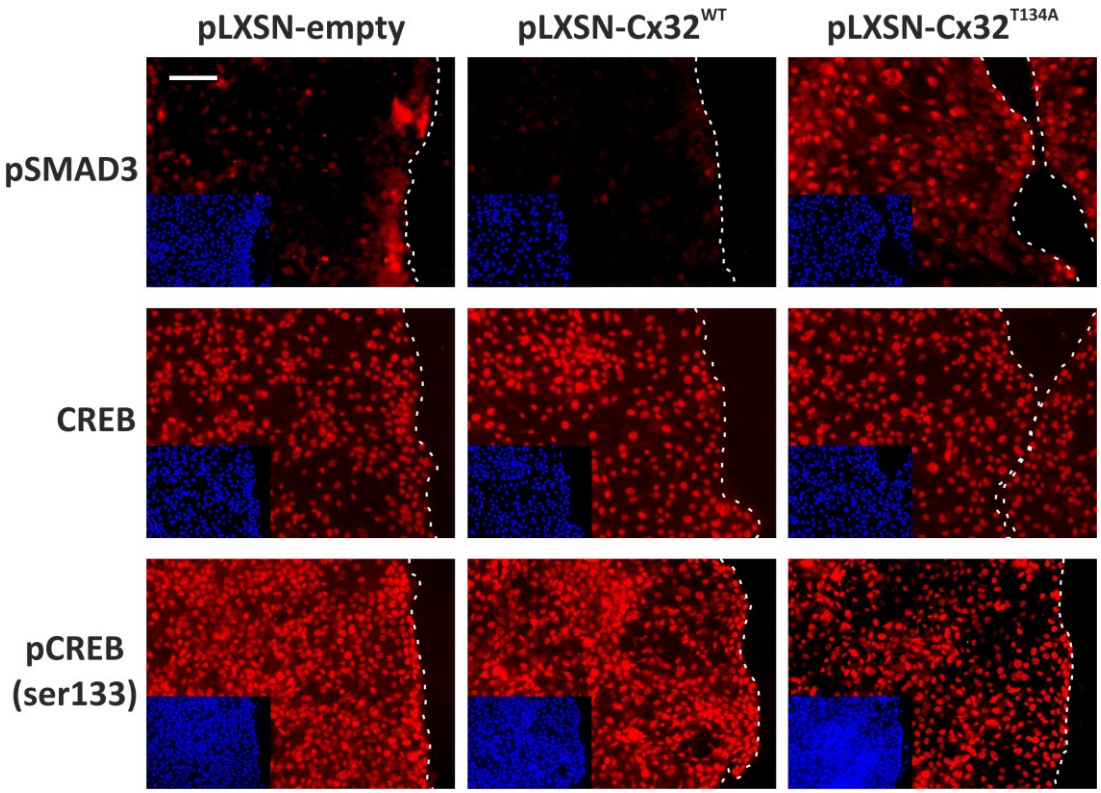

Figure 5.14 Immunofluoresence Labelling of Wounded Cx32^{WT} and Cx32^{T134A} Cultures to Examine pSMAD3 and CREB Protein Localisation.

Y1392 NHU cells transduced with Cx32^{WT} and Cx32^{T134A} overexpression vectors were differentiated by the ABS/Ca^{2+} method on glass slides. Cultures were scratched to generate a wound approximately 750-1000 µm wide and allowed to heal for 8 h before fixing. Indirect immunofluorescence was performed using anti- pSMAD3, CREB and pCREB (ser133) antibodies. Fluorescent microscopy images were taken along the wound edge (shown with white dashed line). Hoechst 33258 images for each region are shown in the corner of each image. Scale bar (top left) = 100 µm.

5.5.6 Examination of SMAD3 and PPARγ protein localisation in wounded $Cx32^{WT}$ and $Cx32^{T134A}$ cultures

As PPARγ has been shown to negatively regulate SMAD3 activation in previous studies, its expression was assessed in wounded $Cx32^{WT}$ and $Cx32^{T134A}$ cultures. Localisation of SMAD3, pSMAD3 and PPARγ was assessed by indirect immunofluoresence in differentiated, Y1284 $Cx32^{WT}$ and $Cx32^{T134A}$ cultures during wound-healing, in regions adjacent to and remote from the wound edge. Furthermore, SMAD3 expression was observed to be of similar intensity in $Cx32^{WT}$ and $Cx32^{T134A}$ cells, with a strong nuclear and weakly cytoplasmic distribution (Fig 5.15 A). SMAD3 expression was observed to be of similar intensity whether cells were adjacent or remote to the wound edge. Activated SMAD3 (pSMAD3) was strongly expressed in $Cx32^{T134A}$ cells with a strong nuclear and weak cytoplasmic distribution (Fig 5.15 B). Expression in $Cx32^{WT}$ cells was weakly cytoplasmic close to the wound edge and not visible in regions remote to the wound edge. PPARγ expression was more distinctly nuclear in $Cx32^{WT}$ cells, where nuclear expression was strong in regions adjacent to and remote from the wound (Fig 5.15 C). A strong nuclear expression was also observed in $Cx32^{T134A}$ cells; however, cytoplasmic labelling was also apparent which gave the appearance of a more diffuse PPARγ distribution throughout the cells. In order to quantitatively assess the PPARγ distribution, image analysis was performed in order to determine relative PPARγ fluorescence in nuclear and cytoplasmic cell compartments. Image analysis of PPARγ fluorescence (using Tissue Gnostics software), confirmed the observation that PPARγ expression was more distinctly nuclear in $Cx32^{WT}$ cells (Fig 5.15 D). The PPARγ nuclear:cytoplasmic labelling intensity across the culture was found to be significantly higher in $Cx32^{WT}$ than $Cx32^{T134A}$ cells.

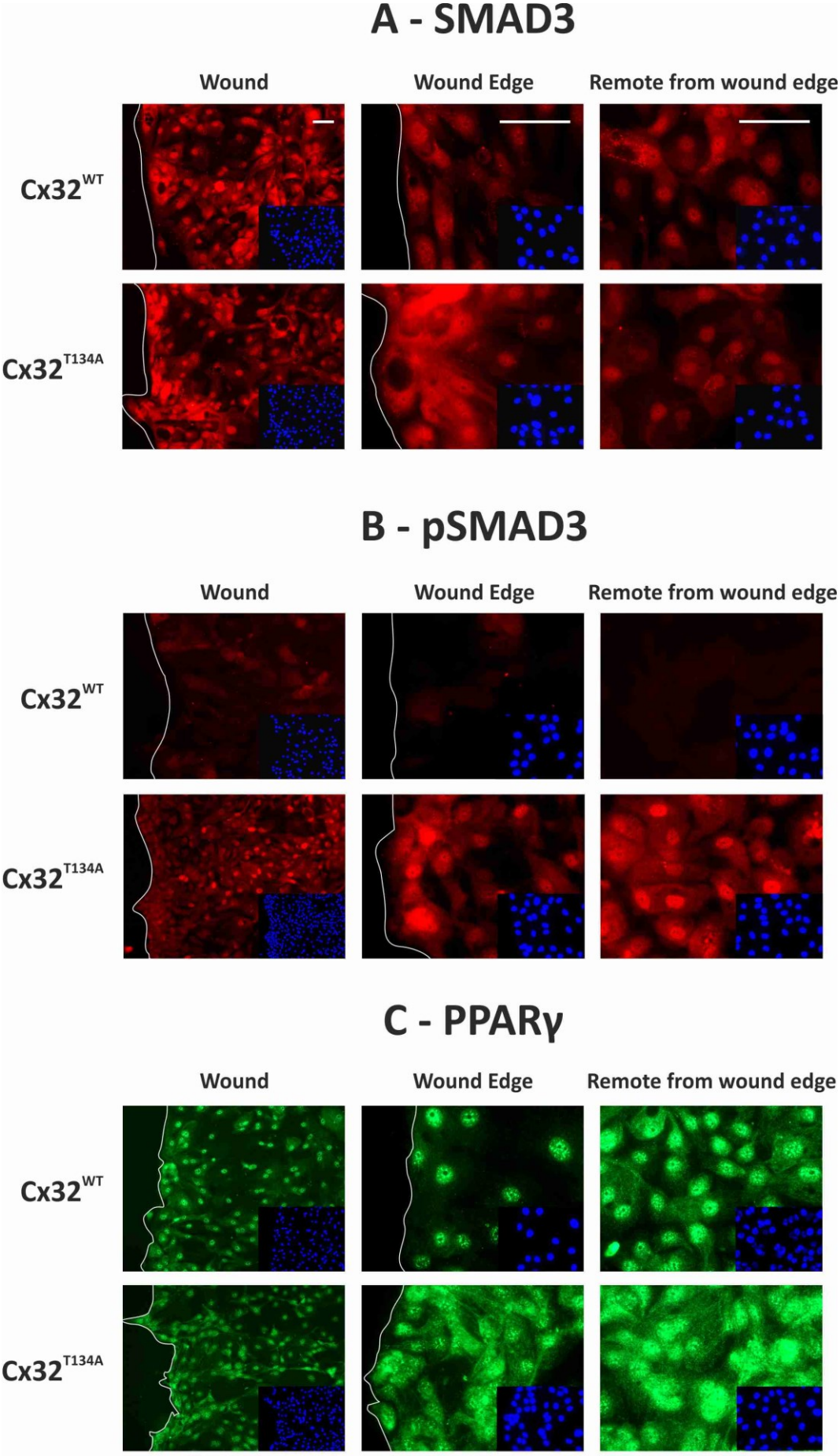
A - SMAD3
Wound
Wound Edge
Remote from wound edge
Cx32WT
Cx32T134A
B - pSMAD3
Wound
Wound Edge
Remote from wound edge
Cx32WT
Cx32T134A
C - PPARγ
Wound
Wound Edge
Remote from wound edge
Cx32WT
Cx32T134A

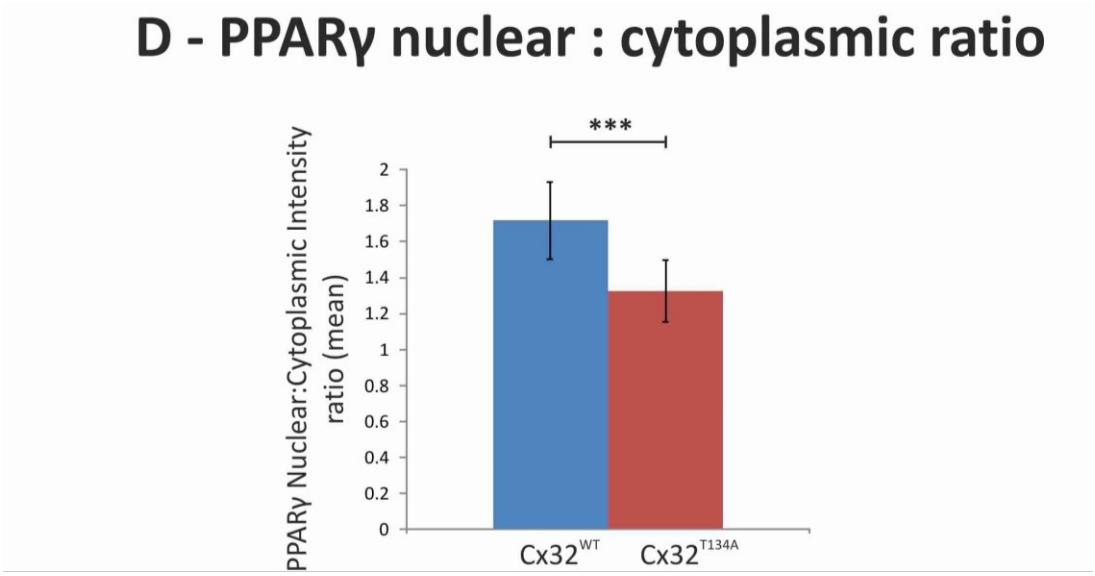

Figure 5.15 Immunofluoresence labelling of wounded Cx32^{WT} and Cx32^{T134A} cultures to examine SMAD3 and PPARγ protein localisation.

Y1284 NHU cells transduced with Cx32^{WT} and Cx32^{T134A} overexpression vectors were differentiated with ABS and Ca^{2+} on glass slides. Cultures were scratched to generate a wound approximately 750-1000 µm wide and allowed to heal for 8 h before fixing. Indirect immunofluorescence was performed using antibodies raised against SMAD3 (A), pSMAD3 (ser423/425) (B) and PPARγ (clone E8 which is specific for an epitope present in the C-terminal ligand binding domain) (C). Lower and higher magnification images were taken along the wound edge (scratch border is depicted by white line) and higher magnification images taken of a region in the centre of the culture (remote from wound edge). Hoechst 33258 images for each region are shown in the corner of each image. Scale bars for each vertical row are shown in the top image and represent 50 µm.

*PPARγ labelling in nuclear and cytoplasmic regions was quantified using TissueQuest software, with the Hoechst 33258 image used to set the nuclear mask algorithm for separation of nuclear and cytoplasmic components. Mean relative fluorescence intensities within nuclear and cytoplasmic compartments of a 1.5 mm^2 area (including the wound edge) was calculated and a ratio of nuclear:cytoplasmic intensity plotted (D). ***P<0.0001 (unpaired t-test)*

5.6 Morphology of Differentiated NHU cells During Wound Repair

5.6.1 Tight junction expression and distribution during differentiated NHU wound healing

To examine whether the migratory behaviour in differentiated urothelial cultures (non-transduced) coincided with a loss of cell polarity, the distribution of several tight junction proteins as well as Cx32 was examined during wound-healing (8 h post-wounding). Cx32 was localised to cell borders and was expressed in all cells, including those at the wound-margin, with no changes in expression close to the wound-edge (Fig 5.16A). A similar trend was observed with the tight junction proteins occludin, ZO-1 and claudin 5. The tight junction proteins examined were distributed at cell borders with no evidence of enhanced or reduced expression towards the wound margin.

To assess if Cx32 overexpression (in wild-type or dominant-negative form) affected the expression of tight junctions and adherens junctions during wounding, immunoblotting of differentiated non-wounded and wounded transduced NHU cultures was performed (Fig 6.16B). In non-wounded cultures there was no change in expression of E-cadherin, occludin or claudin 5, in Cx32 wild-type or dominant-negative overexpressing cells compared with empty vector control. In addition, there was no observed change in expression of these proteins in any of the transductants during the process of wound-healing, as assessed at 1 h and 6 h post-wounding.

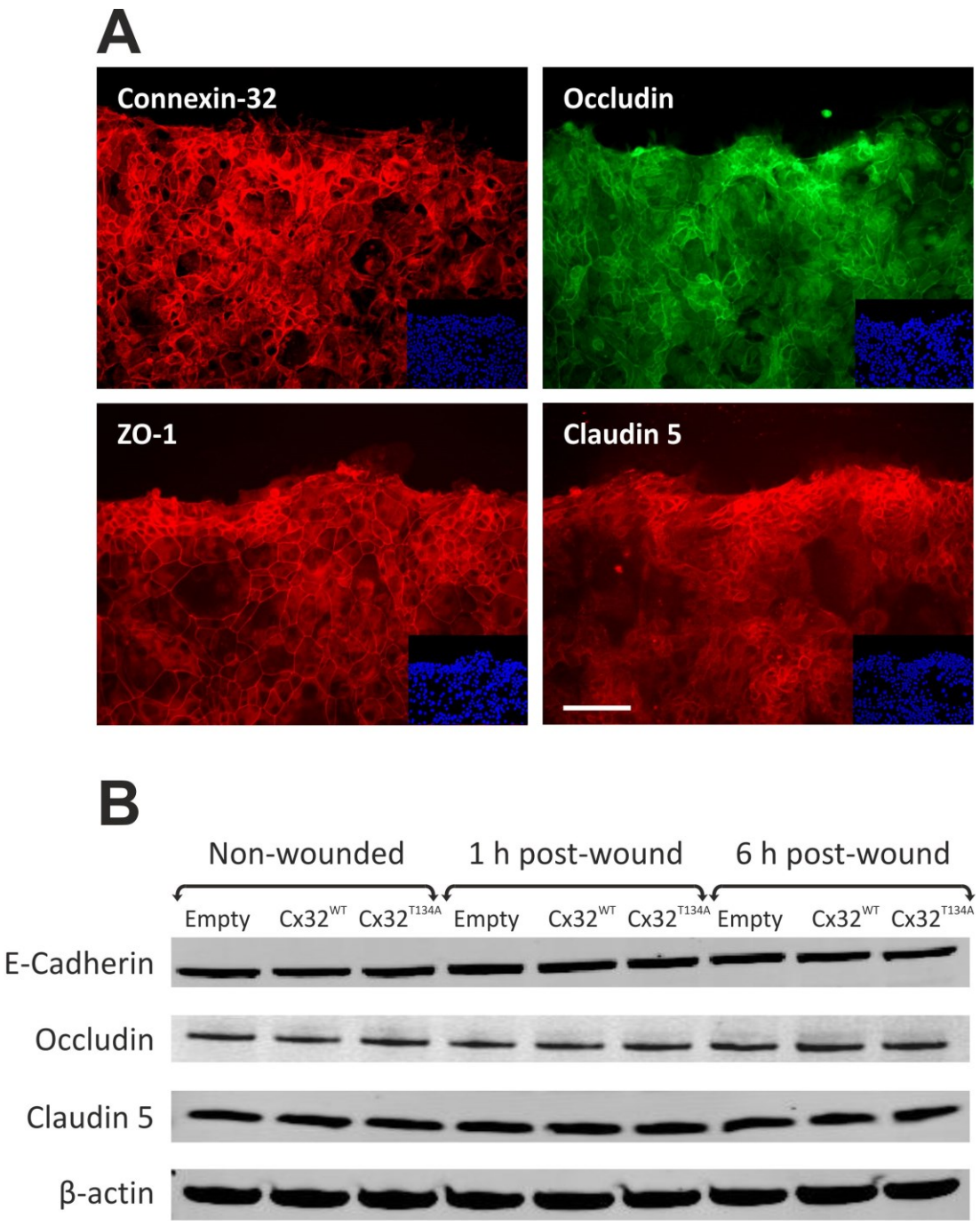

Figure 5.16 Assessment of Cx32 and Tight Junction Proteins During Wound-healing of Differentiated NHU Cultures (Non-transduced and Cx32 Overexpressing).

(A) *Y1268 (P3) non-transduced NHU cells were differentiated on 12-well glass slides using the ABS/Ca^{2+} method. A single scratch of approximately 750 µM wide was generated across each well and cultures were returned to the incubator for 8 h before fixation. Cells were immunolabelled with anti-Cx32, occludin, ZO-1 and*

Claudin 5 antibodies, as indicated. Images showing nuclei labelled with Hoechst 33258 are shown in the bottom corner of each image. Scale bar = 100 µm

(B) *Y1270 (P4) cells transduced with pLXSN-empty, pLXSN-Cx32^{WT} and pLXSN-Cx32^{T134A} retroviral vectors were seeded onto 6 cm culture dishes and differentiated following the ABS/Ca^{2+} procedure. Whole-cell lysates were harvested from non-wounded cultures and cultures at 1 h and 6 h post-wounding with a pipette tip (see Fig 5.2). Immunoblotting was performed using antibodies to label E-cadherin, occludin and claudin 5 to assess cell adhesion and polarity, as well as β-actin as a loading control.*

5.6.2 Assessment of Ki67 expression in differentiated Cx32^{WT} and Cx32^{T134A} transduced NHU cells during wound healing

The proliferative capacity of Cx32^{WT} and Cx32^{T134A} overexpressing cultures during wound healing was examined by assessment of Ki67 expression, a cellular marker associated with proliferation. Immunocytochemistry in ABS/Ca^{2+} wounded cultures demonstrated that Cx32^{T134A} (pore closed) cultures had a high proportion of cells which were Ki67 positive (49%), reflecting high cell cycle activity (Fig 5.18A). However, Ki67 expression was notably absent from cultures in which Cx32^{WT} was overexpressed (0% of cells considered to be above the positive threshold set using Tissue Gnostics TissueFAXS software). Transcript expression of Ki67 was not observed in non-wounded Cx32^{WT} cell cultures, but expression was weakly upregulated as a response to wounding, with low expression observed at 4 h following wounding (Fig 5.18B). In Cx32^{T134A} cultures, Ki67 transcript expression was apparent in both non-wounded and wounded cultures, with expression enhanced by 4 h post-wounding compared to non-wounded cultures.

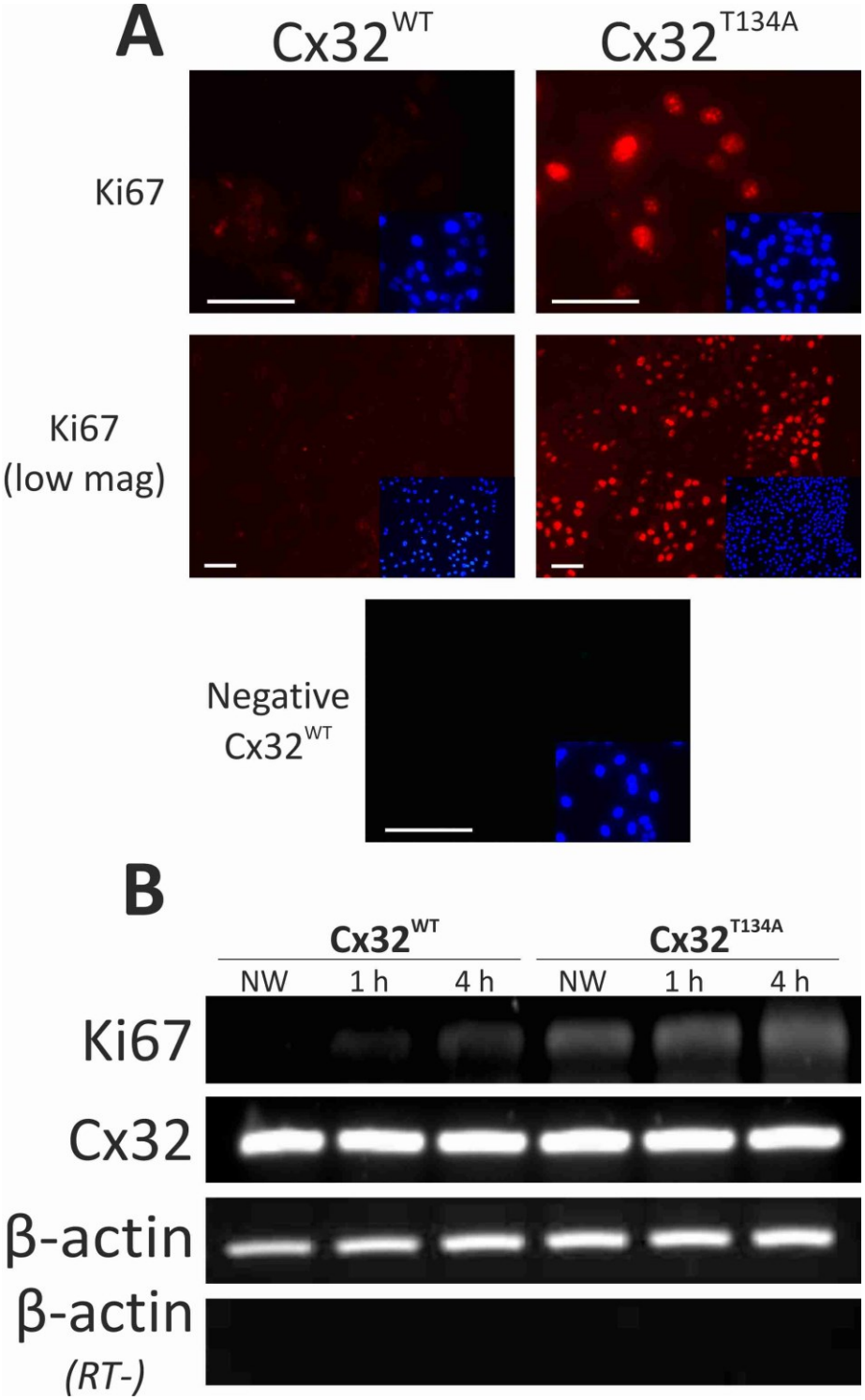

Figure 5.18 Expression of the proliferation marker Ki67 in wounded $Cx32^{WT}$ and $Cx32^{T134A}$ overexpressing cultures.

A - Y1284 (P4) cells transduced with pLXSN-$Cx32^{WT}$ and pLXSN-$Cx32^{T134A}$ retroviral vectors were seeded onto glass slides and differentiated following the ABS/Ca^{2+} procedure. A single scratch of approximately 750 µM wide was generated across each well and cultures were

returned to the incubator for 8 h, before fixation and immunolabelling with an anti-Ki67 antibody. A no-primary antibody, negative control was included. Images showing nuclei labelled with Hoechst 33258 are shown in the bottom corner of each image. Scale bar = 50 µm, Low mag = low magnification image.

B – Y1284 (P4) cells transduced with pLXSN-Cx32^{WT} and pLXSN-Cx32^{T134A} retroviral vectors were differentiated in 6cm cell culture dishes following the ABS/Ca^{2+} method. RNA was harvested from non-wounded (NW) cultures and cultures at 1 h and 4 h post-wounding with a pipette tip (see Fig 5.2). RT-PCR was performed using primers to amplify Ki67 and Cx32 from each culture. Reaction controls included: β-actin (to demonstrate equivalent loading) and a reverse transcription negative (RT-) control (to rule out amplicon/genomic contamination).

5.7 Discussion

The key function of urothelium is to provide a protective urinary barrier; if this is damaged it must be rapidly repaired through a series of wound healing events which involve both migratory and proliferative mechanisms (Kreft et al. 2005, Shabir et al. 2008, Fleming et al. 2012). Data presented in this chapter using methods to study the rates of wound-healing and migration in differentiated NHU cultures, suggests that Cx32 expression has a potent and negative effect on the migratory and proliferative behaviour of NHU cells during scratch wound repair.

5.7.1 Cx32 and migration of NHU cultures

When Cx32 function was inhibited, either by shRNA knock-down or overexpression of a dominant-negative pore-closed mutant, the resulting cultures were faster migrating and showed enhanced ability to restore barrier function upon wounding. Conversely, forced overexpression of functional (wild-type) Cx32 retarded the rate of scratch wound healing and barrier restoration.

Since connexins appear to have communication-associated functions as well as alternative structural functions (for example integration into tight junctions), it is relevant to dissect whether the effects of Cx32 on wound migration are driven by a communication-dependent mechanism.

Overexpression of functional Cx32 had an opposite effect on wound migration compared with pore-closed Cx32, supporting the conclusion that a communication-dependent behaviour is responsible for driving a less-migratory phenotype in differentiated NHU cells. This indicates that specific signalling events through Cx32 channels are likely to be exerting a negative influence on wound healing. Whilst the rate of migration was supressed in $Cx32^{WT}$ overexpressing cells, the resulting

effect on the population was a delay in wound-healing as these cultures were capable of completing the repair in time.

5.7.2 Cx32 and wound healing in the liver

Cx32 is a well-studied marker of differentiation in liver and its expression in hepatocytes *in vitro* is often used as a tool to confirm differentiation. The liver is known to have a remarkable regenerative capacity and a small number of studies in rodents have demonstrated links between Cx32 expression and the rate of liver regeneration following partial hepatectomy (Kren et al. 1993, Dagli et al. 2004). In the Kren study, a temporary reduction in Cx32 and Cx26 mRNA and protein were observed in rat livers following 70% partial hepatectomy suggesting that down regulation of Cx32 is associated with wound-healing. The Dagli study observed a delay in liver regeneration in transgenic mice expressing a dominant-negative mutant Cx32 (driven under a liver-specific albumin promoter), due to reduced levels of hepatocyte proliferation in mutant livers. The mutant Cx32 used in the study (V139M) was defective for membrane localisation and thus the delayed regeneration cannot be presumed to be associated with Cx32-mediated communication. Nevertheless, the results of the study might suggest that Cx32 in the mouse liver regulates regeneration, which contradicts both the Kren study and the results observed in the present study performed in human urothelial cells.

The Dagli study also reported increased susceptibility to chemical-induced hepatocarcinogenesis in the same dominant-negative mice, for which no clear explanation was suggested. It was acknowledged that Cx32 appeared to be playing a role in promoting a wound-healing phenotype, but at the same time acting in a tumour-suppressive fashion. Other studies support the latter finding, where transgenic mice deficient in Cx32 appear to manifest a higher susceptibility to chemical hepatocarcinogenesis (Evert et al. 2002); however, without chemical treatment these mice do not exhibit higher levels of tumour development. A

further study was able to show that cells with membrane-associated Cx32 were suppressive for the development of hepatocellular carcinoma (Li et al. 2007), however, when Cx32 expression was forced in hepatocellular carcinoma cell lines, localisation was aberrant (golgi/cytoplasmic) and resulted in enhanced motility and potential for metastasis.

5.7.3 Connexins and cell migration in the other systems

Although liver regeneration is heavily dependent on increased hepatocyte proliferation, the evidence from several model/experimental systems is that some connexins can directly regulate cell migration. Brain slices from Cx43 knock-out mice show an irregular distribution of astrocytes (Perez Velazquez et al. 1996) and several other studies support a role for Cx43 in supporting neuronal migration (Nadarajah et al. 1997, Wiencken-Barger et al. 2007). However, evidence from a study in which different mutants of Cx43 were probed suggests that Cx43 channel communication properties are not essential for promoting migration and the study indicates that gap junction-mediated adhesion is crucial for neuronal migration (Elias et al. 2007).

Recent studies in human skin models have demonstrated that Cx43 channels also exert an anti-migratory influence in keratinocytes. Cx43 expression is reduced at wound margins during wound healing of normal skin and expression of Cx43 at wound margins was observed to be associated with poor wound healing rates in diabetic non-healing ulcers (Brandner et al. 2004). Although the Cx43 gap junction network in the epidermis is rapidly remodelled to support migration of cells into the wound space, this does not appear to occur with Cx32 expression during migration of differentiated NHU cultures, since Cx32 expression was not downregulated during wound migration. Transfected expression of Cx32 in HeLa cells was found to significantly increase cell adhesion and inhibit cell migration (Yang et al. 2011), as measured by counting cell aggregates. However this was reversible by addition of a

general gap junction inhibitor oleamide, enabling the authors to conclude that Cx32-mediated communication was responsible for inhibition of migration.

Blockade of Cx43 function using a connexin-mimetic peptide (GAP27) was observed to stimulate skin wound healing, even in growth conditions which are known to mimic type II diabetes (Wright et al. 2009, Wright et al. 2013). The authors of the latter study suggest that one possibility is that connexin-mimetic peptides may interfere with cell-cell adhesion (via interference with Cx43 interactions with PDZ domains, found for example in ZO-1) or cell-ECM adhesion, although these mechanisms were not considered as part of that particular study. However, a recent study in mice demonstrated that Cx43 deficiency accelerated skin wound healing and ECM remodelling (Cogliati et al. 2015).

Some analogies may be drawn between Cx43 in repair of the skin and Cx32 in the repair of NHU cultures. Application of Cx43 antisense oligonucleotides had an effect of speeding up the rate of migration of keratinocytes and similarly, so did application of connexin mimetic peptides which can block the communication properties of docked gap junctions, reviewed in (Becker et al. 2012). This suggests that Cx43-mediated communication acts to inhibit the rate of migration, rather than merely expression, similar to the findings with Cx32 in the current study. In addition, treatment of keratinocytes with Cx43 antisense oligonucleotides, increased the expression of TGFβ-1, supporting a role for Cx43 in the suppression of the TGFβ signalling pathway, as observed in the present study with Cx32. However, the $Cx32^{T134A}$ dominant negative cells used in the current study did not appear to alter their expression of TGFβ-1, only the downstream expression of SMAD3 suggesting that effects on this pathway may occur downstream of ligand binding.

5.7.4 Cx32 and cell adhesion

In the present study, expression of proteins associated with cell-cell adhesion (tight junction and E-cadherin proteins), were not compromised in rapidly migrating Cx32 pore-closed mutant cell cultures. Differentiated NHU cultures (non-transduced) appear to migrate in a manner in which the integrity of tight and adherens junctions is largely maintained, ruling out a typical epithelial-mesenchymal transition. Although the role of Cx32 in promoting a more adhesive phenotype (less migratory) was considered, the effects of Cx32 expression on cell-ECM interactions was not and may form an interesting avenue for further study.

5.7.5 Migratory signalling pathways in the urothelium

In the current study the Rho-kinase and TGFβR pathways were two signalling routes selected for analysis, due to the changes observed in the migratory behaviour of urothelial cultures in response to changes in the pore state of Cx32 channels. The Rho-kinase pathway is a key mediator of cell shape and motility (Van Aelst et al. 2002); however the current study did not find any major changes in regulation of RhoA/ROCK signalling as a response to changes in Cx32-mediated cell-cell communication. This was with the exception of a rare population of cells observed only in faster migrating $Cx32^{T134A}$ cultures (pore-closed), in which expression of the RhoA downstream mediators ROCK1 and 2 was observed to be membrane-associated. It is reported that ROCK can act directly at cell membrane ruffles to induce actomyosin contraction (Fackler et al. 2008). Since the $Cx32^{T134A}$ were more migratory than $Cx32^{WT}$ cell cultures, it may be expected that more ROCK activity be observed, however it is unclear as to why membrane expression would be so rare within the rapidly migrating $Cx32^{T134A}$ cell population and the findings were too subtle for clear interpretation. cAMP-induced phosphorylation of RhoA at serine 188 renders it inactive, thus exherting negative effects on the Rho kinase signalling pathway (Ellerbroek et al. 2003). However, changes in expression of pRhoA (ser188) were not observed in $Cx32^{WT}$ cultures, suggesting that it is unlikely that inhibition of ROCK signalling via this mechanism occurs in $Cx32^{WT}$ overexpressing

NHU cultures. The roles of cdc42 and Rac in directed forward movement of NHU cells and the presence of lamellipodia and filopodia were not directly studied in this project (see introduction Fig 1.4 A), however further studies as to the directional movement of NHU cultures provide huge scope for further study.

Cell signalling through TGFβ-receptor activation is associated with increased cell migration and invasion in several human cancer cell lines (Muraoka et al. 2002, Halder et al. 2005) and a potent inhibitor of TGFβRI kinase activity (SB-431542), was observed to inhibit repair of wounded differentiated NHU cultures (Fleming et al. 2012). In the latter study, evidence suggested that the repair of differentiated urothelial cultures was mediated in part by pSMAD3 activation at the wound edge. These findings were confirmed in the present study; SMAD3 was weakly activated (phosphorylated) in control cultures and became more apparent during migration at the wound edge. In Cx32-overexpressing cultures (both $Cx32^{WT}$ and $Cx32^{T134A}$), SB-431542 acted to inhibit wound healing rates, whilst addition of exogenous TGFβ1 acted to promote migration rate of wounded differentiated urothelial cultures. This further supports the role of autocrine/paracrine TGFβR signalling in urothelial repair and suggests that inhibition or activation of this pathway has the ability to modulate the rate at which migration occurs in this system.

Cx32 (wild-type) overexpression resulted in downregulation of activated pSMAD3 coinciding with retarded wound-healing, suggesting that Cx32 expression has an inhibitory effect on this pathway. Conversely, overexpression of pore-closed mutant Cx32 (T134A) had the opposite effect, enhanced expression of nuclear pSMAD3 with rapid wound-healing rates. This further supports SMAD3 activation as a key event in urothelial wound healing, but also demonstrates that Cx32-mediated cell-cell communication is involved in regulating this process, with high levels of Cx32-mediated communication resulting in cultures where wound-healing is largely impaired.

There were two key findings as part of this study which suggested that TGFβ ligand or receptor were unlikely to be involved in explaining the differences observed in wound-healing rates between the wild-type and dominant negative Cx32-overexpressing cultures. Firstly, there were no observed differences in transcript expression of TGFβ (I and II) and TGFβR (I and II) between $Cx32^{WT}$ and $Cx32^{T134A}$ cultures. Secondly, treatment of NHU cells with conditioned medium from $Cx32^{WT}$ or $Cx32^{T134A}$ cultures (wounded and non-wounded), neither inhibited nor enhanced pSMAD3 expression, implying that differences in the release of TGFβR ligands by the two cell types (thus affecting SMAD3 phosphorylation downstream) was not supported.

Furthermore, expression of a key transcriptional coactivator of pSMAD3, CREB was unaltered between in wounded $Cx32^{WT}$ or $Cx32^{T134A}$ cultures. When activated, CREB is phosphorylated at serine 133 and interacts directly with pSMAD3 and a second coactivator P300, to drive expression of key genes including a subset involved in ECM biosynthesis (Ghosh et al. 2000, Schiller et al. 2010).

Inactivation of SMAD3 has been proposed to occur in response to activation of the nuclear receptor PPARγ in several studies; PPARγ ligands have been demonstrated to inhibit TGFβ-induced phenotypic changes in retinal pigment epithelial cells by influence on SMAD3 (Hatanaka et al. 2012). PPARγ-null mouse embryonic fibroblasts show constitutive SMAD3 phosphorylation and interaction with its transcriptional co-activator P300, coinciding with enhanced collagen biosynthesis, even in the absence of exogenous TGFβ (Ghosh et al. 2008). A further study demonstrated that PPARγ exerts negative effects on SMAD3 activity by direct binding to SMAD3, thus blocking its phosphorylation by TGFβRI (Fu et al. 2001).

5.7.6 PPARγ activation and wound migration

The question therefore arises as to whether wound healing in differentiated NHU cultures is inhibited in response to PPARγ activation, with effects on SMAD3 activation in a mechanism independent of ligand binding to TGFβR. Immunocytochemistry demonstrated that PPARγ expression is significantly more nuclear in $Cx32^{WT}$ overexpressing cultures than $Cx32^{T134A}$ cultures which may imply enhanced activity, although future studies to assess potential interactions between PPARγ and SMAD3 would be required to shed further light on this theory.

In differentiated NHU cultures, the immediate and predominant feature of wound-closure was shown to be cell migration with some proliferation as indicated by expression of Ki67 further back from the wound edge (Fleming et al. 2012).

5.7.7 Cx32 and proliferation of NHU cultures

Ki67 expression is observed during all active phases of the cell cycle (late G1, S, G2 and mitosis), but is absent from resting cells (G0) making it an excellent marker for estimating the population of cells undergoing growth (reviewed in Scholzen et al. 2000). In the present study, enhanced expression of Ki67 suggested an unusually high rate of proliferation when Cx32 function was inhibited by overexpression of the dominant negative channel. This was also the case in non-wounded cultures suggesting changes in cell-cycle control were observed in the cell community in general, rather than as a response to wound-healing. Natural and synthetic PPARγ ligands have been demonstrated to inhibit proliferation of NHU cells *in vitro,* arresting cells in the G0/G1 phase of the cell cycle (Kawakami et al. 2002).

In the present study Ki67 labelling was not performed on Cx32 shRNA knock-down cultures. However, given that Cx32 shRNA cultures are significantly faster at wound repair than control cultures using the scratch model system, this would be a worthy

follow up experiment. It would determine whether the effects on proliferation are linked to Cx32 expression rather than the Cx32-mediated GJIC. This would be of particular interest given the channel-independent roles of connexins on cell growth, in particular through the C-terminal tail (reviewed in (Vinken et al. 2012)).

In addition, other markers which would give further insight into the effects of Cx32 overexpression on the cell cycle of NHU cultures would be worthy of study. Whilst Ki67 provides evidence that cells are in active stages of the cell cycle, it does not give direct evidence of proliferation and BrdU pulsing of NHU cultures followed by antibody labelling would provide more direct evidence of proliferation. One study demonstrated that enhanced expression of Cx43 resulted in a delay in cell cycle progression in HeLa cells and human fibroblasts, in association with increased expression of the cell cycle inhibitor p21 (WAF1/CIP1) (Johnstone et al. 2010). p21 is a potent cyclin-dependent kinase inhibitor and prevents progression of the cell cycle between G1 and S phase and it would be relevant to consider the expression of p21 in Cx32 overexpressing (WT and T134A) cultures, especially following wounding. It has been demonstrated that proliferation of vascular smooth muscle cells can be stimulated in response to activation of a SMAD3/ERK MAPK signalling pathway, in a process which involves nuclear export of the cyclin-dependent kinase inhibitor p27 (Suwanabol et al. 2012). Given the links observed between SMAD3 activity and Ki67 in the current study, it would also be worth studying the expression of activated ERK and p27, as part of a larger panel to shed light on the pathways promoting proliferation following inhibition of Cx32 signalling.

SMAD3 knock-out mice show reduced susceptibility to chemical carcinogenesis in skin, compared with wild-type litters (Li et al. 2004) and there is mounting evidence that TGFβ signalling through SMAD mediators is a positive regulator of tumour growth and metastasis in many systems (Massague 2012). The TGFβ pathway has been linked to bladder cancer progression (Miyamoto et al. 1995, Hung et al. 2008) and it has recently been demonstrated that TGFβ secreted by cancer-associated

fibroblasts drives EMT and a more invasive phenotype in urothelial bladder cancer cells (Zhuang et al. 2015). It may therefore be of critical importance to NHU cells that Cx32 channel signalling acts to balance the level of SMAD3 activation, for controlled cell growth and balanced proliferation when needed.

5.7.8 Overview

In other systems such as skin and liver, connexins have been shown to be down regulated during tissue repair. In line with these findings, data presented here confirms that Cx32-mediated cell-cell communication acts to supress the repair rate of differentiated NHU cultures and that this is likely to be mediated in part by suppression of SMAD3 activity, a critical element of the machinery which supports migration in differentiated urothelial cultures, but also in part by a reduced capacity for proliferation in wild-type overexpressing NHU cultures. It is possible that PPARγ activity plays a role in inhibition of SMAD3 activity, but could also contribute to the reduction in proliferation capacity.

Several questions arise from these findings. What messenger molecules might be signalling through Cx32 channels to control migration? Whilst the general nature of messenger molecules which are gap junction permeable are similar for all gap junctions (<1 kDa, water-soluble), it has been observed that different connexins display permeability preferences (Goldberg et al. 2002, Goldberg et al. 2004), although the biochemistry underlying this selectivity is poorly understood. In a system in which several connexins are expressed the potential for function overlap would make this a challenging challenging question to answer. Some second messengers such as inositol 1,4,5-triphosphate (IP3) (Niessen et al. 2000) and adenosine (Goldberg et al. 2002), have been identified as having preferential passage through Cx32 channels when compared with other selected connexins. As a starting point for future work, it may be exciting to pursue the possibility that natural ligands of PPARγ might pass through Cx32 channels. For example the

prostaglandin 15-deoxy PGJ(2) has a molecular mass of 316 Da, comfortably within the range which could be accommodated by Cx32 gap junction pores. This would be of particular interest due to the increased nuclear expression of PPARγ in $Cx32^{WT}$ overexpressing cells, suggesting that activated PPARγ is more abundant when Cx32 is overexpressed. It has been demonstrated that ligands of PPARγ suppress cell proliferation in Th17 cells (Kim et al. 2015) and also that PPARγ can interfere with SMAD3 activity and therefore PPARγ may be the common factor which interferes with both proliferative and migratory pathways.

Another question of interest is why might Cx32 expression physiologically important *in vivo* in supressing migration of human urothelium? The urothelium can be damaged in a variety of ways including injury caused by microorganisms, urinary toxins, mechanical damage or in disease states. Treatment of rat bladders with protamine sulphate invokes selective sloughing of superficial cells in a model used to mimic interstitial cystitis, which results in loss of TER and increased urothelial permeability (Lavelle et al. 2002). Repair occurs rapidly and it is thought that basal/intermediate cells proliferate and migrate to heal the wound, before differentiation at the superficial surface to generate new umbrella cells. Since Cx32 expression *in vivo* was found to be restricted to the basolateral membrane of umbrella cells (chapter 2), damage or shedding of the superficial cells might prove to be a key event in promoting regeneration. Insult resulting in a loss of superficial cells would remove the population of Cx32 expressing cells, thereby reversing the Cx32 channel-mediated block on cell proliferation and migration, which might initiate wound repair at an appropriate time. When urothelial cells are cultured in serum-free medium, they adopt a basal-like phenotype with high proliferation rates and lose expression of markers associated with differentiation (Southgate et al. 1994, Varley et al. 2005), including Cx32 (chapter 2). In non-diseased states *in vivo*, the urothelium is a quiescent epithelium (Walker 1960) and it is plausible that differentiation-induced expression of Cx32 is key to maintaining this state.

A potential physiological role for Cx32 in the urothelium is that it may or may not function in a hemichannel state. In intestinal epithelial cells, connexin hemichannels composed of Cx26, Cx32 and Cx43 have been located to the basal membrane (Clair et al. 2008). It is believed that bacterial invasion promotes hemichannel opening in this setting, allowing release of ATP which in turn enhances bacterial dissemination (Tran Van Nhieu et al. 2003). Whether connexin hemichannels are located in the urothelium and play a role in the spread of urinary tract infection is not known, however subsets of patients suffer recurrent urinary tract infection and the study of Cx hemichannels may certainly prove relevant to this. Additionally, stretch-evoked release of ATP from urothelial cells has been demonstrated to act on P2X receptors in afferent nerves to transmit signals of bladder filling (Cockayne et al. 2000). It has been suggested that release of ATP from stretched urothelial cells occurs in response to elevated Ca^{2+} levels and that ATP may be released through anion channels or Cx hemichannels (Miyamoto et al. 2014). However there is currently little evidence to support this hypothesis, although it seems a likely area for future mechanosensation studies.

It is possible that Cx32 gap junctions are critical for the delicate balance required to achieve a differentiated, low-turnover, impermeable epithelium which can rapidly switch to regeneration when necessary due to Cx32 loss. Data presented in this chapter suggests that normal Cx32 function exerts a negative effect on NHU cell proliferation and migration.

6. Conclusions

6.1 Overview

It is considered that the urothelium serves as the tightest barrier epithelium in the human body (Negrete et al. 1996) ; barrier function is maintained by intercellular tight junctions and apical membrane plaques. Furthermore the urothelium has an impressive capacity to switch into a migratory and proliferative phenotype following damage to ensure barrier restitution. A role for gap junctions in directing the balance between barrier development and epithelial tissue repair has not previously been considered, however *in vitro* studies using normal human urothelial (NHU) cells provided an ideal model system to pursue this.

Prior to this thesis, the expression of Cx26 and Cx43 had previously been reported in human and rat bladders (Grossman et al. 1994, Lorentz et al. 2012, Sunagawa et al. 2015), however a detailed analysis of the expression and localisation of connexin isoforms in urothelium had not previously been reported.

The present study provides the first detailed characterisation of connexin expression in the urothelium, demonstrating that NHU cells alter their connexin expression profile during cytodifferentiation to produce specific channels. The results provide the first evidence for a direct functional role for Cx32 in urothelial homeostasis. Cx32 gap junctions were upregulated as part of the urothelial differentiation programme in response PPARγ activation and were identified *in vitro* as a key element in controlling both differentiation and regenerative behaviours.

6.2 Urothelial expression of connexins

Eight connexins were identified with gene expression in normal human urothelial cells. Of particular interest was Cx32, since its expression uniquely coincided with NHU cell differentiation and immunochemical studies indicated localisation of Cx32 protein to cell borders in the barrier-forming superficial cell layer *in situ*. Thus Cx32 can be considered alongside tight junction proteins, uroplakins and cytokeratins to

be a molecular marker of urothelial cytodifferentiation. Of particular relevance was the finding that knock-down of Cx32 resulted in compromised urothelial cytodifferentiation *in vitro*, suggesting that Cx32 expression is a requirement for the normal development of a functional barrier urothelium. It was further shown that tight junctions, which are paramount in defining the tight barrier properties, were disrupted as a consequence of Cx32 shRNA knock-down, resulting in a significant reduction in barrier function in knock-down cultures from three independent Cx32 shRNA's, demonstrating that Cx32 expression is closely associated with tight junction development.

6.3 Connexins and tight junctions.

Previous studies have demonstrated that some connexins (including Cx32) have the ability to influence the assembly of both tight and adherens junctions (Kojima et al. 2001, Talhouk et al. 2008, Herve et al. 2012). In the current study, the finding that Cx32 shared molecular interactions with ZO-2 and occludin indicated that in urothelium, Cx32 forms a structural component of tight junction complexes. Given that forced expression of a pore-closed dominant negative Cx32 channel did not impact on barrier development, it is probable that the influence of Cx32 on tight junction development is structural and independent of Cx32 channel function. In other tissue networks such as intestinal and airway epithelia and in liver, close relationships have been observed between connexins and tight junctions in both communication-dependent and independent mechanisms and it is therefore in keeping with findings from other studies that Cx32 was observed at tight junction strands with influence on barrier function in urothelial cells.

The Cx32 mutant (T134A) generated in this study was predicted to function as a dominant negative (Beahm et al. 2006). This property has been demonstrated in studies for other connexins as this particular residue is strictly conserved amongst α- and β-connexin subgroups. However, this is the first investigation to have demonstrated loss of function with this mutation for Cx32 and may prove to be a

useful experimental tool for investigating Cx32 function in both *in vitro* and *in vivo* studies.

6.4 Cx32 and the regenerative phenotype

A surprising finding was that Cx32-mediated cell-cell communication exerted a negative impact on both the migration and proliferative capacity (loss of Ki67 expression) of differentiated NHU cultures following scratch wounding. Data presented here provides compelling evidence that signalling events occurring through Cx32 gap junction channels act to block the regenerative capacity of NHU cells. A comparison may be drawn to liver regeneration, in which Cx32 was found to be downregulated prior to stimulation of proliferation in hepatocytes, but then re-expressed during the differentiation which occurs following repair (Neveu et al. 1995).

Whilst the exact mechanisms underpinning this process are largely unknown, exploration of molecular pathways which promote urothelial repair indicated that this process involved suppression of SMAD3 activity, a critical element of the machinery which supports migration in differentiated urothelial cultures (Fleming et al. 2012). The synchronous increase in the nuclear localisation of PPARγ which was observed may prove to be key to unravelling the effects of Cx32 channel behaviour on regeneration. Active PPARγ has previously been demonstrated to be inhibitory to SMAD3 activity (Fu et al. 2001, Ghosh et al. 2008, Hatanaka et al. 2012) and PPARγ ligands have been demonstrated to inhibit proliferation of NHU cells *in vitro* (Kawakami et al. 2002, Varley et al. 2008). Pursuing a potential link between PPARγ behaviour and SMAD3-driven NHU cell migration would be a clear goal for future studies arising from this thesis.

In vitro, NHU cells exhibited a switch to a regenerative phenotype when Cx32 channel activity was blocked. *In vivo*, this could occur as a direct result of shedding of the Cx32-expressing superficial cells, which may occur as a response to insult or injury. Another possibility is that a more complex control system exists in NHU cells

involving Cx32 channel gating, as has been extensively demonstrated in Cx43 channels (Moreno 2005), where phosphorylation events and changes in voltage are impact on channel gating. This would enable NHU cells to open/close Cx32 channels to block or drive a proliferative and migratory phenotype as necessary (see Fig 6.1).

In summary, the evidence presented in this thesis suggests that Cx32 gap junctions are of ultimate importance to urothelial barrier function where they play a role in the delicate balance required to achieve a differentiated, low-turnover, impermeable epithelium which can rapidly regenerate when necessary, followed by restitution of barrier function. The working hypothesis (chapter 1) that specific connexins may be involved in a differentiated urothelial phenotype and barrier function was demonstrated to be true for Cx32 in this study. However, evidence presented here supports a clear inhibitory role for Cx32-mediated GJIC in wound migration, which although not anticipated, does compare with connexins in other systems (e.g. Cx43 in migration of keratinocytes).

6.5 Future Work Plans

Since it has been described as the tightest barrier epithelium in the body, the close association of Cx32 with tight junctions is of particular relevance to the urothelium. However, whilst worthy of reporting, there are many tissue types including liver, gut and airway epithelial cells in which Cx32 has been demonstrated to interact at tight junction strands. Therefore future work plans to follow up from this study would focus on the role of Cx32-mediated intercellular communication on the suppression of NHU cell proliferation and migration, since these findings provide scope for a more unique study into Cx32 biology. Further work to determine the proliferative capacity of Cx32 overexpressing cells (both WT and T134A dominant negative) might include a more detailed analysis of the cell cycle in these transductants, considering markers such as PCNA, cyclins, p21, p27 and pERK as well as performing growth curves of these transduced cells in a differentiated state. These growth curves were not performed as part of this study as it was previously

believed that differentiated NHU cells do not proliferate unless wounded, however mutant $Cx32^{T134A}$ cells may have a greater proliferative capacity even in the absence of wounding).

Give the close associations between hyperproliferation and sustained SMAD3 activity with carcinogenesis/metastasis in many tissues (including bladder), alongside evidence which suggests that both Cx32 and PPARγ are candidate tumour suppressor genes, it seems highly relevant to pursue a more detailed analysis of Cx32 in bladder cancers. I would propose a detailed immunohistochemical analysis of Cx32 in bladder tumours, combined with a study of Cx32 gene and protein expression in a range of bladder cancer cell lines of different stages and grades. A study in which Cx32 is overexpressed in selected cancer cell lines might offer some interesting findings on cancer cell growth and differentiation capacity, especially in light of the data presented here which suggests PPARγ may be modified by Cx32-mediated GJIC. Activated SMAD3 would serve as an excellent marker for TGFβ-pathway involvement and it would be worth linking expressionof Cx32 to pSMAD3 in a variety of tumours and/or cancer cells. Finally, an examination of the bladders of Cx32 knock-out mice might provide further insight as to how essential Cx32 is to bladder physiology and whether there is evidence of hyperplasia or compromised differentiation and barrier function in these animals.

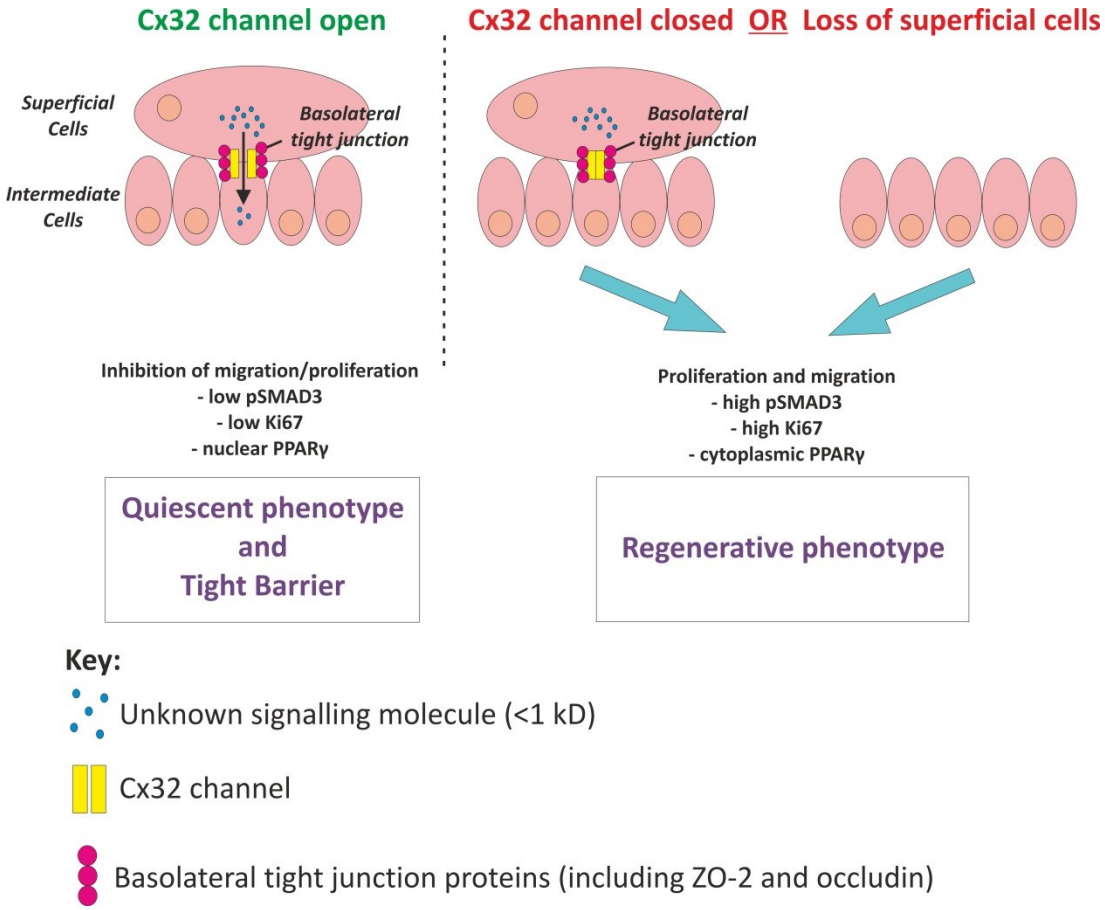

Figure 6.1 Proposed mechanisms for the balance between urothelial barrier function and regeneration.

Appendix 1 – Suppliers

Company Name	Web Address
Abcam Ltd	www.abcam.com
Agar Scientific	www.agarscientific.com
Agilent	www.genomics.agilent.com
Ambion	www.lifetechnologies.com
Applied Biosystems	www.appliedbiosystems.com
BD Biosciences	www.bdbiosciences.com
Bioline	www.bioline.com
Bio-Rad	www.bio-rad.com
CellPath	www.cellpath.co.uk
Cell Signaling	www.cellsignal.com
Clontech	www.clontech.com
Corning	www.corning.com
Civco Medical Solutions	www.civco.com
DAKO UK Ltd	www.dako.com
Eurofins Genomics	www.eurofinsgenomics.eu
FEI	www.fei.com
Fisher Scientific	www.fisher.co.uk
GraphPad	www.graphpad.com
Greiner	www.greinerbioone.com
Harlan Sera-labs	www.seralab.co.uk
Hycult Biotechnology	www.hycultbiotech.com
Leica Biosystems	www.leicabiosystems.com
Li-Cor	www.licor.com
Jencons	www.jenconsusa.com
Life Technologies Ltd	www.lifetechnologies.com
Merck-Millipore	www.merckmillipore.com
Nalgene	www.thermoscientific.com
New England Biolabs	www.neb.com
Olink Bioscience	www.olink.com

Company Name	Web Address
Olympus	www.olympus.co.uk
Pierce	www.piercenet.com
Promega	www.promega.co.uk
Qiagen	www.qiagen.com
Raymond A Lamb	www.fisher.co.uk
Roche	www.roche.co.uk
R&D Systems	www.rndsystems.com
Sarstedt	www.sarstedt.com
Scientific Laboratory Supplies Ltd (SLS)	www.scientificlabs.co.uk
Sigma-Aldrich Ltd	www.sigmaaldrich.com
SLS	www.scientificlabs.co.uk
Solent Scientific	www.solentsci.com
Starlab (UK) Ltd	www.starlab.co.uk
Syngene	www.syngene.co.uk
Tebu Bio Ltd	www.tebu-bio.com
Thermo Scientific	www.thermoscientific.com
Vector labs	www.vectorlabs.com
VWR	www.uk.vwr.com

Appendix 2 - Recipes for Stock Solutions

Appendix 2.1 General Solutions

Phosphate Buffered Saline (PBS)

137 mM NaCl, 2.7 mM KCl, 3.2 mM Na_2HPO_4, pH 7.2 in ddH_2O. PBS was prepared from tablets (Sigma) and autoclaved.

Tris Buffered Saline (TBS)

50 mM Tris-HCl (pH 7.6) and 150 mM NaCl in dH_2O.

Appendix 2.2 Cell Culture Solutions

Cholera Toxin

Cholera toxin (Sigma) prepared to 30 ng/ml (sterile) in KSFM (without supplements). Aliquots of 5 ml stored at 4^{o}C and diluted 1:1000 in KSFMc for use.

Collagenase IV

Collagenase (Sigma) diluted to a final concentration of 100 U/ml in Hank's Balanced Salt Solution (Invitrogen; containing Ca^{2+} and Mg^{2+}) and 10mM HEPES (pH 7.6). Filter sterilised 5 ml aliquots stored at -20°C.

EDTA

0.1% or 1% (w/v) EDTA (Fisher Scientific) stock solutions made in PBS and autoclaved.

L-Glutamine

5 ml aliquots of L-glutamine (Sigma) stored at -20^{o}C.

Transport Medium

500 ml Hank's Balanced Salt Solution (Invitrogen; containing Ca^{2+} and Mg^{2+}), 10 mM HEPES and 500,000 kallikrein inactivating units (KIU) Aprotinin (Nordic Group).

Stripper Medium

500 ml Hank's balanced salt solution (without Ca^{2+} and Mg^{2+}), 10 mM HEPES, 500,000 KIU Aprotinin (Nordic Group) and 0.1% (w/v) EDTA.

Trypsin in Versene (TV)

20 ml Trypsin (Sigma), 4 ml 1% EDTA, 176 ml Hank's balanced salt solution (without Ca^{2+} and Mg^{2+}). 5 ml aliquots stored at -20^{o}C.

Trypsin Inhibitor (TI)

100mg Trypsin Inhibitor (from Soybean; Sigma) dissolved in 5 ml PBS and filter sterilised. 100 µl aliquots stored at -20^{o}C (note: one aliquot of TI inhibits the activity of 1ml TV).

Appendix 2.3 Histology and Immunohistology Solutions

PBS complete (PBSc)

PBS prepared with 0.5 mM $MgCl_2$ and 0.9 mM $CaCl_2$

Formalin Fixative

3.7% Formalin (v/v) in PBSc

Citric Acid Buffer

10 mM citric acid in dH_2O, adjusted to pH 6.0 with NaOH

Tris-EDTA Buffer

10 mM Tris and 1 mM EDTA in dH_20, adjusted to pH 9.0 before addition of 0.05% (w/v) Tween®20

DAB

One SIGMA*FAST*™ 3,3'-Diaminobenzidine tablet was dissolved in 5mls distilled water with one Urea Hydrogen Peroxide tablet. Vortexed until fully dissolved and prepared fresh for every use (DAB peroxidase substrate tablet set, Sigma)

Mayer's Haematoxylin

0.3 g sodium iodide, 1 g citric acid, 50 g chloral hydrate, 50 g aluminium potassium sulphate added sequentially to 850 ml dH_2O. Add 20 ml ethanol containing 15% (w/v) haematoxylin. Add 120ml glycerol, mix and store in a darkened bottle. Filter prior to use.

Scotts Tap Water

2% (w/v) $MgSO_4$ and 0.35% (w/v) $NaHCO_3$ in dH_2O

Hoechst 33258

1 mg/ml stock in PBS. Filtered and stored in the dark at 4^oC

TBS Azide + BSA

50 mM Tris-HCl (pH7.4), 150 mM NaCl with 0.1% (w/v) sodium azide and 0.1% (w/v) bovine serum albumin (Sigma), dH_2O to 1 L

Antifade

5% Propyl gallate (w/v) in 95% glycerol (w/v) and 5% PBS

Appendix 2.4 Immunoblotting Solutions

SDS Electrophoresis Sample Buffer (2x)

125 mM Tris-HCl (pH6.8), 20% glycerol (w/v), 200 mM sodium fluoride, 2 mM sodium orthovanadate, 40 mM tetra-sodium pyrophosphate, dH_2O to 50 ml. Aliquot (1 ml) and store at -20^{o}C.

Ponceau (10x)

5 g Ponceau, 10 ml glacial acetic acid, dH_2O to 100 ml

Western Blot Transfer Buffer

20 mM Tris, 150 mM glycine, 20% methanol (v/v), dH_2O to 1 L

Appendix 2.5 Molecular Biology Solutions

DEPC (nuclease-free) water

0.1% Diethylpyrocarbonate (Sigma) in 1 L dH_2O. Autoclavedmto inactivate.

10 x TBE

108 g Tris, 55 g Boric acid, 20 ml 1M EDTA, to 1 L in dH_2O

Luria Bertani (LB) broth

5 g yeast extract, 10 g bacto-tryptone, 10 g NaCl, adjust to pH 7.0 with NaOH, dH_2O to 1 L. Aliquot (200 ml) into glass bottles and autoclave to sterilise.

LB-Agar plates

5 g yeast extract, 10 g bacto-tryptone, 10 g NaCl, adjust to pH 7.0 with NaOH, add dH_2O to 1 L then supplement with 15 g agar. Aliquot (200 ml) into glass bottles and autoclave to sterilise (store at ambient temperature). Melt to 40^{o}C and pour into plastic petri dishes and allow to solidify before storage at 4^{o}C for up to 1 month

Appendix 3 – Primers Used for RT-PCR and RTqPCR

PCR Product (gene name)	Forward Primer (5'–3')	Reverse Primer (5'-3')	Product Size (base pairs)	Optimal Annealing temperature (°C)
Connexin 25 (GJB7)	TCTACATGGTGGCAGCAGAG	TTGGGACAAGGCTTCAAATC	388	60
Connexin 26 (GJB2)	GCCTACCGGAGACATGAGAA	GACATTCAGCAGGATGCAAA	336	60
Connexin 29/30.2/31.3 (GJC3)	TCTGGGTCTTCCAGGTCATC	CGGGACAGATTGCAGGTTAT	325	62
Connexin 30 (GJB6)	GGCGAGGAGAGAAGAGGAAT	CAACTCTGCCACGTTAAGCA	311	62
Connexin 30.3 (GJB4)	GCTGAGCCTCATCTTCAAGG	GGACAGAGTTCCCATCCTCA	359	62
Connexin 31 (GJB3)	TATACGTGGTGGCTGCAGAG	ATTGAAGCCATGCCAGAGAG	368	58
Connexin 31.1 (GJB5)	CACAAGGACTTCGACTGCAA	GCTTGGAGATGAAGCAGTCC	397	61
Connexin 31.9 (GJD3)	CAAGAGGAGTTCGTGTGCAA	GTGCATGGAGTAGACGACGA	150	60
Connexin 32 (GJB1)	TTTGTACACCTTGCTCAGTGG	GGAGATGGGGAAGAATTGGT	202	62
Connexin 36 (GJD2)	TAACCAGGCCTGCTATGACC	GATGCAGTGCGTAGACCTGA	369	60

PCR Product (gene name)	Forward Primer (5'–3')	Reverse Primer (5'-3')	Product Size (base pairs)	Optimal Annealing temperature (°C)
Connexin 37 (GJA4)	GACGGTGCTCTTCATCTTCC	ATAGGTGCCCATCAGTGCTC	388	57
Connexin 40 (GJA5)	CTACTGGGTGCTGCAGATCA	GCCGGGATACGTAACAGTTG	374	62
Connexin 40.1 (GJD4)	AAAGCTCTGGTTCGTCCTCA	GTGCAGGACATAGACGCTGA	229	61
Connexin 43 (GJA1)	AAGGGAAAGAGCGACCCTTA	GCTGGTCCACAATGGCTAGT	364	58
Connexin 45 (GJC1)	CACCCGTTTTATGTGTGCAG	GCCTTGTTTTGCTTGTAGGC	338	55
Connexin 46 (GJA3)	GCCCAGAGGGTCTTAGCTCT	GAGGGCAACTGCTCTTTGTC	216	55
Connexin 47/46.6 (GJC2)	ATGAGCTGGAGCTTCCTGAC	AAGGCGTCATAGCAGACGTT	203	61
Connexin 50 (GJA8)	TCATCTTCCGGATCCTCATC	CAGCCGGAACTTCTTAGTGC	341	61
Connexin 59 (GJA9)	CAGTCTGGCTTCATCTGCAA	CAACCACAGAGCGAGTGAAA	358	61
Connexin 62 (GJA10)	GGGACAGCAATCAGACCATT	TCTGTGCCCAGTGACTGAAG	385	60

PCR Product (gene name)	Forward Primer (5'–3')	Reverse Primer (5'-3')	Product Size (base pairs)	Optimal Annealing temperature (°C)
Uroplakin 3a (UPK3a)	CGGAGGCATGATCGTCATC	CAGCAAAACCCACAAGTAGAAAGA	68	58
β-actin (ACTB)	ATCATGTTTGAGACCTTCAA	CATCTCTTGCTCGAAGTC	318	56
Ki67 (MKI67)	CAAGAGCATCAGAACGTTTAAGGA	TTCTTGGCCACTTCTTCATTCC	86	59
TGFβI (TGFB1)	TACCTGAACCCGTGTTGCTC	AGAAGTTGGCATGGTAGCCC	537	60
TGFβII (TGFB2)	GCGCTACATCGACAGCAAAG	CAATAGGCCGCATCCAAAGC	381	59
TGFβRI (TGFBR1)	AGCGGTCTTGCCCATCTTC	CTATGAGCAATGGCTGGCTTT	65	60
TGFβRII (TGFBR2)	TGTCTGTGGATGACCTGGCTAA	TTCTGGAGCCATGTATCTTGCA	62	60
Aquaporin 3* (AQP3)	GTCACTCTGGGCATCCTCAT	CTATTCCAGCACCCAAGAAGG	157	60
GAPDH* (GAPDH)	CAAGGTCATCCATGACAACTTTG	GGGCCATCCACAGTCTTCTG	90	60

*Primers used for RT-qPCR

Abbreviations List

ABS – Adult bovine serum

AQP – aquaporin

AUM –asymmetric unit membrane

CK - cytokeratin

Cx – Connexin

dsDNA (double-stranded deoxyribonucleic acid)

FBS - Fetal bovine serum

GJIC – Gap Junctional Intercellular Communication

IC – interstitial cystitis

KSFM – Keratinocyte Serum Free Medium

LY – Lucifer Yellow

NHU – Normal Human Urothelial

PPAR - Peroxisome Proliferator-activated receptor

PPRE - peroxisome proliferator response elements

RhoD – Rhodamine-dextran

RXR- retinoid x receptor

SDM – Site-directed mutagenesis

SPRINP- Single-Primer Reactions In Parallel

TJ – tight junction

TER – Transepithelial Electrical Resistance

UTI – urinary tract infection

References

Ai, Z., A. Fischer, D. C. Spray, A. M. Brown and G. I. Fishman (2000). "Wnt-1 regulation of connexin43 in cardiac myocytes." J Clin Invest **105**(2): 161-171.
Anderson, J. M. and C. M. Van Itallie (2009). "Physiology and function of the tight junction." Cold Spring Harb Perspect Biol **1**(2): a002584.
Angelow, S., K. J. Kim and A. S. Yu (2006). "Claudin-8 modulates paracellular permeability to acidic and basic ions in MDCK II cells." J Physiol **571**(Pt 1): 15-26.
Beahm, D. L., A. Oshima, G. M. Gaietta, G. M. Hand, A. E. Smock, S. N. Zucker, M. M. Toloue, A. Chandrasekhar, B. J. Nicholson and G. E. Sosinsky (2006). "Mutation of a conserved threonine in the third transmembrane helix of alpha- and beta-connexins creates a dominant-negative closed gap junction channel." J Biol Chem **281**(12): 7994-8009.
Beaudoin, M. S., L. A. Snook, A. M. Arkell, A. Stefanson, Z. Wan, J. A. Simpson, G. P. Holloway and D. C. Wright (2014). "Novel effects of rosiglitazone on SMAD2 and SMAD3 signaling in white adipose tissue of diabetic rats." Obesity (Silver Spring) **22**(7): 1632-1642.
Becker, D. L., C. Thrasivoulou and A. R. Phillips (2012). "Connexins in wound healing; perspectives in diabetic patients." Biochim Biophys Acta **1818**(8): 2068-2075.
Bedner, P., H. Niessen, B. Odermatt, M. Kretz, K. Willecke and H. Harz (2006). "Selective permeability of different connexin channels to the second messenger cyclic AMP." J Biol Chem **281**(10): 6673-6681.
Bell, S. M., L. Zhang, A. Mendell, Y. Xu, H. M. Haitchi, J. L. Lessard and J. A. Whitsett (2011). "Kruppel-like factor 5 is required for formation and differentiation of the bladder urothelium." Dev Biol **358**(1): 79-90.
Berthoud, V. M., S. Bassnett and E. C. Beyer (1999). "Cultured chicken embryo lens cells resemble differentiating fiber cells in vivo and contain two kinetic pools of connexin56." Exp Eye Res **68**(4): 475-484.
Berthoud, V. M., P. J. Minogue, J. G. Laing and E. C. Beyer (2004). "Pathways for degradation of connexins and gap junctions." Cardiovasc Res **62**(2): 256-267.
Blanquart, C., O. Barbier, J. C. Fruchart, B. Staels and C. Glineur (2003). "Peroxisome proliferator-activated receptors: regulation of transcriptional activities and roles in inflammation." J Steroid Biochem Mol Biol **85**(2-5): 267-273.
Brandner, J. M., P. Houdek, B. Husing, C. Kaiser and I. Moll (2004). "Connexins 26, 30, and 43: differences among spontaneous, chronic, and accelerated human wound healing." J Invest Dermatol **122**(5): 1310-1320.
Böck, M., J. Hinley, C. Schmitt, T. Wahlicht, S. Kramer and J. Southgate (2014). "Identification of ELF3 as an early transcriptional regulator of human urothelium." Dev Biol **386**(2): 321-330.
Clair, C., L. Combettes, F. Pierre, P. Sansonetti and G. Tran Van Nhieu (2008). "Extracellular-loop peptide antibodies reveal a predominant hemichannel organization of connexins in polarized intestinal cells." Exp Cell Res **314**(6): 1250-1265.
Clarke, T. C., O. J. Williams, P. E. Martin and W. H. Evans (2009). "ATP release by cardiac myocytes in a simulated ischaemia model: inhibition by a connexin mimetic and enhancement by an antiarrhythmic peptide." Eur J Pharmacol **605**(1-3): 9-14.
Clements, R. T., F. L. Minnear, H. A. Singer, R. S. Keller and P. A. Vincent (2005). "RhoA and Rho-kinase dependent and independent signals mediate TGF-beta-induced pulmonary endothelial cytoskeletal reorganization and permeability." Am J Physiol Lung Cell Mol Physiol **288**(2): L294-306.
Cockayne, D. A., S. G. Hamilton, Q. M. Zhu, P. M. Dunn, Y. Zhong, S. Novakovic, A. B. Malmberg, G. Cain, A. Berson, L. Kassotakis, L. Hedley, W. G. Lachnit, G. Burnstock, S. B. McMahon and A. P. Ford (2000). "Urinary bladder hyporeflexia and reduced pain-related behaviour in P2X3-deficient mice." Nature **407**(6807): 1011-1015.

Cogliati, B., M. Vinken, T. C. Silva, C. M. Araujo, T. P. Aloia, L. M. Chaible, C. M. Mori and M. L. Dagli (2015). "Connexin 43 deficiency accelerates skin wound healing and extracellular matrix remodeling in mice." J Dermatol Sci.
Cross, W. R., I. Eardley, H. J. Leese and J. Southgate (2005). "A biomimetic tissue from cultured normal human urothelial cells: analysis of physiological function." Am J Physiol Renal Physiol **289**(2): F459-468.
Dagli, M. L., H. Yamasaki, V. Krutovskikh and Y. Omori (2004). "Delayed liver regeneration and increased susceptibility to chemical hepatocarcinogenesis in transgenic mice expressing a dominant-negative mutant of connexin32 only in the liver." Carcinogenesis **25**(4): 483-492.
Dbouk, H. A., R. M. Mroue, M. E. El-Sabban and R. S. Talhouk (2009). "Connexins: a myriad of functions extending beyond assembly of gap junction channels." Cell Commun Signal **7**: 4.
Diez, J. A., M. Elvira and A. Villalobo (1998). "The epidermal growth factor receptor tyrosine kinase phosphorylates connexin32." Mol Cell Biochem **187**(1-2): 201-210.
Duffy, H. S., M. Delmar and D. C. Spray (2002). "Formation of the gap junction nexus: binding partners for connexins." J Physiol Paris **96**(3-4): 243-249.
Eckert, J. J., A. McCallum, A. Mears, M. G. Rumsby, I. T. Cameron and T. P. Fleming (2005). "Relative contribution of cell contact pattern, specific PKC isoforms and gap junctional communication in tight junction assembly in the mouse early embryo." Dev Biol **288**(1): 234-247.
Edelheit, O., A. Hanukoglu and I. Hanukoglu (2009). "Simple and efficient site-directed mutagenesis using two single-primer reactions in parallel to generate mutants for protein structure-function studies." BMC Biotechnol **9**: 61.
Elias, L. A., D. D. Wang and A. R. Kriegstein (2007). "Gap junction adhesion is necessary for radial migration in the neocortex." Nature **448**(7156): 901-907.
Ellerbroek, S. M., K. Wennerberg and K. Burridge (2003). "Serine phosphorylation negatively regulates RhoA in vivo." J Biol Chem **278**(21): 19023-19031.
Elvira, M., J. A. Diez, K. K. Wang and A. Villalobo (1993). "Phosphorylation of connexin-32 by protein kinase C prevents its proteolysis by mu-calpain and m-calpain." J Biol Chem **268**(19): 14294-14300.
Evans, W. H., E. De Vuyst and L. Leybaert (2006). "The gap junction cellular internet: connexin hemichannels enter the signalling limelight." Biochem J **397**(1): 1-14.
Evert, M., T. Ott, A. Temme, K. Willecke and F. Dombrowski (2002). "Morphology and morphometric investigation of hepatocellular preneoplastic lesions and neoplasms in connexin32-deficient mice." Carcinogenesis **23**(5): 697-703.
Fackler, O. T. and R. Grosse (2008). "Cell motility through plasma membrane blebbing." J Cell Biol **181**(6): 879-884.
Falk, M. M., R. M. Kells and V. M. Berthoud (2014). "Degradation of connexins and gap junctions." FEBS Lett **588**(8): 1221-1229.
Farquhar, M. G. and G. E. Palade (1963). "Junctional complexes in various epithelia." J Cell Biol **17**: 375-412.
Fenteany, G., P. A. Janmey and T. P. Stossel (2000). "Signaling pathways and cell mechanics involved in wound closure by epithelial cell sheets." Curr Biol **10**(14): 831-838.
Ferguson, D. R., I. Kennedy and T. J. Burton (1997). "ATP is released from rabbit urinary bladder epithelial cells by hydrostatic pressure changes--a possible sensory mechanism?" J Physiol **505 (Pt 2)**: 503-511.
Fleming, J. M., S. Shabir, C. L. Varley, L. A. Kirkwood, A. White, J. Holder, L. K. Trejdosiewicz and J. Southgate (2012). "Differentiation-associated reprogramming of the transforming growth factor beta receptor pathway establishes the circuitry for epithelial autocrine/paracrine repair." PLoS One **7**(12): e51404.

Fleming, T. P., M. R. Ghassemifar and B. Sheth (2000). "Junctional complexes in the early mammalian embryo." Semin Reprod Med **18**(2): 185-193.
Fortes, F. S., I. L. Pecora, P. M. Persechini, S. Hurtado, V. Costa, R. Coutinho-Silva, M. B. Braga, F. C. Silva-Filho, R. C. Bisaggio, F. P. De Farias, E. Scemes, A. C. De Carvalho and R. C. Goldenberg (2004). "Modulation of intercellular communication in macrophages: possible interactions between GAP junctions and P2 receptors." J Cell Sci **117**(Pt 20): 4717-4726.
Fromter, E. and J. Diamond (1972). "Route of passive ion permeation in epithelia." Nat New Biol **235**(53): 9-13.
Fry, C. H., G. P. Sui, A. J. Kanai and C. Wu (2007). "The function of suburothelial myofibroblasts in the bladder." Neurourol Urodyn **26**(6 Suppl): 914-919.
Fu, M., J. Zhang, X. Zhu, D. E. Myles, T. M. Willson, X. Liu and Y. E. Chen (2001). "Peroxisome proliferator-activated receptor gamma inhibits transforming growth factor beta-induced connective tissue growth factor expression in human aortic smooth muscle cells by interfering with Smad3." J Biol Chem **276**(49): 45888-45894.
Furuse, M., M. Hata, K. Furuse, Y. Yoshida, A. Haratake, Y. Sugitani, T. Noda, A. Kubo and S. Tsukita (2002). "Claudin-based tight junctions are crucial for the mammalian epidermal barrier: a lesson from claudin-1-deficient mice." J Cell Biol **156**(6): 1099-1111.
Garrod, D. and M. Chidgey (2008). "Desmosome structure, composition and function." Biochim Biophys Acta **1778**(3): 572-587.
Gee, J., M. Tanaka and H. B. Grossman (2003). "Connexin 26 is abnormally expressed in bladder cancer." J Urol **169**(3): 1135-1137.
Ghosh, A. K., J. Wei, M. Wu and J. Varga (2008). "Constitutive Smad signaling and Smad-dependent collagen gene expression in mouse embryonic fibroblasts lacking peroxisome proliferator-activated receptor-gamma." Biochem Biophys Res Commun **374**(2): 231-236.
Ghosh, A. K., W. Yuan, Y. Mori and J. Varga (2000). "Smad-dependent stimulation of type I collagen gene expression in human skin fibroblasts by TGF-beta involves functional cooperation with p300/CBP transcriptional coactivators." Oncogene **19**(31): 3546-3555.
Goldberg, G. S., A. P. Moreno and P. D. Lampe (2002). "Gap junctions between cells expressing connexin 43 or 32 show inverse permselectivity to adenosine and ATP." J Biol Chem **277**(39): 36725-36730.
Goldberg, G. S., V. Valiunas and P. R. Brink (2004). "Selective permeability of gap junction channels." Biochim Biophys Acta **1662**(1-2): 96-101.
Gong, X. Q., S. Nakagawa, T. Tsukihara and D. Bai (2013). "A mechanism of gap junction docking revealed by functional rescue of a human-disease-linked connexin mutant." J Cell Sci **126**(Pt 14): 3113-3120.
Gonzaga-Jauregui, C., F. Zhang, C. F. Towne, S. D. Batish and J. R. Lupski (2010). "GJB1/Connexin 32 whole gene deletions in patients with X-linked Charcot-Marie-Tooth disease." Neurogenetics **11**(4): 465-470.
Grossman, H. B., M. Liebert, I. W. Lee and S. W. Lee (1994). "Decreased connexin expression and intercellular communication in human bladder cancer cells." Cancer Res **54**(11): 3062-3065.
Halder, S. K., R. D. Beauchamp and P. K. Datta (2005). "A specific inhibitor of TGF-beta receptor kinase, SB-431542, as a potent antitumor agent for human cancers." Neoplasia **7**(5): 509-521.
Harnden, P., A. Allam, A. D. Joyce, A. Patel, P. Selby and J. Southgate (1995). "Cytokeratin 20 expression by non-invasive transitional cell carcinomas: potential for distinguishing recurrent from non-recurrent disease." Histopathology **27**(2): 169-174.
Hatanaka, H., N. Koizumi, N. Okumura, E. P. Kay, E. Mizuhara, J. Hamuro and S. Kinoshita (2012). "Epithelial-mesenchymal transition-like phenotypic changes of retinal pigment epithelium induced by TGF-beta are prevented by PPAR-gamma agonists." Invest Ophthalmol Vis Sci **53**(11): 6955-6963.

Heldin, C. H., M. Landstrom and A. Moustakas (2009). "Mechanism of TGF-beta signaling to growth arrest, apoptosis, and epithelial-mesenchymal transition." Curr Opin Cell Biol **21**(2): 166-176.
Herve, J. C., M. Derangeon, D. Sarrouilhe, B. N. Giepmans and N. Bourmeyster (2012). "Gap junctional channels are parts of multiprotein complexes." Biochim Biophys Acta **1818**(8): 1844-1865.
Hicks, R. M. (1975). "The mammalian urinary bladder: an accommodating organ." Biol Rev Camb Philos Soc **50**(2): 215-246.
Hu, P., S. Meyers, F. X. Liang, F. M. Deng, B. Kachar, M. L. Zeidel and T. T. Sun (2002). "Role of membrane proteins in permeability barrier function: uroplakin ablation elevates urothelial permeability." Am J Physiol Renal Physiol **283**(6): F1200-1207.
Hung, T. T., H. Wang, E. A. Kingsley, G. P. Risbridger and P. J. Russell (2008). "Molecular profiling of bladder cancer: involvement of the TGF-beta pathway in bladder cancer progression." Cancer Lett **265**(1): 27-38.
Huse, M., T. W. Muir, L. Xu, Y. G. Chen, J. Kuriyan and J. Massague (2001). "The TGF beta receptor activation process: an inhibitor- to substrate-binding switch." Mol Cell **8**(3): 671-682.
Iacobas, D. A., S. Iacobas and D. C. Spray (2007). "Connexin-dependent transcellular transcriptomic networks in mouse brain." Prog Biophys Mol Biol **94**(1-2): 169-185.
John, S., D. Cesario and J. N. Weiss (2003). "Gap junctional hemichannels in the heart." Acta Physiol Scand **179**(1): 23-31.
Johnstone, S. R., A. K. Best, C. S. Wright, B. E. Isakson, R. J. Errington and P. E. Martin (2010). "Enhanced connexin 43 expression delays intra-mitotic duration and cell cycle traverse independently of gap junction channel function." J Cell Biochem **110**(3): 772-782.
Kameritsch, P., N. Khandoga, U. Pohl and K. Pogoda (2013). "Gap junctional communication promotes apoptosis in a connexin-type-dependent manner." Cell Death Dis **4**: e584.
Kanaporis, G., P. R. Brink and V. Valiunas (2011). "Gap junction permeability: selectivity for anionic and cationic probes." Am J Physiol Cell Physiol **300**(3): C600-609.
Kawakami, S., G. Arai, T. Hayashi, Y. Fujii, G. Xia, Y. Kageyama and K. Kihara (2002). "PPARgamma ligands suppress proliferation of human urothelial basal cells in vitro." J Cell Physiol **191**(3): 310-319.
Khandelwal, P., S. N. Abraham and G. Apodaca (2009). "Cell biology and physiology of the uroepithelium." Am J Physiol Renal Physiol **297**(6): F1477-1501.
Kim, D. H., H. J. Ihn, C. Moon, S. S. Oh, S. Park, S. Kim, K. W. Lee and K. D. Kim (2015). "Ciglitazone, a peroxisome proliferator-activated receptor gamma ligand, inhibits proliferation and differentiation of th17 cells." Biomol Ther (Seoul) **23**(1): 71-76.
Kim, K. K., M. C. Kugler, P. J. Wolters, L. Robillard, M. G. Galvez, A. N. Brumwell, D. Sheppard and H. A. Chapman (2006). "Alveolar epithelial cell mesenchymal transition develops in vivo during pulmonary fibrosis and is regulated by the extracellular matrix." Proc Natl Acad Sci U S A **103**(35): 13180-13185.
Kimura, T. E., A. J. Merritt and D. R. Garrod (2007). "Calcium-independent desmosomes of keratinocytes are hyper-adhesive." J Invest Dermatol **127**(4): 775-781.
Kleopa, K. A. (2011). "The role of gap junctions in Charcot-Marie-Tooth disease." J Neurosci **31**(49): 17753-17760.
Koizumi, J., T. Kojima, R. Kamekura, M. Kurose, A. Harimaya, M. Murata, M. Osanai, H. Chiba, T. Himi and N. Sawada (2007). "Changes of gap and tight junctions during differentiation of human nasal epithelial cells using primary human nasal epithelial cells and primary human nasal fibroblast cells in a noncontact coculture system." J Membr Biol **218**(1-3): 1-7.

Kojima, T., Y. Kokai, H. Chiba, M. Yamamoto, Y. Mochizuki and N. Sawada (2001). "Cx32 but not Cx26 is associated with tight junctions in primary cultures of rat hepatocytes." Exp Cell Res **263**(2): 193-201.
Kojima, T., T. Mitaka, D. L. Paul, M. Mori and Y. Mochizuki (1995). "Reappearance and long-term maintenance of connexin32 in proliferated adult rat hepatocytes: use of serum-free L-15 medium supplemented with EGF and DMSO." J Cell Sci **108 (Pt 4)**: 1347-1357.
Kreft, M. E., M. Sterle, P. Veranic and K. Jezernik (2005). "Urothelial injuries and the early wound healing response: tight junctions and urothelial cytodifferentiation." Histochem Cell Biol **123**(4-5): 529-539.
Kremer, M., G. Son, K. Zhang, S. M. Moore, A. Norris, G. Manzini, M. D. Wheeler and I. N. Hines (2014). "Smad3 signaling in the regenerating liver: implications for the regulation of IL-6 expression." Transpl Int **27**(7): 748-758.
Kren, B. T., N. M. Kumar, S. Q. Wang, N. B. Gilula and C. J. Steer (1993). "Differential regulation of multiple gap junction transcripts and proteins during rat liver regeneration." J Cell Biol **123**(3): 707-718.
Kretz, M., C. Euwens, S. Hombach, D. Eckardt, B. Teubner, O. Traub, K. Willecke and T. Ott (2003). "Altered connexin expression and wound healing in the epidermis of connexin-deficient mice." J Cell Sci **116**(Pt 16): 3443-3452.
Kumar, N. M. and N. B. Gilula (1992). "Molecular biology and genetics of gap junction channels." Semin Cell Biol **3**(1): 3-16.
Kurzrock, E. A., D. K. Lieu, L. A. Degraffenried, C. W. Chan and R. R. Isseroff (2008). "Label-retaining cells of the bladder: candidate urothelial stem cells." Am J Physiol Renal Physiol **294**(6): F1415-1421.
Laird, D. W. (2005). "Connexin phosphorylation as a regulatory event linked to gap junction internalization and degradation." Biochim Biophys Acta **1711**(2): 172-182.
Laird, D. W., P. Fistouris, G. Batist, L. Alpert, H. T. Huynh, G. D. Carystinos and M. A. Alaoui-Jamali (1999). "Deficiency of connexin43 gap junctions is an independent marker for breast tumors." Cancer Res **59**(16): 4104-4110.
Lampe, P. D. and A. F. Lau (2004). "The effects of connexin phosphorylation on gap junctional communication." Int J Biochem Cell Biol **36**(7): 1171-1186.
Lavelle, J., S. Meyers, R. Ramage, S. Bastacky, D. Doty, G. Apodaca and M. L. Zeidel (2002). "Bladder permeability barrier: recovery from selective injury of surface epithelial cells." Am J Physiol Renal Physiol **283**(2): F242-253.
Leiby, B. E., J. R. Landis, K. J. Propert, J. E. Tomaszewski and G. Interstitial Cystitis Data Base Study (2007). "Discovery of morphological subgroups that correlate with severity of symptoms in interstitial cystitis: a proposed biopsy classification system." J Urol **177**(1): 142-148.
Leithe, E. and E. Rivedal (2004). "Epidermal growth factor regulates ubiquitination, internalization and proteasome-dependent degradation of connexin43." J Cell Sci **117**(Pt 7): 1211-1220.
Lewis, S. A. and J. L. de Moura (1982). "Incorporation of cytoplasmic vesicles into apical membrane of mammalian urinary bladder epithelium." Nature **297**(5868): 685-688.
Leybaert, L., K. Braet, W. Vandamme, L. Cabooter, P. E. Martin and W. H. Evans (2003). "Connexin channels, connexin mimetic peptides and ATP release." Cell Commun Adhes **10**(4-6): 251-257.
Li, A. G., S. L. Lu, M. X. Zhang, C. Deng and X. J. Wang (2004). "Smad3 knockout mice exhibit a resistance to skin chemical carcinogenesis." Cancer Res **64**(21): 7836-7845.
Li, B., L. C. Tsoi, W. R. Swindell, J. E. Gudjonsson, T. Tejasvi, A. Johnston, J. Ding, P. E. Stuart, X. Xing, J. J. Kochkodan, J. J. Voorhees, H. M. Kang, R. P. Nair, G. R. Abecasis and J. T. Elder (2014). "Transcriptome analysis of psoriasis in a large case-control sample: RNA-seq provides insights into disease mechanisms." J Invest Dermatol **134**(7): 1828-1838.

Li, M. W., D. D. Mruk, W. M. Lee and C. Y. Cheng (2010). "Connexin 43 is critical to maintain the homeostasis of the blood-testis barrier via its effects on tight junction reassembly." Proc Natl Acad Sci U S A **107**(42): 17998-18003.
Li, Q., Y. Omori, Y. Nishikawa, T. Yoshioka, Y. Yamamoto and K. Enomoto (2007). "Cytoplasmic accumulation of connexin32 protein enhances motility and metastatic ability of human hepatoma cells in vitro and in vivo." Int J Cancer **121**(3): 536-546.
Liu, H. T., J. H. Shie, S. H. Chen, Y. S. Wang and H. C. Kuo (2012). "Differences in mast cell infiltration, E-cadherin, and zonula occludens-1 expression between patients with overactive bladder and interstitial cystitis/bladder pain syndrome." Urology **80**(1): 225 e213-228.
Lobban, E. D., B. A. Smith, G. D. Hall, P. Harnden, P. Roberts, P. J. Selby, L. K. Trejdosiewicz and J. Southgate (1998). "Uroplakin gene expression by normal and neoplastic human urothelium." Am J Pathol **153**(6): 1957-1967.
Locke, D., T. Stein, C. Davies, J. Morris, A. L. Harris, W. H. Evans, P. Monaghan and B. Gusterson (2004). "Altered permeability and modulatory character of connexin channels during mammary gland development." Exp Cell Res **298**(2): 643-660.
Lorentz, R., Q. Shao, T. Huang, G. I. Fishman and D. W. Laird (2012). "Characterization of gap junction proteins in the bladder of Cx43 mutant mouse models of oculodentodigital dysplasia." J Membr Biol **245**(5-6): 345-355.
Martin, P. E. and M. van Steensel (2015). "Connexins and skin disease: insights into the role of beta connexins in skin homeostasis." Cell Tissue Res **360**(3): 645-658.
Massague, J. (2012). "TGFbeta signalling in context." Nat Rev Mol Cell Biol **13**(10): 616-630.
McHugo, J. and M. Whittle (2001). "Enlarged fetal bladders: aetiology, management and outcome." Prenat Diagn **21**(11): 958-963.
Meng, W. and M. Takeichi (2009). "Adherens junction: molecular architecture and regulation." Cold Spring Harb Perspect Biol **1**(6): a002899.
Milatz, S., S. M. Krug, R. Rosenthal, D. Gunzel, D. Muller, J. D. Schulzke, S. Amasheh and M. Fromm (2010). "Claudin-3 acts as a sealing component of the tight junction for ions of either charge and uncharged solutes." Biochim Biophys Acta **1798**(11): 2048-2057.
Miyamoto, H., Y. Kubota, T. Shuin, S. Torigoe, Y. Dobashi and M. Hosaka (1995). "Expression of transforming growth factor-beta 1 in human bladder cancer." Cancer **75**(10): 2565-2570.
Miyamoto, T., T. Mochizuki, H. Nakagomi, S. Kira, M. Watanabe, Y. Takayama, Y. Suzuki, S. Koizumi, M. Takeda and M. Tominaga (2014). "Functional role for Piezo1 in stretch-evoked Ca(2)(+) influx and ATP release in urothelial cell cultures." J Biol Chem **289**(23): 16565-16575.
Moorby, C. and M. Patel (2001). "Dual functions for connexins: Cx43 regulates growth independently of gap junction formation." Exp Cell Res **271**(2): 238-248.
Moreno, A. P. (2005). "Connexin phosphorylation as a regulatory event linked to channel gating." Biochim Biophys Acta **1711**(2): 164-171.
Mrsny, R. J., G. T. Brown, K. Gerner-Smidt, A. G. Buret, J. B. Meddings, C. Quan, M. Koval and A. Nusrat (2008). "A key claudin extracellular loop domain is critical for epithelial barrier integrity." Am J Pathol **172**(4): 905-915.
Muraoka, R. S., N. Dumont, C. A. Ritter, T. C. Dugger, D. M. Brantley, J. Chen, E. Easterly, L. R. Roebuck, S. Ryan, P. J. Gotwals, V. Koteliansky and C. L. Arteaga (2002). "Blockade of TGF-beta inhibits mammary tumor cell viability, migration, and metastases." J Clin Invest **109**(12): 1551-1559.
Murphy, S. M., J. Polke, H. Manji, J. Blake, L. Reiniger, M. Sweeney, H. Houlden, S. Brandner and M. M. Reilly (2011). "A novel mutation in the nerve-specific 5'UTR of the GJB1 gene causes X-linked Charcot-Marie-Tooth disease." J Peripher Nerv Syst **16**(1): 65-70.

Nadarajah, B., A. M. Jones, W. H. Evans and J. G. Parnavelas (1997). "Differential expression of connexins during neocortical development and neuronal circuit formation." J Neurosci **17**(9): 3096-3111.
Nagasawa, K., H. Chiba, H. Fujita, T. Kojima, T. Saito, T. Endo and N. Sawada (2006). "Possible involvement of gap junctions in the barrier function of tight junctions of brain and lung endothelial cells." J Cell Physiol **208**(1): 123-132.
Nakata, Y., M. Iwai, S. Kimura and T. Shimazu (1996). "Prolonged decrease in hepatic connexin32 in chronic liver injury induced by carbon tetrachloride in rats." J Hepatol **25**(4): 529-537.
Negrete, H. O., J. P. Lavelle, J. Berg, S. A. Lewis and M. L. Zeidel (1996). "Permeability properties of the intact mammalian bladder epithelium." Am J Physiol **271**(4 Pt 2): F886-894.
Nelles, E., C. Butzler, D. Jung, A. Temme, H. D. Gabriel, U. Dahl, O. Traub, F. Stumpel, K. Jungermann, J. Zielasek, K. V. Toyka, R. Dermietzel and K. Willecke (1996). "Defective propagation of signals generated by sympathetic nerve stimulation in the liver of connexin32-deficient mice." Proc Natl Acad Sci U S A **93**(18): 9565-9570.
Neveu, M. J., J. R. Hully, K. L. Babcock, J. Vaughan, E. L. Hertzberg, B. J. Nicholson, D. L. Paul and H. C. Pitot (1995). "Proliferation-associated differences in the spatial and temporal expression of gap junction genes in rat liver." Hepatology **22**(1): 202-212.
Niessen, H., H. Harz, P. Bedner, K. Kramer and K. Willecke (2000). "Selective permeability of different connexin channels to the second messenger inositol 1,4,5-trisphosphate." J Cell Sci **113 (Pt 8)**: 1365-1372.
Park, D. J., C. J. Wallick, K. D. Martyn, A. F. Lau, C. Jin and B. J. Warn-Cramer (2007). "Akt phosphorylates Connexin43 on Ser373, a "mode-1" binding site for 14-3-3." Cell Commun Adhes **14**(5): 211-226.
Patel, P. I. and J. R. Lupski (1994). "Charcot-Marie-Tooth disease: a new paradigm for the mechanism of inherited disease." Trends Genet **10**(4): 128-133.
Penuela, S., R. Gehi and D. W. Laird (2013). "The biochemistry and function of pannexin channels." Biochim Biophys Acta **1828**(1): 15-22.
Perez Velazquez, J. L., M. Frantseva, C. C. Naus, J. F. Bechberger, S. C. Juneja, A. Velumian, P. L. Carlen, G. M. Kidder and L. R. Mills (1996). "Development of astrocytes and neurons in cultured brain slices from mice lacking connexin43." Brain Res Dev Brain Res **97**(2): 293-296.
Piechocki, M. P., R. M. Toti, M. J. Fernstrom, R. D. Burk and R. J. Ruch (2000). "Liver cell-specific transcriptional regulation of connexin32." Biochim Biophys Acta **1491**(1-3): 107-122.
Poyet, C., L. Buser, F. Roudnicky, M. Detmar, T. Hermanns, D. Mannhard, A. Hohn, J. Ruschoff, Q. Zhong, T. Sulser, H. Moch and P. J. Wild (2015). "Connexin 43 expression predicts poor progression-free survival in patients with non-muscle invasive urothelial bladder cancer." J Clin Pathol **68**(10): 819-824.
Quist, A. P., S. K. Rhee, H. Lin and R. Lal (2000). "Physiological role of gap-junctional hemichannels. Extracellular calcium-dependent isosmotic volume regulation." J Cell Biol **148**(5): 1063-1074.
Rebel, J. M., W. I. De Boer, C. D. Thijssen, M. Vermey, E. C. Zwarthoff and T. H. Van der Kwast (1994). "An in vitro model of urothelial regeneration: effects of growth factors and extracellular matrix proteins." J Pathol **173**(3): 283-291.
Richard, G., F. Rouan, C. E. Willoughby, N. Brown, P. Chung, M. Ryynanen, E. W. Jabs, S. J. Bale, J. J. DiGiovanna, J. Uitto and L. Russell (2002). "Missense mutations in GJB2 encoding connexin-26 cause the ectodermal dysplasia keratitis-ichthyosis-deafness syndrome." Am J Hum Genet **70**(5): 1341-1348.

Rickard, A., N. Dorokhov, J. Ryerse, D. J. Klumpp and J. McHowat (2008). "Characterization of tight junction proteins in cultured human urothelial cells." In Vitro Cell Dev Biol Anim **44**(7): 261-267.
Robino, L., P. Scavone, L. Araujo, G. Algorta, P. Zunino, M. C. Pirez and R. Vignoli (2014). "Intracellular bacteria in the pathogenesis of Escherichia coli urinary tract infection in children." Clin Infect Dis **59**(11): e158-164.
Rosenthal, R., S. Milatz, S. M. Krug, B. Oelrich, J. D. Schulzke, S. Amasheh, D. Gunzel and M. Fromm (2010). "Claudin-2, a component of the tight junction, forms a paracellular water channel." J Cell Sci **123**(Pt 11): 1913-1921.
Rubenwolf, P. C., N. T. Georgopoulos, L. A. Clements, S. Feather, P. Holland, D. F. Thomas and J. Southgate (2009). "Expression and localisation of aquaporin water channels in human urothelium in situ and in vitro." Eur Urol **56**(6): 1013-1023.
Saez, J. C., A. C. Nairn, A. J. Czernik, D. C. Spray, E. L. Hertzberg, P. Greengard and M. V. Bennett (1990). "Phosphorylation of connexin 32, a hepatocyte gap-junction protein, by cAMP-dependent protein kinase, protein kinase C and Ca2+/calmodulin-dependent protein kinase II." Eur J Biochem **192**(2): 263-273.
Saez, J. C., M. A. Retamal, D. Basilio, F. F. Bukauskas and M. V. Bennett (2005). "Connexin-based gap junction hemichannels: gating mechanisms." Biochim Biophys Acta **1711**(2): 215-224.
Saffitz, J. E., K. Y. Hames and S. Kanno (2007). "Remodeling of gap junctions in ischemic and nonischemic forms of heart disease." J Membr Biol **218**(1-3): 65-71.
Scherer, S. S., L. J. Bone, S. M. Deschenes, A. Abel, R. J. Balice-Gordon and K. H. Fischbeck (1999). "The role of the gap junction protein connexin32 in the pathogenesis of X-linked Charcot-Marie-Tooth disease." Novartis Found Symp **219**: 175-185; discussion 185-177.
Scherer, S. S., Y. T. Xu, E. Nelles, K. Fischbeck, K. Willecke and L. J. Bone (1998). "Connexin32-null mice develop demyelinating peripheral neuropathy." Glia **24**(1): 8-20.
Schiller, M., S. Dennler, U. Anderegg, A. Kokot, J. C. Simon, T. A. Luger, A. Mauviel and M. Bohm (2010). "Increased cAMP levels modulate transforming growth factor-beta/Smad-induced expression of extracellular matrix components and other key fibroblast effector functions." J Biol Chem **285**(1): 409-421.
Schiller, M., F. Verrecchia and A. Mauviel (2003). "Cyclic adenosine 3',5'-monophosphate-elevating agents inhibit transforming growth factor-beta-induced SMAD3/4-dependent transcription via a protein kinase A-dependent mechanism." Oncogene **22**(55): 8881-8890.
Schwartz, M. A. and S. J. Shattil (2000). "Signaling networks linking integrins and rho family GTPases." Trends Biochem Sci **25**(8): 388-391.
Scott, C. A., D. Tattersall, E. A. O'Toole and D. P. Kelsell (2012). "Connexins in epidermal homeostasis and skin disease." Biochim Biophys Acta **1818**(8): 1952-1961.
Scriven, S. D., C. Booth, D. F. Thomas, L. K. Trejdosiewicz and J. Southgate (1997). "Reconstitution of human urothelium from monolayer cultures." J Urol **158**(3 Pt 2): 1147-1152.
Sha, W., K. Thompson, J. South, M. Baron and A. Leask (2012). "Loss of PPARgamma expression by fibroblasts enhances dermal wound closure." Fibrogenesis Tissue Repair **5**: 5.
Shabir, S., W. Cross, L. A. Kirkwood, J. F. Pearson, P. A. Appleby, D. Walker, I. Eardley and J. Southgate (2013). "Functional expression of purinergic P2 receptors and transient receptor potential channels by the human urothelium." Am J Physiol Renal Physiol **305**(3): F396-406.
Shabir, S. and J. Southgate (2008). "Calcium signalling in wound-responsive normal human urothelial cell monolayers." Cell Calcium **44**(5): 453-464.
Shin, K., J. Lee, N. Guo, J. Kim, A. Lim, L. Qu, I. U. Mysorekar and P. A. Beachy (2011). "Hedgehog/Wnt feedback supports regenerative proliferation of epithelial stem cells in bladder." Nature **472**(7341): 110-114.

Slobodov, G., M. Feloney, C. Gran, K. D. Kyker, R. E. Hurst and D. J. Culkin (2004). "Abnormal expression of molecular markers for bladder impermeability and differentiation in the urothelium of patients with interstitial cystitis." J Urol **171**(4): 1554-1558.
Smith NJ, Hinley JS, Varley C, Eardley I, L. Trejdosiewicz and S. J (2015). "The human urothelial tight junction: claudin 3 and the ZO-1α+ switch." Bladder **2**(1).
Solan, J. L. and P. D. Lampe (2007). "Key connexin 43 phosphorylation events regulate the gap junction life cycle." J Membr Biol **217**(1-3): 35-41.
Sosinsky, G. E., J. L. Solan, G. M. Gaietta, L. Ngan, G. J. Lee, M. R. Mackey and P. D. Lampe (2007). "The C-terminus of connexin43 adopts different conformations in the Golgi and gap junction as detected with structure-specific antibodies." Biochem J **408**(3): 375-385.
Southgate, J., P. Harnden and L. K. Trejdosiewicz (1999). "Cytokeratin expression patterns in normal and malignant urothelium: a review of the biological and diagnostic implications." Histol Histopathol **14**(2): 657-664.
Southgate, J., K. A. Hutton, D. F. Thomas and L. K. Trejdosiewicz (1994). "Normal human urothelial cells in vitro: proliferation and induction of stratification." Lab Invest **71**(4): 583-594.
Southgate, J., W. Kennedy, K. A. Hutton and L. K. Trejdosiewicz (1995). "Expression and in vitro regulation of integrins by normal human urothelial cells." Cell Adhes Commun **3**(3): 231-242.
Southgate J, M. J. R. W., Trejdosiewicz L K (2002). "Culture of Human Urothelium." Culture of Epithelial Cells: 381-399.
Southgate, J., C. L. Varley, M. A. Garthwaite, J. Hinley, F. Marsh, J. Stahlschmidt, L. K. Trejdosiewicz and I. Eardley (2007). "Differentiation potential of urothelium from patients with benign bladder dysfunction." BJU Int **99**(6): 1506-1516.
Spector, D. A., J. B. Wade, R. Dillow, D. A. Steplock and E. J. Weinman (2002). "Expression, localization, and regulation of aquaporin-1 to -3 in rat urothelia." Am J Physiol Renal Physiol **282**(6): F1034-1042.
Sunagawa, M., A. Wolf-Johnston, M. Nomiya, N. Sawada, K. E. Andersson, T. Hisamitsu and L. A. Birder (2015). "Urinary bladder mucosal responses to ischemia." World J Urol **33**(2): 275-280.
Suwanabol, P. A., S. M. Seedial, X. Shi, F. Zhang, D. Yamanouchi, D. Roenneburg, B. Liu and K. C. Kent (2012). "Transforming growth factor-beta increases vascular smooth muscle cell proliferation through the Smad3 and extracellular signal-regulated kinase mitogen-activated protein kinases pathways." J Vasc Surg **56**(2): 446-454.
Talhouk, R. S., R. Mroue, M. Mokalled, L. Abi-Mosleh, R. Nehme, A. Ismail, A. Khalil, M. Zaatari and M. E. El-Sabban (2008). "Heterocellular interaction enhances recruitment of alpha and beta-catenins and ZO-2 into functional gap-junction complexes and induces gap junction-dependant differentiation of mammary epithelial cells." Exp Cell Res **314**(18): 3275-3291.
Tavares, A. L., M. E. Mercado-Pimentel, R. B. Runyan and G. T. Kitten (2006). "TGF beta-mediated RhoA expression is necessary for epithelial-mesenchymal transition in the embryonic chick heart." Dev Dyn **235**(6): 1589-1598.
Temme, A., A. Buchmann, H. D. Gabriel, E. Nelles, M. Schwarz and K. Willecke (1997). "High incidence of spontaneous and chemically induced liver tumors in mice deficient for connexin32." Curr Biol **7**(9): 713-716.
Thiery, J. P., H. Acloque, R. Y. Huang and M. A. Nieto (2009). "Epithelial-mesenchymal transitions in development and disease." Cell **139**(5): 871-890.
Toyofuku, T., M. Yabuki, K. Otsu, T. Kuzuya, M. Hori and M. Tada (1998). "Direct association of the gap junction protein connexin-43 with ZO-1 in cardiac myocytes." J Biol Chem **273**(21): 12725-12731.

Tran Van Nhieu, G., C. Clair, R. Bruzzone, M. Mesnil, P. Sansonetti and L. Combettes (2003). "Connexin-dependent inter-cellular communication increases invasion and dissemination of Shigella in epithelial cells." Nat Cell Biol **5**(8): 720-726.
Trosko, J. E. and R. J. Ruch (1998). "Cell-cell communication in carcinogenesis." Front Biosci **3**: d208-236.
Umeda, K., J. Ikenouchi, S. Katahira-Tayama, K. Furuse, H. Sasaki, M. Nakayama, T. Matsui, S. Tsukita, M. Furuse and S. Tsukita (2006). "ZO-1 and ZO-2 independently determine where claudins are polymerized in tight-junction strand formation." Cell **126**(4): 741-754.
Unger, V. M., N. M. Kumar, N. B. Gilula and M. Yeager (1999). "Three-dimensional structure of a recombinant gap junction membrane channel." Science **283**(5405): 1176-1180.
Van Aelst, L. and M. Symons (2002). "Role of Rho family GTPases in epithelial morphogenesis." Genes Dev **16**(9): 1032-1054.
Van Itallie, C. M., A. S. Fanning, A. Bridges and J. M. Anderson (2009). "ZO-1 stabilizes the tight junction solute barrier through coupling to the perijunctional cytoskeleton." Mol Biol Cell **20**(17): 3930-3940.
Varley, C., G. Hill, S. Pellegrin, N. J. Shaw, P. J. Selby, L. K. Trejdosiewicz and J. Southgate (2005). "Autocrine regulation of human urothelial cell proliferation and migration during regenerative responses in vitro." Exp Cell Res **306**(1): 216-229.
Varley, C. L., E. J. Bacon, J. C. Holder and J. Southgate (2009). "FOXA1 and IRF-1 intermediary transcriptional regulators of PPARgamma-induced urothelial cytodifferentiation." Cell Death Differ **16**(1): 103-114.
Varley, C. L., M. A. Garthwaite, W. Cross, J. Hinley, L. K. Trejdosiewicz and J. Southgate (2006). "PPARgamma-regulated tight junction development during human urothelial cytodifferentiation." J Cell Physiol **208**(2): 407-417.
Varley, C. L. and J. Southgate (2008). "Effects of PPAR agonists on proliferation and differentiation in human urothelium." Exp Toxicol Pathol **60**(6): 435-441.
Varley, C. L., J. Stahlschmidt, W. C. Lee, J. Holder, C. Diggle, P. J. Selby, L. K. Trejdosiewicz and J. Southgate (2004a). "Role of PPARgamma and EGFR signalling in the urothelial terminal differentiation programme." J Cell Sci **117**(Pt 10): 2029-2036.
Varley, C. L., J. Stahlschmidt, B. Smith, M. Stower and J. Southgate (2004b). "Activation of peroxisome proliferator-activated receptor-gamma reverses squamous metaplasia and induces transitional differentiation in normal human urothelial cells." Am J Pathol **164**(5): 1789-1798.
Vinken, M., E. Decrock, L. Leybaert, G. Bultynck, B. Himpens, T. Vanhaecke and V. Rogiers (2012). "Non-channel functions of connexins in cell growth and cell death." Biochim Biophys Acta **1818**(8): 2002-2008.
Vlaskovska, M., L. Kasakov, W. Rong, P. Bodin, M. Bardini, D. A. Cockayne, A. P. Ford and G. Burnstock (2001). "P2X3 knock-out mice reveal a major sensory role for urothelially released ATP." J Neurosci **21**(15): 5670-5677.
Walker, B. E. (1960). "Renewal of cell populations in the female mouse." Am J Anat **107**: 95-105.
Wallis, S., S. Lloyd, I. Wise, G. Ireland, T. P. Fleming and D. Garrod (2000). "The alpha isoform of protein kinase C is involved in signaling the response of desmosomes to wounding in cultured epithelial cells." Mol Biol Cell **11**(3): 1077-1092.
Watanabe, T., K. Sato and K. Kaibuchi (2009). "Cadherin-mediated intercellular adhesion and signaling cascades involving small GTPases." Cold Spring Harb Perspect Biol **1**(3): a003020.
Wei, C. J., R. Francis, X. Xu and C. W. Lo (2005). "Connexin43 associated with an N-cadherin-containing multiprotein complex is required for gap junction formation in NIH3T3 cells." J Biol Chem **280**(20): 19925-19936.

Wezel, F., J. Pearson and J. Southgate (2014). "Plasticity of in vitro-generated urothelial cells for functional tissue formation." Tissue Eng Part A **20**(9-10): 1358-1368.
White, T. W., R. Bruzzone, S. Wolfram, D. L. Paul and D. A. Goodenough (1994). "Selective interactions among the multiple connexin proteins expressed in the vertebrate lens: the second extracellular domain is a determinant of compatibility between connexins." J Cell Biol **125**(4): 879-892.
Wiencken-Barger, A. E., B. Djukic, K. B. Casper and K. D. McCarthy (2007). "A role for Connexin43 during neurodevelopment." Glia **55**(7): 675-686.
Winder, M., G. Tobin, D. Zupancic and R. Romih (2014). "Signalling molecules in the urothelium." Biomed Res Int **2014**: 297295.
Wright, C. S., R. F. Berends, D. J. Flint and P. E. Martin (2013). "Cell motility in models of wounded human skin is improved by Gap27 despite raised glucose, insulin and IGFBP-5." Exp Cell Res **319**(4): 390-401.
Wright, C. S., M. A. van Steensel, M. B. Hodgins and P. E. Martin (2009). "Connexin mimetic peptides improve cell migration rates of human epidermal keratinocytes and dermal fibroblasts in vitro." Wound Repair Regen **17**(2): 240-249.
Wu, X. R., J. H. Lin, T. Walz, M. Haner, J. Yu, U. Aebi and T. T. Sun (1994). "Mammalian uroplakins. A group of highly conserved urothelial differentiation-related membrane proteins." J Biol Chem **269**(18): 13716-13724.
Wu, X. R., M. Manabe, J. Yu and T. T. Sun (1990). "Large scale purification and immunolocalization of bovine uroplakins I, II, and III. Molecular markers of urothelial differentiation." J Biol Chem **265**(31): 19170-19179.
Yamaguchi, D. T. and D. Ma (2003). "Mechanism of pH regulation of connexin 43 expression in MC3T3-E1 cells." Biochem Biophys Res Commun **304**(4): 736-739.
Yang, J., B. Liu, Q. Wang, D. Yuan, X. Hong, Y. Yang and L. Tao (2011). "Connexin 32 and its derived homotypic gap junctional intercellular communication inhibit the migration and invasion of transfected HeLa cells via enhancement of intercellular adhesion." Mol Med Rep **4**(5): 971-979.
Yu, Z., J. Mannik, A. Soto, K. K. Lin and B. Andersen (2009). "The epidermal differentiation-associated Grainyhead gene Get1/Grhl3 also regulates urothelial differentiation." EMBO J **28**(13): 1890-1903.
Zaravinos, A., G. I. Lambrou, I. Boulalas, D. Delakas and D. A. Spandidos (2011). "Identification of common differentially expressed genes in urinary bladder cancer." PLoS One **6**(4): e18135.
Zavadil, J. and E. P. Bottinger (2005). "TGF-beta and epithelial-to-mesenchymal transitions." Oncogene **24**(37): 5764-5774.
Zhou, Y., W. Yang, M. M. Lurtz, Y. Ye, Y. Huang, H. W. Lee, Y. Chen, C. F. Louis and J. J. Yang (2007). "Identification of the calmodulin binding domain of connexin 43." J Biol Chem **282**(48): 35005-35017.
Zhuang, J., Q. Lu, B. Shen, X. Huang, L. Shen, X. Zheng, R. Huang, J. Yan and H. Guo (2015). "TGFbeta1 secreted by cancer-associated fibroblasts induces epithelial-mesenchymal transition of bladder cancer cells through lncRNA-ZEB2NAT." Sci Rep **5**: 11924.